OPTIMIZATION OF ENVIRONMENTALLY FRIENDLY SOLAR ASSISTED ABSORPTION COOLING SYSTEMS

Berhane Hagos Gebreslassie

ISBN: 978-84-693-7673-7
Dipòsit Legal: T-1752-2010

UNIVERSITAT ROVIRA I VIRGILI
OPTIMIZATION OF ENVIRONMENTALLY FRIENDLY SOLAR ASSISTED ABSORPTION COOLING SYSTEMS
Berhane Hagos Gebreslassie
ISBN: 978-84-693-7673-7/DL:T-1752-2010

DOCTORAL THESIS

Berhane Hagos Gebreslassie

Optimization of environmentally friendly solar assisted absorption cooling systems

Department of Mechanical Engineering

UNIVERSITAT ROVIRA I VIRGILI

UNIVERSITAT ROVIRA I VIRGILI
OPTIMIZATION OF ENVIRONMENTALLY FRIENDLY SOLAR ASSISTED ABSORPTION COOLING SYSTEMS
Berhane Hagos Gebreslassie
ISBN: 978-84-693-7673-7/DL:T-1752-2010

Berhane Hagos Gebreslassie

Optimization of environmentally friendly solar assisted absorption cooling systems

Doctoral Thesis

Supervised by: Dr. Dieter T. Boer
Dr. Gonzalo Guillén Gosálbez
Dr. Laureano Jiménez Esteller

Department of Mechanical Engineering

UNIVERSITAT ROVIRA I VIRGILI

Tarragona

2010

UNIVERSITAT ROVIRA I VIRGILI
OPTIMIZATION OF ENVIRONMENTALLY FRIENDLY SOLAR ASSISTED ABSORPTION COOLING SYSTEMS
Berhane Hagos Gebreslassie
ISBN: 978-84-693-7673-7/DL:T-1752-2010

Acknowledgements

First, I am heartily thankful to my supervisors, Dr. Dieter Boer, Dr. Gonzalo Guillén Gosálbez and Dr. Laureano Jiménez Esteller whose encouragement, guidance and support throughout the whole course enabled me to develop my research ability tremendously. They have made available their support in numerous ways. I would like to thank all members of the SUSCAPE research group who helped me in different forms. It was a great opportunity to study in such a multidisciplinary research group. Thank you so much indeed.

I would like to acknowledge the University of Rovira i Virgili for providing me a four year scholarship to realize my masters and the PhD study.

I am grateful to all members of all Mechanical Engineering Department especially the dean Dr. Ildefonso Cuesta, the secretary Samuel Garcia, the PhD students Jerko Labus and Iván Andrés Montero and the postgraduate coordinators Ms. Núria Juanpere and Ms. Laura Cortés for their administrative help from the beginning to the end of my study.

I am thankful to the committee of the tribunals of PhD thesis presentation Dr. Luisa Cabeza, Dr. Montse Meneses, Dr. António Mortal, Dr. Moises Graells, Dr. José Caballero, Dr. Ildefonso Cuesta and Dr. Francesc Castells for their cooperation and the precious time they spent to read and evaluate my work.

I offer my regards and blessings for the help I received from Ms. Pilar Secanell, Ethiopian URV students, and to all of those who supported me in any respect during the completion of the thesis.

Lastly, my wife presence during my study was important and my greatest and sincere appreciation goes to my wife Hidat Hagos, to my father, mother, brothers and sisters for their continued support. Liwamey just thank you. I love you all.

UNIVERSITAT ROVIRA I VIRGILI
OPTIMIZATION OF ENVIRONMENTALLY FRIENDLY SOLAR ASSISTED ABSORPTION COOLING SYSTEMS
Berhane Hagos Gebreslassie
ISBN: 978-84-693-7673-7/DL:T-1752-2010

Resumen

Tanto las limitadas reservas de combustibles fósiles como su impacto ambiental han motivado, entre otras causas, la optimización de los sistemas de generación de energía. Los equipos de refrigeración y otros sistemas de enfriamiento tienen un elevado consumo energético y contribuyen al incremento de las emisiones de CO_2. Existen alternativas más sostenibles a los ciclos de compresión convencionales. Estos sistemas requieren mejoras para ser competitivos.

El objetivo de esta tesis doctoral es la mejora de sistemas de refrigeración por absorción mediante optimización y modelización matemática. Se incluye, por un lado el análisis energético, exergético y termoeconómico y por otro la optimización multiobjetivo, incluyendo el efecto de la incertidumbre del precio de la energía en el diseño del ciclo de absorción.

Se ha realizado el análisis termodinámico para varias configuraciones de los ciclos por absorción incluyendo el análisis energético, exergético y estructural [1, 2]. En concreto, en [1] se ha comparado el coeficiente de rendimiento y la eficiencia exergética de diferentes configuraciones de los ciclos de absorción de agua-LiBr. En [2] se lleva a cabo un análisis energético, exergético y estructural de ciclos de absorción de amoniaco-agua de simple efecto con diferentes grados de integración de calor. A partir del análisis de exergético se determinan las irreversibilidades de las diferentes unidades y de todo el ciclo. Como las irreversibilidades por sí solos no indican la manera de mejorar el ciclo, se ha integrado el análisis estructural mediante los coeficientes de interacción estructural (CSB).

A partir del análisis estructural se ha estudiado la optimización termoeconómica. Se ha formulado una ecuación relativamente que determina el

UNIVERSITAT ROVIRA I VIRGILI
OPTIMIZATION OF ENVIRONMENTALLY FRIENDLY SOLAR ASSISTED ABSORPTION COOLING SYSTEMS
Berhane Hagos Gebreslassie
ISBN: 978-84-693-7673-7/DL:T-1752-2010

área óptima de los intercambiadores de calor en sistemas térmicos. Para una descripción detallada consultar [3].

La optimización termoeconómica únicamente considera una única función objetivo y examina un subconjunto de posibles alternativas. Para superar esta limitación se introduce un método riguroso basado en programación matemática. La metodología sistemática para el diseño de sistemas de refrigeración por absorción más sostenibles se describe en [4]. El método se basa en la formulación de un problema de programación no lineal (PNL) bi-criteria que considera la minimización del coste total y del impacto ambiental.

El impacto ambiental se evalúa a partir del análisis del ciclo de vida, que incluye los daños causados en todas las etapas del ciclo de vida del sistema de refrigeración. El método de solución para la optimización multiobjetivo (restricción ϵ) y los conceptos de la frontera de Pareto se describen en [4]. Sólo hemos considerado el impacto ambiental durante la operación suponiendo que el impacto debido a la fabricación es insignificante en comparación con el impacto debido a la operación. Los resultados muestran que se puede reducir el impacto ambiental si el se está dispuesto a sacrificar parcialmente el rendimiento económico del sistema.

Basado en la formulación matemática en [4] se ha considerado el efecto de la variabilidad de los precios de la energía. El problema se formuló como un modelo de PNL bi-criterio estocástico. En [5] se describen el escenario múltiple bi-criteria de formulación del modelo estocástico, el modelo del coste total previsto y el de riesgo financiero. En este trabajo el riesgo financiero se mide mediante el downside risk, evitando así la definición de variables binarias y obteniendo un mejor rendimiento numérico.

En [6] el diseño del sistema de refrigeración por absorción se completa incluyendo el subsistema de producción de calor. Se han sido considerados dos fuentes alternativas de calor: gas natural y energía solar térmica. Se han considerado los siguientes tipos de colectores: tres de placa plana, tres de tubos evacuados y uno del tipo de compuesto parabólico. En este trabajo, además del impacto durante la operación del sistema, se ha incluido el debido a la fabricación de las unidades. La selección del colector y del número de

UNIVERSITAT ROVIRA I VIRGILI
OPTIMIZATION OF ENVIRONMENTALLY FRIENDLY SOLAR ASSISTED ABSORPTION COOLING SYSTEMS
Berhane Hagos Gebreslassie
ISBN: 978-84-693-7673-7/DL:T-1752-2010

colectores en cada módulo se representan mediante una disyunción utilizando la formulación *big-M*. El enfoque propuesto se ilustra mediante estudios de casos teniendo en cuenta los datos meteorológicos de Barcelona y Tarragona. Los resultados muestran que se puede lograr una reducción significativa en el impacto ambiental con una mayor inversión en el subsistema de captación solar, aumentando así la fracción solar del sistema de refrigeración. La selección del tipo de colector solar depende de las condiciones específicas de funcionamiento y de los datos meteorológicos considerados en el análisis.

Finalmente se ha evaluado el impacto de ciclos de absorción apoyados con energía solar para la reducción del calentamiento global. Hemos estudiado como afectan las diferentes tecnologías, la tasa de emisión de gases de efecto invernadero y qué efecto tiene el precio del combustible en la selección del sistema [7]. El estudio incluye cómo estos parámetros favorecen el reemplazamiento del gas natural por la energía solar. Los resultados revelan que en situaciones de precios altos del combustible y considerando el impuesto sobre las emisiones de CO_2 los ciclos de absorción apoyados con energía solar son técnica y económicamente viables.

UNIVERSITAT ROVIRA I VIRGILI
OPTIMIZATION OF ENVIRONMENTALLY FRIENDLY SOLAR ASSISTED ABSORPTION COOLING SYSTEMS
Berhane Hagos Gebreslassie
ISBN: 978-84-693-7673-7/DL:T-1752-2010

Summary

Optimization of energy conversion systems becomes more important due to limitations of fossil fuels and the environmental impact during their use. Among these systems cooling and refrigeration devices have an increasing share in the total energy consumption and the contribution to CO_2 emissions. There exist more sustainable cooling systems, which represent an alternative to conventional compression cycles. However, they still have to be improved in order to become competitive.

This thesis focuses on mathematical modeling and optimization of environmentally friendly absorption cooling systems. We include on the one hand energy, exergy and structural analysis and thermoeconomic optimization, and on the other hand optimization of the cooling system considering two contradicting objective functions, and optimization of absorption cycles under uncertainty of energy prices.

The thermodynamic analysis has been performed for different configurations of the absorption cooling cycles. The detailed description of energy, exergy and the structural analysis of the different configurations are presented in [1, 2]. Specifically, in [1] different configurations of water-LiBr absorption cycles have been compared based on the coefficient of performance and the exergetic efficiency. Moreover, in [2] energy, exergy and structural analysis of single effect ammonia-water absorption cooling cycles with different degree of heat integration are performed. From the exergy analysis irreversibilities of the units and the cycle are determined. Since the irreversibilities do not indicate how to improve the cycle, the structural analysis using the coefficients of structural bonds *(CSB)* has been applied.

Based on the structural analysis presented in [2] the thermoeconomic optimization is studied. An equation that determines the optimal area of the

UNIVERSITAT ROVIRA I VIRGILI
OPTIMIZATION OF ENVIRONMENTALLY FRIENDLY SOLAR ASSISTED ABSORPTION COOLING SYSTEMS
Berhane Hagos Gebreslassie
ISBN: 978-84-693-7673-7/DL:T-1752-2010

heat exchangers in thermal systems is formulated. A detailed description is presented in [3].

The thermoeconomic optimization relays only in a single economic objective function and examines a subset of feasible alternatives. To overcome this short coming a rigorous mathematical programming method is introduced. The systematic approach for the design of sustainable absorption cooling systems is described in [4]. The method relies on formulating a bi-criteria nonlinear programming (NLP) problem that accounts for the minimization of the total annualized cost and the environmental impact of the cycle.

The environmental performance is measured according to the principles of life cycle assessment (LCA), which accounts for the damage caused in all the stages of the life cycle of the cooling system. The solution method for the multi-objective optimization ($(the\ \epsilon - constraint)$) and the Pareto frontier concepts are described in [4]. We have considered initially only the environmental impact during the operation of the cooling system assuming that the impact due to manufacturing is negligible compared to the impact due to operation. The results show that a reduction in the environmental impact caused by the cycle can be attained if the decision maker is willing to compromise the economic performance of the system.

Based on the mathematical formulation in [4] a systematic approach for the design of absorption cooling cycles considering the variability of the energy price is studied. This is achieved by formulating the design task as a bi-criteria stochastic NLP model. In [5] the multi-scenario bi-criteria stochastic model formulation, the expected total cost, and the financial risk are described. In this work the financial risk is measured using the downside risk, which avoids the definition of binary variables, thus leading to better numerical performance.

In [6] the design of absorption cooling cycle is modified to include the heat production subsystem. Two heat sources are considered: natural gas and solar energy. Three types of flat plate, three types of evacuated tube and one type of compound parabolic collectors are considered. In this work in addition to the environmental impact during operation of the system we

UNIVERSITAT ROVIRA I VIRGILI
OPTIMIZATION OF ENVIRONMENTALLY FRIENDLY SOLAR ASSISTED ABSORPTION COOLING SYSTEMS
Berhane Hagos Gebreslassie
ISBN: 978-84-693-7673-7/DL:T-1752-2010

include the environmental impact during manufacturing of the units. The selection of module of the collector and the number of collectors in each module are represented by a disjunction, reformulated using the big-M formulation. The proposed approach was illustrated through case studies considering the weather data of Barcelona and Tarragona. The results show that significant reductions in the environmental impact can be achieved if the decision-maker is willing to invest on the solar collector's subsystem. These reductions are achieved by increasing the number of collectors installed, which increases the solar fraction of the cooling system. The type of solar collector dependents on the particular operating conditions and weather data considered in the analysis.

Finally, solar assisted absorption cycles have been considered for the reduction of the global warming impact of the cooling system. We have studied how greenhouse gas emissions tax and the fuel price affect the greenhouse gas emissions reduction by giving preference to different technologies [7]. The study includes how these parameters force the model to shift the energy consumption from natural gas to solar energy. The optimization results reveal that with high fuel prices including the CO_2 emissions tax, solar assisted absorption cooling systems are technically and economically feasible.

UNIVERSITAT ROVIRA I VIRGILI
OPTIMIZATION OF ENVIRONMENTALLY FRIENDLY SOLAR ASSISTED ABSORPTION COOLING SYSTEMS
Berhane Hagos Gebreslassie
ISBN: 978-84-693-7673-7/DL:T-1752-2010

Table of contents

UNIVERSITAT ROVIRA I VIRGILI
OPTIMIZATION OF ENVIRONMENTALLY FRIENDLY SOLAR ASSISTED ABSORPTION COOLING SYSTEMS
Berhane Hagos Gebreslassie
ISBN: 978-84-693-7673-7/DL:T-1752-2010

UNIVERSITAT ROVIRA I VIRGILI
OPTIMIZATION OF ENVIRONMENTALLY FRIENDLY SOLAR ASSISTED ABSORPTION COOLING SYSTEMS
Berhane Hagos Gebreslassie
ISBN: 978-84-693-7673-7/DL:T-1752-2010

Chapter 1

Introduction

The design of energy conversion systems becomes more important due to limitations of fossil fuels and the environmental impact during their use. Energy systems are complex as they involve in economic, technical, environmental, legal and political factors and supporting our daily life and economic development [8, 9]. Nowadays, 94 % of the CO_2 emissions in Europe are attributed to the energy sector, due to the combustion of fossil fuels (oil: 50 %, natural gas: 22 % and coal: 28 % [10]).

The building sector represents 40 % of the total primary energy demand in European Union countries and one third of the GHG emissions [11]. A significant part of the emissions attributed to the building sector are due to air conditioning (AC) systems, which are based mainly on electricity driven compression cycles. Particularly, during the last years there has been a proliferation of vapor compression air conditioning [11–13]. The cooling demand has been increasing rapidly during the last decade, especially in moderate climates [12, 13]. As a result, the electricity demand threatens the stability of electricity grids and increases the environmental problems associated with the generation of electricity. In Spain, the summer peak electricity consumption became higher than the winter peak electricity demand. The summer peak in the southern part of the country increased by 20 % in 2003 and by another 20 % in 2004 [11].

Hence, it seems clear that a durable change in the energy structure should be made in order to adopt more sustainable solutions to fulfill the increasing

UNIVERSITAT ROVIRA I VIRGILI
OPTIMIZATION OF ENVIRONMENTALLY FRIENDLY SOLAR ASSISTED ABSORPTION COOLING SYSTEMS
Berhane Hagos Gebreslassie
ISBN: 978-84-693-7673-7/DL:T-1752-2010

cooling demand. Mainly, environmentally friendly and energy efficient technologies have to be promoted so that the environmental impact of cooling applications is minimized without compromising their economic performance. In this line, there has been a growing interest on thermal energy activated cooling machines. They provide an environmentally friendly alternative to standard compression chillers [14–16]. The most common types of thermally driven chillers are absorption and adsorption chillers. The benefits of absorption systems are [17]:

- Absorption chillers can be driven by low grade thermal energy, as waste heat, biomass, solar thermal energy or heat from cogeneration.
- Absorption chillers are silent and vibration free.
- Absorption chillers do not pose a threat to ozone layer depletion as they don't use CFC's or HCFC's and may have less impact on global warming.
- Absorption chillers are economically attractive if the fuel costs are substantially lower than the electricity costs.

Absorption cycles use a mixture of a refrigerant and an absorbent. The most widely employed mixtures are water-lithium-bromide (water as refrigerant) and ammonia-water (ammonia as refrigerant). $H_2O - LiBr$ has certain merits over the $NH_3 - H_2O$ supported chillers. For example, they have higher performance, and do not require rectification to purify the refrigerant. However, its working range is limited by the freezing point of the refrigerant (water) and the crystallization risk of the solution. Especially at higher temperatures it is corrosive. The ammonia-water system is used typically for low temperature cooling or freezing and it does not have crystallization problems. The need of further rectification after desorption reduces the chiller efficiency.

Even though, these technologies can use renewable energy, thus decreasing the associated environmental impact, they need a higher number of units (absorber, desorber and heat recovery units). This leads to higher capital

ISBN: 978-84-693-7673-7/DL:T-1752-2010

costs than those associated with conventional cooling systems (*i.e.*, vapor compression system). Hence, optimization strategies based on both, thermodynamic and economic insights are needed to improve their operational and economic performance.

In this regard, the thermoeconomic optimization which merges the thermodynamic and economic analysis within a single framework has been applied to thermal systems [18–24]. In the process system engineering community, the mathematical programming approach is extensively used. However, for thermal systems, and in particular for cooling systems its use is rather limited. Recently, mathematical programming has been used in the optimization of cooling systems [25–27]. This approach is based on formulating optimization problems that can be solved via the standard techniques for linear, nonlinear, mixed integer linear and mixed integer non linear problems. This method offers a suitable framework to address the environmental performance of different design alternatives, energy resources and also permit to include the uncertainties of the design parameters at the design stage.

To my knowledge works that integrate the environmental and the economic performance measure in the framework of multi objective optimization have not been addressed yet for cooling systems. Therefore, this PhD thesis is aimed at filling this gap. The main novelties of this dissertation lie in: 1) comparison of the performance of different configuration of absorption cycles considering only the unavoidable exergy destruction rates. 2) The thermoeconomic optimization based on the structural method for ammonia-water absorption cycles. 3) The integration of the life cycle analysis methodologies to evaluate the design of the solar assisted absorption cooling system alternatives that are systematically generated by the mathematical programming optimization tools in the framework of multi-objective optimization; 4) The integration of the financial risk management to evaluate the design of the absorption cooling system alternatives, which are systematically generated by the optimization tools considering the uncertainties of the future energy price.

This PhD thesis is structured in four main sections. Next the objective of the PhD thesis is presented followed by the problem statement. The section

ISBN: 978-84-693-7673-7/DL:T-1752-2010

that follows will discus the optimization methods based on exergy analysis and the mathematical programming. The third section presents the objective functions considered. Last, the conclusions of the work are drawn and future works are included.

1.1 General objective

The overall objective of the PhD thesis is the optimization of environmentally friendly solar assisted absorption cooling cycle in the framework of multi-objective, robust and multi-period optimization problem.

Specific objectives

- Exergy analysis of different configurations of absorption cycles and comparison based on the coefficient of performance, irreversibilities and the exergetic efficiency.
- Thermoeconomic optimization of single effect $NH_3 - H_2O$ absorption cycles using coefficients of structural bonds (CSB).
- Multi-objective optimization of environmentally friendly single effect $NH_3 - H_2O$ absorption cycle using mathematical programming.
- Include uncertainty of the energy prices to improve the robustness of the optimization problem of the aforementioned mathematical programming.
- Modify the model of the absorption cycle to include the heat production subsystem, which includes the solar thermal collectors, and optimize the modified problem.
- Study how solar assisted absorption cooling cycles can be real alternatives, if a carbon dioxide tax is introduced. Also, study how fuel prices affect the competitiveness of the more sustainable technologies.

UNIVERSITAT ROVIRA I VIRGILI
OPTIMIZATION OF ENVIRONMENTALLY FRIENDLY SOLAR ASSISTED ABSORPTION COOLING SYSTEMS
Berhane Hagos Gebreslassie
ISBN: 978-84-693-7673-7/DL:T-1752-2010

1.2 Problem statement

This PhD thesis addresses the optimal design of solar assisted absorption cooling cycle following two approaches.

1. Thermoeconomic optimization method which merges the thermodynamic and the economic analysis to a single objective function. Energy, exergy and structural analysis for different configurations of the absorption cycles have been performed.

2. Mathematical programming method is employed to optimize the cooling system in the framework of multi-objective optimization. Two contradicting objective functions are used: cost and environmental performance or cost and financial risk.

In both approaches the given data are the cooling capacity of the system, the inlet and outlet temperatures of the external fluids (heat source temperature for the second approach is a variable), the overall heat transfer coefficients of the heat exchangers and capital and operating cost parameters. For the second approach LCA related information is given (*i.e.*, life cycle inventory of emissions and feedstocks, parameters of the damage model, global warming potential parameters for the greenhouse gas emissions). It is assumed that the energy cost cannot be perfectly forecasted, and its variability can be represented by a set of scenarios with a given probability of occurrence. Monthly weather data (ambient temperature and global daily solar radiation) and performance equations of the solar collectors are also given data. The goal is to determine the optimal design and associated operating conditions at minimum total cost for the thermoeconomic optimization and in the case of multi-objective optimization at the optimal trade-off designs. Moreover, quantified environmental benefits, by incorporating the solar energy to the cooling system is evaluated.

UNIVERSITAT ROVIRA I VIRGILI
OPTIMIZATION OF ENVIRONMENTALLY FRIENDLY SOLAR ASSISTED ABSORPTION COOLING SYSTEMS
Berhane Hagos Gebreslassie
ISBN: 978-84-693-7673-7/DL:T-1752-2010

Chapter 2

Optimization methods

Optimization of thermal systems is the modification of structure and design variables to minimize (maximize) a given objective function (*e.g*, the production cost, profit, environmental impact, environmental benefit, reliability, flexibility, etc) that simultaneously fulfills the process constraints. Typical constraints are the physical laws, the boundary conditions associated with material availability, financial resources, protection of environment, governmental regulation, safety, maintainability, etc. A widely used method is based on the thermoeconomic optimization [18–24]. Details of this method can be found in [3, 28, 29] and a brief description is given in section 2.1.

Using mathematical programming several compromise solutions (a multi-objective) that represent the optimal trade-off between the objective functions can be provided at the design stage. Hence, the decision maker can make a rational decision based on this information. Details of this method can be found [4–6, 30] and a brief description could be found in section 2.2.

2.1 Exergy based methods

Absorption cycles are generally evaluated according to their coefficient of performance (COP). Starting with the basic single effect cycle, more complex and efficient cycles can be obtained. Multi-stage cycles have higher COP's; however, they need higher driving temperatures. The triple effect has the highest energetic efficiency followed by double and single effect cycles. The

ISBN: 978-84-693-7673-7/DL:T-1752-2010

half effect cycle (also called double lift) has the lowest COP but can work with lower driving temperatures. Thus the quality of the driving energy of these cycles differs considerably.

The energy conservation law does not differentiate between different forms of energy to evaluate the coefficient of performance. A convenient way of introducing and quantifying the quality of energy is based on the maximum possible work that can be obtained from a given form of energy using environmental parameters as reference state. This standard energy quality is commonly called exergy [28]. In other words, exergy is the maximum possible reversible work obtainable in bringing the state of a system to equilibrium with the environment. It enables us to compare different types of energy for example heat and work, and it takes into account the different quality of heat at different temperature levels.

2.1.1 Exergy analysis

A detailed discussion of exergy analysis and thermoeconomic optimization in thermal systems can be found [28, 29]. In particular, exergy destruction analysis and evaluation of the exergetic efficiency of water-LiBr absorption cycles can be found in [31–35]. Ammonia-water absorption cycle are considered in [36, 37].

First law analysis of water-LiBr multiple effect absorption cycles was carried out by Grossman *et al.* [38]. However, for high temperature range the thermodynamic properties are evaluated by extrapolating the existing thermodynamic property correlations. Lee *et al.* [39] made the first and second law thermodynamic analysis of triple effect cycles. However, the exergy destruction rates were evaluated without distinguishing the avoidable and unavoidable parts. Morosuk and Tsatsaronis [40] proposed splitting the exergy destruction rate into avoidable and unavoidable parts. The exergy destruction rates which can not be further reduced by design improvement represent unavoidable exergy destruction. Therefore, a designer has to focus on the exergy destruction rates with potential room for improvement. To my knowledge, the energy and exergy analysis that compares half, single,

UNIVERSITAT ROVIRA I VIRGILI
OPTIMIZATION OF ENVIRONMENTALLY FRIENDLY SOLAR ASSISTED ABSORPTION COOLING SYSTEMS
Berhane Hagos Gebreslassie
ISBN: 978-84-693-7673-7/DL:T-1752-2010

double, and triple effect on rational base and that does not depend on the design specifications are not covered. Hence, to fill this gap a comparison of multiple effect cycles based on the coefficient of performance and exergy efficiency which considers only the unavoidable exergy destruction rate are performed in Gebreslassie *et al.* [1]. As expected, the coefficient of performance increases from half effect to the multiple effects. However, the increase in exergetic efficiency is not as pronounced as the coefficient of performance. The maximum coefficient of performance and the exergetic efficiency are obtained close to the cut off temperature of the generator, which represents the lowest feasible temperature.

Exergy analysis include the evaluation of exergy of each stream, the irreversibility, exergy loses and exergy efficiency of each unit and the system. Furthermore, exergy analysis enable us to determine the coefficients of structural bonds (CSB) of each unit [28, 41, 42]. The CSB is used in making decisions where the thermoeconomic optimization has to be performed.

Coefficients of structural bonds can be determined as function of the variable (x) that influence the efficiency of the unit, irreversibility rate of the unit k ($\dot{I}_k$) and the system ($\dot{I}_t$) as given in eqn. (2.1)

$$CSB_k = \left(\frac{\frac{\partial \dot{I}_t}{\partial x}}{\frac{\partial \dot{I}_t}{\partial x}} \right)_{x=var} \tag{2.1}$$

Structural coefficients consider how the irreversibility of the whole system changes when the irreversibility of one component is modified by modifying its efficiency. If a slight decrease of the irreversibility of one component due to a higher efficiency causes an important improvement in the total irreversibility of the cycle, it will be wise to put much of the design effort to improve the efficiency of this component. In the case of a high coefficient of structural bonds, the benefit of a more efficient (*i.e.*, more expensive) unit on the performance of the whole cycle is considerable. Otherwise, if the coefficient of structural bonds is low (*i.e.*, near unity), an improvement of the efficiency of the unit is not economically worthwhile. Details can be found in [2, 28, 43].

UNIVERSITAT ROVIRA I VIRGILI
OPTIMIZATION OF ENVIRONMENTALLY FRIENDLY SOLAR ASSISTED ABSORPTION COOLING SYSTEMS
Berhane Hagos Gebreslassie
ISBN: 978-84-693-7673-7/DL:T-1752-2010

2.1.2 Thermoeconomic optimization

The thermoeconomic optimization is a discipline that combines exergy and economic analysis. This work follows the structural method introduced by Beyer [41, 42] which is based on the coefficients of structural bonds explained in section 3.2 of Gebreslassie *et al.* [3] and the local cost of the irreversibility. The main goal of a thermoeconomic optimization is to give a balance between the expenditure on investment costs and exergy costs which results in minimum total cost of the system under a given structure of the system. This method was applied for a vapor compression refrigerator by Dingeç *et al.* [21], for a condenser of compression cycle by Dentice d'Accadia *et al.* [22] and recently for water-LiBr absorption cycle by Kizllkan *et al.* [24]. The key point of this approach is the selection of an appropriate efficiency related variable x. The variable x should be directly related to the efficiency and the investment cost of the unit under consideration. This is because the final optimization problem depends on the capital and irreversibility cost of this unit.

2.2 Mathematical programming methods

Mathematical programming is the study of a problem in which one has to minimize or maximize a function by systematically choosing the value of a real or integer variable from the allowed set of variables. The previous optimization method may leads to sub-optimal solution, while the mathematical programming method is a rigorous approach and systematically evaluates all alternatives of the feasible solutions.

2.2.1 Mathematical model

The mathematical model describes the system behavior in terms of relations of physical laws. The model should describe the manner in which all relations are connected and the way in which variables affect the performance measures [29, 30]. The mathematical model for an optimization problem should include an objective function and constraints (equality or inequality).

UNIVERSITAT ROVIRA I VIRGILI
OPTIMIZATION OF ENVIRONMENTALLY FRIENDLY SOLAR ASSISTED ABSORPTION COOLING SYSTEMS
Berhane Hagos Gebreslassie
ISBN: 978-84-693-7673-7/DL:T-1752-2010

The objective function can be the total cost, the environmental impact or the financial risk due to energy price variability of the cooling system. There are set of variables that control the value of the objective functions as the thermodynamic properties of each streams and the capacity of each unit of the cooling system.

Constraints are expressions which allow that variables can take certain values but exclude others. The equality and inequality constraints should be provided by appropriate thermodynamic, economic, and environmental models with boundary conditions. These models generally include mass and energy conservation equations, relations associated to engineering designs (*e.g*, minimum and maximum temperature, pressure, minimum temperature approaches, etc), environmental impacts and thermodynamic properties of the streams. The model also include inequalities that specify the allowable operating ranges, the minimum and maximum performance requirements, the bounds on the availability of resources, etc

An optimization problem can be stated as shown in eqn. (2.2).

$$\begin{aligned} \text{(M)} \quad \min_{x} \quad & U(x) = \{f_1(x), f_2(x), ..\} \\ \text{s.t.} \quad & h(x) = 0 \\ & g(x) \leq 0 \\ & x \in \Re \end{aligned} \tag{2.2}$$

Here, $U(x)$ refers to the objective function. This can include single objective function (if only $f_1(x)$ is minimized) or multiple objective functions. $h(x)$ and $g(x)$ represents the equality and inequality constraints respectively. x refers to the set of design variables. Optimization problems can be classified based on the nature the equations involved in eqn. (2.2) (linear and nonlinear), based on the nature of the permissible design variables (continues or integer), based on the nature of the design variables (static or dynamic), based on the nature of constraints (constraint or unconstrained), based on the nature of the variables (stochastic or deterministic), based on the number of objective functions (single or multiple), and so on.

UNIVERSITAT ROVIRA I VIRGILI
OPTIMIZATION OF ENVIRONMENTALLY FRIENDLY SOLAR ASSISTED ABSORPTION COOLING SYSTEMS
Berhane Hagos Gebreslassie
ISBN: 978-84-693-7673-7/DL:T-1752-2010

2.2.2 Selection of the appropriate solvers

The General Algebraic Modeling System (GAMS) is a modeling environment [44]. It is integrated with different external solvers. These solvers are capable of solving linear, nonlinear, and mixed-integer optimization problems. The most widely used solvers of NLP problems are CONOPT, MINOS and SNOPT. These algorithms attempt to find local optimum unless the NLP problem is convex. If the NLP problem is convex the local minimum becomes a global minimum. As rule of thumb, if the model under consideration has highly nonlinear constraints, as in this thesis, CONOPT is more suitable. However, if the model involves less nonlinearity outside the objective function, either MINOS, or SNOPT are probably more adequate. For constrained nonlinear systems (CNS), for models with few degrees of freedoms, and if the model has roughly the same number of constraints and variables it is recommended to start with CONOPT (*i.e.*, CONOPT3, but not CONOPT1 or CONOPT2). CONOPT is designed for large and sparse models which are like the type of models that can be encountered in this work, hence for the NLP models of this work CONOPT is used [44].

The NLP solvers can not be used for Mixed Integer Nonlinear Programming (MINLP) problems. In the thesis this type of problems are encountered when the heat production sub-system is integrated to the absorption cycle as discussed in Gebreslassie *et al.* [6]. In these systems the type of collector and the number of collectors are represented as integer variables while the rest of variables represent linear or nonlinear variables. For solving such type of problems DICOPT and SBB solvers are used [44].

The MINLP algorithm inside DICOPT solves a series of NLP and Mixed Integer Programming (MIP) sub-problems. DICOPT is the local optimizer. However, it has provisions to handle non-convexities [44]. In this work the NLP sub-problem is solved with CONOPT and the MIP sub-problem we use CPLEX. SBB supports all type of discrete variables and it is based on the combination of the standard Branch and Bound known from MILP. For the NLP sub-problems CONOPT, MINOS and SNOPT can be used [44].

UNIVERSITAT ROVIRA I VIRGILI
OPTIMIZATION OF ENVIRONMENTALLY FRIENDLY SOLAR ASSISTED ABSORPTION COOLING SYSTEMS
Berhane Hagos Gebreslassie
ISBN: 978-84-693-7673-7/DL:T-1752-2010

In both solvers, the Relaxed Mixed Integer Nonlinear Programming (RMINLP) is initially solved using the starting point provided. In this work, the same model is simulated in Engineering Equation Solver (EES) [45] and the results are used as starting point in GAMS. The solver will stop if it gives unbounded or infeasible solutions. However, if the solution of the RMINLP is an integer, the solver will return this solution as optimal integer solution. Otherwise, the current solution is stored and for DICOPT solver the outer approximation procedure will start. However, if the solver is SBB the Branch and Bound procedure will start [44].

2.2.3 Solution techniques for multi-objective optimization applications

The bi-criteria optimization problem results a set of efficient or Pareto optimal points representing alternative process designs, each achieving a unique combination of environmental and economic performances [4, 6, 7] or Downside Risk and the expected total cost performance [5].

The general concept of Pareto frontier is explained in section 4 of Gebreslassie *et al.* [4–6]. The mathematical definition of Pareto optimality states that a design objective vector f^* is Pareto optimal if there does not exist another design objective vector f in the feasible design space such that $f_i \leq f_i^*$ for all $i \in \{i = 1, 2, ..., n\}$ and $f_i < f_i^*$ for at least one $i \in \{i = 1, 2, ..., n\}$. Thus, given a Pareto solution A, it is impossible to find another solution B that performs better than A for each objective. For the calculation of the Pareto set, two main methods exist in the literature. These are the $weighted - sum$ and $\epsilon - constraint$. The weighted-sum method is only rigorous for the case of convex problems, whereas the $\epsilon - constraint$ method is rigorous for convex and non-convex problems. In general, the thermodynamic correlations, the capital cost correlations, the minimum temperature difference constraints introduce non-convexities to the model. Thus, the $\epsilon - constraint$ method is better suited to the problems formulated in this work.

UNIVERSITAT ROVIRA I VIRGILI
OPTIMIZATION OF ENVIRONMENTALLY FRIENDLY SOLAR ASSISTED ABSORPTION COOLING SYSTEMS
Berhane Hagos Gebreslassie
ISBN: 978-84-693-7673-7/DL:T-1752-2010

Chapter 3

Applications of optimization

The objective functions we have considered in the PhD thesis are presented in this section. This includes the economic performance indicator, the environmental performance indicator and the financial risk performance indicator.

3.1 Economic performance

To measure the economic performance we use the total cost of the cooling system. It encompasses the capital cost and the operation cost. The total investment amortization cost is considered in this case based on the capital recovery factor. The Chemical Engineering Plant Cost Index (CEPCI) [46] is used to consider the inflation of the investment cost. For the operation cost we considered the cost of steam, natural gas, electricity, and cooling water. A detailed discussion can be found in [4] (section 3.3.1), [5] (section 3.2.1), [6], (section 3.3.1), and [7] (appendix B).

3.2 Life Cycle Assessment of thermal systems

LCA is used to assess the environmental performance of the process, whereas optimization techniques are used for generating in a systematic way different technological alternatives and identifying the best ones in terms of economic and environmental criteria. Examples on the application can be found in [47–49].

UNIVERSITAT ROVIRA I VIRGILI
OPTIMIZATION OF ENVIRONMENTALLY FRIENDLY SOLAR ASSISTED ABSORPTION COOLING SYSTEMS
Berhane Hagos Gebreslassie
ISBN: 978-84-693-7673-7/DL:T-1752-2010

In this thesis, the environmental performance of the system is measured by the Eco-indicator 99 [4, 6], and Global Warming Potential (GWP) [7] metrics. The Eco-indicator 99 accounts for 11 impact categories that are aggregated into three types of damages: human health, ecosystem quality and resource depletion. Eco-indicator 99 is described in detail in [50]. GWP is a relative scale which compares the impact of a given chemical with that of the same impact of carbon dioxide (whose GWP by convention is equivalent to 1). The GWP is calculated over a specific time interval that must be stated beforehand [51, 52]. We follow the Intergovernmental Panel on Climate Change (IPCC) 2007 and the Kyoto Protocol [52] considering a time horizon of 100 years. Details about the LCA methodology can be found elsewhere [53].

The calculation of the Eco-indicator 99 and GWP follows the main LCA stages [53]: (1) goal and scope definition, (2) inventory analysis, (3) damage assessment and (4) interpretation. These stages are described in the context of the PhD work in section 3.3.2 of [4–6].

3.3 Financial risk

Most of the strategies that address the optimal design and modeling of thermal systems such as compression refrigeration and absorption cooling are mainly deterministic, that is, based on nominal values for design parameters [20, 54–57]. Deterministic optimization assumes that all parameters are known with certainty or fail to recognize the presence of probable situations other than the most likely one. However, resource availability, technology development, unit cost of energy, end user demand, cooling and heating demand are fraught with uncertainty. This affects the optimization result and has to be taken into account in the decision making process [8, 9, 58].

The sources of uncertainties and their classification are explained in [59]. First the uncertainties are classified as *short term* which includes day to day process and parameter variations such as flow rates and temperatures. The system responds the variability within short period of time. The *long term* uncertainty includes product demand, product sales, raw material purchase

ISBN: 978-84-693-7673-7/DL:T-1752-2010

and equipment purchase uncertainty. These uncertainties occur over an extended time horizon.

Alternatively, they are classified by Pistikopoulos [60] into four categories:

i. *Model inherent uncertainty:* include kinetic constants, physical properties, transfer coefficients. They can be described either by range or by probability distribution function.

ii. *Process inherent uncertainty*: include flow rate and temperature variations which are usually described by a probability distribution function.

iii. *External uncertainty:* include feed stream availability, product demands, prices and environmental conditions. They are described based on historical data and customer orders are usually used to obtain a probability distribution.

iv. *Discrete uncertainty:* include uncertainties such as equipment availability and other random discrete events. A (discrete) probability distribution function can commonly be obtained from available data and manufacturer's specifications.

A number of approaches have been proposed in the literatures for the quantification of uncertainty in the design, planning, and scheduling of process plants and energy systems. These approaches have contributed to a better understanding of how uncertainty affects the design and planning performances. The main approaches to optimization under uncertainty are reviewed in detail by Sahinidis [58]. These are: i). Stochastic programming which is extensively used in process system engineering planning and scheduling by considering the uncertainties such as product demand, customer satisfaction, and the environmental metrics [61–66]. It can be expressed as recourse models, robust models and probabilistic models. ii). Fuzzy programming examples can be found in energy sector planning under uncertainty [8, 9, 67–69]. It could be possibilistic and flexible programming. iii). Stochastic dynamic programming [70].

UNIVERSITAT ROVIRA I VIRGILI
OPTIMIZATION OF ENVIRONMENTALLY FRIENDLY SOLAR ASSISTED ABSORPTION COOLING SYSTEMS
Berhane Hagos Gebreslassie
ISBN: 978-84-693-7673-7/DL:T-1752-2010

Optimization under uncertainty have followed a variety of modeling philosophies, including the minimization of expected total cost which is the one adopted in this work [5], maximization of expected net present value [64], minimization of deviations from goals, and optimization over soft constraints [58]. Usually, designs with minimum expected total cost performs better for higher financial risk, so they tend to have a trade-off between the objectives.

UNIVERSITAT ROVIRA I VIRGILI
OPTIMIZATION OF ENVIRONMENTALLY FRIENDLY SOLAR ASSISTED ABSORPTION COOLING SYSTEMS
Berhane Hagos Gebreslassie
ISBN: 978-84-693-7673-7/DL:T-1752-2010

Chapter 4

Conclusions and perspectives

Aligned with the objectives optimization of environmentally friendly solar assisted absorption cooling cycle in the framework of multi-objective, robust and multi-period optimization problem is performed. The methodology presented in this work is intended to promote a more sustainable design of cooling applications by guiding the decision-makers towards the adoption of alternatives that promote less environmental impact and reduce the consumption of primary energy resources. The conclusions withdrawn from the successive work to accomplish the specific objectives are listed below.

- From the results of energy and exergy analysis of the different configurations of water-LiBr absorption cycles an increase in COP is observed from half (0.458) to triple effect (2.32) cycles. However, the increase in exergetic efficiency from effect to effect is not as pronounced as the COP which varies from 0.359 (half effect) to 0.473 (triple effect cycle). The results show that the maximum COP and the exergetic efficiencies are near to the minimum feasible generator temperature (cut-off temperature). As the generator temperature increases COP decrease slowly however, exergetic efficiencies decrease drastically. In all cycles, the effect of the heat source temperature on the exergy destruction rates is similar for the same type of components.

- Results of the structural analysis confirm that, it is more important to improve the efficiency of units with high $\triangle T_{min}$ (or low $UA - values$)

UNIVERSITAT ROVIRA I VIRGILI
OPTIMIZATION OF ENVIRONMENTALLY FRIENDLY SOLAR ASSISTED ABSORPTION COOLING SYSTEMS
Berhane Hagos Gebreslassie
ISBN: 978-84-693-7673-7/DL:T-1752-2010

rather than units which already operate with low $\triangle T_{min}$ (or high $UA-values$). The unit with highest value of the CSB is the refrigerant heat exchanger. The CSB's of the refrigerant heat exchanger, the evaporator, the condenser, the generator and the absorber are higher than one and therefore, an improvement of these units will improve the cycle performance. The dephlegmator shows a different behaviour due to its strong interactions with the rest of the cycle. Differences between the cycle configurations are generally small. However, the optimum values of the efficiency of each component depend also on the energy cost and the capital investment and the annual operation time.

- Using the thermoeconomic optimization based on structural method an equation is formulated that enables to estimate the optimal heat exchanger area. This optimal area leads to minimum total cost and the equation is generally valid for thermal systems (*i.e.*, not limited to absorption cycles). The optimum result agrees very well with the one obtained from the integrated optimization algorithm of Engineering Equation Solver (EES). In particular for a high operation cost (i.e, if the operation time is high, 6000 h/year) the error between the proposed equation and the numerical optimum is only 1.1 %. If the operation time is less (2000 h/year) the results show about 3 % error. Because of its easy application the proposed equation is useful at the design stage of the thermal system.

- A bi-criteria nonlinear programming optimization problem that integrates the environmental performance based on Eco-indicator 99 and the total cost of an ammonia-water absorption cycle is developed. The results reveal that a reduction by 5.5 % environmental impact (*i.e.*, relative to the minimum total cost design) caused by the cycle can be attained if the decision maker is willing to compromise the economic performance of the system. These reductions are achieved by decreasing the energy consumption, which on the other hand requires an increase in the total cost of the cycle.

UNIVERSITAT ROVIRA I VIRGILI
OPTIMIZATION OF ENVIRONMENTALLY FRIENDLY SOLAR ASSISTED ABSORPTION COOLING SYSTEMS
Berhane Hagos Gebreslassie
ISBN: 978-84-693-7673-7/DL:T-1752-2010

- The solar assisted absorption cooling system formulation and solution approach is illustrated through a case study. A significant reduction in the environmental impact (70.5 %) can be achieved if the decision-maker is willing to invest on the solar collector's subsystem. These reductions can be attained by increasing the number of collectors installed, which increases the solar fraction of the cooling system. It has also been shown that the type of collector selected depends on the particular operating conditions and weather data considered in the analysis. For Barcelona weather data the results show that the Sydney type evacuated tube collector is selected for all Pareto alternatives. However, for Tarragona weather data flat plates collectors are selected in higher environmental impact Pareto alternative designs.

- Even though, the results of the optimization problem shows that technically reducing the global warming potential is viable at the current energy prices and without considering governmental subsidies on solar technologies, the use of solar energy in cooling applications is not profitable. The method presented in this study is aimed in facilitating the task of policy makers when deciding on the tax rates to promote more sustainable technological alternatives. For example the case study results reveal that if the GHG emissions tax rate is increased beyond 58 $€/tonCO_{2-eq}$, and the fuel cost beyond 0.0635 $€/kWh$ the solar assisted absorption cycles are not only attractive in environmental performance but also economically becomes attractive.

UNIVERSITAT ROVIRA I VIRGILI
OPTIMIZATION OF ENVIRONMENTALLY FRIENDLY SOLAR ASSISTED ABSORPTION COOLING SYSTEMS
Berhane Hagos Gebreslassie
ISBN: 978-84-693-7673-7/DL:T-1752-2010

Future works

- The absorption cycle model in GAMS can be modified to include the detail distillation column models, different type of heat exchangers, and $H_20 - LiBr$ absorption cycles.
- The exergy and thermoeconomic analysis of the system could be integrated in the GAMS model and used in the optimization.
- The solar assisted absorption cooling system assumes a steady state for each month of the year. However, this could be improved to hourly steady state operation. In this case the use of thermal storages could improve the performance of the solar assisted absorption cycle. Therefore, at this stage the model could be modified in order to include the thermal storages. Moreover, the monthly cooling load was assumed as constant parameter for the whole time horizon but this could be modified to monthly/hourly cooling load.
- The uncertainty of the energy price is considered in the design of an absorption cycle. This could be extended to the solar assisted absorption cooling system. The uncertainties in the environmental metrics, design parameters, cooling demand, and weather data can be included following the same procedures.
- The collector type and the number of collectors are determined based on the collector performance equations and the module area. However, the arrangement of the collectors is not studied. Therefore, the model could be extended considering possible configurations.

UNIVERSITAT ROVIRA I VIRGILI
OPTIMIZATION OF ENVIRONMENTALLY FRIENDLY SOLAR ASSISTED ABSORPTION COOLING SYSTEMS
Berhane Hagos Gebreslassie
ISBN: 978-84-693-7673-7/DL:T-1752-2010

Nomenclature

Abbreviations

AC	Air conditioning
CFC	Chlorofluorocarbon
CPC	Compound parabolic collector
CSB	Coefficients of structural bonds
ETC	Evacuated tube collector
FPC	Flat plate collector
GHG	Greenhouse gas emissions
GWP	Global warming potential
$HCFC$	Hydro chlorofluorocarbon
$IPCC$	Intergovernmental Panel on Climate Change
LCA	Life cycle assessment
LP	Linear programming problem
$MINLP$	Mixed integer nonlinear programming problem
NLP	Nonlinear programming problem
$RMINLP$	Relaxed mixed integer nonlinear programming problem

Variables and parameters

UA	Thermal conductance [kW/K]
$\triangle T_{min}$	Heat exchanger minimum temperature difference (K)
$ECO99$	Eco-indicator 99 [points]
COP	Coefficient of performance [-]
$\dot{I}_k$	Irreversibility rate of unit k [kW]

UNIVERSITAT ROVIRA I VIRGILI
OPTIMIZATION OF ENVIRONMENTALLY FRIENDLY SOLAR ASSISTED ABSORPTION COOLING SYSTEMS
Berhane Hagos Gebreslassie
ISBN: 978-84-693-7673-7/DL:T-1752-2010

$\dot{I}_t$	Total irreversibility rate of the cooling system [kW]
x	Set of design variables

Subscripts

k	Unit (equipment) of the cooling system
t	The whole cooling system

UNIVERSITAT ROVIRA I VIRGILI
OPTIMIZATION OF ENVIRONMENTALLY FRIENDLY SOLAR ASSISTED ABSORPTION COOLING SYSTEMS
Berhane Hagos Gebreslassie
ISBN: 978-84-693-7673-7/DL:T-1752-2010

References

UNIVERSITAT ROVIRA I VIRGILI
OPTIMIZATION OF ENVIRONMENTALLY FRIENDLY SOLAR ASSISTED ABSORPTION COOLING SYSTEMS
Berhane Hagos Gebreslassie
ISBN: 978-84-693-7673-7/DL:T-1752-2010

References

[1] Gebreslassie BH, Medrano M, Boer D. Exergy analysis of multi-effect water-libr absorption systems: From half to triple effect. Renewable Energy 2010;35(8):1773 –82.

[2] Boer D, Gebreslassie BH, Medrano M, Miquel N. Effect of internal heat recovery in ammonia-water absorption cooling cycles: Exergy and structural analysis. International Journal of Thermodynamics 2009;12:17–27.

[3] Gebreslassie BH, Medrano M, Mendes F, Boer D. Optimum heat exchanger area estimation using coefficients of structural bonds: Application to an absorption chiller. International Journal of Refrigeration 2010;33:529–37.

[4] Gebreslassie BH, Guillén-Gosálbez G, Jiménez L, Boer D. Design of environmentally conscious absorption cooling systems via multi-objective optimization and life cycle assessment. Applied Energy 2009;86:1712–22.

[5] Gebreslassie BH, Guillén-Gosálbez G, Jiménez L, Boer D. Economic performance optimization of an absorption cooling system under uncertainity. Applied Thermal Engineering 2009;29:3491–500.

[6] Gebreslassie BH, Guillén-Gosálbez G, Jiménez L, Boer D. A systematic tool for the minimization of the life cycle impact of solar assisted absorption cooling systems. Energy 2010;DOI: 10.1016/j.energy.2010.05.039.

[7] Gebreslassie BH, Guillén-Gosálbez G, Jiménez L, Boer D. Solar assisted absorption cooling cycles for reduction of global warming: a multi-

ISBN: 978-84-693-7673-7/DL:T-1752-2010

objective optimization approach. Renewable Energy 2010;Under revision .

[8] Cai YP, Huang GH, Yang ZF, Tan Q. Identification of optimal strategies for energy management systems planning under multiple uncertainties. Applied Energy 2009;86(4):480–95.

[9] Lin QG, Huang GH, Bass B, Qin XS. Iftem: An interval-fuzzy two-stage stochastic optimization model for regional energy systems planning under uncertainty. Energy Policy 2009;37:868–78.

[10] Commission of the European Communities C. Towards a european strategy for the security of energy supply. Tech. Rep.; 2000.

[11] Casals XG. Solar absorption cooling in spain: Perspectives and outcomes from the simulation of recent instalations. Renewable Energy 2006;31:1371–89.

[12] Balaras CA, Grossman G, Henning HM, Ferreira CAI, Podesser E, Wang L, et al. Solar air conditioning in Europe–an overview. Renewable and Sustainable Energy Reviews 2007;2:299 – 314.

[13] Henning HM. Solar assisted air conditioning of buildings - an overview. Applied Thermal Engineering 2007;27:1734–49.

[14] Rosiek S, Batlles FJ. Integration of the solar thermal energy in the construction: Analysis of the solar-assisted air-conditioning system installed in ciesol building. Renewable Energy 2009;34:1423–31.

[15] Doukas H, Patlitzianas KD, Kagiannas AG, Psarras J. Renewable energy sources and rationale use of energy development in the countries of *GCC*: Myth or reality? Renewable Energy 2006;34:755–70.

[16] Jaruwongwittaya T, Chen G. A review: Renewable energy with absorption chillers in thailand. Renewable and Sustainable Energy Reviews 2009;14:1437–44.

[17] Dorgan CB, Leight SP, Dorgan CE. Application guide for absorption cooling/refrigeration using recovered heat. 1995.

[18] Misra RD, Sahoo PK, Sahoo S, Gupta A. Thermoeconomic otimization of a single effect water/libr vapour absorption refrigeration system. International Journal of Refrigeration 2003;26(2):158–69.

[19] Misra RD, Sahoo PK, Gupta A. Thermoeconomic evaluation and optimization of a double-effect h 2o/libr vapour-absorption refrigeration system. International Journal of Refrigeration 2005;28(3):331–43.

[20] Misra R, Sahoo P, Gupta A. Thermoeconomic evaluation and optimization of an aqua-ammonia vapour-absorption refrigeration system. International Journal of Refrigeration 2006;29(1):47–59.

[21] Dingeç H, Ileri A. Thermoeconomic optimization of simple refrigerators. International Journal of Energy Research 1999;23(11):949–62.

[22] Dentice M, Vanoli L. Thermoeconomic optimisation of the condenser in a vapour compression heat pump. International Journal of Refrigeration 2004;27(4):433–41.

[23] Selbas R, Kizilkan Ö, Sencan A. Thermoeconomic optimization of subcooled and superheated vapor compression refrigeration cycle. Energy 2006;31:2108–28.

[24] Kizilkan Ö, Sencan A, Kalogirou SA. Thermoeconomic optimization of a libr absorption refrigeration system. Chemical Engineering and Processing: Process Intensification 2007;46(12):1376–84.

[25] Chavez-Islas LM, Heard CL. Design and analysis of an ammonia-water absorption refrigeration cycle by means of an equation-oriented method. Industrial & Engineering Chemistry Research 2009;48(4):1944–56.

[26] Chavez-Islas LM, Heard CL. Optimization of a simple ammonia-water absorption refrigeration cycle by application of mixed-integer nonlinear programming. Industrial & Engineering Chemistry Research 2009;48(4):1957–72.

[27] Chavez-Islas LM, Heard CL, Grossmann IE. Synthesis and optimization of an ammonia-water absorption refrigeration cycle considering different types of heat exchangers by application of mixed-integer nonlinear programming. Industrial & Engineering Chemistry Research 2009;48(6):2972–90.

[28] Kotas TJ. The exergy method of thermal plant analysis. Krieger Publishing Company; 1995.

[29] Bejan A, Tsatsaronis G, Moran M. Thermal Design & Optimization. John Wiley & Sons Inc.; 1996.

[30] Edgar TF, Himmelblau DM, Lasdon LS. Optimization of chemical processes. McGraw-Hill; 2001.

[31] Anand DK, Lindler KW, Schweitzer S, Kennish WJ. Second law analysis of solar powered absorption cooling cycles and systems. Journal of Solar Energy Engineering, Transactions of the ASME 1984;106(3):291–8.

[32] Koehler WJ, Ibele WE, Soltes J, Winter ER. Availability simulation of a lithium bromide absorption heat pump. Heat Recovery Systems and CHP 1988;8(2):157–71.

[33] Aphornratana S, Eames I. Thermodynamic analysis of absorption refrigeration cycles using the second law of thermodynamics method. International Journal of Refrigeration 1994;18(4):244–52.

[34] Talbi M, Agnew B. Exergy analysis: An absorption refrigerator using lithium bromide and water as the working fluids. Applied Thermal Engineering 2000;20:619–30.

[35] Kilic M, Kaynakli O. Second law-based thermodynamic analysis of water-lithium bromide absorption refrigeration system. Energy 2007;32(8):1505–12.

ISBN: 978-84-693-7673-7/DL:T-1752-2010

[36] Ataer E, Gögüs Y. Comparative study of irreversibilities in an aqua-ammonia absorption refrigeration system. International Journal of Refrigeration 1991;14(2):86–92.

[37] Best R, Islas J, Martínez M. Exergy efficiency of an ammonia-water absorption system for ice production. Applied Energy 1993;45:241–56.

[38] Grossman G, Wilk M, De Vault RC. Simulation and performance analysis of triple-effect absorption cycles. ASHRAE Transactions 1994 1994;100(1):452–62.

[39] Lee SF, Sherif S. Second-law analysis of multi-effect lithium bromide/water absorption chillers. In: ASHRAE Transactions; vol. 105. 1999,.

[40] Morosuk T, Tsatsaronis G. A new approach to the exergy analysis of absorption refrigeration machines. Energy 2008;33(6):890–907.

[41] Beyer J. Strukturuntersuchungen-notwendiger bestandteil der effektivitä tsanalyse von waermeverbrauchersystemen. Energieanwendung 1970;19(12):358–61.

[42] Beyer J. Struktur waermetechnischer systeme und oekonomische optimierung der systemparameter. Energieanwendung 1974;23(9):274–9.

[43] Boer D, Medrano M, Nogués M. Exergy and structural analysis of an absorption cooling cycle and the effect of efficiency parameters. International Journal of Thermodynamics 2005;8(4):191–8.

[44] Brooke A, Kendrik D, Meeraus A, Raman R, Rosenthal RE. GAMS - A User's Guide. GAMS Development Corporation, Washington; 1998.

[45] F-Chart Software . Engineering Equation Solver, (EES). www.fchart.com 2008.

[46] Chemical Engineering . Chemical Engineering Plant Cost Index (CEPCI). Tech. Rep. 2009.

ISBN: 978-84-693-7673-7/DL:T-1752-2010

[47] Guillén-Gosálbez G, Grossmann IE. A global optimization strategy for the environmentally conscious design of chemical supply chains under uncertainty in the damage assessment model. Computers & Chemical Engineering 2010;34(1):42–58.

[48] Hugo A, Ciumei C, Buxton A, Pistikopoulos EN. Environmental impact minimization through material substitution: a multi-objective optimization approach. Green Chemistry 2004;6:407–17.

[49] Azapagic A. Life cycle assessment and its application to process selection, design and optimisation. Chemical Engineering Journal 1999;73:1–21.

[50] PRé-Consultants . The eco-indicator 99, a damage oriented method for life cycle impact assessment. methodology report and manual for designers. Tech. Rep.; PRé Consultants, Amersfoort, The Netherlands; 2000.

[51] PRé-Consultants . SimaPro 7 LCA software. The Netherlands (www.pre.nl/simapro/default.htm); 2008.

[52] Metz B, Davidson O, Bosch P, Dave R, Meyer L. IPCC, 2007: Summary for Policymakers. In: Climate Change 2007: Mitigation. Contribution of Working Group III to the Fourth Assessment Report of the International Panel on Climate Change. Cambridge University Press, Cambridge, United Kingdom and Newyork, NY, USA.; 2007.

[53] IRAM-ISO 14040 . Environmental management-Life cycle assessment-Principles and frame work. 2006.

[54] Tveit TM, Savola T, Gebremedhin A, Fogelholm CJ. Multi-period $MINLP$ model for optimising operation and structural changes to CHP plants in district heating networks with long-term thermal storage. Energy Conversion and Management 2009;50:639–47.

ISBN: 978-84-693-7673-7/DL:T-1752-2010

[55] Savola T, Fogelholm CJ. $MINLP$ optimisation model for increased power production in small-scale CHP plants. Applied Thermal Engineering 2007;27(1):89–99.

[56] Wang J, Dai Y, Gao L. Parametric analysis and optimization for a combined power and refrigeration cycle. Applied Energy 2008;85(11):1071–85.

[57] Zhao Y, Shigang Z, Haibe Z. Optimization study of combined refrigeration cycles driven by an engine. Applied Energy 2003;76(4):379 –89.

[58] Sahinidis NV. Optimization under uncertainty: state-of-the-art and opportunities. Computers & Chemical Engineering 2004;28(6-7):971–83.

[59] Subrahmanyam S, Pekny JF, Reklaitis GV. Design of batch chemical plants under market uncertainty. Industrial & Engineering Chemistry Research 1994;33(11):2688–701.

[60] Pistikopoulos EN. Uncertainty in process design and operations. Computers & Chemical Engineering 1995;19(Supplement 1):553–63.

[61] Lahdelma R, Makkonen S, Salminen P. Two ways to handle dependent uncertainties in multi-criteria decision problems. Omega 2009;37(1):79–92.

[62] Durbach IN, Stewart TJ. Using expected values to simplify decision making under uncertainty. Omega 2009;37(2):312–30.

[63] Azaron A, Brown KN, Tarim SA, Modarres M. A multi-objective stochastic programming approach for supply chain design considering risk. International Journal of Production Economics 2008;116:129–38.

[64] Guillen G, Mele FD, Bagajewicz MJ, Espuña A, Puigjaner L. Multi-objective supply chain design under uncertainty. Chemical Engineering Science 2005;60(6):1535–53.

ISBN: 978-84-693-7673-7/DL:T-1752-2010

[65] Barbaro A, Bagajewicz MJ. Managing financial risk in planning under uncertainty. Aiche Journal 2004;50(5):963–89.

[66] Gupta A, Maranas CD. Managing demand uncertainty in supply chain planning. Computers & Chemical Engineering 2003;27(8-9):1219–27.

[67] Mavrotas G, Demertzis H, Meintani A, Diakoulaki D. Energy planning in buildings under uncertainty in fuel costs: The case of a hotel unit in greece. Energy Conversion and Management 2003;44(8):1303–21.

[68] Sadeghi M, Mirshojaeian Hosseini H. Energy supply planning in iran by using fuzzy linear programming approach (regarding uncertainties of investment costs). Energy Policy 2006;34(9):993–1003.

[69] Yokoyama R, Ito K. Optimal design of energy supply systems based on relative robustness criterion. Energy Conversion and Management 2002;43(4):499–514.

[70] Petkov SB, Maranas CD. Design of multiproduct batch plants under demand uncertainty with staged capacity expansions. Computers & Chemical Engineering 1998;22:S789–92.

UNIVERSITAT ROVIRA I VIRGILI
OPTIMIZATION OF ENVIRONMENTALLY FRIENDLY SOLAR ASSISTED ABSORPTION COOLING SYSTEMS
Berhane Hagos Gebreslassie
ISBN: 978-84-693-7673-7/DL:T-1752-2010

Appendix A

Appendices

A.1 List of publications

five published, one accepted and one under revision

1. **B. H. Gebreslassie**, M. Medrano, and D. Boer. Exergy analysis of multi-effect water-LiBr absorption systems: From half to triple effect. *Renewable Energy*, 35(8):1773-1782 , 2010.

2. D. Boer, **B. H. Gebreslassie**, M. Medrano, M. Nogues. Effect of internal Heat Recovery in Ammonia-Water Absorption Cooling Cycles: Exergy and structural Analysis. *International Journal of Thermodynamics*, 12(1):17–27, 2009.

3. **B. H. Gebreslassie**, M. Medrano, L.F. Mendes and D. Boer. Thermoeconomic Optimization of Absorption Cooling Cycle Using Structural Coefficient. *International Journal of Refrigeration*, 33(3):529-537, 2010.

4. **B. H. Gebreslassie**, G. Guillen-Gosalbez, L. Jimenez, D. Boer. Design of environmentally conscious absorption cool-

UNIVERSITAT ROVIRA I VIRGILI
OPTIMIZATION OF ENVIRONMENTALLY FRIENDLY SOLAR ASSISTED ABSORPTION COOLING SYSTEMS
Berhane Hagos Gebreslassie
ISBN: 978-84-693-7673-7/DL:T-1752-2010

ing systems via multi-objective optimization and life cycle assessment. *Applied Energy*, 86(9):1712-1722, 2009.

5. **B. H. Gebreslassie**, G. Guillen-Gosalbez, L. Jimenez, D. Boer. Economic performance optimization of an absorption cooling system under uncertainty. *Applied Thermal Engineering*, 29(17-18):3491-3500, 2009.

6. **B. H. Gebreslassie**, G. Guillen-Gosalbez, L. Jimenez, D. Boer. A systematic tool for the minimization of the life cycle impact of solar assisted absorption cooling systems. *Energy*, DOI: 10.1016/j.energy.2010.05.039, 2010.

7. **B. H. Gebreslassie**, G. Guillen-Gosalbez, L. Jimenez, D. Boer. Solar assisted absorption cooling cycles for reduction of global warming: a multi-objective optimization approach. *Submitted to Renewable Energy*, 2010.

A.2 Congress contributions

1. **B. H. Gebreslassie**, M. Jimenez, G. Guillen-Gosalbez, L. Jimenez, D. Boer. Multi-objective optimization of solar assisted absorption cooling system. 20^{th} *European Symposium on Computer Aided Chemical Engineering (ESCAPE20) Ischia, Italy*, June 2010.

2. **B. H. Gebreslassie**, G. Guillen-Gosalbez, L. Jimenez, D. Boer. Optimization of the Economic and Environmental Performance of an Ammonia-Water Absorption Cooling Cycle. *2009 AIChE Annual Meeting. Nashville, TN*

ISBN: 978-84-693-7673-7/DL:T-1752-2010

(USA), November 2009.

3. **B. H. Gebreslassie**, G. Guillen-Gosalbez, L. Jimenez, Dieter Boer,. Optimización económica de sistemas de refrigeración por absorción considerando el impacto medioambiental y la incertidumbre de los parámetros. *VI Jornadas de Ingenier Termodinamica, Cordoba (Spain)*, 2009.

4. **B. H. Gebreslassie**, G. Guillen-Gosalbez, L. Jimenez, D. Boer. Design of environmentally friendly absorption cooling systems via multi-objective optimization. *ESCAPE 19 Cracow, Poland*, June 2009.

5. **B. H. Gebreslassie**, G. Guillen-Gosalbez, L. Jimenez, D. Boer. A systematic method for the environmentally conscious design of absorption cooling cycles. 11^{th} *Mediterranean Congress of Chemical Engineering, Barcelona (SPAIN)*, 2008.

6. G. Guillen-Gosalbez, F.D. Mele, **B. H. Gebreslassie**, L. Jimenez. Strategic planning of supply chains for biofuels production via multi-objective optimization and life cycle assessment. 11^{th} *Mediterranean Congress of Chemical Engineering, Barcelona (SPAIN)*, 2008.

7. Mendes L.F, J.P. Cardoso, A.Mortal, Boer, D, **B.H. Gebreslassie**, M. Medrano. Thermoeconomic optimization of a solar absorption cooling system. *Solar Air Conditioning* 2^{nd} *International Conference of Solar Air-Conditioning. Tarragona (Spain)*, Pages: 172-177, 2007.

UNIVERSITAT ROVIRA I VIRGILI
OPTIMIZATION OF ENVIRONMENTALLY FRIENDLY SOLAR ASSISTED ABSORPTION COOLING SYSTEMS
Berhane Hagos Gebreslassie
ISBN: 978-84-693-7673-7/DL:T-1752-2010

8. Mendes L.F, J.P. Cardoso, A.Mortal, Boer, D, **B. H. Gebreslassie**, M. Medrano. Exergy analysis of a solar absorption cooling system". Presentation of a communication. 2^{nd} *International Conference of Solar Air-Conditioning. Tarragona (Spain)*, Pages :166-171, 2007.

A.3 Book chapters

1. **B. H. Gebreslassie**, M. Jimenez, G. Guillen-Gosalbez, L. Jimenez, D. Boer. Multi-objective optimization of solar assisted absorption cooling system. *Computer Aided Chemical Engineering* , Elsevier, Vol. 28: 1033-1038, ISBN: 978-0-444-53569-6, 2010.

2. **B. H. Gebreslassie**, G. Guillen-Gosalbez, L. Jimenez, D. Boer. Design of environmentally friendly absorption cooling systems via multi-objective optimization. *Computer Aided Chemical Engineering*, Elsevier, Vol. 26: 1099-1103, ISBN: 978-0-444-53441-5, 2009.

Renewable Energy 35 (2010) 1773–1782

Contents lists available at ScienceDirect

Renewable Energy

journal homepage: www.elsevier.com/locate/renene

Exergy analysis of multi-effect water–LiBr absorption systems: From half to triple effect

Berhane H. Gebreslassie [a], Marc Medrano [b], Dieter Boer [a,*]

[a] Departament d'Enginyeria Mecànica, Universitat Rovira i Virgili, Av. Països Catalans 26, 43007 Tarragona, Spain
[b] GREA Innovació Concurrent, Edifici CREA, Universitat de Lleida, Pere de Cabrera s/n, 25001 Lleida, Spain

ARTICLE INFO

Article history:
Received 3 September 2009
Accepted 8 January 2010
Available online 8 February 2010

Keywords:
Absorption cycle
Water–Lithium bromide
Exergy analysis
Double effect
Triple effect
Half effect

ABSTRACT

An exergy analysis, which only considers the unavoidable exergy destruction, is conducted for single, double, triple and half effect Water–Lithium bromide absorption cycles. Thus, the obtained performances represent the maximum achievable performance under the given operation conditions.

The coefficient of performance (COP), the exergetic efficiencies and the exergy destruction rates are determined and the effect of the heat source temperature is evaluated. As expected, the COP increases significantly from double lift to triple effect cycles. The exergetic efficiency varies less among the different configurations. In all cycles the effect of the heat source temperature on the exergy destruction rates is similar for the same type of components, while the quantitative contributions depend on cycle type and flow configuration. Largest exergy destruction occurs in the absorbers and generators, especially at higher heat source temperatures.

1. Introduction

The thermal refrigeration or thermally activated refrigeration, is based on the use of a heat driven absorption unit [1]. In this cooling system the energy input to the generator can be heat from renewable energies such as solar thermal energy and biomass (Fig. 1). Depending on the available temperature level different cycle configurations can be used. These cycles are generally evaluated in terms of their Coefficient of Performance (COP). Compression cycles have significant higher COP's than absorption cycles. Among the absorption cycles, multi-stage cycles have higher COP's than the basic configuration, but need higher driving heat temperatures. Best energetic efficiency is obtained by triple effect configurations, followed by double effect and single effect. For very low heat input temperatures the half effect (also called double lift) configuration can be applied, but it presents the lowest COP.

This change in driving temperature and thus quality of the input energy is not taken into account by the COP, but it is considered in the exergy analysis [2–4]. Using exergy efficiencies we can compare on a rational basis cycles with different types of energy input, in form of heat at different temperature levels or work. The exergy analysis of absorption cycles started in the eighties with publications describing the methodology and the evaluation of the exergy destruction rates and exergy efficiencies [5–7]. Studies focussing on the effect of operation temperatures and heat exchangers effectiveness has been done for single effect cycles with both the water–LiBr [8–10] or the ammonia-water working pair [11,12]. The working pairs have also been directly compared [5,13]. Anand et al. [5] considered the influence of the effectiveness of the heat exchangers on the cycle, and found the highest increase of the exergetic efficiency by improving solution and refrigerant heat exchangers. Koehler et al. [6] reported for a water–LiBr cycle a large effect of the solution heat exchanger, while the refrigerant heat exchanger was less important. They also stated a high interdependence between various components. Meunier et al. [14] compared for different sorption systems, namely, adsorption, chemical reaction and liquid absorption heat pumps, the main contributions to entropy generation.

Besides the single effect configuration different authors determined also for double effect [5,15–20] and triple effect cycles [16] exergy destruction rates and exergetic efficiencies. Jeong et al. [21] used the exergy analysis to obtain an optimum design for an absorption cycle. Sencan et al. [22] evaluated for a water–LiBr single effect cycle the effect of the operating conditions on COP and exergetic efficiency and discussed the main factors which cause the exergy destruction in absorption systems.

Results of the different studies are often difficult to compare and differ in the conclusions obtained, especially if different cycle configurations are analyzed. Basically this is due to the different methodologies and assumptions considered in each analysis. An

* Corresponding author. Fax: +34 977559691.
E-mail address: Dieter.Boer@urv.net (D. Boer).

0960-1481/$ – see front matter © 2010 Elsevier Ltd. All rights reserved.
doi:10.1016/j.renene.2010.01.009

Nomenclature

COP	Coefficient of performance [–]
e_{ph}	Specific physical exergy [kJ/kg]
h	Specific enthalpy [kJ/kg]
$\dot{E}_D$	Exergy destruction rate [kW]
$\dot{E}_F$	Exergy input (Fuel F) [kW]
$\dot{E}_P$	Exergy output (Product P) [kW]
$\dot{m}$	Mass flow rate [kJ/s]
P	Pressure [kPa]
$\dot{Q}$	Heat transfer rate [kW]
s	Specific entropy [kJ/kg K]
T	Temperature [°C or K]
$\dot{W}_{pump}$	Mechanical power of the pump [kW]
x	Mass concentration of Lithium bromide [%]
UA	Product of overall heat transfer coefficient and heat exchanger area [kW/K]

Greek symbols

Ψ	Exergetic efficiency [–]
τ	Dimensionless exergetic temperature [–]

Subscripts

e	exit
h	high
i	inlet
k	component
l	low
m	middle
0	thermodynamic environment

Abbreviations

A	Absorber
C	Condenser
CG	Condenser-Generator
DS	Double effect series flow
DP	Double effect parallel flow
DR	Double effect reverse flow
E	Evaporator
G	Generator
H	Half effect
HE	Solution heat exchanger
LiBr	Lithium bromide
S	Single effect
TS	Triple effect series flow
TP	Triple effect parallel flow

approach comparing three different cycles has been proposed by [16]. Their study evaluates for a single, a double and a triple effect cycle COP's and exergetic efficiencies for given UA value of the components. The results obtained are valid for these designs, but may change for other design specifications.

Indeed, in the former analysis the exergy destruction rates were always evaluated without distinguishing the avoidable and unavoidable part. Morosuk and Tsatsaronis [23] proposed splitting the exergy destruction into endogenous/exogenous and unavoidable/avoidable parts, in order to facilitate the understanding and the improvement of the considered systems. The exergy destruction rate, which cannot be further reduced by design improvements, represents the unavoidable part. The designer has to focus on the avoidable part, which represents the potential for improving. In thermoeconomic analysis its cost can be compared with the avoidable investment costs, and improvements can center on the most relevant components [24]. Parameters as the modified exergoeconomic factor based on the avoidable costs can be introduced [25].

The purpose of this paper is to compare different configurations of absorption cycles taking into account only the unavoidable exergy destruction. Thus, the results represent the maximum obtainable performance and are not affected by design specifications. The exergy analysis of seven different multi-stage absorption cycles (Table 1) has been achieved applying the same methodology and assumptions for all cycles. The exergetic efficiencies for the different cycles and exergy destruction rates in the main components depending on the heat source temperature have been obtained. Thus, the origin of the exergy destruction in the different cycles can be quantified and compared. The analysis will consider typical cooling conditions with fixed temperatures of the chilled water and cooling water, while the heat source temperature will be varied.

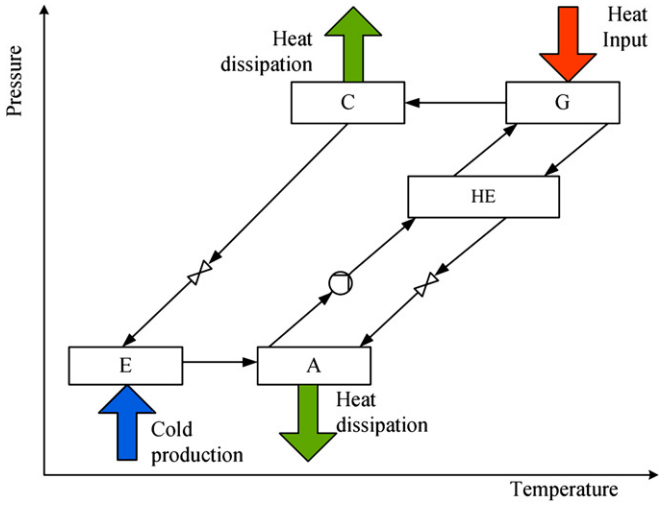

Fig. 1. Basic absorption cycle.

2. Description of the absorption cycle configurations

The operation and the configuration of absorption cycles already have been described in detail elsewhere [1]. Therefore, only the schematics of the different configurations will be presented (Figs. 2–8), starting with the basic single effect configuration. The cycles are presented in pressure–temperature diagrams. Based on the single effect cycle, more complicated cycles can be obtained in order to improve the energy efficiency or the achievable

Table 1
Considered multi-effect water–LiBr cycles.

Cycle	Abbreviations
Half effect	H
Single effect	S
Double effect series flow	DS
Double effect parallel flow	DP
Double effect reverse flow	DR
Triple effect series flow	TS
Triple effect parallel flow	TP

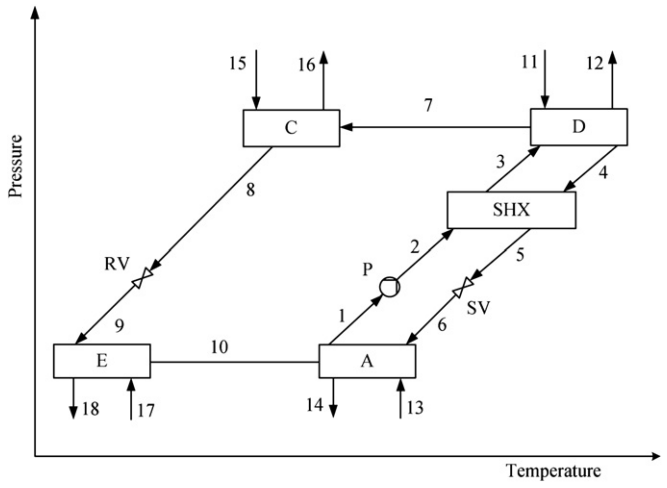

Fig. 2. Single effect absorption cycle.

temperature lift between evaporator and absorber [26]. The so-called double and triple-effect cycles obtain higher COP's than the single-effect cycle, but they need an energy supply at higher temperatures. The solution flow between absorber and generator can be achieved in series, parallel of reverse flow. Compared to the single-effect cycle in the double (Figs. 3–5) and triple effect (Figs. 6 and 7) cycles additional internal heat exchanges take place in the condenser-generator assemblies "CG". Here the heat released on the hot side of the heat exchanger (condenser) by the condensing vapor is producing more vapor in the solution on the cold side (generator). Thus the generation of refrigerant vapor is distributed among more generators.

The difference between series (Figs. 3–6), parallel (Figs. 4–7) and reverse flow (Fig. 5) is in the way the solution is distributed between the different generators. In the series flow it is directly pumped from the absorber "A" to the high temperature generator "G", while in the parallel flow it is distributed among the different generators ("G" and "CG"). In the reverse flow, the solution is first pre-concentrated in the lower generator "CG", before being pumped to the high temperature generator "G". These configurations achieve higher COP's than the single effect, but require a higher operation temperature in the high temperature generator "G".

The half effect (also called double-lift) cycle (Fig. 8) includes two solution circuits. Both of them include a generator and an absorber.

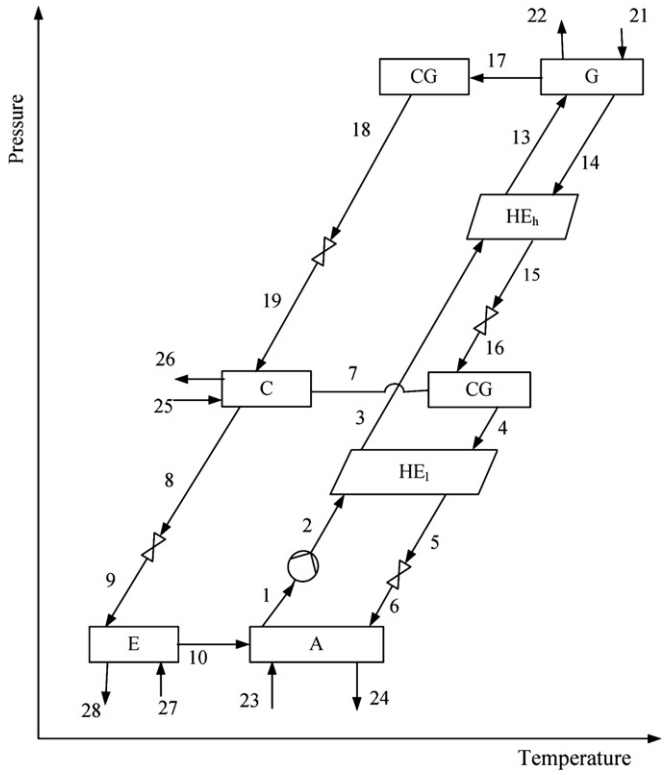

Fig. 3. Double effect series flow cycle.

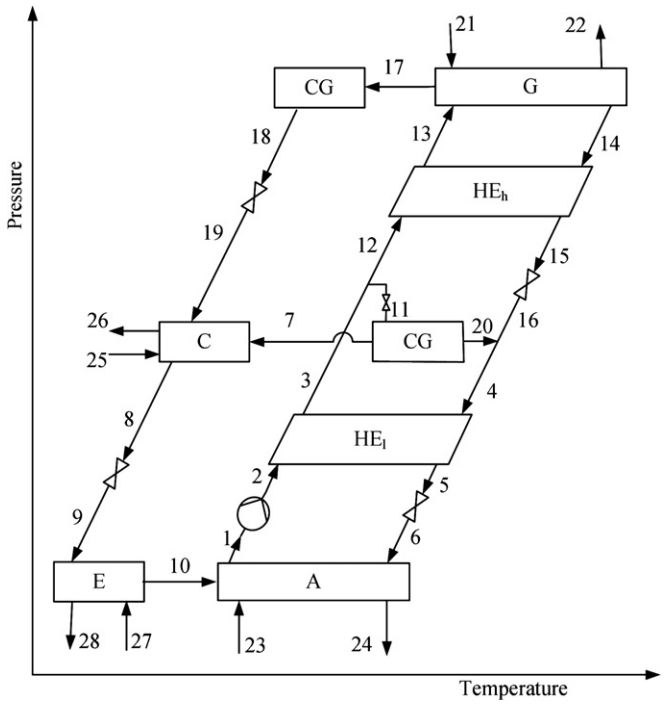

Fig. 4. Double effect parallel flow cycle.

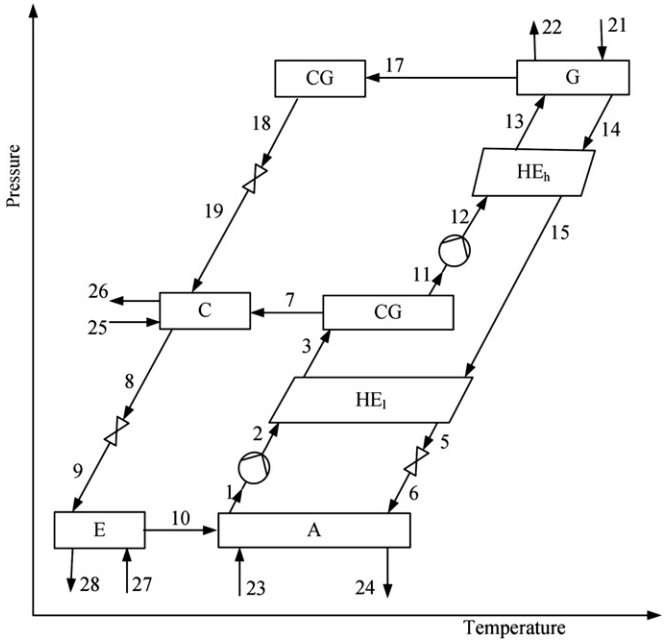

Fig. 5. Double effect reverse flow cycle.

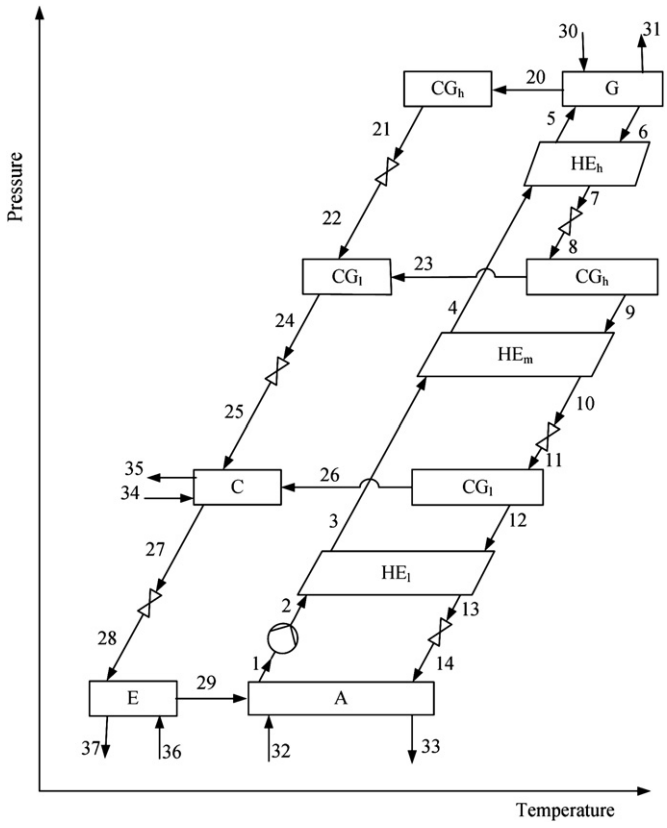

Fig. 6. Triple effect series flow cycle.

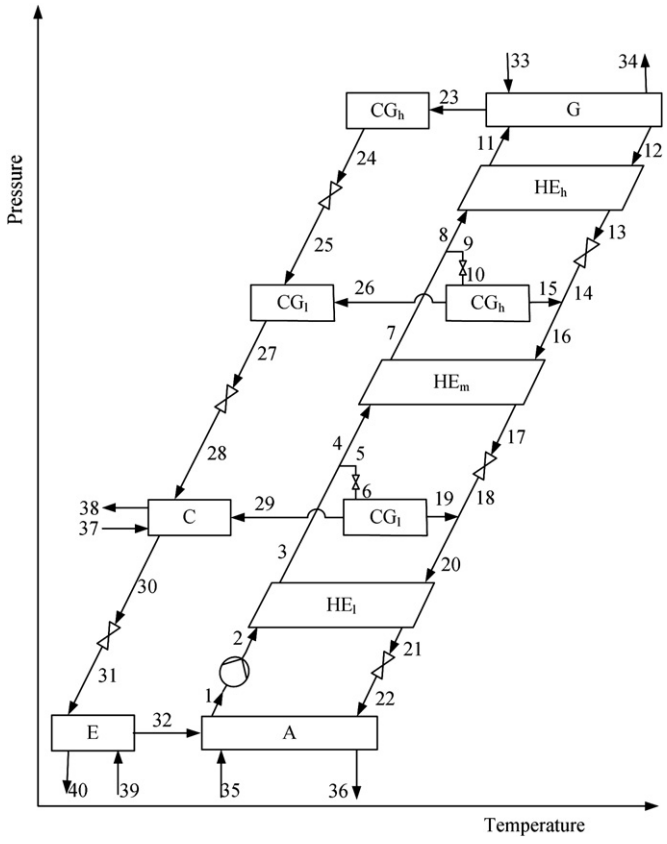

Fig. 7. Triple effect parallel flow cycle.

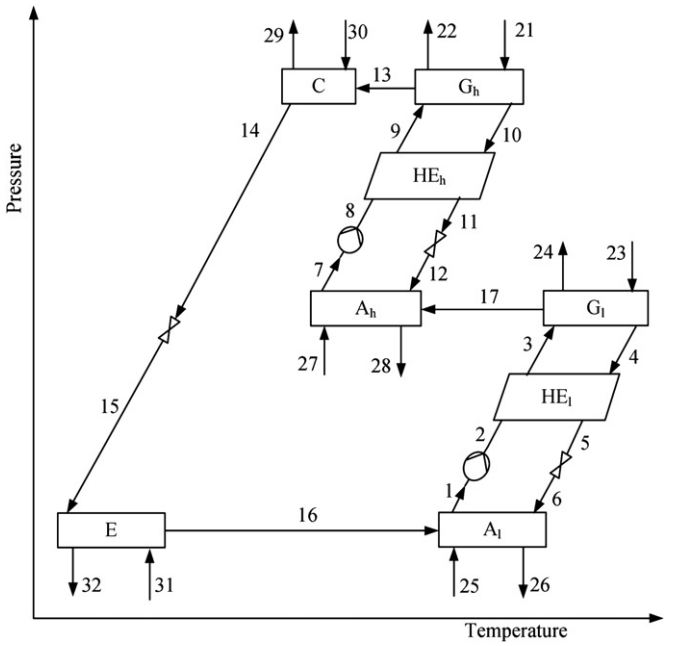

Fig. 8. Half effect cycle.

The vapor generated in the generator of the low pressure circuit "G_l" enters in the absorber of the high pressure circuit "$\boldsymbol{A}_h$". Heat is supplied at the same temperature to both generators and dissipated at an intermediate temperature in the condenser and the low and high absorber. This configuration can work at a considerably lower generator temperature, than the single-effect cycle, but at the cost of a lower COP.

3. Methodology of the simulation

A computer code for simulating the cycles has been established using the program Engineering Equation Solver [27]. Properties for water–LiBr have been evaluated by the correlations from [28]. These correlations are valid for temperatures up to 210 °C, as required in the triple effect cycles. Properties for all state point have been evaluated.

The input data, output data and main assumptions are presented below. For this study, typical cooling operating conditions have been chosen [29,30]. In order to consider only unavoidable irreversibilities the minimum temperature difference in the heat exchangers is fixed to a value of 0.2 K [23] and heat and pressure losses are not considered. The characteristic parameters are given in Table 2. The generator temperature is varied in the feasible range. The lowest temperature (cut-off temperature) corresponds to a concentration difference between the entering and leaving solution in one of the absorbers or generators of the cycle, which approaches zero and thus leads to very high solution flow rates. The

Table 2
Characteristic parameters.

Evaporator cooling capacity $\dot{Q}_E$	1000 kW
Temperatures	
Chilled water inlet/outlet (E)	11.7/7.2 °C
Cooling water inlet/outlet (parallel flow through A and C)	29.4 °C/32 °C
Minimum temperature difference in heat exchangers	0.2 K
Environmental temperature T_0	298 K
Environmental pressure p_0	100 kPa

upper generator temperature is limited by crystallization of the water–LiBr solution.

The following assumptions were made:

- Steady state.
- Heat losses are not considered.
- Pressure losses in pipes and components are not considered.
- Heat is supplied to the generators in the form of condensing steam, except for the half effect cycle, where it is hot water.
- The refrigerant leaving the condensers is saturated liquid.
- The refrigerant leaving the evaporator is saturated vapor.
- The solution and refrigerant valves are isenthalpic.
- The refrigerant vapor leaving the generators is at the mean temperature between incoming and leaving solution.

3.1. Mass, energy and entropy balances

Modeling includes first and second law analysis. Considering the assumptions made steady state mass (Eqs. 1 and 2), energy (Eq. (3)) and entropy balances (Eq. (4)) for each of the components k are established. The governing equations of mass and type of material conservation are:

$$0 = \Sigma \dot{m}_i - \Sigma \dot{m}_e \tag{1}$$

$$0 = \Sigma \dot{m}_i x_i - \Sigma \dot{m}_e x_e \tag{2}$$

where $\dot{m}$ is the mass flow rate and x is mass concentration of LiBr in the solution. Neglecting heat losses the first and second law of thermodynamics yield the energy and entropy balances of each component:

$$0 = \Sigma \dot{m}_i h_i - \Sigma \dot{m}_e h_e - \dot{W} \tag{3}$$

$$0 = \Sigma \dot{m}_i s_i - \Sigma \dot{m}_e s_e + \dot{S}_{\mathrm{gen,k}} \tag{4}$$

$\dot{S}_{\mathrm{gen,k}}$ represents the entropy generation in component k. The exergy destruction rate $\dot{E}_{\mathrm{D,k}}$ in component k results as

$$\dot{E}_{\mathrm{D,k}} = T_0 \dot{S}_{\mathrm{gen,k}} \tag{5}$$

The output data obtained are:

- The pressures, temperatures, concentrations, mass flow rates, enthalpies and entropies of each current.
- The heat rates or, in the case of the solution pump, the power and the exergy destruction rates of the components.

3.2. COP and exergetic efficiency

For the complete cycles the first and second law performances are evaluated in terms of the Coefficient of Performance (COP) and the exergetic efficiency ϵ. The COP is defined as the useful heat rate from the evaporator (the chilled water production) $\dot{Q}_{\mathrm{E}}$ divided by the required heat rate to the generator (the steam consumption) $\dot{Q}_{\mathrm{G}}$ (Eq. (6)).

$$\mathrm{COP} = \frac{\dot{Q}_{\mathrm{E}}}{\dot{Q}_{\mathrm{G}}} = \frac{[\dot{m}(h_e - h_i)]_{\text{chilled water}}}{[\dot{m}(h_i - h_e)]_{\text{steam/hot water}}} \tag{6}$$

The exergetic efficiency of a cycle Ψ is defined as the useful exergy output (Product P) $\dot{E}_{\mathrm{P}}$ divided by the required exergy input (Fuel F) $\dot{E}_{\mathrm{F}}$. The input is given by the reduction of the exergy rate of the steam in the generator and the pump power. The product is represented by the increase in the exergy rate of the chilled water (Eq. (7)).

Table 3
Comparison of operation conditions for single effect cycle.

	Ref. [29,30]	Present work	Error (%)
p_h [kPa]	5356	5401	0,84
p_l [kPa]	0,902	0,9007	0,14
$\dot{m}_7$ [kg/s]	0,01773	0,01769	0,23
$\dot{m}_4$ [kg/s]	0,4359	0,4743	8,81
$\dot{m}_1$ [kg/s]	0,4536	0,492	8,47
x_4 [%]	58,86	58,61	0,42
x_1 [%]	56,56	56,50	0,11
$x_4 - x_1$ [%]	2,30	2,11	8,26

$$\Psi = \frac{\dot{E}_{\mathrm{P}}}{\dot{E}_{\mathrm{F}}} = \frac{\left[\dot{m}\left(e_{\mathrm{ph},e} - e_{\mathrm{ph},i}\right)\right]_{\text{chilled water}}}{\left[\dot{m}\left(e_{\mathrm{ph},i} - e_{\mathrm{ph},e}\right)\right]_{\text{steam/hot water}} + \dot{W}_{\mathrm{pump}}} \tag{7}$$

The specific physical exergy e_{ph} of the water is evaluated in Eq. (8):

$$\mathrm{eph} = h - h_0 - T_0(s - s_0) \tag{8}$$

The terms h and s represent the enthalpy and entropy of the fluid, whereas, h_0 and s_0 are the enthalpy and entropy of the fluid at environmental temperature T_0 and pressure p_0. The specific exergy of the water–LiBr mixture has not to be evaluated, as we use entropy balances.

3.3. Error analysis

The programs for the cycles have been validated by comparison with available data from similar cycle simulations. A detailed comparison with [29] and [30] is presented for the single effect configuration. Their characteristic parameters have been integrated in our program in order to obtain the same UA values and cooling power. The operating conditions are compared in Table 3. The subscripts used refer to Fig. 2. The main difference is found in the evaluation of the concentration, resulting in a difference of 8% in the solution concentration difference. This results in a similar difference in the solution mass flow rates. This is due to different correlations used for the evaluation of properties. In our work properties for water–LiBr have been evaluated by the correlations from Kaita [28] which have the advantages to cover a larger temperature range. Table 4 shows the heat transfer rates and the COP. As can be observed the error in the final results is less than 1%. The same conclusions can be made for the other cycle configurations, as the type of calculations is basically the same as for the single effect.

4. Results and discussion

4.1. First law analysis

The further calculation have been achieved with the assumptions presented above, especially fixing for the heat exchangers the minimum temperature difference. Thermodynamics properties at each state points of some of the cycles are given in (Table 5–8). The

Table 4
Comparison of heat transfer rate and COP.

	Heat Transfer Rate [kW]		
	Ref. [29,30]	Present work	Error (%)
Absorber	56,29	56,74	0,80
Generater	44,18	44,00	0,41
Condenser	41,88	41,88	0,00
Evaporator	58,59	58,85	0,44
COP [–]	0,7148	0,7116	0,45

Table 5
Operating conditions of the single effect cycle.

State Point	T [°C]	p [kPa]	x [%]	$\dot{m}$ [kg/s]	h [kJ/kg]	s [kJ/kg K]
1	32.0	1.00	52.25	5.11	73.2	0.22
2	32.0	4.81	52.25	5.11	73.2	0.22
3	64.5	4.81	52.25	5.11	141.7	0.43
4	69.8	4.81	56.94	4.69	164.1	0.43
5	32.2	4.81	56.94	4.69	89.4	0.20
6	32.2	1.00	56.94	4.69	89.4	0.20
7	67.1	4.81		0.42	2626.0	8.61
8	32.2	4.81		0.42	134.9	0.47
9	7.0	1.00		0.42	134.9	0.48
10	7.0	1.00		0.42	2514.0	8.97
11	70.0	31.20		0.49	2626.0	7.75
12	70.0	31.20		0.49	293.1	0.96
13	29.4	101.00		101.40	123.3	0.43
14	32.0	101.00		101.40	134.2	0.46
15	29.4	101.00		96.36	123.3	0.43
16	32.0	101.00		96.36	134.2	0.46
17	11.7	101.00		52.96	49.3	0.18
18	7.2	101.00		52.96	30.4	0.11

tabulated values correspond approximately to the generator temperature which yields to the maximum COP. COP and exergetic efficiency are plotted versus the generator temperature in order to compare the different cycles. The results presented here differ from the literature [16], as only the unavoidable exergy destruction has been considered. Thus the lowest feasible generator temperatures are lower and the resulting COP's are higher. They represent the theoretically feasible maximum performance for the considered cycle configurations. Fig. 9 shows the variation of the COP for the different cycles with the generator temperature. As expected the COP increases from the half effect, to the single, double and triple effect. The maximum performance is achieved at generator temperatures close to the minimum feasible temperature, the cut-off temperature. The COP decreases for higher generator temperatures. The maximum generator temperature is limited by crystallization. For double and triple effect the parallel flow configuration shows slightly higher performance and higher achievable maximum generator temperature, although differences are very small.

Table 6
Operating conditions of double effect series flow cycle.

State Point	T [°C]	P [kPa]	x [%]	$\dot{m}$ [kg/s]	h [kJ/kg]	s [kJ/kg K]
1	32.0	1.00	52.25	4.75	73.1	0.22
2	32.0	32.30	52.25	4.75	73.2	0.22
3	64.8	32.30	52.25	4.75	142.3	0.44
4	70.6	4.81	57.32	4.33	167.0	0.43
5	32.2	4.81	57.32	4.33	91.1	0.19
6	32.2	1.00	57.32	4.33	91.1	0.19
7	67.8	4.81	0.00	0.19	2627.1	8.62
8	32.2	4.81	0.00	0.42	134.9	0.47
9	7.0	1.00	0.00	0.42	134.9	0.48
10	7.0	1.00	0.00	0.42	2513.7	8.97
13	106.0	32.30	52.25	4.75	230.9	0.68
14	109.8	32.30	54.90	4.52	241.4	0.67
15	65.0	32.30	54.90	4.52	148.3	0.41
16	65.0	4.81	54.90	4.52	148.3	0.41
17	107.9	32.30	0.00	0.23	2700.0	7.94
18	70.8	32.30	0.00	0.23	296.4	0.97
19	32.2	4.81	0.00	0.23	296.4	1.00
21	110.0	143.38		0.28	2691.1	7.24
22	110.0	143.38		0.28	461.4	1.42
23	29.4	100.00		101.57	123.3	0.43
24	32.0	100.00		101.57	134.2	0.47
25	29.4	100.00		47.08	123.3	0.43
26	32.0	100.00		47.08	134.2	0.47
27	11.7	100.00		52.96	49.2	0.18
28	7.2	100.00		52.96	30.4	0.11

Table 7
Operating conditions of the triple effect series flow cycle.

State Point	T [°C]	P [kPa]	x [%]	$\dot{m}$ [kg/s]	h [kJ/kg]	s [kJ/kg K]
1	32.0	1.00	52.23	5.80	73.0	0.22
2	32.0	134.10	52.23	5.80	73.1	0.22
3	63.9	134.10	52.23	5.80	140.5	0.43
4	103.9	134.10	52.23	5.80	226.2	0.67
5	147.4	134.10	52.23	5.80	321.6	0.91
6	149.8	134.10	53.78	5.63	326.2	0.90
7	104.1	134.10	53.78	5.63	227.9	0.65
8	104.1	29.46	53.78	5.63	227.9	0.65
9	107.8	29.46	55.11	5.50	237.6	0.66
10	64.1	29.46	55.11	5.50	147.2	0.41
11	64.1	4.81	55.11	5.50	147.2	0.41
12	68.5	4.81	56.31	5.38	159.5	0.42
13	32.2	4.81	56.31	5.38	86.8	0.20
14	32.2	1.00	56.31	5.38	86.8	0.20
20	148.6	134.10		0.17	2771.3	7.47
21	108.0	134.10		0.17	453.1	1.40
22	68.7	29.46		0.17	453.1	1.42
23	105.9	29.46		0.14	2696.6	7.98
24	68.7	29.46		0.30	287.5	0.94
25	32.2	4.81		0.30	287.5	0.97
26	66.3	4.81		0.12	2624.3	8.61
27	32.2	4.81		0.42	134.9	0.47
28	7.0	1.00		0.42	134.9	0.48
29	7.0	1.00		0.42	2513.7	8.97
30	150.0	476.20		0.21	2745.9	6.84
31	150.0	476.20		0.21	632.2	1.84
32	29.4	100.00		101.24	123.3	0.43
33	32.0	100.00		101.24	134.2	0.46
34	29.4	100.00		30.99	123.3	0.43
35	32.0	100.00		30.99	134.2	0.46
36	11.7	100.00		52.96	49.2	0.18
37	7.2	100.00		52.96	30.4	0.11

4.2. Exergetic efficiencies

Tendencies are similar for the exergetic efficiency. The maximum exergetic efficiencies are lowest for the half effect, followed by the single effect. Highest values are found for double and

Table 8
Operating conditions of the half effect cycle.

State Point	T [°C]	P [kPa]	x [%]	$\dot{m}$ [kg/s]	h [kJ/kg]	s [kJ/kg K]
1	32.0	1.00	52.30	8.52	73.2	0.22
2	32.0	2.10	52.30	8.52	73.2	0.22
3	48.2	2.10	52.30	8.52	107.1	0.33
4	49.8	2.10	55.00	8.10	117.5	0.32
5	32.2	2.10	55.00	8.10	81.7	0.21
6	32.2	1.00	55.00	8.10	81.7	0.21
7	32.0	2.10	43.50	8.52	64.7	0.29
8	32.0	4.81	43.50	8.52	64.7	0.29
9	48.3	4.81	43.50	8.52	102.8	0.41
10	49.8	4.81	45.70	8.10	105.0	0.40
11	32.2	4.81	45.70	8.10	64.9	0.27
12	32.2	2.10	45.70	8.10	64.9	0.27
13	49.1	4.81		0.42	2591.6	8.51
14	32.2	4.81		0.42	134.9	0.47
15	7.0	1.00		0.42	134.9	0.48
16	7.0	1.00		0.42	2513.7	8.97
17	49.0	2.10		0.42	2592.2	8.89
21	50.0	100.00		1272.16	209.4	0.70
22	49.8	100.00		1272.16	208.6	0.70
23	50.0	100.00		1349.13	209.4	0.70
24	49.8	100.00		1349.13	208.6	0.70
25	29.4	100.00		100.78	123.3	0.43
26	32.0	100.00		100.78	134.2	0.46
27	29.4	100.00		97.92	123.3	0.43
28	32.0	100.00		97.92	134.2	0.46
29	29.4	100.00		95.03	123.3	0.43
30	32.0	100.00		95.03	134.2	0.46
31	11.7	100.00		52.96	49.2	0.18
32	7.2	100.00		52.96	30.4	0.11

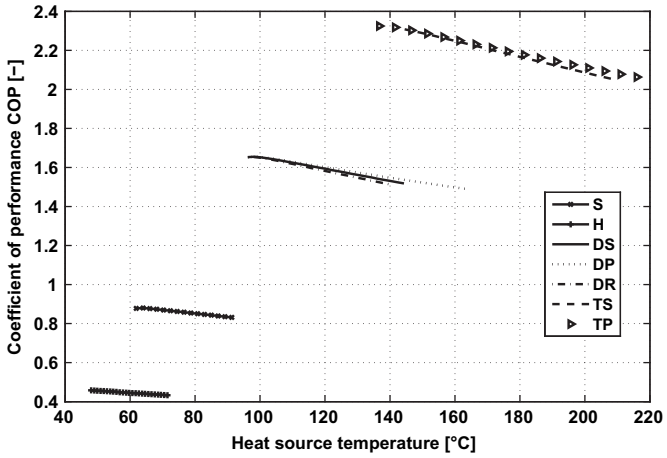

Fig. 9. Comparison of the coefficient of performance.

triple effect. Little difference is found between the flow configurations. The exergetic efficiencies achieve a maximum at slightly lower heat source temperatures than the COP (Fig. 10). Furthermore, the decrease with increasing heat source temperature is more accentuated than for the COP. This behavior is due to a nearly constant denominator in the COP, the heat input rate $\dot{Q}_G$, while the denominator in the equation for the exergetic efficiency $\dot{E}_F$ increases. This is shown in Eq. (9), where T represents the temperature of the condensing steam. The second term ($\tau = 1-T_0/T$) is also called dimensionless exergetic temperature [3] and increases with the temperature T, approaching for very high temperatures one. The maximum values of COP and exergetic efficiencies of the different cycles are summarized in Table 9.

$$\dot{E}_{F,G} = \dot{Q}_G\left(1-\frac{T_0}{T}\right) \tag{9}$$

4.3. Exergy destruction rates

To understand the differences among the cycles and the effect of the changing heat source temperature on the performance, the exergy destruction rates in all the main components have been evaluated and plotted in Figs. 11–15. The exergy destruction rate of the evaporator is constant in all cycles as its operating conditions have been fixed.

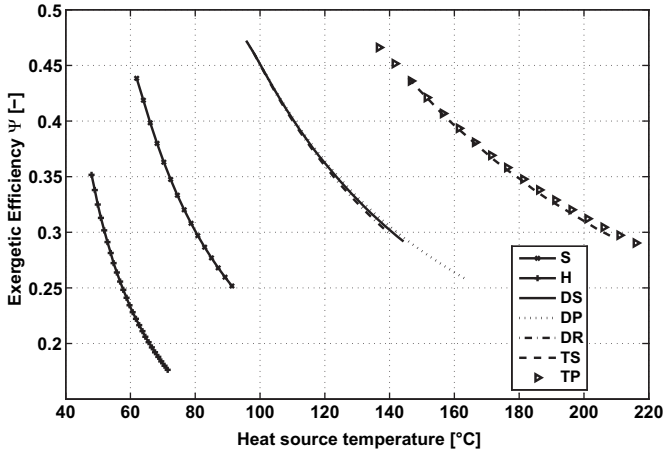

Fig. 10. Comparison of exergetic efficiency.

Table 9
Maximum COP's and exergetic efficiencies of the cycles.

Cycle	COP	Ψ
Half effect	0.458	0.359
Single effect	0.880	0.438
Double effect series flow	1.655	0.473
Double effect parallel flow	1.656	0.473
Double effect reverse flow	1.654	0.473
Triple effect series flow	2.312	0.447
Triple effect parallel flow	2.321	0.470

4.3.1. Single effect cycle

For the single effect cycle (Fig. 11) exergy destruction rates in the condenser and the solution heat exchanger are nearly independent of the generator temperature. This differs from the behavior of a real solution heat exchanger with fixed heat exchange area. Since mass flow rate becomes large when it gets closer to the cut-off temperature solution, the exergy destruction rate of a real solution heat exchanger increases significantly when it approaches low generator temperatures [13]. As in our study the minimum temperature difference is fixed the solution heat exchanger area would have to increase in order to maintain these conditions. Therefore if only unavoidable exergy destruction rates are considered the decrease of the cycle COP close to the cut-off temperatures results less important than in the case of a real machine with a fixed solution heat exchanger area. On the other hand the exergy destruction rates in the absorber and generator increase with the generator temperature as the concentration difference between weak and strong solution increases. The absorber shows higher exergy destruction than the generator as mixing of streams at different temperatures between the solution and the colder vapor from the evaporator takes place. The origin of exergy destruction is further discussed in [22].

4.3.2. Double effect cycles

For the double effect cycles (Figs. 12–14) differences in the flow configurations become clearer observing the exergy destruction rates in the components. As expected no difference is found for the evaporator and condenser. Exergy destruction in the generators and its increment with the generator temperature is lower than for the single effect cycle: This is due to the fact that the thermal power $\dot{Q}_G$ supplied to the double effect cycles is significantly less than for the single effect and the separation process is now distributed between the high temperature generator and the generator condenser assembly. The exergy destruction rates in the generators

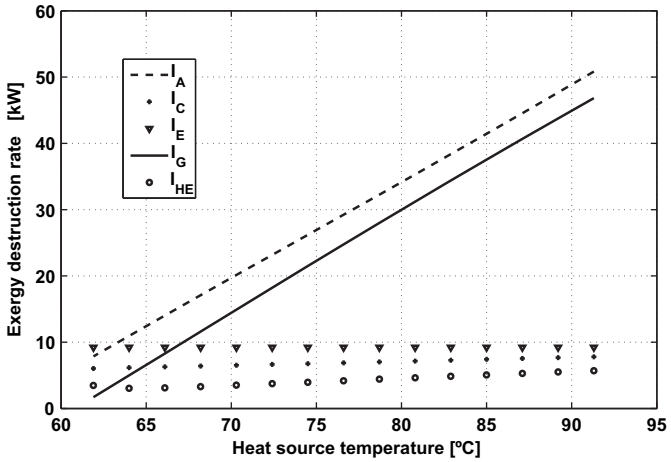

Fig. 11. Exergy destruction rates in the main components of a single effect absorption cycle as function of heat source temperature.

UNIVERSITAT ROVIRA I VIRGILI
OPTIMIZATION OF ENVIRONMENTALLY FRIENDLY SOLAR ASSISTED ABSORPTION COOLING SYSTEMS
Berhane Hagos Gebreslassie
ISBN: 978-84-693-7673-7/DL:T-1752-2010

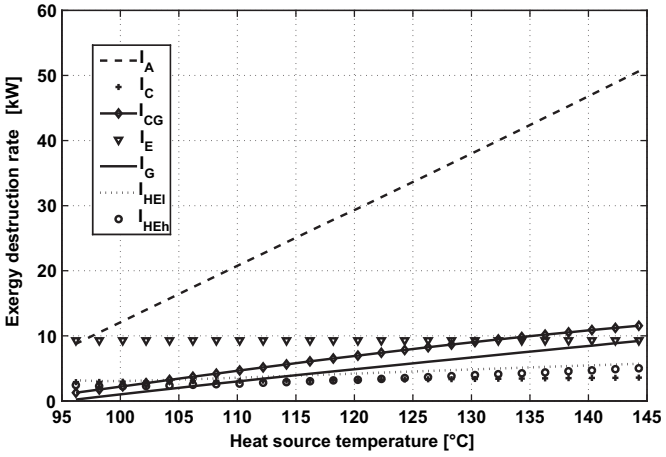

Fig. 12. Exergy destruction rates in the main components of a double effect series flow absorption cycle as function of the heat source temperature.

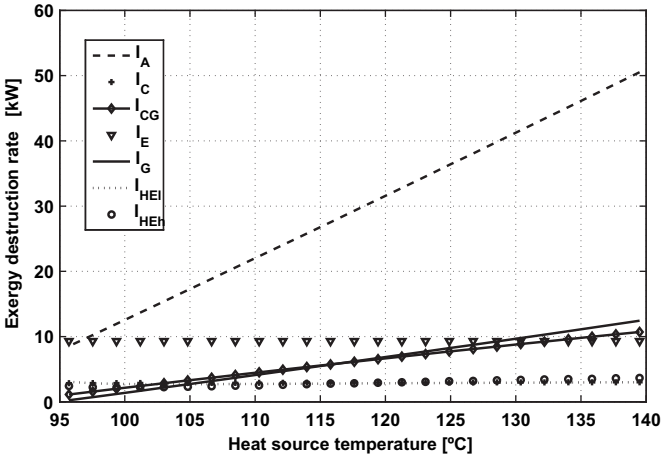

Fig. 14. Exergy destruction in the main components of double effect reverse flow absorption cycle as function of heat source temperature.

for the different flow configurations for the same heat source temperatures are similar for series and reverse flow, but higher for parallel flow. We can observe that exergy destruction increases with the concentration difference in the solutions, which is similar for series and reverse flow, but higher for parallel flow. The same is valid for the different condenser-generator assemblies, where again the parallel flow has the highest concentration difference and the highest exergy destruction rate. Exergy destruction in the solution heat exchangers is due the heat capacity rate mismatch, resulting in larger temperature differences, which is the highest in the high temperature solution heat exchanger for the parallel flow and the low temperature heat exchanger of the series flow. As it occurs for the generator, the absorber exergy destruction increases with a larger solution concentration difference. In the parallel flow the concentration difference and the exergy destruction rate is significantly lower than in the other flow configurations. Thus for parallel flow the higher exergy destruction in the generators is compensated by a lower exergy destruction in the absorber.

4.3.3. Triple effect cycles

The same observations as for double effect configurations can be made for triple effect configurations. The main difference is that now the separation process is distributed among three generators and the exergy destruction rate of each of them is again smaller as the corresponding component in the double effect. While in the parallel flow exergy destruction rates are higher in the generator, this is again compensated by lower values in the absorber.

4.3.4. Half effect cycle

The half effect cycle (Fig. 15) includes two absorbers. Both have the largest exergy destruction rates in the cycle followed by the two generators. Again for absorbers and generators the exergy destruction increases with the generator temperature, as solution concentration differences become larger. The exergy destruction rate of the whole cycle is the highest among the analyzed cycles, which explains the significantly lower exergetic efficiency (Fig. 10).

4.3.5. Discussion

In our analysis only unavoidable exergy destruction is considered. For the minimum temperature difference in the heat exchangers a very small value of 0.2 K has been fixed and pressure losses are neglected. The above results show similar tendencies for all cycles. The absorber exergy destruction rate is dominant, followed by the one of the generator. As the heat source temperature increases, the concentration differences between incoming and leaving solutions in generators and absorbers increase. This is accompanied by larger exergy destruction rates. In the other components like condenser and solution heat exchanger exergy

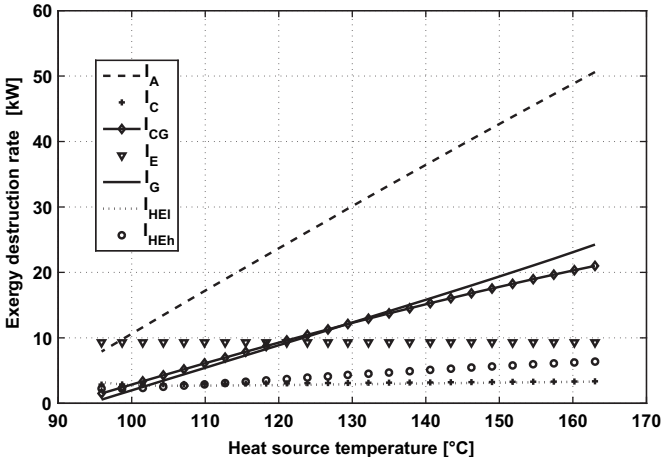

Fig. 13. Exergy destruction rates in the main components of a double effect parallel flow absorption cycle as function of the heat source temperature.

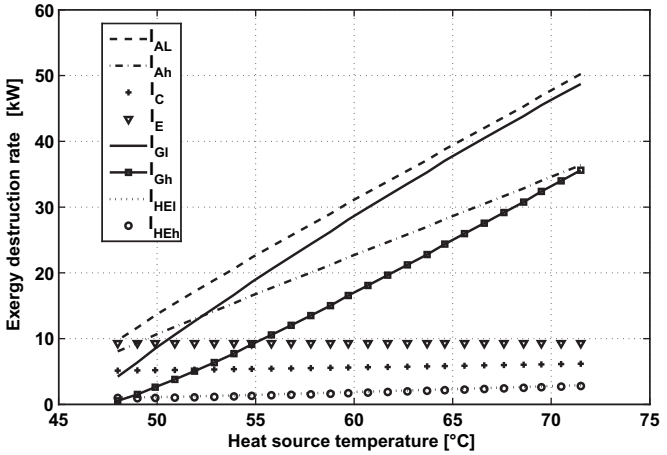

Fig. 15. Exergy destruction rates in the main components of a half effect absorption cycle as function of the heat source temperature.

destruction rates are only slightly affected by the generator temperature. The evaporator exergy destruction rate is not changing among cycles as its operating conditions remain unchanged and is not affected by the heat source temperature.

These results differ from other studies which evaluate both unavoidable and avoidable exergy destruction. In this conventional exergetic evaluation the design of the heat exchangers is fixed for example by given UA values. The minimum temperature differences in the heat exchangers will change, if the operating conditions change. The behavior of the solution heat exchanger, the generator and absorber will be different. At low heat source temperatures, near the cut-off temperature, the solution concentration differences are small. Therefore the solution mass flow rates become large. Thus if the heat source temperature decreases in this temperature range, the heat rate in the solution heat exchanger increases significantly. The temperature difference between hot and cold fluid becomes larger. The solutions enter at a lower temperature in the generator and at a higher temperature in the absorber. Both heat rates in generator and absorber increase, if the cooling capacity has to remain constant. The COP decreases significantly. As a consequence close to the cut-off temperature, the exergy destruction rates in absorber, generator and solution heat exchangers becomes very high. With increasing generator temperature the exergy destruction rates in absorber and generator pass through a clear minimum, which corresponds to a maximum of the exergetic efficiency. For higher heat source temperatures absorber and generator exergy destruction rates increase again. The last phenomena is also observed in our study, as the solution flow rates are decreasing and the relative contribution of the exergy destruction due to the temperature difference becomes smaller. Therefore main differences in our results are found at generator temperatures close to the cut-off temperature, which corresponds to small concentration differences and large mass flow rates of the solution, while tendencies for higher heat source temperatures are similar.

5. Conclusions

The performance of seven different water–LiBr absorption cooling cycles has been evaluated applying first and second law analysis. Only unavoidable exergy destruction is considered in order to compare the cycles on a rational basis. Effects of the avoidable exergy destructions are eliminated at this stage of the theoretical analysis, but should be considered at the design stage. The present study enables us to distinguish and quantify these parts. The avoidable part shows where the main potential for improvement of the cycle is. This is not necessarily the component with the largest exergy destruction, if the exergy destruction is mainly due to the unavoidable part.

The effect of the heat source temperature has been evaluated for typical cooling operating conditions. The COP increases from half to triple effect and shows for each cycle a maximum, which is slightly higher than the cut-off temperature. The values of the COP are higher than in studies which include both avoidable and unavoidable exergy destruction and maintain these high values also close to the cut-off temperature. At higher heat source temperatures the COP decreases slowly. The same qualitative behavior is found for the exergetic efficiency. But the decrease at higher heat source temperatures is more significant as in the denominator of the exergetic efficiency the heat rate to the generator is nearly constant, while its temperature and thus the dimensionless exergetic temperature is increasing. As a consequence the exergy input (Fuel) increases, while the output (Product) in the numerator is fixed. The maximum exergy efficiencies are lowest for the half effect, followed by the single effect. Highest values are found for double and triple effect. Little difference is found among the flow configurations (reverse, series and parallel flow).

Furthermore, the exergy destruction rates of the heat exchangers are determined. For condenser and solution heat exchanger the exergy destruction is practically independent of the heat source temperature. For absorber and generator the exergy destruction rates increase with the heat source temperature, as the solution concentration differences become larger. Differences to studies which consider both avoidable and unavoidable exergy destruction are found at low generator temperatures near the cut-off temperature. In this temperature range, in real heat exchangers exergy destruction due to temperature difference is dominant. In our study it is not included, as it represents an avoidable exergy destruction. Results for higher heat source temperatures are similar to other studies.

The purpose of this study is a comparison of the exergy efficiencies and the exergy destruction in different absorption cycle configurations taking into account only the unavoidable exergy destruction. Thus cycles can be compared on a rational basis. Results do not depend on design specifications, as for example UA values. The next step in this type of analysis would be the advanced exergy analysis proposed by [23], where the total exergy destruction is splitted into avoidable and unavoidable parts. This makes it easier to understand the thermodynamic inefficiencies and should be considered in the termoeconomic optimization [25]. An example of how this type of advanced exergetic evaluation helps to improve the design is presented in [24].

Acknowledgements

Berhane H. Gebreslassie expresses his gratitude for the financial support received from University Rovira i Virgili. The authors also wish to acknowledge support of this research work from the Spanish Ministry of Education and Science (projects DPI2002-00706, DPI2008-04099, PHB2008-0090-PC and BFU2008-863 00196) and the Spanish Ministry of External Affairs (projects A/8502/07, HS2007-864 0006 and A/020104/08).

References

[1] Herold KE, Radermacher R, Klein SA. Absorption chillers and heat pumps. Boca Raton, Florida: CRC Press; 1996.
[2] Bejan A, Tsatsaronis G, Moran M. Thermal design & optimization. John Wiley & Sons Inc; 1996.
[3] Kotas TJ. The exergy method of thermal plant analysis. Krieger Publishing Company; 1995.
[4] Szargut J, Morris D, Steward F. Exergy analysis of thermal, chemical, and metallurgical processes. N.Y.: Hemisphere; 1988.
[5] Anand DK, Lindler KW, Schweitzer S, Kennish W. Second-law analysis of solar-powered absorption cooling cycles and systems. Journal of Solar Energy Engineering; 1984.
[6] Koehler WJ, Ibele WE, Soltes J, Winter ER. Availability simulation of a lithium bromide absorption heat pump. Heat Recovery Systems and CHP 1988;8(2):157–71.
[7] Le Goff P, Louis G, Ramadane A. pompes a chaleur a absorption, multi-etagees: analyse exergetique. principes de realisation [Multi-stage absorption heat pumps: exergetic analysis. Techniques for construction]. Revue Generale de Thermique 1988;27(320–321):451–63.
[8] Aphornratana S, Eames IW. Thermodynamic analysis of absorption refrigeration cycles using the second law of thermodynamics method. International Journal of Refrigeration 1994;18(4):244–52.
[9] Talbi M, Agnew B. Exergy analysis: an absorption refrigerator using lithium bromide and water as the working fluids. Applied Thermal Engineering 2000;20:619–30.
[10] Kilic M, Kaynakli O. Second law-based thermodynamic analysis of water–lithium bromide absorption refrigeration system. Energy 2007;32(8):1505–12.
[11] Ataer EO, Gögus Y. Comparative study of irreversibilities in an aqua–ammonia absorption refrigeration system. International Journal of Refrigeration 1991; 14(2):86–92.
[12] Best R, Islas J, Martinez M. Exergy efficiency of an ammonia–water absorption system for ice production. Applied Energy 1993;45:241–56.

[13] Karakas A, Egrican N, Uygur S. Second-law analysis of solar absorption-cooling cycles using lithium bromide/water and ammonia/water as working fluids. Applied Energy 1990;37(3):169–87.
[14] Meunier F, Kaushik SC, Neveu P, Poyelle F. A comparative thermodynamic study of sorption systems: second law analysis. International Journal of Refrigeration 1996;19(6):414–21.
[15] Izquierdo M, de Vega M, Lecuona A, Rodriguez P. Compressors driven by thermal solar energy: entropy generated, exergy destroyed and exergetic efficiency. Solar Energy 2002;72(4):363–75.
[16] Lee SF, Sherif SA. Second-law analysis of multi-effect lithium bromide/water absorption chillers. ASHRAE Transactions 1999;105.
[17] Ravikumar TS, Suganthi L, Samuel AA. Exergy analysis of solar assisted double effect absorption refrigeration system. Renewable Energy 1998; 14(1–4):55–9.
[18] Gomri R. Second law comparison of single effect and double effect vapour absorption refrigeration systems. Energy Conversion and Management 2009;50(5):1279–87.
[19] Gomri R, Hakimi R. Second law analysis of double effect vapour absorption cooler system. Energy Conversion and Management 2008;49(11):3343–8.
[20] Kaushik SC, Arora A. Energy and exergy analysis of single effect and series flow double effect water–lithium bromide absorption refrigeration systems. International Journal of Refrigeration 2009;32(6):1247–58.
[21] Jeong J, Saito K, and Sunao K. Optimum design method for a single effect absorption refrigerator based on the first and, second law analysis. In: 21st IIR international congress of refrigeration, Washington, DC (USA): 2003; 1–9.
[22] Sencan A, Yakut KA, Kalogirou SA. Exergy analysis of lithium bromide/water absorption systems. Renewable Energy 2005;30(5):645–57.
[23] Morosuk T, Tsatsaronis G. A new approach to the exergy analysis of absorption refrigeration machines. Energy 2008;33(6):890–907.
[24] Morosuk T, Tsatsaronis G. Advanced exergetic evaluation of refrigeration machines using different working fluids. Energy 2009;34(12):2248–58.
[25] Tsatsaronis G, Park MH. On avoidable and unavoidable exergy destructions and investment costs in thermal systems. Energy Conversion and Management 2002;43(9–12):1259–70.
[26] Alefeld G. Rules for the design of multistage absorber machines. Brennstoff-Wärme-Kraft 1982;34(2):64–73.
[27] EES. Engineering Equation Solver. F-chart software, www.fchart.com; 1992–2009.
[28] Kaita Y. Thermodynamic properties of litium bromide-water solutions at high htemperatures. International Journal of Refrigeration 2001;24:374–90.
[29] Gommed K, Grossman G. Performance analysis of staged absorption heat pumps: water–lithium bromide systems. ASHRAE Transactions 1990;96(1):1590–8.
[30] Grossman G, Wilk M, De Vault RC. Simulation and, performance analysis of triple-effect absorption cycles. ASHRAE Transactions 1994;100(1):452–62.

Int. J. of Thermodynamics **Vol. 12 (No. 1), pp. 17-27, March 2009**
ISSN 1301-9724 **www.icatweb.org/journal.htm**

Effect of Internal Heat Recovery in Ammonia-Water Absorption Cooling Cycles: Exergy and Structural Analysis

Dieter Boer[1]*, Berhane Hagos Gebreslassie[2], Marc Medrano[3], Miquel Nogués[4]

[1,2]Department of Mechanical Engineering,
University of Rovira i Virgili, Tarragona, Spain
Phone: (+34) 977 559631
E-mail: [1]Dieter.Boer@urv.net;
[2]Berhane.Gebreslassie@urv.net

[3,4]GREA Innovació Concurrent,
Universitat de Lleida Lleida, Spain
E-mail: [3]mmedrano@diei.udl.cat;
[4]mnogues@diei.udl.cat

Abstract

First and second law analysis have been conducted for three low temperature driven ammonia-water absorption cooling cycles with increasing internal heat recovery. Based on the results of exergy analysis the structural analysis has been achieved. The obtained Coefficients of Structural Bonds (CSB) consider how the irreversibility of the whole cycle is affected by a change in the irreversibility related to an efficiency improvement of a single component. Trends for the different configurations are similar, while quantitative differences among the main heat exchangers are considerable. The highest values of the CSB are found for the refrigerant heat exchanger. Also the evaporator, the condenser, the generator and the absorber show values higher than unity. The lowest CSB's are obtained in the solution heat exchanger. In general, CSB's decrease with increasing efficiency. That means that for very efficient heat exchangers, a further improvement looks less attractive. The dephlegmator is an exception as it shows a singularity of the CSB value due to its complex interactions with the other components. Once the CSB's are obtained for the main components, they can be used in the structural method of the thermoeconomic optimisation. This method enables us to find the optimum design of a component in a straightforward calculation.

Keywords: Absorption cycle, ammonia-water, exergy analysis, structural analysis.

1. Introduction

Combining thermodynamics and economics, the thermoeconomic or exergoeconomic analysis can be achieved (Kotas, 1995; Bejan et al., 1996; El-Sayed, 2003). The objective of exergoeconomic optimization is the minimization of the total cost, mainly composed of capital and energy costs. In the field of refrigeration thermoeconomic analysis was applied initially to compression cycles (Wall, 1986; Dentice d'Accadia et al., 1998; Dingeç et al., 1999; Ferrer et al., 2001; Dentice d'Accadia et al., 2004; Zhang et al., 2004) and later to absorption cycles (Tozer et al., 1999; Sahin et al., 2002; Misra et al., 2003; Misra et al., 2005; Misra et al., 2006; KizIlkan et al., 2007).

One methodology used in exergoeconomic optimisation is the structural method introduced by Beyer (1970 and 1974). It is based on structural coefficients, which show how local irreversibilities in the components affect the overall irreversibility rate of the cycle. The coefficient of structural bonds (*CSB*) of a component *k*, which is obtained by variation of a parameter x_i, is defined as

$$CSB_{k;i} = \left(\frac{\partial \dot{I}_t}{\partial \dot{I}_k} \right)_{xi=\text{var}} \quad (1)$$

where $\dot{I}_k$ is the irreversibility rate of component *k*, and $\dot{I}_t$ is the irreversibility rate of the whole cycle. Structural coefficients show how the irreversibility of the whole cycle and a single component are related. If a slight decrease in the irreversibility of one component due to an increased efficiency causes a significant improvement in the total irreversibility of the cycle (high *CSB*), it will be wise to put much of the design effort in improving the efficiency of this component. Otherwise (low *CSB*), an improvement of the efficiency of the considered component is not worthwhile. These coefficients can help us to determine for one selected component of the system its optimum efficiency, for which a minimum total cost is achieved (Kotas, 1995).

In the present study, this method will be applied to the analysis of absorption cycles. The analysed cycles are ammonia-water absorption cooling cycles with increasing internal heat recovery. A similar approach has been applied by Sözen (2001) for an ammonia-water refrigeration cycle. Modelling starts with the first law analysis, followed by the exergy analysis (Karakas et al., 1990; Ataer et al., 1991; Best et al., 1993).

Once the irreversibilities of the components and the whole cycle are evaluated, the coefficients of structural bonds can be evaluated. Compared to a former study (Boer et al., 2005), here the *CSB*'s are not constant, but their dependence on the efficiencies is shown and their behaviour is quantified and compared for different cycle configurations. These *CSB*'s can be used in the structural method of exergoeconomic optimisation (Beyer, 1974). The final purpose is the design of more cost-effective absorption cycles. The application of the *CSB*'s is described in KizIlkan et al. (2007) and will be summarized briefly. More details can be found in Kotas (1995).

The optimum efficiency specification for a component will be determined in order to obtain the minimum annual

*Corresponding author

UNIVERSITAT ROVIRA I VIRGILI
OPTIMIZATION OF ENVIRONMENTALLY FRIENDLY SOLAR ASSISTED ABSORPTION COOLING SYSTEMS
Berhane Hagos Gebreslassie
ISBN: 978-84-693-7673-7/DL:T-1752-2010

operating cost. This operating cost is composed mainly of the fuel and capital costs.

$$C_i(x_i) = t_{op} c^e_{in} \dot{E}_{in}(x_i) + a^c \sum_{l=1}^{n} C^c_l(x_i) + b^c \quad (2)$$

The first term of the right hand side represents the fuel cost, the second one the capital investment amortisation and the third one other cost factors that are not affected by the optimisation, for example maintenance costs. The capital recovery factor is given by

$$a^c = \frac{i(1+i)^n}{(1+i)^n - 1} \quad (3)$$

At the optimum point

$$t_{op} c^e_{in} CSB_{k,i} \frac{\partial \dot{I}_k}{\partial x_i} = -a^c \frac{\partial C^c_k}{\partial x_i} \quad (4)$$

Equation (4) depends only on parameters of component k, which is optimised. The interaction with the system is taken into account by the *CSB*. $\partial \dot{I}_k / \partial x_i$ describes the effect of the efficiency parameter x_i on the irreversibility of the component. $\partial C^c_k / \partial x_i$ takes into account the dependence of the component cost on x_i. Both parameters depend on the efficiency of the analysed component. From equation (4) the efficiency that results in the lowest operating cost C_t can be obtained (KizIlkan et al., 2007).

2. Description of the cycles

For this study an ammonia-water absorption cycle has been selected (Figure 1). Basic components are the absorber (*A*), the condenser (*C*), the generator (*G*), and the evaporator (*E*). The cycle is completed by the solution heat exchanger (*SHE*), the dephlegmator (*D*) and the rectification plates (*R*). To obtain the necessary pressure changes, the cycles include the solution pump (*P*), the refrigerant expansion valve (*RV*) and solution expansion valve (*SV*).

For cycle I, the solution circulates between the absorber, where the refrigerant is absorbed at low pressure, and the generator, where the refrigerant is desorbed at high pressure (state points 1 to 6). The strong solution leaves the absorber (1), is preheated in the solution heat exchanger (3), and enters the rectification column. The column has three theoretical stages, which is sufficient in cooling applications (Roriz et al., 2003). The feed enters in central plate two. Vapour and liquid in equilibrium leave plate two towards plates one and three, respectively, while saturated liquid from plate three and saturated vapour from plate one enter plate two. Temperature and concentration of ammonia in the vapour increase from plate one to plate three. The generator acts as the reboiler of the rectification column. The weak solution (4) leaves towards the absorber. In the dephlegmator, the necessary liquid reflux is obtained, while the rest of the vapour (9) condenses completely in the condenser (10). The condensate expands in the refrigerant throttling valve, causing partial vaporisation (12), and enters the evaporator. Due to the water content of the mixture, the temperature increases during the vaporisation process as the liquid contains less and less ammonia, which is the more volatile component. Vaporisation in the evaporator is only partial, as total evaporation would require too large of a temperature gradient. The cycle is closed when the vapour with a small liquid fraction (13) enters the absorber. Streams 15 to 22 are the external heat transfer fluids (in all cases this is water), which deliver or extract the heat to or from the cycle.

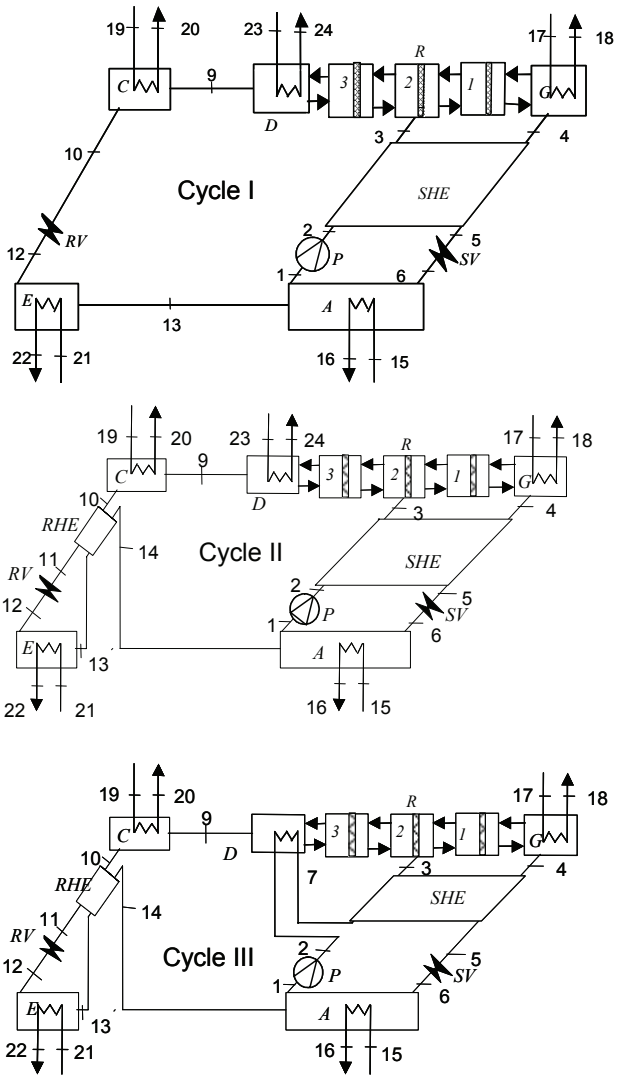

Figure 1. Ammonia-water absorption cycles with increasing internal heat recovery.

Cycle II is similar to Cycle I except for the refrigerant heat exchanger (*RHE*). In Cycle II after leaving the condenser the condensate (10) is subcooled (11) in order to supply heat for the partial vaporisation in the evaporator (14).

An additional feature of Cycle III is a heat exchange between the strong solution after the solution pump (2) and the dephlegmator (*D*). Preheating the strong solution (7) eliminates the use of cooling water in the rectifier.

3. Methodology of the simulation

A computer code for simulating the cycle has been established using the Engineering Equation Solver EES program. Properties for ammonia water are given by Tillner-Roth and Friend (1998). Typical cooling operation conditions are assumed as follows:

Evaporator cooling capacity	1000 kW
Temperatures:	
Chilled water inlet/outlet (*E*)	12/6ºC
Cooling water inlet/outlet (parallel flow through *A* and *C*)	27ºC/32ºC

Hot water inlet (*G*)	90ºC
Minimum temperature difference in the dephlegmator *D*	15 K
Minimum temperature difference in the rest of heat exchangers	5 K

The hot water outlet temperature in the generator is adjusted to minimise the mismatch of heat capacity rates (product of mass flow and specific heat) in the generator. This means that the temperature differences between the hot and cold streams are the same on the hot and the cold sides of the generator (Kotas, 1995). In the same way the degree of evaporation in the evaporator is chosen to obtain the same temperature difference at the inlet and outlet of the evaporator.

The main assumptions are:

- Steady state.
- Heat losses are not considered.
- Pressure losses are not considered.
- The refrigerant leaving the condensers is saturated liquid.
- The mass exchange efficiencies in absorber and generator are 0.9.
- The liquid and vapour leaving the adiabatic rectification plates are in equilibrium.
- The solution and refrigerant valves are adiabatic.
- The pump efficiency is 0.6.

Modeling starts with a first law analysis. Steady state mass and energy balances for the components of the cycles are established as follows:

Global mass balance:

$$\Sigma \dot{m}_i = \Sigma \dot{m}_e \tag{5}$$

Mass balance for ammonia:

$$\Sigma \dot{m}_i z_i = \Sigma \dot{m}_e z_e \tag{6}$$

Energy balance:

$$0 = \dot{Q} - \dot{W} + \sum_i \dot{m}_i h_i - \sum_e \dot{m}_e h_e \tag{7}$$

For adiabatic components the energy balance is:

$$\Sigma \dot{m}_i h_i = \Sigma \dot{m}_e h_e + \dot{W} \tag{8}$$

The mechanical power only appears in the energy balance of the pump. The mass exchange efficiency for absorber and generator takes into account that thermodynamic equilibrium is not totally reached at the outlet (Ataer et al., 1991) and is defined as:

$$\varepsilon_m = \frac{(z_i - z_e)_{real}}{(z_i - z_e)_{equilibrium}} \tag{9}$$

The coefficient of performance (*COP*) is defined by the cooling output divided by the driving heat input.

$$COP = \frac{\dot{m}_{21}(h_{22} - h_{21})}{\dot{m}_{17}(h_{18} - h_{17})} \tag{10}$$

The driving heat is delivered by the hot water. The subscripts in Eqns (10) and (16) correspond to the numeration of state points presented in *Figure 1*. The general exergy balance is given by Kotas (1995):

$$0 = \sum_i (1 - \frac{T_0}{T_i})\dot{Q}_i - \dot{W} + \sum_i \dot{m}_i e_i - \sum_e \dot{m}_e e_e - \dot{I} \tag{11}$$

Considering components as adiabatic, the above equation can be simplified as

$$\Sigma \dot{m}_i e_i = \Sigma \dot{m}_e e_e + \dot{W} + \dot{I} \tag{12}$$

Specific exergy (Eq. 13) considers only the physical exergy (Jonsson et al., 2000). The chemical exergy of water and ammonia cancels out in the exergy balances as entering and leaving quantities are the same (Kotas, 1995). Mixing entropy has already been taken into account in the calculation of the entropy of the mixture.

$$e = h - h_0 - T_0(s - s_0) \tag{13}$$

The properties indicated with the subscript *0* refer to the environmental state, which is taken as 25ºC and 1 bar. Using exergy flow rates

$$\dot{E} = \dot{m} e \tag{14}$$

it follows

$$\Sigma \dot{E}_i = \Sigma \dot{E}_e + \dot{W} + \dot{I} \tag{15}$$

Irreversibilities are obtained from the exergy analysis. The resulting equations for the different components are given by Karakas et al. (1990). The exergy efficiency is defined as the useful exergy output divided by the required exergy input. For the cycle the exergy input is given by the reduction of the exergy flow of the external heating fluid in the generator and the pump work. The exergy output produced in the evaporator is given by the increase in the exergy flow of the chilled water.

$$\Psi = \frac{\dot{m}_{21}(e_{21} - e_{22})}{\dot{m}_{17}(e_{18} - e_{17}) + \dot{W}_{pump}} \tag{16}$$

The output data obtained are:

- The pressures, temperatures, concentrations, mass flows, enthalpies, entropies and exergies of each state point of streams.
- The thermal or, in the case of the solution pump, mechanical power and irreversibility rate of the main components.
- The COP and the exergetic efficiency.

Once the irreversibilities of the components and the whole cycle have been determined, a parametric study can be achieved. The *UA* values in *Table 1* correspond to minimum temperature differences ΔT_{min} in the heat exchangers for the base case taken as 5 K, except for the dephlegmator, where it is 15 K. *UA* values for all components are maintained constant (Boer et al., 2005), except for the one which is analysed. For this selected component, the minimum temperature difference is varied, which results in a variation of *UA*. The variation of ΔT_{min} for any component is typically between 1 and 10 K, if operation is feasible, except for the dephlegmator where variations were achieved between 5 and 30 K. This range is limited by the operating conditions in order to avoid high solution flow ratios of operation with low performance. As a result, the influence of the heat transfer efficiency of this component on its own irreversibility and also on the irreversibility of the whole cycle is evaluated. These data can be used to determine the *CSB* (Eqn. 1) for a given set of

ISBN: 978-84-693-7673-7/DL:T-1752-2010

Table 1: UA Values Corresponding to the Fixed ΔT_{min} in the Base Case.

Component	Cycle		
	I	II	III
	UA [kW/K]		
A	269.2	264.3	233.4
C	144.8	136.3	136.5
G	318.5	299.8	297.6
E	131.4	131.4	131.4
D	6.2	5.9	7.3
RHE	-	6.3	6.4
SHE	254.6	239.5	229.5

operating conditions, which is the main objective of this analysis.

4. Results

4.1 First and second law analysis

Results of the energetic analysis for the different state points are presented in Table 2, 3 and 4. The corresponding thermal or mechanical power of the components are given in Table 5.

The exergy balances have been achieved for the different components in order to obtain the irreversibilities (Table 6). For all cycles, the highest irreversibilities were found in the solution heat exchanger (*SHE*) followed by the absorber (*A*), the evaporator (*E*) the condenser (*C*) and the generator (*G*).

The irreversibilities of the solution expansion valve (*SV*) and the dephlegmator (*D*) were less important. The irreversibility of the refrigerant expansion valve (*RV*) is considerably reduced by the introduction of the refrigerant heat exchanger (*RHE*). The refrigerant heat exchanger (*RHE*) and the rectification (*R*) contribute less to the irreversibilities. Irreversibilities in the adiabatic rectification plates were low and caused by mixing of streams with different temperatures and concentrations.

Table 2: Operating Conditions for Cycle I.

State Point	T [C]	P [bar]	z [kg kg^{-1}]	$\dot{m}$ [kg s^{-1}]	h [kJ kg^{-1}]	s [kJ kg^{-1}K^{-1}]	e [kJ kg^{-1}]	$\dot{E}$ [kW]
1	32	4.452	0.513	9.321	72.05	1.025	27.31	254.6
2	32.6	14.29	0.513	9.321	73.27	1.025	28.7	267.6
3	74.7	14.29	0.513	9.321	273.4	1.638	46.09	429.6
4	85	14.29	0.46	8.411	299.3	1.687	57.28	481.8
5	37.6	14.29	0.46	8.411	77.43	1.026	32.64	274.5
6	37.8	4.452	0.46	8.411	77.43	1.029	31.5	264.9
9	47	14.29	0.999	0.91	1666	5.766	207.4	188.8
10	37	14.29	0.999	0.91	518	2.07	162	147.4
12	1	4.452	0.999	0.91	518	2.113	149	135.6
13	7	4.452	0.999	0.91	1617	6.119	53.48	48.67
15	27	1	0	69.434	113.3	0.395	0.028	1.939
16	32	1	0	69.434	134.2	0.464	0.338	23.48
17	90	1.702	0	38.371	377.1	1.193	26.05	999.5
18	80.1	1.702	0	38.371	335.6	1.077	19.09	732.5
19	27	1	0	49.97	113.3	0.395	0.028	1.395
20	32	1	0	49.97	134.2	0.464	0.338	16.9
21	12	1	0	39.71	50.51	0.181	1.22	48.54
22	6	1	0	39.71	25.32	0.091	2.652	105.3
23	27	1	0	5.192	113.3	0.395	0.028	0.145
24	32	1	0	5.192	134.2	0.464	0.338	1.756

Table 3: Conditions for Cycle II.

State Point	T [C]	P [bar]	z [kg kg^{-1}]	$\dot{m}$ [kg s^{-1}]	H [kJ kg^{-1}]	s [kJ kg^{-1}K^{-1}]	e [kJ kg^{-1}]	$\dot{E}$ [kW]
1	32	4.453	0.513	8.771	72.06	1.025	27.31	239.6
2	32.6	14.29	0.513	8.771	73.28	1.025	28.7	251.7
3	74.7	14.29	0.513	8.771	273.4	1.638	46.08	404.2
4	85	14.29	0.46	7.914	299.3	1.687	57.28	453.3
5	37.6	14.29	0.46	7.914	77.44	1.026	32.64	258.3
6	37.8	4.453	0.46	7.914	77.44	1.029	31.5	249.3
9	47	14.29	0.999	0.857	1666	5.766	207.4	177.7
10	37	14.29	0.999	0.857	518	2.07	162	138.7
11	22.8	14.29	0.999	0.857	449.3	1.843	160.9	137.8
12	1	4.453	0.999	0.857	449.3	1.862	155	132.8
13	7	4.453	0.999	0.857	1617	6.118	53.48	45.81
14	32	4.453	0.999	0.857	1685	6.354	51.98	44.53
15	27	1	0	68.16	113.3	0.395	0.028	1.903
16	32	1	0	68.16	134.2	0.464	0.338	23.05
17	90	1.702	0	36.104	377.1	1.193	26.05	940.4
18	80.1	1.702	0	36.104	335.6	1.077	19.09	689.2
19	27	1	0	47.029	113.3	0.395	0.028	1.313
20	32	1	0	47.029	134.2	0.464	0.338	15.91
21	12	1	0	39.71	50.51	0.181	1.222	48.54
22	6	1	0	39.71	25.32	0.091	2.652	105.3
23	27	1	0	4.886	113.3	0.395	0.02792	0.1364
24	32	1	0	4.886	134.2	0.464	0.3382	1.652

Table 4: Operating Conditions for Cycle III.

State point	T [C]	p [bar]	z [kg kg^{-1}]	$\dot{m}$ [kg s^{-1}]	h [kJ kg^{-1}]	s [kJ kg^{-1}K^{-1}]	E [kJ kg^{-1}]	$\dot{E}$ [kW]
1	32	4.452	0.513	8.769	72.05	1.025	27.31	239.5
2	32.6	14.29	0.513	8.769	73.27	1.025	28.7	251.7
3	74.9	14.29	0.513	8.769	274.6	1.641	46.26	405.6
4	85	14.29	0.46	7.912	299.3	1.687	57.28	453.2
5	40.1	14.29	0.46	7.912	88.75	1.062	33.14	262.2
6	40.2	4.452	0.46	7.912	88.75	1.066	32.01	253.3
7	35.1	14.29	0.513	8.769	84.7	1.062	29.03	254.6
9	47.6	14.29	0.999	0.856	1668	5.772	207.5	177.8
10	37	14.29	0.999	0.856	517.9	2.069	161.9	138.6
11	22.6	14.29	0.999	0.856	448.6	1.84	160.8	137.7
12	1	4.452	0.999	0.856	448.6	1.86	155	132.7
13	7	4.452	0.999	0.856	1616	6.117	53.48	45.8
14	32	4.452	0.999	0.856	1686	6.354	51.96	44.51
15	27	1	0	72.443	113.3	0.395	0.028	2.023
16	32	1	0	72.443	134.2	0.464	0.338	24.5
17	90	1.702	0	36.039	377.1	1.193	26.05	938.7
18	80.2	1.702	0	36.039	335.8	1.078	19.12	689.2
19	27	1	0	47.11	113.3	0.395	0.028	1.315
20	32	1	0	47.11	134.2	0.464	0.338	15.93
21	12	1	0	39.71	50.51	0.181	1.222	48.54
22	6	1	0	39.71	25.32	0.091	2.652	105.3

Table 5: Thermal or Mechanical Power for a Fixed Cooling Capacity.

Component	Cycle		
	I	II	III
	Power [kW]		
A	1451	1425	1514
C	1044	983	985
G	1593	1499	1488
E	1000	1000	1000
D	109	102	100
RHE		59	59
SHE	1866	1756	1666
P	19	18	18

UNIVERSITAT ROVIRA I VIRGILI
OPTIMIZATION OF ENVIRONMENTALLY FRIENDLY SOLAR ASSISTED ABSORPTION COOLING SYSTEMS
Berhane Hagos Gebreslassie
ISBN: 978-84-693-7673-7/DL:T-1752-2010

Table 6: Irreversiblities.

Component	Cycle		
	I	II	III
	Irreversibility [kW]		
A	37.46	33.10	35.78
C	25.87	24.35	24.49
G	13.36	12.57	12.42
E	30.17	30.20	30.17
D	9.29	8.75	7.34
RHE	-	2.23	2.24
SHE	45.24	42.57	39.95
P	5.93	5.58	5.58
RV	11.83	5.03	4.99
SV	9.61	9.04	8.99
R	1.68	1.58	1.48

The main source of irreversibilities is the temperature between hot and cold streams. Irreversibilities for *SHE* are high due to the low generator temperature. The concentration difference between weak and strong solution is small and solution flow rates large. Results agree with Best et al. (1993), except in the generator. In our case the generator shows lower irreversibilities, as the mismatch of the heat capacity rates has been minimized.

Heat integration affected the irreversibilities in the following way. The main effect of the refrigerant heat exchanger (component *RHE* in Cycles II and III) was a strong reduction in the irreversibility of the refrigerant expansion valve due to the change in working conditions. The refrigerant valve inlet temperature (state points 10 and 11 for Cycles I and II, respectively) decreased from 37ºC to about 22.8ºC, thus reducing the enthalpy h_{12} in the evaporator inlet from 518 kJ/kg to about 449 kJ/kg. This led to an increase in the enthalpy difference in the evaporator and, for a fixed cooling power, the refrigerant mass flow decreased from 0.91 kg/s to 0.857 kg/s. Consequently, the solution flow rate also decreased. The reduction of the irreversibility in the refrigerant valve is greater than the irreversibility added by the refrigerant heat exchanger. The irreversibility of absorber (*A*) decreased because the vapour (14) entered with less difference in temperature with regard to the solution (6) and the mixing took place at a more uniform temperature. Because of the reduction in the mass flows, all irreversibilities were generally smaller.

The combined solution preheater and dephlegmator (component *D* in Cycle III) irreversibility in the solution heat exchanger was also reduced by preheating of the solution. The strong solution entered the solution heat exchanger at 35.1ºC (T_7) compared to 32.6ºC (T_2) in Cycle II. At the same time, however, T_5 increased from 37.6ºC in Cycle II to 40.1ºC in Cycle III, and thus increased the absorber irreversibility. Thus, the reduction of irreversibility in the dephlegmator and solution heat exchanger is partially compensated for by the increase in the absorber.

These reductions in irreversibilities due to the better heat integration improved the *COP* and the exergetic efficiencies Ψ of the cycles (*Table 7*). The refrigerant heat exchanger had a greater effect (+6%) than the solution preheating (compared to Cycle II less than 1%).

Table 7: Energetic (COP) and Exergetic Efficiencies (Ψ).

Cycle	I	II	III
COP	0.628	0.667	0.672
Increase of *COP* compared to Cycle I (%)	-	6.2	7.0
Ψ	0.199	0.211	0.212
Increase of Ψ compared to Cycle I (%)	-	6.0	6.5

4.2 Grassmann diagrams

The exergy flows and irreversibilities can be represented in graphical form. The Grassmann diagram (Szargut et al., 1988; Kotas, 1995) can be used to illustrate cyclic processes and their components with their corresponding irreversibilities, the exergy flows and the recirculation of exergy in the cycle. The inlet exergy flow is on one side of each component, and in the component itself, part of this exergy flow is degraded due to irreversibilities. On the other side of the component exergy flows are leaving. Each component represents a graphical exergy balance and shows how part of the exergy input is lost in the successive energy transformation in the cycles. The widths of the lines are proportional to their exergy flow. This type of diagram already has been employed for absorption cycles (Anand et al., 1984; Szargut et al., 1988; Jeong et al., 2003). The thermal exergy flows E^Q correspond to the change in the exergy flow rate of the external fluids.

Figure 2 represents the exergy flows of Cycle I. The description starts with the external heat and exergy transfer. The exergy input E^Q_G represents the reduction in hot water exergy and the exergy output E^Q_E represents the increase in chilled water exergy. The exergy flows E^Q_A, E^Q_C and E^Q_D are dissipated by the cooling water.

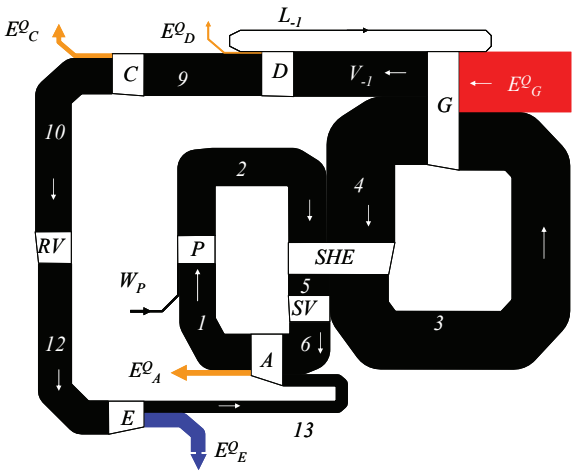

Figure 2. Grassmann diagrams of Cycle I.

With regard to the cycle itself, on the right side is situated the solution circuit with the strong solution (points 1 to 3) and the weak solution (points 4 to 6). The exergy input to the cycle is given by the thermal exergy E^Q_G supplied to the generator and the pump work W_P. This exergy is used to increase the exergy of the solution (points 3 to 4) and generate vapour flow V_{-1}. In the dephlegmator thermal exergy E^Q_D is dissipated and a reflux L_{-1} is created. In *Figures 2, 3* and *4* the exergy destruction in the rectifier is included in the exergy destruction in the generator and the dephlegmator in order to simplify the figure. The vapour (point 9) enters the condenser, where again thermal

UNIVERSITAT ROVIRA I VIRGILI
OPTIMIZATION OF ENVIRONMENTALLY FRIENDLY SOLAR ASSISTED ABSORPTION COOLING SYSTEMS
Berhane Hagos Gebreslassie
ISBN: 978-84-693-7673-7/DL:T-1752-2010

exergy E^Q_C is dissipated. The refrigerant passes through the refrigerant expansion valve and enters the evaporator, where the useful thermal exergy output E^Q_E is produced. The vapour (point 13) enters the absorber, where the refrigerant joins the solution circuit and the thermal exergy E^Q_A is dissipated. The strong solution exergy is increased in the solution heat exchanger (points 2 to 3) while the weak solution exergy is reduced (points 4 to 5). It can also be observed that the irreversibilities in the solution pump and solution expansion valve are relatively small.

In the Grassmann diagram for Cycle II (Figure 3), the refrigerant heat exchanger has been added. A new loop for the refrigerant flow is therefore added on the left hand side. The lines representing the exergy flows are slightly narrower than for Cycle I due to the reduction in the mass flows. In the Grassmann diagram for Cycle III (Figure 4), the cooling of the dephlegmator by cooling water is replaced by a heat exchange, which preheats the strong solution. The dissipation of the thermal exergy flow E^Q_D is therefore eliminated. The vapour flow V_{-1} and the strong solution 2 should enter on the same side but in order to obtain a clearer presentation an exception has been made in this case.

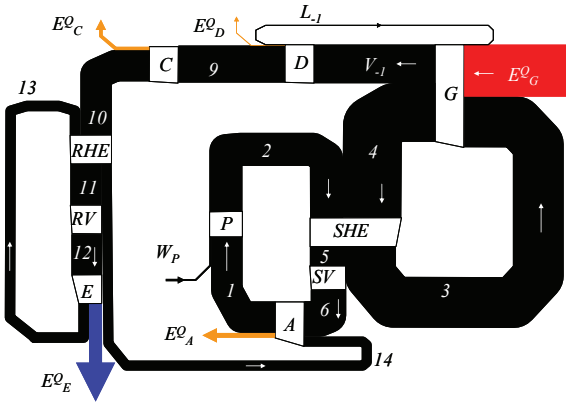

Figure 3. Grassmann diagrams of Cycle II.

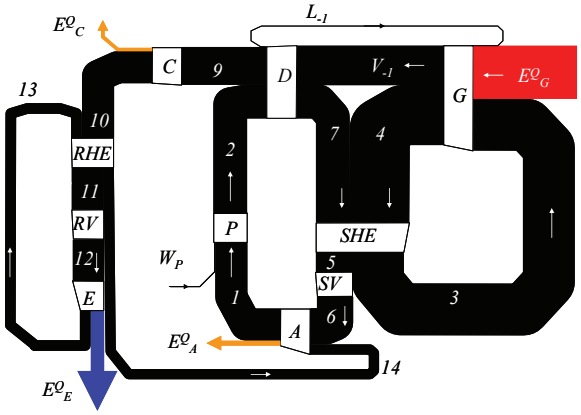

Figure 4. Grassmann diagrams of Cycle III.

4.3 Structural analysis

Once the irreversibilities are obtained, it can be checked how a change of the irreversibility of one component affects the rest of the cycle. In the component, where the minimum temperature difference is modified, the irreversibility increases with a higher minimum temperature difference. For the other components the irreversibilities can increase or decrease depending on the interactions among the components.

The analysis starts with the absorber. The minimum temperature difference $\Delta T_{A,min}$ between solution and cooling water is modified. In *Figure 5* can be observed how the irreversibility of the absorber and of the other components are affected. As $\Delta T_{A,min}$ increases, the concentration difference between weak and strong solution decreases. In order to maintain the cooling capacity, the solution flow rate has to increase. As a direct consequence, the irreversibilities in the solution heat exchanger, the generator, the solution valve and the pump increase. This effect is more accentuated at temperature differences above 5 K, in which case as the absorber $\Delta T_{A,min}$ increases the irreversibility of all components increases. *Figure 5* also shows that the irreversibilities of the absorber and solution heat exchanger are the main contributors to the total irreversibility, followed by the evaporator and condenser.

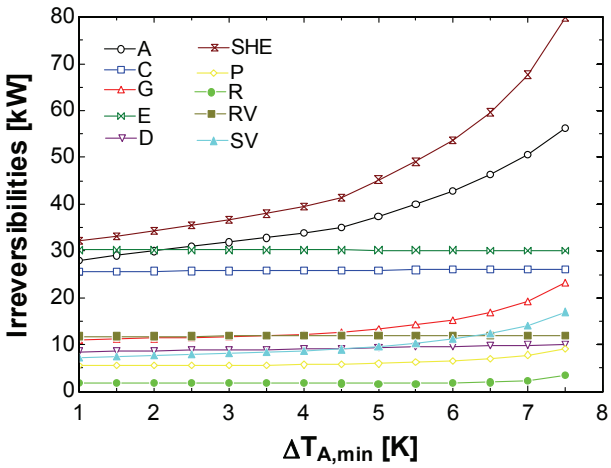

Figure 5: Irreversibilities due to a variation of absorber minimum temperature difference for Cycle I.

Figure 6 presents the total irreversibility of the whole cycle versus the irreversibility of the absorber due to the variations of ΔT_{min} for the cycle configurations considered. The trends for the different cycle configurations are similar, although there are slight differences among the values and slopes of the curves.

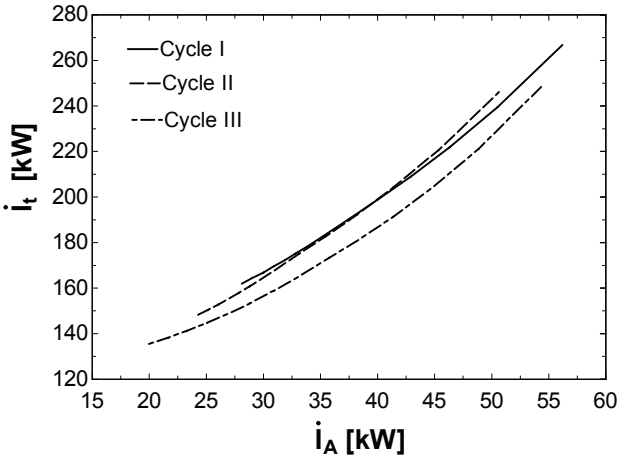

Figure 6: Total irreversibility change versus absorber irreversibility for change of absorber minimum temperature difference.

These observations will be quantified by the *CSB*'s as they correspond to the slope of the curves representing the

ISBN: 978-84-693-7673-7/DL:T-1752-2010

total irreversibility versus the irreversibility of the absorber. Their values are determined by application of Eqn. 1. For the absorber case, such an equation can be rewritten as:

$$CSB_{A;\Delta T_A} = \left(\frac{\Delta \dot{I}_t}{\Delta \dot{I}_A} \right)_{\Delta T_{A,\min}=\text{var}, UA(comp \neq A)=const} \quad (9)$$

Values of the *CSB* for the absorber for the three configurations cycles are presented in *Figure 7*. At higher ΔT_{min} the *CSB*'s are higher. This means that the benefit of increasing the efficiency of a less efficient heat exchange is higher than for an already efficient heat exchanger with a low ΔT_{min}. If the value of the *CSB* is lower than one, the reduction of the irreversibility of the component under consideration is offset by an increase in the irreversibility of the other components. This means that a further improvement of this component is not worthwhile. Cycles I and II have very similar values of *CSB*'s, while cycle III has lower *CSB*'s for minimum temperature differences below 6 K. In the considered range *CSB* values are between 1.7 and 4.5. This means that in all cases a reduction in the irreversibility of the absorber is accompanied by a greater reduction in the cycle's total irreversibility. The change in the slope at a ΔT_{min} of about 4.5 K corresponds to the point where the ΔT_{min} shifts from the hot to the cold side of the heat exchanger. The same phenomenon explains also sudden shifts in the slopes of the *CSB*'s for other components. Once the dependence of the *CSB*'s of the component efficiencies are obtained, we can apply Eqn. 4 to determine the optimum efficiency, which results in the lowest operating cost.

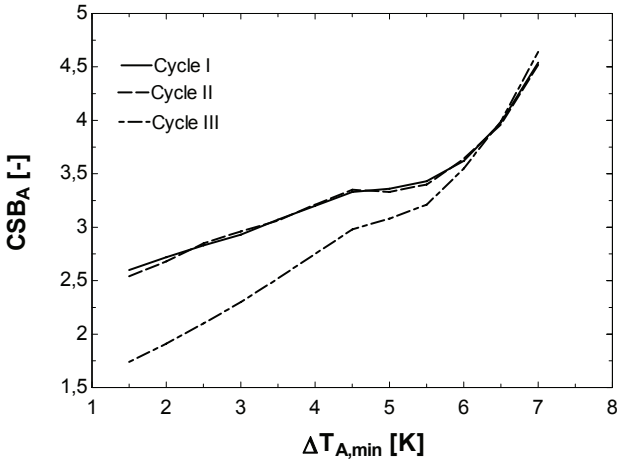

Figure 7: CSB for the absorber.

The same procedure is applied to the other main components of the different cycles in order to obtain the corresponding *CSB*'s (

Figure 8). Comparing the different configurations, very similar values for cycles I and II are found, while values for cycle III are generally slightly higher.

Comparing the different components, the highest *CSB* results are for the refrigerant heat exchanger. Even at small temperature differences values are still much higher than unity. The condenser and evaporator have similar *CSB*'s with values above two. For the generator and solution heat exchanger it seems less interesting to improve their heat transfer efficiencies once ΔT_{min} is below 5 K, as in this range *CSB*'s are near unity. The dephlegmator shows a totally different behaviour with a singularity. While at minimum temperature differences above 15 K *CSB*'s are negative, they change to positive values for lower ΔT_{min}. This means that we should operate at a ΔT_{min} between 10 to 15 K. For lower ΔT_{min} the *CSB* approaches zero and further improvement makes no sense. These different tendencies are due to the strong interactions of the dephlegmator with the rest of the cycle. As the heat exchange efficiency improves the leaving ammonia becomes more pure, but there is an increase in other parameters, namely the heat which has to be dissipated, the temperature difference along the rectification column, and the reflux.

The interactions between the different components can be better understood observing the changes in the irreversibilities in detail. *Table 8* represents the effect of the improvement of one component on the irreversibility of the other components for the three cycle configurations. For each component changes in irreversibilities are presented in two columns, the left in kW and the right in %. The values correspond to the differences of the irreversibility for ΔT_{min} of 1 K and 5 K, except for the dephlegmator (5 K and 30 K). A positive number represents an improvement, which is a reduction in irreversibility. Moreover, there is also a positive interaction if the reduction in the irreversibility of one component also causes a reduction in the irreversibility of other components. A grey background marks the effect on the component itself. A bold number indicates an important improvement (>10%), while an italic number corresponds to strong losses (>10%).

The reduction of the ΔT_{min} of all main components (absorber, generator, evaporator and condenser) affects the pressures and concentrations and leads to a reduction in the solution mass flow ratio. As a consequence, the irreversibility of the solution heat exchanger *SHE* is always reduced. This also benefits other components of the solution circuit such as the pump *P* and the solution expansion valve *SV*.

An improvement of the absorber *A* reduces the solution flow rate and irreversibilities of all components in the solution circuit, including the rectification column and the generator. The same effect occurs with the condenser. As its ΔT_{min} decreases, the high pressure of the cycle is reduced and the solution leaving the generator is weaker in ammonia. The irreversibilities in all components except the absorber are reduced.

The irreversibility is given by the difference between exergy input and exergy output. For the absorber we obtain (for Cycle I):

$$\dot{I}_A = \left[\dot{E}_6 + \dot{E}_{13} - \dot{E}_1\right] - \left[\dot{E}_{16} - \dot{E}_{15}\right] \quad (17)$$

As the heat dissipation increases, the amount of exergy output $\left[\dot{E}_{16} - \dot{E}_{15}\right]$ through the cooling water increases. As the solution flow rate increases, higher exergy flow rates of the solution circuit are obtained. But the exergy of the leaving strong solution $\dot{E}_1$ increases more than the exergy of the entering weak solution $\dot{E}_6$. So, the exergy input $\left[\dot{E}_6 + \dot{E}_{13} - \dot{E}_1\right]$ becomes smaller. Consequently the irreversibility of the absorber decreases.

If in the generator ΔT_{min} decreases the weak solution outlet temperature increases for a fixed hot source temperature. Also, the temperature difference along the rectification column and its irreversibility increases. On the other hand, the component for which a decrease in

ISBN: 978-84-693-7673-7/DL:T-1752-2010

irreversibility results in a decrease in irreversibiilties in all weak solution becomes weaker in ammonia and the solution flow rate decreases, which in general decreases the irreversibility of the other components of the solution circuit.

In the evaporator case, a reduction in the ΔT_{min} increases the refrigerant temperature for given temperatures of the chilled water. The low pressure of the cycle and as a consequence the strong solution concentration of ammonia in the absorber will increase. Due to the higher driving forces for the mass transfer the irreversibility of the absorber increases. The irreversibility of the rectification column increases as the irreversibility on the first plate above the generator mixes liquid and vapour with a higher concentration difference. The irreversibilities for the other components of the solution circuit decrease as the solution flow rate decreases.

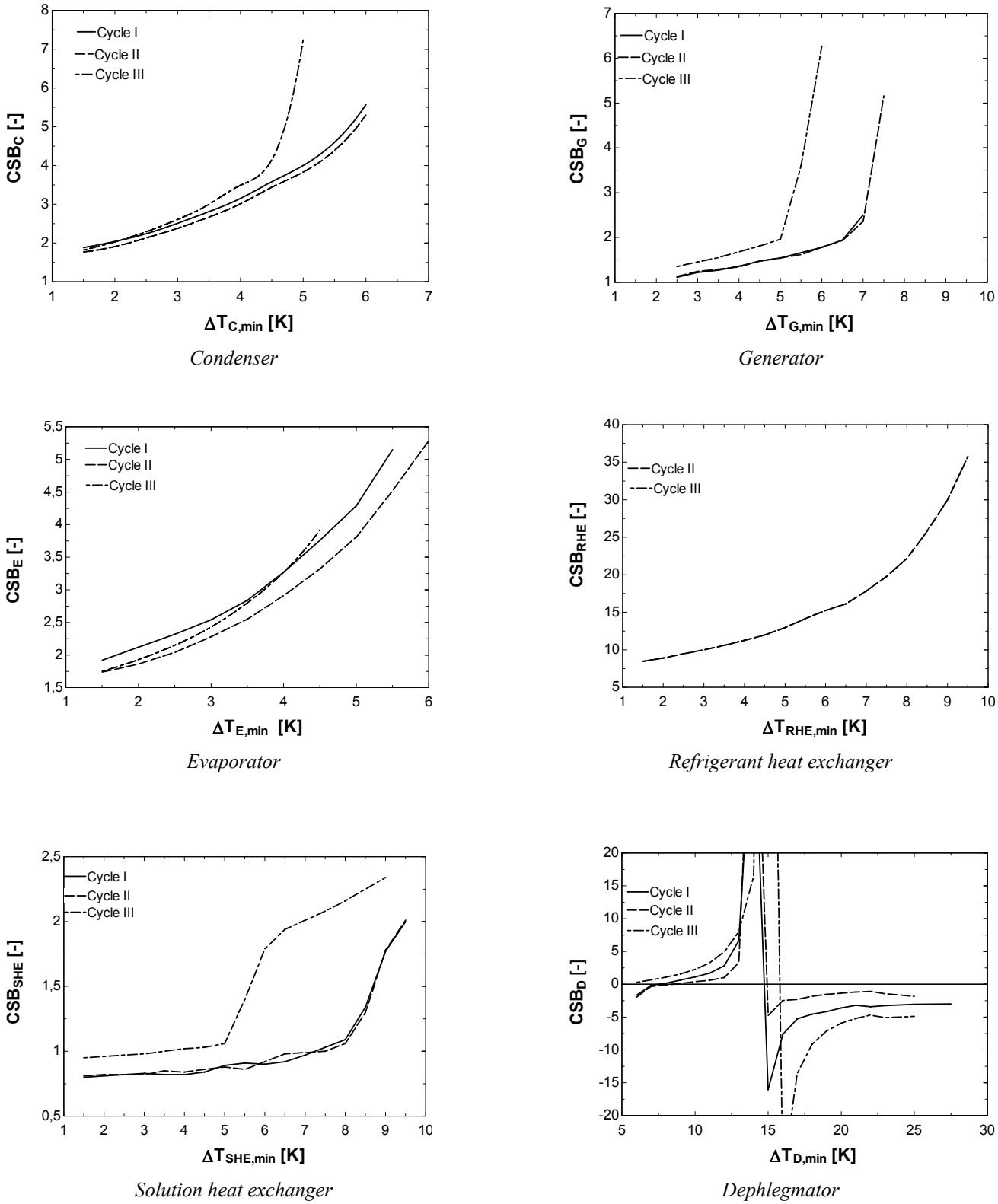

Figure 8: CSB for the main components.

ISBN: 978-84-693-7673-7/DL:T-1752-2010

Table 8: Interactions Between Components (Values Correspond to the Differences of the Irreversibility for ΔT_{min} of 1K and 5K, Except the Dephlegmator (5K And 30K)).

		Effect of the improvement of											
	on the irreversibility of	A		C		G		E		RHE		SHE	
		kW	%	kW	%	kW	%	kW	%	kW	%	kW	%
Cycle I	R	-0.2	-12	-0.1	-4	-0.3	-16	-0.3	-16			0.2	13
	A	9.4	25	-8.9	-24	-4.9	-13	-5.6	-15			-2.9	-8
	C	0.3	1	12.6	49	-0.2	-1	0.6	2			-0.4	-2
	G	2.3	17	4.3	32	12.3	92	3.5	26			4.1	31
	E	0	0	0.1	0	0	0	15.6	52			0.1	0
	D	0.8	9	0.8	8	-0.7	-7	1.2	13			-1.3	-14
	RHE												
	SHE	13.1	29	14.8	33	6.8	15	20.2	45			16.2	36
	P	0.4	7	3.4	57	1.4	24	1.1	19			-0.4	-8
	RV	0	0	2.5	21	0	0	2.5	21			0	0
	SV	2.4	25	3.6	37	1.5	16	3.7	39			-2.1	-22
	Cycle	28.5	15	33	17	15.9	8	42.3	22			13.3	7
Cycle II	R	-0.2	-12	-0.1	-4	-0.3	-16	-0.2	-16	0	-0.1	0.2	13
	A	8.8	27	-8.6	-26	-4.6	-14	-6.2	-19	0	0.1	-2.7	-8
	C	0.2	1	11.8	48	-0.2	-1	0.2	1	0.4	1.5	-0.4	-2
	G	2.2	17	3.8	30	11.6	92	3	24	0.4	3.2	3.9	31
	E	0	0	0.1	0	0	0	15.6	52	0	0	0.1	0
	D	0.8	9	0.7	8	-0.6	-7	1	12	0.1	0.7	-1.3	-14
	RHE	0	1				-1	0.6	25	0.4	15.9		
	SHE	12.3	29	13.6	32	6.4	15	18.6	44	0.9	2.2	15.3	36
	P	0.4	7	3.2	56	1.3	24	1	17	0.1	2.3	-0.4	-7
	RV	0	-1	1.1	21	0	0	0.8	17	0.7	13.4	0	1
	SV	2.3	25	3.3	36	1.4	16	3.4	38	0.2	1.9	-2.1	-22
	Cycle	26.7	15	29.3	17	15.1	9	37.7	22	3.2	1.8	12.7	7
Cycle III	R	-0.7	-44	-0.1	-4	-0.2	-15	-0.2	-13	0	0.3	0.3	19
	A	15.8	44	-6.1	-17	-3	-8	-2.7	-8	0.2	0.5	-0.6	-2
	C	0.9	4	11.6	47	-0.3	-1	0	0	0.4	1.5	-1.3	-4
	G	2.5	20	4	32	11.5	93	3	25	0.5	3.8	3.8	31
	E	-0.1	0	0.1	0	0	0	15.6	52	0	0	0.1	0
	D	0.4	5	1.1	15	-0.3	-4	1.5	21	0.1	0.8	-0.6	-8
	RHE	0.1	5			0	-1	0.5	24	0.4	16	-0.1	-3
	SHE	15.6	39	13.7	34	7.5	19	18.3	46	1.2	2.9	14.2	36
	P	0.2	4	3.1	55	1.3	24	0.8	15	0.1	2.4	-0.3	-5
	RV	-0.1	-2	1.1	22	0	1	0.9	17	0.7	13.5	0.1	1
	SV	3.3	37	3.5	39	1.6	18	3.8	42	0.2	2	-1.6	-18
	Cycle	38	22	32.5	19	18.2	11	41.6	24	3.6	2.1	14	8

A component for which a decrease in irreversibility results in a decrease in irreversibiilties in all components is the refrigerant heat exchanger. Not only is this component's irreversibility reduced if ΔT_{min} is reduced, but also there is a considerable reduction in the irreversibilities of the refrigerant valve and solution heat exchanger. One way to explain this effect is that for a fixed cooling demand, if the refrigerant heat exchanger is more efficient, the enthalpy of the refrigerant entering the evaporator becomes lower, while the evaporator exit enthalpy remains constant. Therefore a lower refrigerant mass flow is needed for a given cooling power. This induces a reduction in all mass flows in the cycle. As a consequence, a strong reduction in the solution heat exchanger irreversibility is found. These high values of *CSB* appear both for Cycles II and III. As the thermal power of the refrigerant heat exchanger is only small, its effect on the total irreversibility remains limited to 7 to 8 %.

The improvement of the solution heat exchanger in Cycle I and II has a small impact on the other components except the generator and the rectification column due to the increase of the solution temperature entering the rectification plates. This is reflected by lower *CSB* values than in Cycle III.

In general strong interactions between the components can be observed, which in general cannot be quantified easily. Since *CSB* values depend on the components, their interactions with the rest of the cycle and the operating conditions, their use simplifies exergy analyses as direct positive or negative interactions can be found observing the value of the *CSB*'s. It can be concluded that the *CSB's* are helpful parameters, which enable us to better understand the behaviour of absorption cycles and offer a possibility to gain more insight in the thermodynamics of absorption cycles. Furthermore they can be used in economic optimisation.

5. Conclusions

Energy, exergy and structural analyses have been achieved for different configurations of ammonia-water absorption cooling cycles. The exergy analysis determines the irreversibilities of the different components and the whole cycle. But irreversibilities alone do not indicate how to improve the cycle in order to obtain the largest benefit.

To do so, the structural analysis using the coefficients of structural bonds (*CSB*) is applied. The *CSB*'s indicate how the irreversibility change in one component affects the rest of the system. This analysis includes a variation of the minimum temperature difference ΔT_{min} or *UA*-value of one component, while the *UA*-values of the other components are fixed. In this way, the effect on the irreversibility change in all the considered components of the whole cycle can be quantified by the *CSB*'s. They are different for each component and cycle configuration and also vary with the ΔT_{min} or *UA*-value.

Results show, as expected, that it is more beneficial to improve less efficient components with high ΔT_{min} or low *UA*-values rather than components which already operate with low ΔT_{min}. The components with the highest impact on the cycle as a whole are identified, and the refrigerant heat exchanger has the highest *CSB* values. Values which are in general significantly higher than unity can be seen in the evaporator, the condenser, the generator and the absorber. Values around unity are found for the solution heat exchanger. The dephlegmator shows a different behavior due to its strong interactions with the rest of the cycle. Differences between the cycle configurations are generally small.

In summary, once the exergy balances for a cycle have been established and the irreversibilities have been obtained, the structural method presents a useful method for better understanding and quantifying the interactions in the cycle. With the *CSB*, the most cost-effective cycle for a given set of operating parameters can be obtained. However, as is presented in Eqn. 8 the optimum efficiency values of each component depend also on the energy cost and the capital investment and the annual operation time.

Acknowledgements

This research project was financially supported by the "Ministerio de Ciencia y Tecnología – Dirección general de investigación" of Spain (DPI2002-00706).

Nomenclature

a^c	Capital recovery factor (-)
b^c	Part of the annual operation cost which is not affected by the optimisation (€)
c^e_{in}	Unitary cost of input exergy (€/kWh)
$c^l_{k,i}$	Unit cost of irreversibility (€/kWh)
C^c_l	Capital cost of the component l (€)
C_t	Annual operation cost (€)
COP	Coefficient of performance (-)
CSB	Coefficients of structural bonds (-)
e	Specific exergy (kJ kg^{-1})
$\dot{E}$	Exergy flow (kW)
$\dot{E}_{in}$	Input exergy flow (kW)
h	Specific enthalpy (kJ kg^{-1})
i	Interest rate (-)
$\dot{I}$	Irreversibility (kW)
$\dot{m}$	Mass flow (kg s^{-1})
n	Years of repayment
p	Pressure (bar)
s	Specific entropy (kJ kg^{-1} K^{-1})
t_{op}	Annual operation time (h)
T	Temperature (ºC or K)
UA	Product of heat transfer coefficient and heat transfer area (kW/K)
$\dot{W}_{pump}$	Pump power (kW)
x_i	Parameter in the efficiency variation of the *CSB*
z	Mass fraction of ammonia (kg/kg)

Greek letters

ΔT_{min}	Minimum temperature difference in a heat exchanger (K)
$\xi_{k,i}$	Capital cost coefficient (€/kW)
Ψ	Exergetic efficiency of the cycle (-)

Subscripts

i	inlet
e	exit
k	component k
t	total
0	environmental state (25ºC, 1 bar)

Components

A	Absorber
C	Condenser
D	Dephlegmator
E	Evaporator
G	Generator
P	Solution pump
R	Adiabatic rectification plates
RHE	Refrigerant heat exchanger
RV	Refrigerant expansion valve
SHE	Solution heat exchanger
SV	Solution expansion valves

References

Anand, D. K., K. W. Lindler, et al., 1984. "Second-Law Analysis of Solar-Powered Absorption Cooling cycles and systems,." *J. Solar Energy Eng* 106: 291-298.

Ataer, E. and Y. Gögus, 1991. "Comparative study of irreversibilities in an aqua-ammonia absorption refrigeration system." *International Journal of Refrigeration* 14(2): 86-92.

Bejan, A., G. Tsatsaronis, et al., 1996. *Thermal Design & Optimization*. New York, John Wiley & Sons Inc.

Best, R., J. Islas, et al., 1993. "Exergy Efficiency of an Ammonia-Water Absorption System for Ice Production." *Applied Energy* 45: 241-256.

Beyer, J., 1970. Structural analysis- necessary part of efficiency analysis of thermal systems [Strukturuntersuchungen- notwendiger Bestandteil der Effektivitätsanalyse von Wärmeverbrauchersystemen]. *Energie-anwendung* 19(12): 358-361.

Beyer, J., 1974. "Structure of thermal systems and economical optimisation of system parameters [Struktur wärmetechnischer Systeme und ökonomische Optimierung der Systemparameter]." *Energieanwendung* 23(9): 274-279.

Boer, D., M. Medrano, et al., 2005. "Exergy and structural analysis of an absorption cooling cycle and the effect of efficiency parameters." *International Journal of Thermodynamics* 8(4): 191-198.

Dentice d'Accadia, M. and F. de Rossi, 1998. "Thermoeconomic optimization of a refrigeration plant." *International Journal of Refrigeration* 21(3): 42-54.

ISBN: 978-84-693-7673-7/DL:T-1752-2010

Dentice d'Accadia, M. and L. Vanoli, 2004. "Thermoeconomic optimisation of the condenser in a vapour compression heat pump." *International Journal of Refrigeration* 27(4): 433-441.

Dingeç, H. and A. Ileri, 1999. "Thermoeconomic optimization of simple refrigerators." *International Journal of Energy Research* 23(11): 949-962.

El-Sayed, Y. M., 2003. *The Thermoeconomics of energy conversions*. Amsterdam Boston.

Ferrer, M. A., M. A. Lozano, et al., 2001. "Thermoeconomics applied to Air-Conditioning Systems." *ASHRAE Transactions AT-01-9-2*.

Jeong, J., K. Saito, et al., 2003. *Optimum design method for a single effect absorption refrigerator based on the first and second law analysis*. 21st IIR International Congress of Refrigeration, Washington, DC (USA).

Jonsson, M. and Y. Jinyue, 2000. "Exergy and Pinch Analysis of Diesel Engine Bottoming Cycles with Ammonia-Water Mixtures as Working Fluid." *Int.J. Applied Thermodynamics* 3(2): 57-71.

Karakas, A., N. Egrican, et al., 1990. "Second law analysis of solar absorption-cooling cycles using Lithium Bromide/Water and Ammonia/Water as Working Fluids." *Applied Energy* 37: 169-197.

KizIlkan, Ö., A. Sencan, et al., 2007. "Thermoeconomic optimization of a LiBr absorption refrigeration system." *Chemical Engineering and Processing: Process Intensification* 46(12): 1376-1384.

Kotas, T., 1995. *The Exergy Method of Thermal Plant Analysis*. Melbourne, Florida, Krieger Publishing Company.

Misra, R. D., P. K. Sahoo, et al., 2003. "Thermoeconomic optimization of a single effect water/LiBr vapour absorption refrigeration system." *International Journal of Refrigeration* 26(2): 158-169.

Misra, R. D., P. K. Sahoo, et al., 2005. "Thermoeconomic evaluation and optimization of a double-effect H2O/LiBr vapour-absorption refrigeration system." *International Journal of Refrigeration* 28(3): 331-343.

Misra, R. D., P. K. Sahoo, et al., 2006. "Thermoeconomic evaluation and optimization of an aqua-ammonia vapour-absorption refrigeration system." *International Journal of Refrigeration* 29(1): 47-59.

Roriz, L. and A. Mortal, 2003. *Study on distillation solutions for a solar assisted absorption heat pump*. Eurotherm seminar 72: Thermodynamics, heat and mass transfer of refrigeration machines and heat pumps, Valencia, Spain, Ed. Pub. IMST-UPV.

Sahin, B. and A. Kodal, 2002. "Thermoeconomic optimization of a two stage combined refrigeration system: a finite-time approach." *International Journal of Refrigeration* 25(7): 872-877.

Szargut, J., D. Morris, et al., 1988. Exergy Analysis of Thermal, Chemical, and Metallurgical Processes.

Sözen, A., 2001. Effect of heat exchangers on performance of absorption refrigeration systems. *Energy Conversion and Management* 42(14): 1699-1716.

Tillner Roth, R. and D. Friend, 1998. A Helmholtz Free Energy Formulation of the Thermodynamic Properties of the mixture {Ammonia + Water}. *J.Phys.Chem.Ref.Data* 27(1): 63-96.

Tozer, R. and M. A. Lozano, 1999. *Thermo-economic optimisation of a single effect absorption chiller and cooling tower*. International Sorption Heat Pump Conference. Munich: ZAE Bayern.

Wall, G., 1986. "Thermoeconomic Optimization of a Heat-Pump System." *Energy* 11(10): 957-967.

Zhang, G. Q., L. Wang, et al., 2004. "Thermoeconomic optimization of small size central air conditioner." *Applied Thermal Engineering* 24(4): 471-485.

INTERNATIONAL JOURNAL OF REFRIGERATION 33 (2010) 529–537

available at www.sciencedirect.com

ScienceDirect

journal homepage: www.elsevier.com/locate/ijrefrig

Optimum heat exchanger area estimation using coefficients of structural bonds: Application to an absorption chiller

Berhane H. Gebreslassie [a], *Marc Medrano* [b], *Filipe Mendes* [c,d], *Dieter Boer* [a,*]

[a] *Department of Mechanical Engineering, University Rovira i Virgili, Tarragona 43007, Spain*
[b] *GREA Innovació Concurrent, Edifici CREA, Universitat de Lleida, Lleida, Spain*
[c] *Departamento de Física, Instituto Superior Técnico, Technical University of Lisbon, Lisbon, Portugal*
[d] *ICIST, Instituto Superior Técnico, Technical University of Lisbon, Lisbon, Portugal*

ARTICLE INFO

Article history:
Received 4 May 2009
Received in revised form
17 September 2009
Accepted 4 December 2009
Available online 16 December 2009

Keywords:
Absorption system
Chiller
Design
Optimisation
Area
Heat exchanger

ABSTRACT

The optimum allocation of the heat exchange area considers both running and investment cost. The structural method of thermoeconomic optimization is used to derive a simple equation for the estimation of the economic optimum of the area of a heat exchanger integrated in a more complex system. The obtained equation is generally valid for thermal systems. The optimum heat exchange area can be estimated in a straightforward calculation once operation and cost parameters, the overall heat transfer coefficient and the Coefficient of Structural Bonds (CSB) are known. The CSB quantifies the interactions between the units of the thermal system and is obtained from an exergy analysis. Therefore, compared to former work, the proposed equation has the advantage of considering interactions between the units of the system. A case study is presented for an ammonia-water absorption chiller. The optimum area from the proposed formulation is compared with the results obtained from the integrated optimization algorithm of EES (from *F*-Chart) and the base cases for different annual operation time.

Détermination de la surface d'échange de chaleur optimale à l'aide des coefficients des liens structurels: application à un refroidisseur à absorption

Mots clés : Système à absorption ; Refroidisseur ; Conception ; Optimisation ; Surface ; Échangeur de chaleur

* *Corresponding author*. Tel.: +34 977 559631; fax: +34 977 559691.
E-mail address: Dieter.Boer@urv.net (D. Boer).
0140-7007/$ – see front matter © 2009 Elsevier Ltd and IIR. All rights reserved.
doi:10.1016/j.ijrefrig.2009.12.004

Nomenclature

Abbreviations

A	Absorber
C	Condenser
D	Desorber
EES	Engineering Equation solver
E	Evaporator
P	Solution pump
RV	Refrigerant expansion valve
SC	Subcooler
SHX	Solution heat exchanger
SV	Solution expansion valve
yr	Year

Variables

a^c	Capital recovery factor [–]
A_k	Area of heat exchanger k [m^2]
b^c	Cost factors, which are not affected by optimization [euro]
$c^l_{k,i}$	Unit cost of exergy destruction [euro kWh^{-1}]
C_c	Annual capital cost [euro]
C_{op}	Annual running cost [euro]
C_t	Annual total cost [euro]
C^c_k	Capital cost of unit k [euro]
COP	Coefficient of performance [–]
CSB	Coefficient of structural bonds [–]
E_{in}	Rate of fuel exergy consumed [kW]
e_j	Specific exergy of stream j [$kJ\,kg^{-1}$]
h_j	specific enthalpy of stream j [$kJ\,kg^{-1}$]
m_j	Mass flow rate of stream j [$kg\,s^{-1}$]
P_j	Pressure of stream j [MPa]
Q_k	Heat transfer rate to unit k [kW]
s_j	Specific entropy of stream j [$kJ\,kg^{-1}\,K^{-1}$]
S_k	Entropy production in unit k [$kW\,K^{-1}$]
T_j	Temperature of stream j [°C or K]
ΔT^{lm}_k	Logarithmic mean temperature difference [K]
$\Delta \overline{T}_k$	Arithmetic mean temperature difference [K]
$\tilde{T}$	Thermodynamic mean temperature [K]
$\overline{T}$	Arithmetic mean temperature [K]
W_k	Mechanical power done by unit k [kW]
x_i	Parameter related to efficiency of units [m^2 or K]
$z_{i,j}$	Mass fraction of component i in stream j [–]

Greek letters

$\xi_{k,\,i}$	Capital cost coefficient [euro kW^{-1}]

Parameters

b	Specific cost of heat exchanger [euro m^{-2}]
$c_{in}{}^e$	Specific cost of exergy [euro kWh^{-1}]
ir	Interest rate [–]
n	Years for the repayment [yr]
nu	The number of units in absorption cycle [–]
t_{op}	Operation time [$h\,yr^{-1}$]
U_k	Overall heat transfer coefficient of unit k [$kW\,m^{-2}\,K^{-1}$]

Subscripts

0	Environment state
c	Cold
h	Hot
i	Component of a stream
j	Streams
k	Unit
t	Total

Sets

IN(k)	Set of input streams to unit k
OUT(k)	Set of output streams from unit k

1. Introduction

Heat exchangers are important units in thermal systems. The area should be sized to optimize economic performance and be distributed in order to obtain the maximum performance for a given available total area. The optimum refers to the design with the lowest total cost, determined mostly by the investment and running cost. The final purpose is the design of more cost-effective systems.

An example of thermal systems, which are mainly composed by heat exchangers are absorption cycles. In these systems the heat exchangers are the main source of exergy destruction and the dominant investment cost factor. The problem of optimum area allocation has initially been discussed for endoreversible cycles, where the internal exergy destruction is neglected. These approaches indicates how to distribute the heat conductance among the external heat exchangers (Bejan et al., 1995; Herold and Radermacher, 1990; Klein, 1992). The ''square root criterion'' (Summerer, 1996; Ziegler, 1997, 1999) includes the effect of parameters as the specific cost of the heat exchanger surface, the overall heat transfer coefficient and the mean temperature of the heat exchanger. Summerer (1996) performed a large number of numerical simulations of cycles in order to create a database of the best-obtained design options. More recent work used the exergy-based concept of thermoeconomic optimization. Misra et al. (2003, 2006) used an average cost approach and the minimization of the overall running and amortization cost.

Another exergy based method is the structural method, which has been developed by Beyer (1970, 1974). It uses the unitary cost of exergy and structural coefficients. This thermoeconomic optimization methodology has been applied by Dingeç and Ileri (1999) for a vapor compression refrigerator, by Dentice d'Accadia and Vanoli (2004) for the design of a condenser of a compression cycle and recently by KizIlkan et al. (2007), for a water-LiBr absorption refrigeration system. These works used the general optimization equation in order to obtain the numerical solutions for the considered problems.

In this work the structural method is used to derive a simple correlation for the straight forward estimation of the optimum area of a heat exchanger in a thermal system. This correlation has some similarity with the square root criterion developed by Ziegler, but goes further considering also interactions between the units. It describes the effect of the main parameters and includes as a new feature the Coefficient of Structural Bonds (CSB). The CSB is obtained from an exergy analysis and describes the interaction of the different units of a system among each other. Thus, this method enables us to optimize each unit individually, without the need of optimizing simultaneously the whole system. A case study is presented for the analysis of an ammonia water absorption chiller. The results of the proposed correlation are compared with the results obtained by a numerical optimization method. Finally, benefits and limitations are discussed.

2. Problem statement

In this work we address the optimal design of an absorption chiller based on the thermoeconomic optimization that follows structural method. Given are the cooling capacity of the system, the inlet and outlet temperatures of the external fluids and cost data. The goal is to determine the optimal design and the resulting benefits compared to the base case. The mathematical model derived to address this problem is explained in detail in the following sections.

3. Thermoeconomic optimization

The mathematical formulation includes three main types of constraints: (1) general equations based on energy, materials and exergy balances that obeys the first and second law of thermodynamics, (2) the structural method based on the CSB's and (3) objective function equations that assess the economic performances of the system. All sets of equations are described in detail next.

3.1. General constraints

As mentioned before, these equations are added to enforce the mass and energy conservation in steady state. These principles are applied to all the units of the system, each of which is treated as a control volume with inlet and outlet streams, heat transfer and work interactions (Herold et al., 1996; Kotas, 1995) (see Fig. 1). This is accomplished via the following equations:

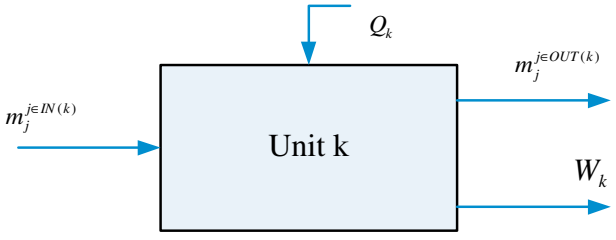

Fig. 1 – A generic unit of the absorption cycle.

$$\sum_{j\in IN(k)} m_j z_{i,j} - \sum_{j\in OUT(k)} m_j z_{i,j} = 0 \quad \forall k, i \tag{1}$$

Eq. (1) represents the mass balances, and states that the total amount of component i that enters unit k must equal the total amount of i that leaves k. In this equation, m_j denotes the mass flow rate of stream j, and $z_{i,j}$ is the mass fraction of component i in stream j. Note that j can be either an inlet or outlet stream. Hence, in this equation IN(k) denotes the set of inlet streams of unit k, whereas OUT(k) represents the set of outlet streams.

$$\sum_{j\in IN(k)} m_j h_j - \sum_{j\in OUT(k)} m_j h_j + Q_k - W_k = 0 \quad \forall k \tag{2}$$

Eq. (2) defines the energy balance in the system assuming no heat losses. Note that the heat transfer rate and mechanical power terms in Eq. (2) can take a zero value in some of the units.

The exergy destruction (I_k) results from the exergy balance given by Eq. (3), where e_j denotes the specific exergy of stream j. T_0 is the environment temperature and T_j the temperatures at which the heat is transferred.

$$\sum_{j\in IN(k)} m_j e_j - \sum_{j\in OUT(k)} m_j e_j + \sum_{j\in IN(k)} \left(1-\frac{T_0}{T_j}\right) Q_k - W_k - I_k = 0 \quad \forall k \tag{3}$$

The coefficient of performance (COP) is determined via Eq. (4) as the ratio between the energy extracted from the chilled water and the total energy supplied to the system (Herold et al., 1996).

$$COP = \frac{Q_{k=E}}{Q_{k=D} + W_{k=P}} \tag{4}$$

The heat exchangers are modeled using the logarithmic mean temperature difference (ΔT_k^{lm}), the heat transfer area (A_k) and the overall heat transfer coefficient (U_k), as shown in Eq. (5).

$$Q_k = U_k A_k \Delta T k^{lm} \quad \forall k \tag{5}$$

3.2. Structural method

The thermoeconomic analysis combines the thermodynamic analysis by first and second law with economics. Initially, the second law analysis is used in order to determine the exergy destruction in the units and the whole system. In continuation a sensitivity analysis shows how a change of the efficiency of 1 unit changes its exergy destruction and affects the exergy destruction of the whole system. In the case of a heat exchanger, the area is varied. This analysis enables us to evaluate the effect of an improvement of this unit on the global performance. The effect can be quantified by the so-called coefficients of structural bonds (CSB). The CSB of a unit k, which is obtained by variation of a parameter x_i is defined by

$$CSB_{k,i} = \left(\frac{dI_t}{dI_k}\right)_{x_i=var} \tag{6}$$

I_k is the exergy destruction rate of unit k, I_t is the exergy destruction rate of the whole system. The parameter x_i is related to the efficiency of the units. The parameter x_i can be the minimum temperature difference, the effectiveness or

the heat exchange area. Structural coefficients consider how the exergy destruction of the whole system and a single unit are related. If a slight decrease of the exergy destruction of 1 unit due to an increased efficiency causes an important decrease in the total exergy destruction of the system (high CSB), it will be wise to put much of the design effort in improving the efficiency of this unit. Otherwise (low CSB), an improvement of the efficiency of the considered unit is not worthwhile. These CSB's can be used in the structural method of the thermoeconomic optimization, the final purpose of which will be the design of more cost-effective systems. The use of the CSB for the thermoeconomic optimization is explained next. More details can be found in Kotas (1995).

3.3. *Objective function*

For a unit, its optimum efficiency specification will be determined in order to obtain the minimum annual total cost C_t, which represents the objective function (Eq. (7)).

$$C_t(x_i) = t_{op} c^e_{in} E_{in}(x_i) + a^c \sum_{l=1}^{nu} C^c_l(x_i) + b^c \tag{7}$$

The first term in the right hand side of Eq. (7) corresponds to the running or fuel cost, which depends on the operation time t_{op}, the specific cost of exergy $c_{in}{}^e$ and the rate of fuel exergy consumed $E_{in}(x_i)$. The second term accounts for the capital investment amortization, which is the sum of the capital cost of the units $\sum_{l=1}^{nu} C^c_l(x_i)$ multiplied by the capital recovery factor a^c. The subindex "l" refers to the lth unit of the system consisting of nu number of units. The capital recovery factor depends on the interest rate 'ir' and the years for the repayment n and is given by Eq. (8).

$$a^c = \frac{ir(ir+1)^n}{(ir+1)^n - 1} \tag{8}$$

The last term b^c includes other cost factors, which are not affected by the optimization, as for example the maintenance costs. Both fuel cost and capital cost depend on the parameter x_i. The best design with the optimum value of x_i corresponds to the lowest possible annual operation cost.

By some reorganization and differentiation of the objective function with respect to x_i results Eq. (9) (see Kotas (1995)).

$$\frac{dC_t}{dx_i} = t_{op} c^l_{k,i} \frac{dI_k}{dx_i} + a^c \frac{dC^c_k}{dx_i} \tag{9}$$

$c_{k,i}{}^l$ denotes the unit cost of exergy destruction given by:

$$c^l_{k,i} = c^e_{in} CSB_{k,i} + \frac{a^c}{t_{op}} \xi_{k,i} \tag{10}$$

The term $\xi_{k,i}$ represents the capital cost coefficient defined as:

$$\xi_{k,i} = \sum_{l'=1}^{nu} \left[\frac{dC^c_{l'}}{dx_i} \right]_{x_i = var, l' \neq k} \tag{11}$$

$\xi_{k,i}$ represents the effect of x_i on the capital cost of the units which are not optimized ($l' \neq k$). k refers to the unit to be optimized. In a first approximation, the contribution of the capital cost coefficient can be neglected (Kotas, 1995). The unit cost of exergy destruction becomes:

$$c^l_{k,i} \approx c^e_{in} CSB_{k,i} \tag{12}$$

In the optimum point Eq. (9) becomes zero, resulting in Eq. (13)

$$t_{op} c^e_{in} CSB_{k,i} \frac{dI_k}{dx_i} = -a^c \frac{dC^c_k}{dx_i} \tag{13}$$

From Eq. (13) the value of x_i, e.g. an area or a minimum temperature difference, which results in the lowest operating cost C_t can be obtained. It depends only on parameters of the unit k, which is the unit under consideration in the optimization. The interaction with the system is taken into account by the CSB. The term dI_k/dx_i describes the effect of the efficiency parameter x_i on the exergy destruction of the unit and dC^c_k/dx_i takes into account the dependence of the unit cost on x_i. Both parameters depend on the efficiency of the analyzed unit. KizIlkan et al. (2007) applied Eq. (13) to each unit of the absorption cycle and obtained the numerical results for the optimum heat transfer areas.

In the present work a different approach is applied in order to obtain a simplified equation which enables us to estimate the optimum area of the heat exchangers in a more straightforward way. Some exactitude will be lost in the results, but more insight in the parameters affecting the optimization problem can be obtained, which represents an advantage compared to a numerical optimization.Eq. (13) can be simplified supposing that the heat exchanger cost is proportional to its area (Ziegler, 1997)

$$Ck^c = bA_k \tag{14}$$

and that the logarithmic mean temperature difference is approximated by the arithmetic mean temperature difference. Eq. (5) can be expressed as:

$$Q_k \approx U_k A_k \Delta\overline{T}_k \tag{15}$$

Combining and differentiating Eqs. (14) & (15) results:

$$\frac{dC^c_k}{d(\Delta\overline{T}_k)} \approx -\frac{bQ_k}{U_k} \frac{1}{\Delta\overline{T}^2_k} \tag{16}$$

The exergy destruction due to the temperature difference in the heat exchange is given by (Ziegler, 1997):

$$I_k = T_0 Q_k \left(\frac{1}{\tilde{T}_c} - \frac{1}{\tilde{T}_h} \right) \tag{17}$$

$\tilde{T}_h$ and $\tilde{T}_c$ are the thermodynamic mean temperatures for the hot and cold fluid in unit k, which are defined by:

$$\tilde{T}_k = \frac{Q_k}{S_k} \tag{18}$$

with $T \gg \Delta T$ Eq. (17) becomes

$$I_k \approx T_0 Q_k \left(\frac{\Delta\overline{T}_k}{\tilde{T}_h \tilde{T}_c} \right) \tag{19}$$

The product of the thermodynamic mean temperature will be approximated by the arithmetic mean temperature of the unit.

$$\tilde{T}_h\tilde{T}_c \approx \overline{T}_k^2 \tag{20}$$

where

$$\overline{T}_k = \frac{T_h^{IN} + T_c^{IN}}{2} \tag{21}$$

leading to

$$\frac{dI_k}{d(\Delta\overline{T}_k)} \approx \frac{T_0 Q_k}{\overline{T}_k^2} \tag{22}$$

Substituting Eqs. (16) & (22) in Eq. (13) results in Eq. (23).

$$\Delta\overline{T}_{k,opt} \approx \sqrt{\frac{a^e b}{t_{op} c_{in}^e CSB_{k,i} U_k}\frac{\overline{T}_k^2}{T_0}} \tag{23}$$

This equation estimates the arithmetic mean temperature difference for the heat exchanger k, which results in the lowest operation cost. Note that units for temperatures are in Kelvin. The value of the optimum temperature difference increases with capital cost (capital recovery factor, specific cost of the heat exchanger) and with the mean temperature of the unit as the entropy flow and thus the exergy destruction for the same heat flow is higher at lower temperatures. It decreases with higher operation time, cost of energy, CSB and heat transfer coefficient. The corresponding heat exchanger area can then be obtained with Eq. (15).

$$A_{k,opt} \approx Q_k \sqrt{\frac{t_{op} c_{in}^e CSB_{k,i}}{a^e b U_k}\frac{T_0}{\overline{T}_k^2}} \tag{24}$$

Eqs. (23) and (24) can be used once the CSB's have been determined from an exergy analysis. The influence of the overall heat transfer coefficient and specific heat exchanger cost is the same as commented by Ziegler (Ziegler, 1998): "Specific cost and heat transfer coefficient are taken into account with the square root. Large driving temperature differences are required for expensive surfaces or bad transfer coefficients. However the driving temperature difference should be somewhat larger in the exchanger at high temperatures." The most significant difference results from the consideration of the interactions between units and cycle by the coefficient of structural bonds. This becomes especially important for large values of the CSB.

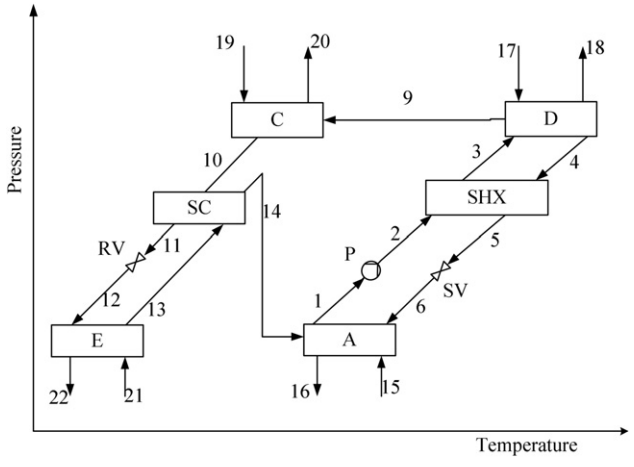

Fig. 2 – Schematics of an ammonia-water absorption chiller.

4. Case study: ammonia–water absorption chiller

The capabilities and limits of our approach are illustrated through a case study that addresses the design of an absorption chiller (see Fig. 2). The system is an absorption chiller driven by low grade heat optimized to be used with compound parabolic concentrator solar collectors (Mendes and Collares-Pereira, 1999). The chiller was built and tested at the Instituto Superior Técnico of the Technical University of Lisbon. It uses ammonia–water as working pair, is indirectly cooled by air (dry cooling tower) and has a nominal cooling capacity of 5 kW.

4.1. *System description*

Compared to a compression cooling cycle, the basic idea of an absorption cycle is to replace the electricity consumption associated with the vapor compression by a thermally driven absorption–desorption system (Herold et al., 1996). This is accomplished by making use of absorption and desorption processes that employs suitable working fluid pairs. The working pair consists of a refrigerant and an absorbent. In this study, without loss of generality, an ammonia-water solution is used as working pair, ammonia being the refrigerant and water the absorbent.

Fig. 2 represents the considered absorption chiller in a pressure–temperature plot. The system provides chilled water for cooling applications and is driven by hot pressurized water at 110 °C. The basic units are the absorber (A), condenser (C), desorber (D) and evaporator (E). The cycle also includes the refrigerant subcooler (SC), refrigerant expansion valve (RV), solution heat exchanger (SHX), solution pump (P), and solution expansion valve (SV). The high pressure equipments are the solution heat exchanger, desorber, and condenser, whereas the low pressure ones are the evaporator and absorber.

The system operation is as follows. The refrigerant in vapor phase (stream 14) coming from the subcooler (SC) is absorbed in absorber (A) by the diluted liquid solution (stream 6). The concentrated solution (stream 1) leaving the absorber is pumped by pump (P) to reach a higher pressure (stream 2) before being preheated in the solution heat exchanger (SHX). Then, the solution (stream 3) enters the desorber, in which the desorption of ammonia takes place. Only the stripping of the distillation section was used in this chiller (Mendes et al., 2007). Since the evaporation temperature is above 0 °C, the enrichment process of ammonia in the rectification column does not bring significant performance improvement (Fernández-Seara and Sieres, 2006), which was experimentally verified by Roriz and Mortal (2003). Vapor refrigerant (stream 9) from the desorber condenses completely in the condenser (C). The liquid refrigerant (stream 10) from the condenser is then subcooled (stream 11) in the subcooler (SC) by the superheating stream (stream 13) that comes from the evaporator (E). The liquid refrigerant (stream 11) flows to the evaporator (E) through the refrigerant expansion valve (RV). The weak liquid

Table 1 – Process data of the absorption cooling cycle.

Heat transfer coefficients U (kW m^{-2} K^{-1})	
Absorber	0.91
Condenser	1.1
Evaporator	1.34
Desorber	1.1
Subcooler	0.26
Solution heat exchanger	0.99
Heat transfer area A (m^2)	
Absorber	2.06
Condenser	1.37
Evaporator	1.00
Desorber	1.05
Subcooler	0.42
Solution heat exchanger	1.20
Temperature data (°C)	
Chilled water inlet/outlet	16/11
Condenser cooling water inlet/outlet	40/49
Desorber heating water temperature	110/103.8
Cost data	
Unitary cost of exergy (euro MW h^{-1})	125
Specific cost of heat exchanger Eq. (14) (euro m^{-2})	500
Interest rate (%)	10
Operation time per year (h)	2000/4000/6000
Amortization period (yr)	15
Other data	
Cooling capacity (kW)	5
Pump efficiency	0.6

solution (stream 4) from the desorber returns back to the absorber (A) through the solution heat exchanger (SHX), which preheats the concentrated solution (stream 2) before being introduced to the desorber. From the heat exchanger, the solution is finally sent to the expansion valve (SV), and then to the absorber (A). Streams 15–22 are external heat transfer fluids. In our case, water is used for energy supply and dissipation.

Table 3 – Thermal and mechanical power exchanged and energy destruction rate of the chiller units.

Unit	Q (kW)	W (kW)	I (kW)
A	8.11		0.12
C	5.94		0.20
D	8.96		0.16
E	5.00		0.10
SC	0.74		0.03
SHX	11.42		0.28
P		0.14	0.06
RV			0.01
SV			0.07
Overall			1.02

The input data of the problem, which includes the cooling capacity of the chiller and the external fluid (water) temperatures, are given in Table 1. These data are the design data of the analyzed chiller except the area of the solution heat exchanger, which has been increased in this case study.

A computer code for simulating the chiller has been established using the program Engineering Equation Solver (EES, from the F-Chart Software Company). Properties for ammonia water are given by Tillner Roth and Friend (1998). Properties for all state points, including specific exergies, have been evaluated. The specific exergy Eq. (25) considers only the physical exergy (Kotas, 1995). The chemical exergy of water and ammonia cancels out as entering and leaving quantity are the same. Mixing entropy is taken into account in the calculation of the entropy of the mixture.

$$e_i = (h_i - h_0) - T_0(s_i - s_0) \quad \forall i \tag{25}$$

Table 2 – Thermodynamic properties of each state point (SP) at the base case.

SP	T (°C)	P (MPa)	z (–)	m (kg s^{-1})	h (kJ kg^{-1})	s (kJ kg^{-1}K^{-1})	e (kJ kg^{-1})	E (kW)
1	46.9	0.55	0.463	0.053	121.0	1.168	44.06	2.35
2	47.1	1.82	0.463	0.053	122.6	1.168	45.62	2.44
3	91.9	1.82	0.463	0.053	336.3	1.793	68.83	3.68
4	104.0	1.82	0.414	0.049	378.7	1.876	85.77	4.18
5	54.6	1.82	0.414	0.049	144.2	1.210	54.53	2.65
6	54.8	0.55	0.414	0.049	144.2	1.215	53.10	2.59
9	94.0	1.82	0.977	0.005	1798.0	6.042	234.00	1.10
10	46.7	1.82	0.977	0.005	540.8	2.189	152.40	0.72
11	14.3	1.82	0.977	0.005	384.4	1.674	153.30	0.72
12	7.3	0.55	0.977	0.005	384.4	1.682	150.60	0.71
13	12.3	0.55	0.977	0.005	1444.0	5.447	61.19	0.29
14	31.3	0.55	0.977	0.005	1600.0	5.982	54.29	0.26
15	43.8	0.20	0.000	0.373	183.6	0.623	1.03	0.38
16	49.0	0.20	0.000	0.373	205.3	0.691	2.01	0.75
17	110.0	0.24	0.000	0.342	461.5	1.419	36.03	12.33
18	103.8	0.24	0.000	0.342	435.3	1.350	30.87	10.56
19	40.0	0.20	0.000	0.373	167.7	0.572	0.53	0.20
20	43.8	0.20	0.000	0.373	183.6	0.623	1.03	0.38
21	16.0	0.20	0.000	0.240	67.4	0.239	1.92	0.46
22	11.0	0.20	0.000	0.240	46.5	0.166	3.26	0.78

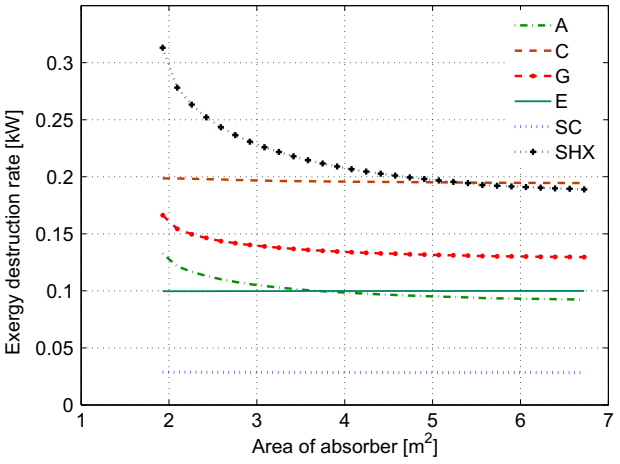

Fig. 3 – Exergy destruction rates in the units due to variation of absorber area.

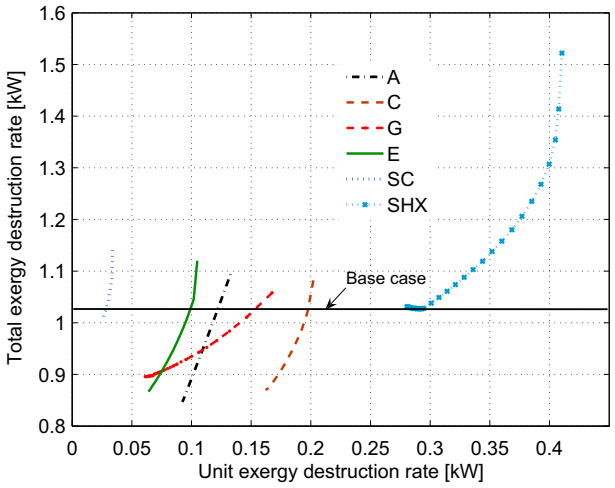

Fig. 5 – Total exergy destruction rate versus exergy destruction rate of each unit.

The properties indicated with the subscript 0 refer to the environment state, which is taken as 32 °C and 0.1 MPa corresponding to typical summer conditions in the Mediterranean region. The main assumptions are:

- Steady state operation.
- Heat losses are not considered.
- Pressure losses are not considered.
- The refrigerant leaves the condenser as a saturated liquid.
- The solutions leave the absorber and desorber as saturated liquids.
- The solution and refrigerant valves are adiabatic.

5. Results and discussions

After achieving the energy and exergy analysis for the base case the CSB for the main units are obtained by a parametric analysis (structural analysis). With these results the optimum design using the approach presented in previous section is determined for different yearly operating times and is finally compared with results from integrated optimization algorism embedded with the EES program (from the *F*-Chart).

5.1. *Energy and exergy analysis*

For the base case results of the energetic analysis for the different state points are presented in Table 2. The corresponding thermal or mechanical power of the units and the corresponding exergy destruction rate are given in Table 3. The COP for the base design is 0.56.

Among the heat exchangers the highest exergy destructions were found in the solution heat exchanger (SHX) followed by the condenser (C). The condenser has a high exergy destruction rate as it also accomplishes part of the function of the dephlegmator, which is not included in this chiller. It follows the desorber (D), the absorber (A) and the evaporator,

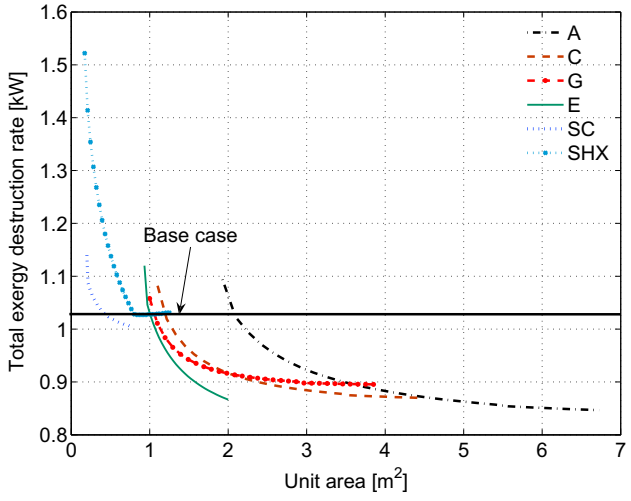

Fig. 4 – Total exergy destruction rates as function of each unit area while keeping the other unit areas constant.

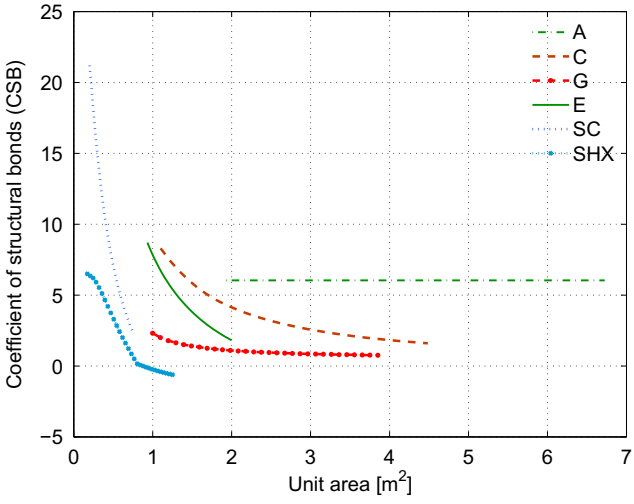

Fig. 6 – Coefficient of structural bonds (CSB) of each unit as function of its area.

Table 4 – Results of thermoeconomic optimization.

t_{op}	2000 (h)			4000 (h)			6000 (h)		
	Base	EES	Eq. (24)	Base	EES	Eq. (24)	Base	EES	Eq. (24)
COP	0.56	0.62	0.56	0.56	0.62	0.62	0.56	0.66	0.64
Area (m^2)									
A	2.06	2.17	1.63	2.06	2.32	2.36	2.06	2.48	3.15
C	1.18	1.37	1.32	1.18	1.42	1.59	1.18	1.85	1.76
D	1.05	1.15	0.94	1.05	1.08	0.95	1.05	0.90	0.98
E	1.00	1.62	1.90	1.00	1.97	2.68	1.00	2.55	3.29
SC	0.42	0.46	0.28	0.42	0.50	0.34	0.42	0.53	0.38
SHX	1.20	0.88	0.59	1.20	0.63	0.57	1.20	0.77	0.56
Annual cost (euro)									
C_c	277	307	267	277	317	341	277	364	406
C_{op}	896	813	887	1892	1618	1611	2688	2349	2338
C_t	1173	1120	1154	2070	1935	1952	2966	2713	2744
% of base case C_t	100	95.5	98.4	100	93.5	94.3	100	91.5	92.5

while the subcooler (SC) has the lowest exergy destruction among the heat exchangers. These observations agree with results from Best et al. (1993) (Fig. 3).

5.2. *Structural analysis*

Once the exergy destructions for the base design are obtained, it can be evaluated how a change of the exergy destruction of 1 unit affects the rest of the system. This analysis is done by modification of the area of the unit under consideration, while the areas of the other units are maintained constant. Results for the absorber are presented in Fig. 3. As expected, the exergy destruction in the absorber increases for a smaller area, but at the same time the absorber affects the other units. In the case of the solution heat exchanger and also the generator the increase of the exergy destruction is important, while for the evaporator, condenser and subcooler nearly no effect can be observed. The effect of the heat exchange area of the units on the total exergy destruction rate of the chiller is presented in Fig. 4. In all cases and especially in the small areas range a decrease in area of the heat exchangers result in a significant increase of the exergy destruction of the chiller. The most significant increase is found in the solution heat exchanger.

Now the exergy destruction rate of the units and the exergy destruction rate of the whole chiller can be related (Fig. 5). The main difference between the units is the magnitude of the individual exergy destruction and the slope of the curve. The slope corresponds to the CSB. A large slope indicates a strong interaction between the unit and the whole chiller, and thus a strong influence of a modification of its area on the other units and the chiller performance. From these results the CSB values of the units can be determined by Eq. (6) (Fig. 6). Values higher than unity indicate that an increase in the area of a unit will also have a positive effect on the other components. The absorber is the only unit with a constant CSB, with a high value of about six. For the other units the CSB increases with decreasing area. This means that the total cost reduction by increasing the area of a less efficient heat exchange is higher than for an already efficient heat exchanger with a large area.

If the value of the CSB is lower than one, the reduction of the exergy destruction of the unit under consideration is compensated by an increase of the exergy destruction of the rest of the units. This means that a further improvement of this unit is not worthwhile. The highest values result for the subcooler, followed by evaporator and condenser. The desorber has relatively small CSB's close to unity and thus a small influence on the chiller performance is expected. In general strong interactions between the units can be observed. The CSB's simplify the exergy analysis, as directly positive or negative interactions can be quantified (Boer et al., 2009).

5.3. *Thermoeconomic optimization*

Based on the results obtained up to now the thermoeconomic optimization can be achieved. The objective is the minimization of the annual operation cost (Eq. (7)). This cost depends principally on the fuel cost and the capital investment amortization, which are function of the heat exchanger areas. The optimum value for the area will be estimated from Eq. (24). The proposed method optimizes a heat exchanger regarding the initial design, and indicates the strong and week points of the design. These values are compared with results from integrated optimization algorism embedded with the EES program(from the F-Chart). In EES the areas of all heat exchangers are used as decision variables, trying to provide the best final solution. Table 4 presents the optimum areas for different operation times (2000, 4000 and 6000 h per year). The resulting designs can be compared with the base design in terms of capital, running and total cost.

General tendencies are similar for the estimation by Eq. (24) and the numerical optimization. In all cases the total cost is reduced compared to the base design. As expected for a larger operation time the areas increase and as a consequence the COP increases, in order to obtain the optimal design. For shorter operation times a less efficient chiller which results in less capital cost is more economic.

Comparing the results of the integrated optimization algorithm of EES and the proposed formulation of this work, Eq. (24) agrees well when the fuel cost (operation cost) dominates the capital cost i.e, at a high annual operation time.

However, at a small operation time the total capital cost is in the same order as the fuel cost. Therefore, the difference in the results of the optimizations become more significant. This is because the effect of the simplifications we made in derivation of Eq. (24) especially in Eq. (12) is more pronounced.

6. Conclusions

The energy, exergy and thermoeconomic analyses of an ammonia-water chiller have been achieved. The exergy destruction rates of the units have been determined. The effect of changes in the heat exchange area on their exergy destruction of the unit and the whole chiller have been evaluated and quantified by the Coefficients of Structural Bonds (CSB). The CSB's indicate how the exergy destruction change in 1 unit affects the rest of the system.

Finally the thermoeconomic optimization of the units has been achieved based on the structural method, which uses the CSB's. This method has been adapted in order to obtain a simplified equation to estimate the optimum heat exchanger area. This equation depends on parameters, which are directly related to the heat exchangers. Thus, it indicates how the area should change if these parameters are modified. The optimum corresponds to the design with the minimum total cost. These results have been compared with a integrated optimization algorithm from EES in order to evaluate the accuracy of the estimation. The application of the proposed equation for the estimation of the heat exchanger area offers an interesting way to determine a close to optimum value by a quick estimation, which can be used as starting value for comprehensive optimization methodologies.

Acknowledgments

Berhane H. Gebreslassie expresses his gratitude for the financial support received from the University Rovira i Virgili. Dr. Marc Medrano would like to thank the Spanish Ministry of Education and Science for his Ramon y Cajal research appointment. The authors also wish to acknowledge support of this research work from the ''Ministerio de Ciencia y Tecnología – Dirección general de investigación'' of Spain (DPI2002-00706).

REFERENCES

Bejan, A., Vargas, J.V.C., Sokolov, M., 1995. Optimal allocation of a heat-exchanger inventory in heat driven refrigerators. Int. J. of Heat and Mass Transfer 38 (16), 2997–3004.

Best, R., Islas, J., Martinez, M., 1993. Exergy efficiency of an ammonia–water absorption system for ice production. Applied Energy 45, 241–256.

Beyer, J., 1970. Strukturuntersuchungen – notwendiger Bestandteil der Effektivitätsanalyse von Wärmeverbrauchersystemen. (Structural analysis – necessary part of efficiency analysis of thermal systems). Energieanwendung 19 (12), 358–361.

Beyer, J., 1974. Struktur wärmetechnischer Systeme und ökonomische Optimierung der Systemparameter. (Structure of thermal systems and economical optimisation of system parameters). Energieanwendung 23 (9), 274–279.

Boer, D., Gebreslassie, B.H., Medrano, M., Nogués, M., 2009. Effect of internal heat recovery in ammonia–water absorption cooling cycles: exergy and structural analysis. Int. J. of Thermodynamics 12 (1), 17–27.

Dentice d'Accadia, M., Vanoli, L., 2004. Thermoeconomic optimisation of the condenser in a vapour compression heat pump. Int. J. of Refrigeration 27 (4), 433–441.

Dingeç, H., Ileri, A., 1999. Thermoeconomic optimization of simple refrigerators. Int. J. of Energy Research 23 (11), 949–962.

Fernández-Seara, J., Sieres, J., 2006. The importance of the ammonia purification process in ammonia-water absorption systems. Energy Conversion and Management 47 (13–14), 1975–1987.

Herold, K., Radermacher, R., Sa, K., 1996. Absorption Chillers and Heat Pumps. CRC Press.

Herold, K., Radermacher, R., 1990. Optimum allocation of heat transfer surface in an absorption heat pump. In: IECEC (Intessociety Energy Conversion and Engineering Conference), vol. 2., Reno, pp. 217–221.

KizIlkan, Ö., Sencan, A., Kalogirou, S., 2007. Thermoeconomic optimization of a LiBr absorption refrigeration system. Chemical Engineering and Processing: Process Intensification 46, 1376–1384.

Klein, S.A., 1992. Design considerations for refrigeration cycles. Int. J. of Refrigeration 15 (3), 181–185.

Kotas, T, J, 1995. The Exergy Method of Thermal Plant Analysis. Krieger Publishing Company.

Mendes, L.F., Collares-Pereira, M., 1999. A solar assisted and air cooled absorption machine to provide small power heating and cooling. In: International Sorption Heat Pump Conference. Munich, Germany, pp. 129–136.

Mendes, L.F., Collares-Pereira, M., Ziegler, F., 2007. A rich solution spray as a refining method in a small capacity, single effect, solar assisted absorption machine with the pair NH_3/H_2O: experimental results. Energy Conversion and Management 48 (11), 2996–3000.

Misra, R.D., Sahoo, P., Sahoo, S., Gupta, A., 2003. Thermoeconomic optimization of a single effect water/LiBr vapour absorption refrigeration system. Int. J. of Refrigeration 26, 158–169.

Misra, R.D., Sahoo, P., Gupta, A., 2006. Thermoeconomic evaluation and optimization of an aqua-ammonia vapour-absorption refrigeration system. Int. J. of Refrigeration 29, 47–59.

Roriz, L., Mortal, A., 2003. Study on distillation solutions for a solar assisted absorption heat pump. In: Corberán, J.M., Royo, R. (Eds.), Eurotherm Seminar 72: Thermodynamics, Heat and Mass Transfer of Refrigeration Machines and Heat Pumps. IMST-UPV, Valencia, Spain.

Summerer, F., 1996. Evaluation of absorption cycles with respect to cop and economics. Int. J. of Refrigeration 19 (1), 19–24.

Tillner Roth, R., Friend, D., 1998. A Helmholtz free energy formulation of the thermodynamic properties of the mixture Ammonia + Water. Journal of Physical and Chemical Reference Data 27 (1), 63–96.

Ziegler, F., 1997. Sorptionswärmepumpen. Forschungsberichte des Deutschen Kälte- und Klimatechnischen Vereins. Deutscher Kälte- und Klimatechnischer Verein (DKV), Stuttgart, Germany.

Ziegler, F., 1998. Design optimization of endo-reversible heat transformation cycles. In: Proc. of ECOS. Nancy, France, pp. 573–580.

Ziegler, F., 1999. Discussion of optimized design of endo-reversible heat transformation cycle. In: International Sorption Heat Pump Conference. ZAE Bayern, Munich, pp. 459–464.

Applied Energy 86 (2009) 1712–1722

Contents lists available at ScienceDirect

Applied Energy

journal homepage: www.elsevier.com/locate/apenergy

Design of environmentally conscious absorption cooling systems via multi-objective optimization and life cycle assessment

Berhane H. Gebreslassie [a], Gonzalo Guillén-Gosálbez [b], Laureano Jiménez [b], Dieter Boer [a,*]

[a] Department of Mechanical Engineering, University Rovira i Virgili, Av. Països Catalans, 26, 43007 Tarragona, Spain
[b] Department of Chemical Engineering, University Rovira i Virgili, Av. Països Catalans, 26, 43007 Tarragona, Spain

ARTICLE INFO

Article history:
Received 20 August 2008
Received in revised form 14 November 2008
Accepted 16 November 2008
Available online 25 December 2008

Keywords:
Absorption refrigeration
Multi-objective optimization
Life cycle assessment (LCA)
Ammonia–water
Cost analysis

ABSTRACT

In this paper, a systematic method based on mathematical programming is proposed for the design of environmentally conscious absorption cooling systems. The approach presented relies on the development of a multi-objective formulation that simultaneously accounts for the minimization of cost and environmental impact at the design stage. The latter criterion is measured by the Eco-indicator 99 methodology, which follows the principles of life cycle assessment (LCA). The design task is formulated as a bi-criteria nonlinear programming (NLP) problem, the solution of which is defined by a set of Pareto points that represent the optimal trade-off between the economic and environmental concerns considered in the analysis. These Pareto solutions can be obtained via standard techniques for multi-objective optimization. The main advantage of this approach is that it offers a set of alternative options for system design rather than a single solution. From these alternatives, the decision-maker can choose the best one according to his/her preferences and the applicable legislation. The capabilities of the proposed method are illustrated in a case study problem that addresses the design of a typical absorption cooling system.

1. Introduction

During the last decade, there has been a growing awareness of the importance of incorporating environmental concerns along with traditional economic criteria in the optimization of industrial process. This trend has been motivated by several issues, a major one being the stringent legislation that aims to mitigate important environmental problems such as the ozone layer depletion and global warming. In this challenging scenario, absorption refrigeration is gaining popularity in the air conditioning system, as it uses refrigerants with almost zero global warming potential and do not contribute to the ozone layer depletion [1–3]. The main difference between an absorption refrigeration system and the conventional compression system is that the former uses heat sources as energy input in order to produce cooling, while the compression system requires mechanical energy for its operation. The heat sources may be fossil fuel, renewable energy resources or waste heat recovered from other thermal systems. Moreover, these systems have also other advantages, such as high reliability, low maintainability and a silent and vibration free operation. Another important merit of these systems is the elimination of CFC's and HCFC's as refrigerants [4].

Unfortunately, absorption cycles require higher number of units to accommodate the absorption and desorption processes. This leads to higher capital costs than those associated with conventional cooling systems (i.e., vapor compression system). Hence, optimization strategies based on both, thermodynamic and economic insights are needed to improve their operational and economic performance so that they can be competitive in the market. Specifically, the preferred method for optimizing these systems has been the *thermoeconomic* optimization [5–8], which merges exergy and economic analysis within a single framework. This approach is based on an iterative procedure that relies on both, a thermodynamic model and a cost model [5,8].

An alternative strategy that has been applied to the optimization of similar industrial process is the simultaneous approach, which relies on systematic optimization methods based on mathematical programming. In this second approach, the design task is posed as an optimization problem, which is solved by standard techniques for linear, nonlinear, mixed integer linear and mixed integer nonlinear (LP, NLP, MILP, MINLP, respectively) problems. These methods have been extensively used in the optimization of chemical processes [9–14]. However, their application to the design of absorption cycles has been rather limited.

Most of the strategies that address the design of absorption cycles focus on reducing the exergy destroyed within the cycle in order to improve the energetic efficiency [5,6,8,15]. Although these approaches may lead to a reduction in the energy consumption, and hence to a decrease in the associated environmental impact, they have the disadvantage of neglecting the damage caused in other stages in the life cycle of the absorption system, such as

* Corresponding author. Tel.: +34 977559631.
E-mail address: Dieter.Boer@urv.cat (D. Boer).

0306-2619/$ - see front matter © 2008 Elsevier Ltd. All rights reserved.
doi:10.1016/j.apenergy.2008.11.019

Nomenclature

A	absorber
C	condenser
D	desorber
E	evaporator
LCA	life cycle assessment
P	solution pump
RV	refrigerant expansion valve
SC	subcooler
SHX	solution heat exchanger
SV	solution expansion valve
yr	year

Indices

b	chemical
d	damage category
i	component of a stream
j	streams
k	unit
r	impact category

Sets

RD(d)	set of impact categories included in the damage category d
IN(k)	set of input streams to unit k
OUT(k)	set of out put streams from unit k

Parameters

c_1	cost parameter (euro/m^2)
c_2	cost parameter (euro)
c_3	cost parameter (euro/kW)
c_q	unitary cost of steam (euro/MW h)
c_e	unitary cost of electricity (euro/MW h)
$cr\,f$	capital recovery factor (–)
dm_{br}	coefficient of damage model associated with chemical b and impact r (impact/kg)
ir	interest rate (–)
is_b	life cycle inventory entry per unit of steam generated (kg/kg)
ie_b	life cycle inventory entry per unit of electricity generated (kg/kW)
n_d	normalization factor (Eco-indicator 99 points/impact)
t_{op}	operational hours (h/yr)
U_k	overall heat transfer co-efficient of unit k (kW/m^2 K)
w_d	weighting factor (–)

Variables

A_k	area of heat exchanger (km^2)
C_c	total capital cost (euro/yr)
C_{exp}	cost of expansion valves (euro)
C_{hxs}	cost of heat exchangers (euro)
C_{op}	total operational cost (euro/yr)
C_p	cost of pump (euro)
COP	coefficient of performance (–)
DAM$_d$	damage in category d (impact)
ECO99	Eco-indicator 99 (Eco-indicator 99 points)
ΔT_k^{lm}	logarithmic mean temperature difference (°C or K)
ΔT_k^{h}	temperature difference in the hot end (°C or K)
ΔT_k^{c}	temperature difference in the cold end (°C or K)
h_j	enthalpy of stream j (kJ/kg)
IMP$_r$	damage in impact r (impact)
LCI$_b$	life cycle inventory entry associated with chemical b (kg)
m_j	mass flow rate of stream j (kg/s)
P_j	pressure of stream j (bar)
Q_k	heat transferred in unit k (kW)
TC	total cost (euro/yr)
T_j	temperature of stream j (°C or K)
W_p	mechanical power of pump (kW)
$x_{i,j}$	mass fraction of component i in stream j (–)

the generation of those utilities consumed by the cycle. Thus, due to their limited scope, these methods can lead to solutions that reduce the impact locally instead of alternatives that mitigate the harmful effects over the entire life cycle of the process.

Life cycle analysis (LCA) arose in response to this situation. LCA is an objective process for evaluating the environmental loads associated with a product, process or activity [9,16]. During the application of LCA, the energy and materials used in a process are firstly identified and quantified along with the wastes released to the environment. This information is further translated in to a set of environmental impacts that can be aggregated into different groups. These impacts are finally used to assess diverse process alternatives that may be implemented to achieve environmental improvements. Today, LCA can be effectively used to restructure any industrial process in order to improve its environmental performance [9]. In energy scenarios, LCA has been traditionally used as a tool to estimate the energy and environmental impacts related to products or services [16–19].

The application of LCA provides valuable insights into the design problem. Unfortunately, LCA does not include a systematic way of generating process alternatives for environmental improvements. This limitation can be overcome by coupling LCA with optimization tools. In this framework, LCA is employed to assess technological solutions from an environmental perspective, whereas optimization tools seek in a systematic way the best ones according to the predefined criteria. Although the advantages of such a combined strategy have been already acknowledged in the literature, specifically in the area of process design [9–14], little research has been conducted to date in this direction. Specifically, Azapagic and Clift [13,14] proposed the application of multi-objective optimization as a tool for system improvements by integrating the economic performance of mineral boron production and life cycle assessment. Fu and Diwekar [20] used multi-objective optimization to simultaneously minimize the green house emissions and the total cost. Guillén-Gosálbez et al. [9] have addressed the incorporation of environmental concerns in the structural optimization of process flowsheets through the combined use of LCA and multi-objective mixed integer nonlinear programming (MINLP) techniques.

To our knowledge, there is no work in the literature that simultaneously considers the integration of LCA and process optimization to improve the economic and environmental performance of absorption cooling cycles. Hence, the aim of this work is to develop a systematic approach for the design of environmentally conscious absorption cooling cycles based on the combined use of LCA and mathematical programming. More precisely, in this work the design task is formulated as a multi-objective nonlinear programming (NLP) problem that accounts for the minimization of the total annualized cost and environmental impact. The environmental impact is determined according to the Eco-indicator 99 methodology [21], which includes eleven environmental impact categories that are further aggregated into a single environmental metric [9,22]. The capabilities of our approach are illustrated through a case study. The obtained results show that significant

environmental savings can be achieved by compromising the economic benefit of the system and vice versa. The methodology presented is intended to promote a more sustainable design of absorption cycles.

2. Problem statement

We address the optimal design of absorption cooling cycles with economic and environmental concerns. Given are the cooling capacity of the system, the inlet and outlet temperatures of the external fluids, capital and operating cost data, and LCA related information (i.e., life cycle inventory of emissions and feedstock requirements, and parameters of the damage model). The goal is to determine the optimal design and associated operating conditions that simultaneously minimize the total annualized cost and environmental impact. The mathematical model derived to address this problem is explained in detail in the following sections.

3. Mathematical model

Compared to a compression cooling cycle, the basic idea of an absorption system is to replace the electricity consumption associated with the vapor compression by a thermally driven absorption–desorption system [2]. This is accomplished by making use of absorption and desorption processes that employ suitable working fluid pairs. The working pair consists of a refrigerant and an absorbent. In this study, without loss of generality, an ammonia/water solution is used as working pair, with the ammonia being the refrigerant and water the absorbent.

3.1. System description

Fig. 1 represents the absorption cycle under study in a pressure temperature plot. The system provides chilled water for cooling applications. The basic components are the absorber (A), condenser (C), desorber (D), and evaporator (E). The cycle also includes the refrigerant subcooler (SC), refrigerant expansion valve (RV), solution heat exchanger (SHX), solution pump (P), and solution expansion valve (SV). The high pressure equipments are the solution heat exchanger, desorber, and condenser, whereas the low pressure ones are the evaporator and absorber.

The system operation is as follows. The refrigerant in vapor phase (stream 14) coming from the subcooler (SC) is absorbed in absorber (A) by the diluted liquid solution (stream 6). The concentrated solution (stream 1) leaving the absorber is pumped by pump (P) to reach a higher pressure (stream 2) before being preheated in the solution heat exchanger (SHX). Then, the solution (stream 3) enters the desorber, in which the desorption of ammonia takes place. Vapor refrigerant (stream 9) from the desorber condenses completely in the condenser (C). The liquid refrigerant (stream 10) from the condenser is then subcooled (stream 11) in the subcooler (SC) by the superheating stream (stream 13) that comes from the evaporator (E). The liquid refrigerant (stream 11) flows to the evaporator (E) through the refrigerant expansion valve (RV). The weak liquid solution (stream 4) from the desorber returns back to the absorber (A) through the solution heat exchanger (SHX), which preheats the concentrated solution (stream 2) before being introduced to the desorber. From the heat exchanger, the solution is finally sent to the expansion valve (SV), then to absorber (A).

Note that streams 15–22 are external heat transfer fluids. In our case, water is used for energy supply and energy extracting. The useful output energy is the heat extracted from the environment of evaporator (Q_E), whereas the input energy is supplied to the desorber (Q_D) [23,24].

3.2. General constraints

A computer code for simulating the cycle was developed using the generic algebraic modeling system GAMS [25]. The mathematical formulation takes the form of a bi-criteria nonlinear programming (NLP) problem, the solution of which comprises a set of trade-off solutions. The main assumptions of the model are:

- Steady state operation.
- Heat losses are not considered.
- Pressure losses are not considered.
- The refrigerant leaves the condenser as a saturated liquid.
- The refrigerant leaves the evaporator as a saturated vapor.
- The solutions leave the absorber and desorber as saturated liquids.
- The solution and refrigerant valves are adiabatic.
- Rectification of ammonia water is not considered.
- The ammonia concentration in the vapor that leaves the desorber is fixed.

The model of the absorption cycle is based on energy and materials balance that ensure the mass and energy conservation. These principles are applied to each unit of the cycle. Specifically, each process unit can be treated as a control volume with inlet and outlet streams, heat transfer and work interactions [2,15] (see Fig. 2). This is accomplished via the following equations:

$$\sum_{j\in \mathrm{IN}(k)} m_j x_{i,j} - \sum_{j\in \mathrm{OUT}(k)} m_j x_{i,j} = 0 \quad \forall k, i \tag{1}$$

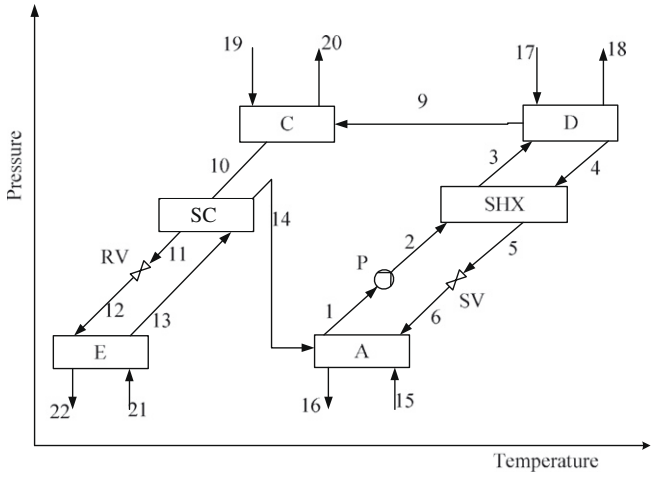

Fig. 1. Ammonia–water absorption cycle with internal heat recovery.

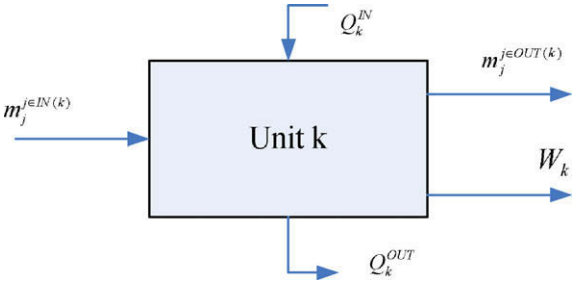

Fig. 2. A generic unit of the absorption cycle with its inlets and outlets.

UNIVERSITAT ROVIRA I VIRGILI
OPTIMIZATION OF ENVIRONMENTALLY FRIENDLY SOLAR ASSISTED ABSORPTION COOLING SYSTEMS
Berhane Hagos Gebreslassie
ISBN: 978-84-693-7673-7/DL:T-1752-2010

Eq. (1) represents the mass balances, and ensures that the total amount of component i that enters unit k must equal the total amount of i that leaves k. In this equation, m_j denotes the mass flow of stream j, and $x_{i,j}$ is the mass fraction of component i in stream j. Note that j can be either an inlet or outlet stream. Furthermore, IN(k) denotes the set of inlet streams of unit k, whereas OUT(k) includes the outlet streams.

$$\sum_{j\in \mathrm{IN}(k)} m_j h_j - \sum_{j\in \mathrm{OUT}(k)} m_j h_j + Q_k^{\mathrm{IN}} - Q_k^{\mathrm{OUT}} - W_k = 0 \quad \forall k \tag{2}$$

Eq. (2) defines the energy balance in the system assuming no heat losses. The difference in energy content between the inlet and outlet streams, plus the heat supplied to the unit (Q_k^{IN}) must equal the heat removed (Q_k^{OUT}) plus the work done (W_k) by the unit. Note that the heat and work terms in Eq. (2) can take a zero value in some of the units, as shown in Eqs. (3)–(5):

$$Q_k^{\mathrm{IN}} = 0 \quad \text{if } k = \left\{ \begin{array}{l} \text{Absorber(A)} \\ \text{Condenser(C)} \\ \text{Subcooler(SC)} \\ \text{Solution heat exchanger(SHX)} \\ \text{Pump(P)} \\ \text{Expansion valves(RV, SV)} \end{array} \right\} \tag{3}$$

$$Q_k^{OUT} = 0 \quad \text{if } k = \left\{ \begin{array}{l} \text{Evaporator(E)} \\ \text{Desorber(D)} \\ \text{Subcooler(SC)} \\ \text{Solution heat exchanger(SHX)} \\ \text{Pump(P)} \\ \text{Expansion valves(RV, SV)} \end{array} \right\} \tag{4}$$

$$W_k = 0 \quad \forall k \neq \text{pump} \tag{5}$$

Furthermore, the enthalpy of a stream is determined from its temperature (T), pressure (P), and composition, as

$$h_j = f(T_j, P_j, x_{i,j}) \quad \forall j \tag{6}$$

In our work, the enthalpies are calculated according to the correlations proposed by Pátek and Komfar [26]. These equations are completely empirical, and allow for the calculation of the properties of a mixture for pressures below 30 bars. These correlations can be easily solved both explicitly and implicitly [27]. Note that any other correlation could be embedded into the mathematical formulation.

The heat exchangers are modeled using the logarithmic mean temperature difference (ΔT_k^{lm}), the heat transfer area (A_k), and the overall heat transfer coefficient (U_k), as

$$Q_k = U_k A_k \Delta T_k^{lm} \quad \forall k \tag{7}$$

The logarithmic mean temperature difference, which is function of the hot and cold end (ΔT_k^h and ΔT_k^c, respectively) temperature differences, is calculated via the Chen's approximation [28]. This avoids the discontinuity of the function at $\Delta T_k^h = \Delta T_k^c$, which in turn improves the robustness of the mathematical formulation and its numerical performance [28]

$$\Delta T_k^{lm} = \left[\Delta T_k^h \Delta T_k^c \frac{\Delta T_k^h + \Delta T_k^c}{2} \right]^{\frac{1}{3}} \quad \forall k \tag{8}$$

Finally, the coefficient of performance (COP) is determined via Eq. (9) as the ratio between the energy extracted from the chilled water and the total energy supplied to the system [2]

$$\mathrm{COP} = \frac{Q_{k=\mathrm{E}}}{Q_{k=\mathrm{D}} + W_{k=\mathrm{P}}} \tag{9}$$

3.3. Objective function

The model previously presented must attain two different targets: minimum total annualized cost and environmental impact.

3.3.1. Economic objective function

The total annualized cost of the system, which is denoted by TC, includes the capital and operating costs (C_c and C_{op}, respectively)

$$\mathrm{TC} = C_c + C_{op} \tag{10}$$

The capital cost includes the cost of the heat exchangers (C_{hxs}), pumps (C_p), and expansion valves (C_{exp}) times the capital recovery factor ($cr\,f$)

$$C_c = (C_{hxs} + C_p + C_{exp}) cr\,f \tag{11}$$

The cost of the heat exchangers is estimated using the linear correlation proposed by Kizllkan et al. [7]

$$C_{hxs} = \sum_{k=heat\ \ exchanger} (c_1 A_k + c_2) \tag{12}$$

In Eq. (12), c_1 and c_2 are the variable and fixed cost parameters, respectively, associated with the heat exchangers used in the system. These parameters relate the area of a heat exchanger with its cost.

The cost of the pump is estimated using the correlation introduced by Siddiqui [29]:

$$C_p = c_3 W_p^{0.4} \tag{13}$$

where W_p denotes the pump work, and c_3 is a cost parameter. Finally, let us note that the cost of the expansion valves can be usually neglected, since their contribution to the system cost is rather small [30,31].

The capital recovery factor ($cr\,f$) is function of the interest rate (ir) and the life span (i.e., number of useful years) of the unit under consideration (n) [8].

$$cr\,f = \frac{ir(ir+1)^n}{(ir+1)^n - 1} \tag{14}$$

Finally, the total annualized operational cost includes the cost of the steam used in the desorber, the electricity consumed by the pump and the cooling water. Usually, the latter term can be neglected compared to the remaining terms, so the operating costs are calculated as follows:

$$C_{op} = (c_q Q_{k=\mathrm{D}} + c_e W_{k=\mathrm{P}}) t_{op} \tag{15}$$

In this equation, c_q and c_e are the unitary costs of the heat and electricity, whereas t_{op} is the total operation time.

3.3.2. Environmental impact assessment based on LCA

In this work, the environmental performance of the cycle is assessed according to the principles of LCA. A general description of the LCA methodology can be found elsewhere [32]. Specifically, here we follow the general LCA methodology [9,21,22], which comprises four steps. These steps are next described in detail in the context of the proposed strategy.

3.3.2.1 Goal and scope definition. In this first step the system boundaries, the impact categories, and the functional unit are defined. The boundaries of the system should include the entire life cycle of the service or process being analyzed. In our specific case, we perform an analysis from the cradle to the grave, including in the study those upstream processes required to generate the utilities consumed by the absorption cycle. Regarding the impact categories, the Eco-indicator 99 proposes eleven impact categories that are further aggregated into three damage categories. These

damage categories are finally translated into a single indicator. The functional unit of the study is the cold produced during the useful life span of the system.

3.3.2.2 Inventory analysis. This second step of LCA quantifies the inputs and outputs of energy and mass associated with the cold production, which are further translated into emissions released and waste generated (i.e., the environmental burdens). In our problem, all the environmental burdens are expressed as function of steam and electricity consumed in the system. Note that both variables are degrees of freedom in the optimization problem.

We should mention that the calculation of the life cycle inventory of emissions requires the inclusion of a process model reproducing the behavior of the utility generation system. Generally, the insertion of such a model significantly increases the complexity of the original formulation. This difficulty can be overcome by making use of specific databases that contain the inventory of emissions of a wide range of industrial processes found in Europe [33–35]. Thus, in general, the inventory of emissions associated with the energy generation will be retrieved from the aforementioned databases and provided as input data to the mathematical model.

3.3.2.3 Impact assessment. In this third step, the life cycle inventory is translated into the corresponding environmental impacts. As mentioned before, three different damage categories are considered in the calculation of the Eco-indicator 99. These are:

- Human health damages, which are measured in disability adjusted life years (DALYs). A damage of one means that one life year of one individual is lost, or one person suffers 4 yr from a disability of 0.25.
- Ecosystem quality damages, that are measured in PDF m^2 yr (potentially disappear fraction of species). A damage of one means that all species disappear from a m^2 over 1 yr, or 10% of all species disappear from 10 m^2 over 1 yr, or 10% of all species disappear from 10 m^2 over 10 yr.
- Damages to resources, which are measured in MJ of surplus energy. A damage of 1 means that due to a certain extraction of resources, further extraction of the same resources in the future will need an additional MJ of energy due to the lower resource concentration or other unfavorable characteristics of the remaining reserves [9,22].

The damage in each impact category are calculated from the life cycle inventory and the impact model, as stated in Eq. (16).

$$\mathrm{IMP}_r = \sum_b dm_{br}\mathrm{LCI}_b \quad \forall r \tag{16}$$

In this equation, IMP_r denotes the damage caused in impact category r, LCI_b is the life cycle inventory entry (i.e., emissions and feedstock requirements) associated with chemical b, and dm_{br} is the coefficient of the damage model associated with chemical b and impact r. As mentioned before, the environmental burdens of the cycle are caused by the energy generation. Hence, the life cycle inventory entries can be expressed as a function of the consumption of steam and electricity, as

$$\mathrm{LCI}_b = \mathrm{LCI}_b^{steam} + \mathrm{LCI}_b^{electricity} = is_b m_s + ie_b W_{k=P} \quad \forall b \tag{17}$$

Here, is_b and ie_b are the life cycle inventory entries per unit of reference flow. In the steam production, the reference flow is 1 kg of steam generated, whereas in the electricity generation, it is 1 MJ of electricity produced. The amount of steam required by the cycle (m_s) is determined via the following equation:

$$m_s = \frac{Q_{k=\mathrm{D}}}{h_{18} - h_{17}} \tag{18}$$

Note that the determination of the environmental burdens associated with the generation of energy requires the expansion of the system boundaries to include the upstream processes. As mentioned before, the data associated with these upstream activities can be retrieved from standard databases [33–35]. Furthermore, the damage factors, which are the link between the results of the inventory phase and the impact categories, are given by specific damage models available for each damage category [22]. Finally, the impact categories r are aggregated into d damage categories (DAM_d), which are further translated into a single metric (ECO99), as stated in Eqs. (19) and (20).

$$\mathrm{DAM}_d = \sum_{r\in \mathrm{RD}(d)} \mathrm{IMP}_r \quad \forall d \tag{19}$$

$$\mathrm{ECO99} = \sum_d n_d w_d \mathrm{DAM}_d \tag{20}$$

Here, RD(d) represents the set of environmental impacts included in the damage category d, and n_d and w_d are specific normalization and weighting factors [22], respectively.

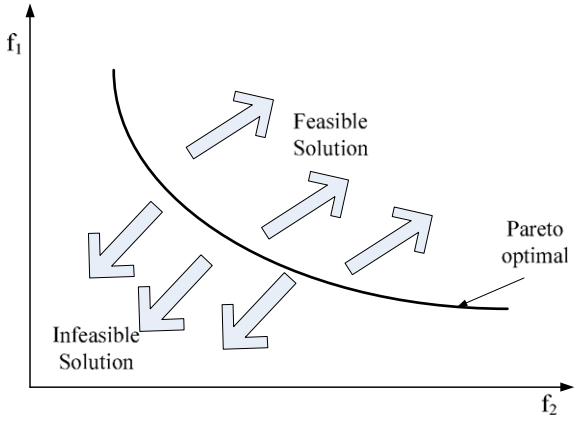

Fig. 3. Pareto curve.

Table 1
Process data of the absorption cooling cycle.

Heat transfer coefficients $U\left(\frac{\mathrm{kW}}{\mathrm{m^2\ K}}\right)$		
Absorber		0.8
Condenser		0.5
Evaporator		1.1
Desorber		1.3
Subcooler		1.0
Solution heat exchanger		0.7
Temperature data (°C)		
Chilled water inlet/outlet		10/5
Condenser cooling water inlet/outlet		27/35
Absorber cooling water		27/35
Desorber heating steam		100
Cost data		
Unitary cost of heat (euro/MW h)		30.00
Unitary cost of electricity (euro/MW h)		100.00
Cost parameters		
Eq. (12)	c_1	516.62
	c_2	268.45
Eq. (13)	c_3	630.00
Interest rate (%)		10
Operation time per year (h)		4000
Amortization period (yr)		15
Other data		
Cooling capacity (kW)		100
Vapor concentration at exit of desorber (x_9)		0.996
Pump efficiency		0.7

Table 2
Normalization and weighting factors.

	Normalization	Weights
Human health	1.54×10^{-2}	400
Ecosystem quality	5.13×10^{3}	400
Resources	8.41×10^{3}	200

Table 3
Environmental data associated with the production of 1 kg of steam and 1 MJ of electricity.

	Impact category	Unit	Steam	Electricity
1	Carcinogens	DALY	4.53×10^{-9}	1.68×10^{-8}
2	Respiratory effects by organic substances	DALY	1.02×10^{-10}	6.96×10^{-11}
3	Respiratory effects by inorganic substances	DALY	6.01×10^{-8}	1.60×10^{-7}
4	Climate change	DALY	4.88×10^{-8}	3.17×10^{-8}
5	Ionizing radiation	DALY	8.10×10^{-11}	4.69×10^{-9}
6	Ozone layer depletion	DALY	3.03×10^{-11}	5.23×10^{-11}
7	Ecotoxicity	PDF m^2 yr	3.63×10^{-23}	2.14×10^{-3}
8	Acidification/eutrophication	PDF m^2 yr	1.55×10^{-3}	3.60×10^{-3}
9	Land use	PDF m^2 yr	1.10×10^{-3}	6.00×10^{-3}
10	Minerals extraction	MJ surplus	3.71×10^{-4}	2.40×10^{-4}
11	Fossil fuels extraction	MJ surplus	5.25×10^{-1}	5.10×10^{-2}

3.3.2.4 Interpretation. The solution of the mathematical model previously presented is defined by a set of Pareto points that represent the optimal trade-off between the objectives considered. From these alternatives, the decision-maker should choose the best one according to his/her preferences and the applicable legislation. Note that the selection of the final alternative needs some articulation of preferences. In our work, the preferences are articulated in the post-optimal analysis of the Pareto solutions. This approach provides further insights into the design problem and allows for a better understanding of the trade-off between the criteria considered in the analysis. In this regard, upon analysis of the trade-off points, decision-makers should try to operate in those regions where significant environmental improvements can be achieved at a marginal increase in the total cost.

4. Solution method

The design task is finally posed as a bi-criteria nonlinear programming (NLP) problem. Multi-objective optimization methods have been extensively applied to the design of sustainable processes [9,12–14,36,37,20]. The problem can therefore be mathematically expressed as follows:

$$\begin{aligned} (\mathrm{M}) \quad \min_{x} \quad & U(x) = \{f_1(x), f_2(x)\} \\ \text{s.t.} \quad & h(x) = 0 \\ & g(x) \leqslant 0 \\ & x \in \Re \end{aligned} \tag{21}$$

The solution to this problem is given by a set of efficient or Pareto optimal points representing alternative process designs, each achieving a unique combination of environmental and economic performances [21,36]. The continuous variables x represents state or design variables (i.e., thermodynamic properties, flows, operating conditions, and sizes of equipment units). The equality constraints $h(x) = 0$ represent thermodynamic property relations, mass and energy balances, cost and LCA calculations. On the other hand, the inequality constraints $g(x) \leqslant 0$ represent the design specifications, such as minimum and maximum equipment capacities and upper and lower limits on process variables. Finally, $f_1(x)$ and $f_2(x)$ denote the economic and environmental performances of the cycle, respectively.

The general concept of Pareto frontier is depicted in Fig. 3. In the figure f_1 and f_2 represent the total cost and environmental impact, respectively. The points that lie in the Pareto curve are the Pareto optimal solutions of the problem. The mathematical definition of Pareto optimality states that a design objective vector f^* is Pareto optimal if there does not exist another design objective vector f

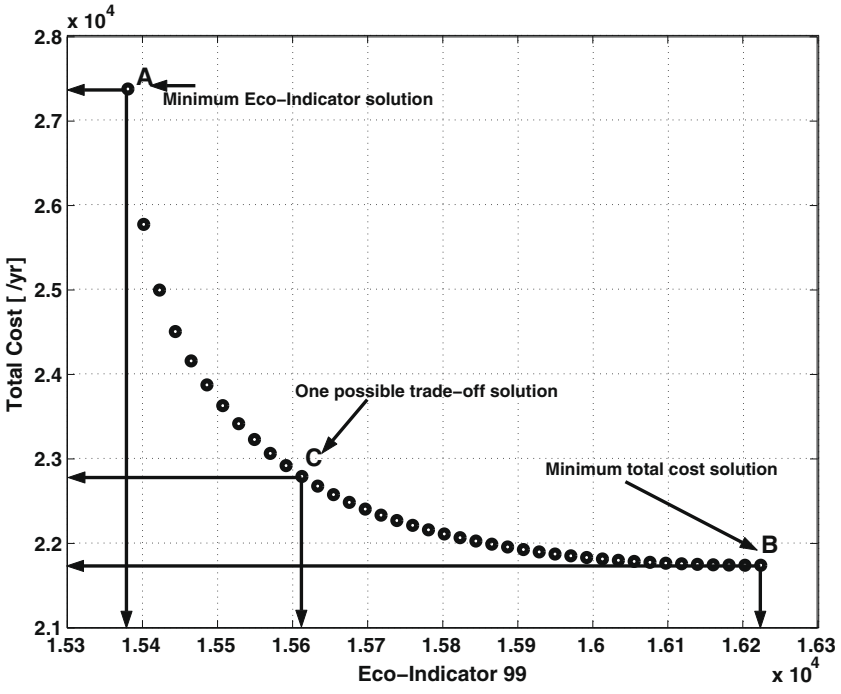

Fig. 4. Pareto set of solutions considering the total annualized cost and Eco-indicator 99 value.

UNIVERSITAT ROVIRA I VIRGILI
OPTIMIZATION OF ENVIRONMENTALLY FRIENDLY SOLAR ASSISTED ABSORPTION COOLING SYSTEMS
Berhane Hagos Gebreslassie
ISBN: 978-84-693-7673-7/DL:T-1752-2010

in the feasible design space such that $f_i \leqslant f_i^*$ for all $i \in \{1,2,\ldots,n\}$ and $f_i < f_i^*$ for at least one $i \in \{1,2,\ldots,n\}$. Thus, given a Pareto solution A, it is impossible to find another solution B that performs better than A for each objective. Notice that no solution exists below the Pareto curve, because this would violate the definition of Pareto optimality (i.e., this solution would dominate some of the Pareto optimal ones, which by definition cannot be dominated).

For the calculation of the Pareto set of (M), two main methods exist in the literature. These are the weighted-sum method and the ϵ-constraint method [9,36]. The weighted-sum method is only rigorous for the case of convex problems, whereas the epsilon constraint (ϵ-constraint) method is rigorous for convex and non-convex problems. In general, the thermodynamic correlations used to determine the enthalpies in model (M) will add non-convexities in the mathematical formulation. Thus, the ϵ-constraint method is better suited to our problem.

This method is based on formulating an auxiliary model (MA), which is obtained by transferring one of the objectives of the original problem (M) to an additional constraint. This constraint imposes an upper limit on the value of the secondary objective.

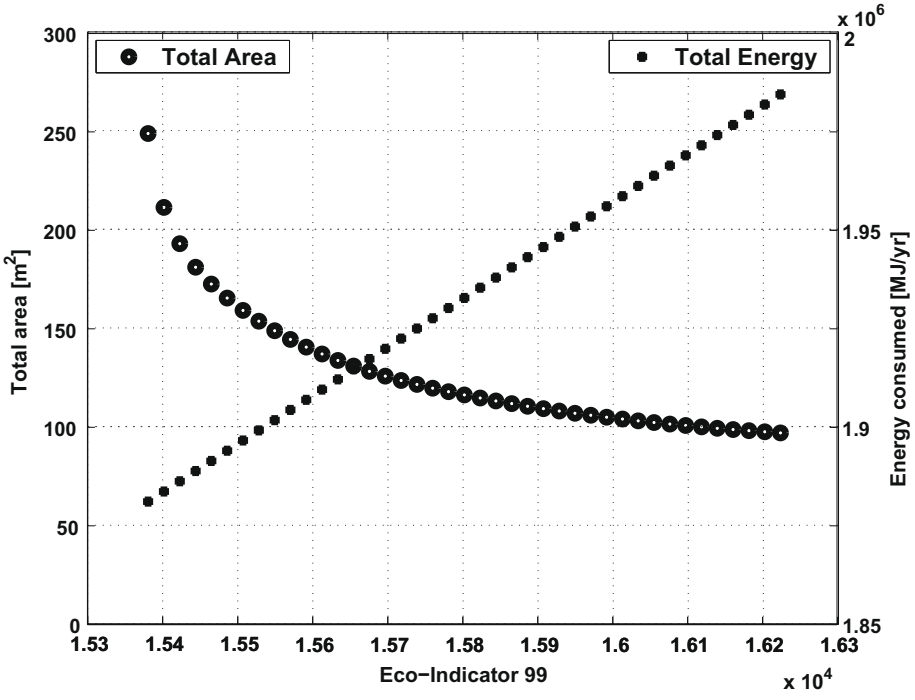

Fig. 5. Total size of heat exchangers and total energy consumed vs. Eco-indicator 99.

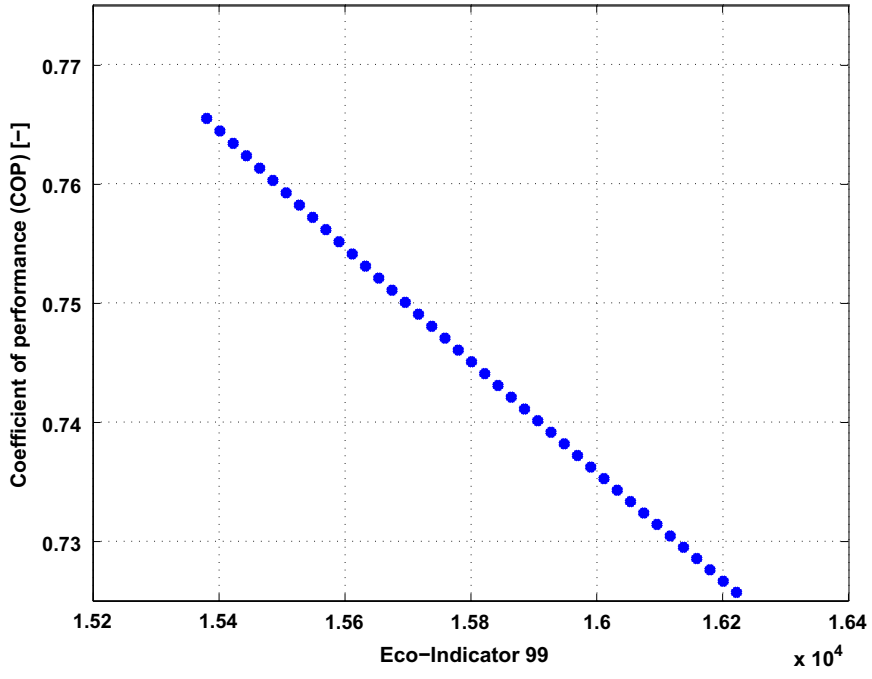

Fig. 6. Coefficient of performance vs. Eco-indicator 99.

Model (MA) is then solved for different values of the auxiliary parameter ϵ in order to generate the entire Pareto set of solutions:

$$\begin{aligned} (\mathrm{MA}) \quad & \min_x \ f_1(x) \\ & \text{s.t.} \quad f_2(x) \leqslant \epsilon \\ & \quad \underline{\epsilon} \leqslant \epsilon \leqslant \bar{\epsilon} \\ & \quad h(x) = 0 \\ & \quad g(x) \leqslant 0 \\ & \quad x \in \Re \end{aligned} \tag{22}$$

Thus, if (MA) is solved for all possible values of ϵ and the resulting solutions are unique, then these solutions represent the entire Pareto set of solutions of the original multi-objective problem. If the solutions to (MA) are not unique for some value(s) of ϵ, then the Pareto point(s) must be picked by direct comparison. The extreme points of the interval $[\underline{\epsilon}, \bar{\epsilon}]$, within which ϵ must fall, $\epsilon \in [\underline{\epsilon}, \bar{\epsilon}]$, can be determined by solving the following single objective problems:

$$\begin{aligned} & \underline{\epsilon} = f_2(\bar{x}^*) \\ \bar{x}^* = \ & \arg\min_x f_2(x) \\ & h(x) = 0 \\ & g(x) \leqslant 0 \\ & x \in \Re \end{aligned} \tag{23}$$

$$\begin{aligned} & \bar{\epsilon} = f_2(\bar{x}^*) \\ \bar{x}^* = \ & \arg\min_x f_1(x) \\ & h(x) = 0 \\ & g(x) \leqslant 0 \\ & x \in \Re \end{aligned} \tag{24}$$

5. Case study

The capabilities of our approach is illustrated through a case study problem that addresses the design of a typical absorption cooling system. The system is driven by low grade heat and utilizes ammonia–water as working pair. The process data and environmental information of the problem are given in Tables 1–3. These data include the operating conditions, heat exchanger design parameters, costs parameters and environmental information. The environmental inventory data were retrieved from the Eco-invent database [33–35]. The Hierarchist damage model and normalization with the Average weighting factors were adopted in the LCA calculations (see Table 3).

6. Results and discussion

A bi-criteria nonlinear programming (NLP) simulation model was implemented in GAMS [25]. The resulting optimization problem contains 165 constraints and 206 continuous variables. Each single-objective problem was solved with CONOPT [38]. This solver attempts to find a local optimum to an NLP model. Since problem (MA) is non-convex, CONOPT cannot guarantee the global optimality of the solutions found. Each of these solutions must therefore be regarded as locally optimal unless a global optimization package like BARON [39] is used.

The problem is first solved by optimizing each single objective separately. This provides the lower and upper limits within which ϵ fall. Then, the interval $[\underline{\epsilon}, \bar{\epsilon}]$ is partitioned into 40 sub-intervals of equal length, and model (MA) is calculated for each of the limits of

Table 5
Thermodynamic properties and mass flow rates at each state point of the cycle in Pareto solution B.

State point	P (bar)	T (°C)	x $\left(\frac{kg}{kg}\right)$	m $\left(\frac{kg}{s}\right)$	h $\left(\frac{kJ}{kg}\right)$
1	0.48	33.1	0.548	0.401	−102.5
2	1.55	33.1	0.548	0.401	−99.2
3	1.55	79.1	0.548	0.401	105.7
4	1.55	95.7	0.429	0.317	189.4
5	1.55	41.1	0.429	0.317	−69.7
6	0.48	41.1	0.429	0.317	−69.7
9	1.55	79.1	0.996	0.084	1417.0
10	1.55	39.8	0.996	0.084	185.8
11	1.55	23.8	0.996	0.084	110.1
12	0.48	3.0	0.996	0.084	110.1
13	0.48	3.0	0.996	0.084	1303.0
14	0.48	38.8	0.996	0.084	1378.6
15	1.00	27.0		4.024	116.2
16	1.00	35.0		4.024	149.7
17	1.00	100.0		0.06	2678.0
18	1.00	100.0		0.06	418.6
19	1.00	27.0		3.087	116.2
20	1.00	35.0		3.087	149.7
21	1.00	10.0		4.785	42.1
22	1.00	5.0		4.785	21.1

Table 4
Thermodynamic properties and mass flow rates at each state point of the cycle in Pareto solution A.

State point	P (bar)	T (°C)	x $\left(\frac{kg}{kg}\right)$	m $\left(\frac{kg}{s}\right)$	h $\left(\frac{kJ}{kg}\right)$
1	0.50	28.1	0.596	0.267	−114.2
2	1.39	28.1	0.596	0.267	−110.1
3	1.39	70.0	0.596	0.267	76.4
4	1.39	93.7	0.416	0.184	180.3
5	1.39	36.1	0.416	0.184	−90.3
6	0.50	36.1	0.416	0.184	−90.3
9	1.39	70.0	0.996	0.083	1404.0
10	1.39	36.0	0.996	0.083	166.8
11	1.39	22.2	0.996	0.083	101.5
12	0.50	4.0	0.996	0.083	101.5
13	0.50	4.0	0.996	0.083	1304.0
14	0.50	35.0	0.996	0.083	1370.0
15	1.00	27.0		3.820	116.2
16	1.00	35.0		3.820	149.7
17	1.00	100.0		0.057	2678.0
18	1.00	100.0		0.057	418.6
19	1.00	27.0		3.076	116.2
20	1.00	35.0		3.076	149.7
21	1.00	10.0		4.785	42.1
22	1.00	5.0		4.785	21.1

Table 6
Thermodynamic properties and mass flow rates at each state point of the cycle in Pareto solution C.

State point	P (bar)	T (°C)	x $\left(\frac{kg}{kg}\right)$	m $\left(\frac{kg}{s}\right)$	h $\left(\frac{kJ}{kg}\right)$
1	0.50	30.1	0.579	0.318	−109.3
2	1.45	30.1	0.579	0.318	−105.6
3	1.45	72.6	0.579	0.318	83.4
4	1.45	92.4	0.431	0.235	172.9
5	1.45	38.1	0.431	0.235	−83.4
6	0.50	38.1	0.431	0.235	−83.4
9	1.45	72.6	0.996	0.083	1408.0
10	1.45	37.4	0.996	0.083	173.7
11	1.45	22.9	0.996	0.083	105.4
12	0.50	4.0	0.996	0.083	105.4
13	0.50	4.0	0.996	0.083	1304.4
14	0.50	36.4	0.996	0.083	1373.0
15	1.00	27.0		3.878	116.2
16	1.00	35.0		3.878	149.7
17	1.00	100.0		0.058	2678.0
18	1.00	100.0		0.058	418.6
19	1.00	27.0		3.078	116.2
20	1.00	35.0		3.078	149.7
21	1.00	10.0		4.785	42.1
22	1.00	5.0		4.785	21.1

Table 7
Operating performance, cost and environmental impact of Pareto solutions A, B, and C.

Design	COP (–)	TC (euro/yr)	C_{op} (euro/yr)	C_c (euro/yr)	A_{total} (m^2)	Steam (kg)	Electricity (MJ)	Total ECO99
ECO99 (A)	0.77	27,366	15,983	11,383	248.5	825,464	15,838	15,381
Cost (B)	0.73	21,737	16,903	4834	96.8	869,737	18,948	16,223
Trade-off (C)	0.76	22,786	16,239	6548	136.8	837,582	16,832	15,612

Table 8
Normalized contribution of each impact category to the total Eco-indicator 99 value in Pareto solution C.

	Impact categories	Impact (steam)	Impact (electricity)	Total trade-off
1	Carcinogens	98.54	7.34	105.90
2	Respiratory effects by organic substances	2.21	0.03	2.24
3	Respiratory effects by inorganic substances	1307.00	69.95	1377.00
4	Climate change	1061.00	13.86	1075.00
5	Ionizing radiation	1.76	2.05	3.81
6	Ozone layer depletion	0.66	0.02	0.68
7	Ecotoxicity	2371.00	2.81	2373.00
8	Acidification/eutrophication	101.07	4.74	105.80
9	Land use	72.05	7.87	79.93
10	Minerals extraction	7.40	0.10	7.50
11	Fossil fuels extraction	10461.00	20.44	10481.00
	ECO99	15484.00	129.20	15613.20

these sub-intervals. The total computation time for the generation of the efficient solutions is 2.75 s in a 1.86 GHz machine. The Pareto points obtained by following this strategy are shown in Fig. 4. As can be observed in the figure, there is a clear trade-off between both objective functions, since a reduction in the total Eco-indicator 99 value can only be achieved at the expense of an increase in the total annualized cost. Points A and B are the optimal design solutions with minimum Eco-indicator 99 and total annualized cost values, respectively. In the optimal solution A, the total annualized cost is 25.9% larger than in solution B, whereas in B, the Eco-indicator 99 is 5.5% larger than in A. Point C represents a possible intermediate Pareto optimal solution in the interval $[\underline{\epsilon}, \overline{\epsilon}]$.

Note that each point in the Pareto set represents a different optimal design which operates under a set of specific conditions. Furthermore, each trade-off solution involves a different compromise between both criteria. The environmental impact is decreased along the Pareto curve by reducing the consumption of energy (i.e., steam and electricity), which in turn decreases the environmental loads and, hence, the impact caused. This is accomplished by increasing the area of the heat exchangers of the cycle. Ideally, the size of the heat exchangers and the energy consumption should be simultaneously minimized in order to decrease the total cost and environmental impact. However, this is not possible, since a reduction in the size of the heat exchangers leads to an increase in the thermal energy demand (i.e., steam consumption), which turns out to be the main contributor to the total environmental impact, and vice versa. This is clearly shown in Fig. 5, which depicts for the obtained Pareto solutions, the total area and energy consumption as a function of the Eco-indicator 99 value.

Let us note that in the cost and environmental assessment analysis, there is an inherent trade-off between energy consumption and size of the cycle. In the cost analysis, we have that bigger areas lead to higher capital cost but on the other hand to lower energy consumption. In the environmental analysis, we find that greater equipments reduce the impact due to the energy production but on the other hand increase the impact associated with their construction. In both cases, each of these terms is penalized with a different factor (energy and capital cost in the former case, and energy and equipment impact in the latter). These weighting factors (i.e., cost and environmental impact parameters) will conduct the optimization search towards a particular solution. Hence, the minimum cost alternative will not be in general the same as the minimum environmental impact one, since both solutions will depend on the specific values of the economic and environmental

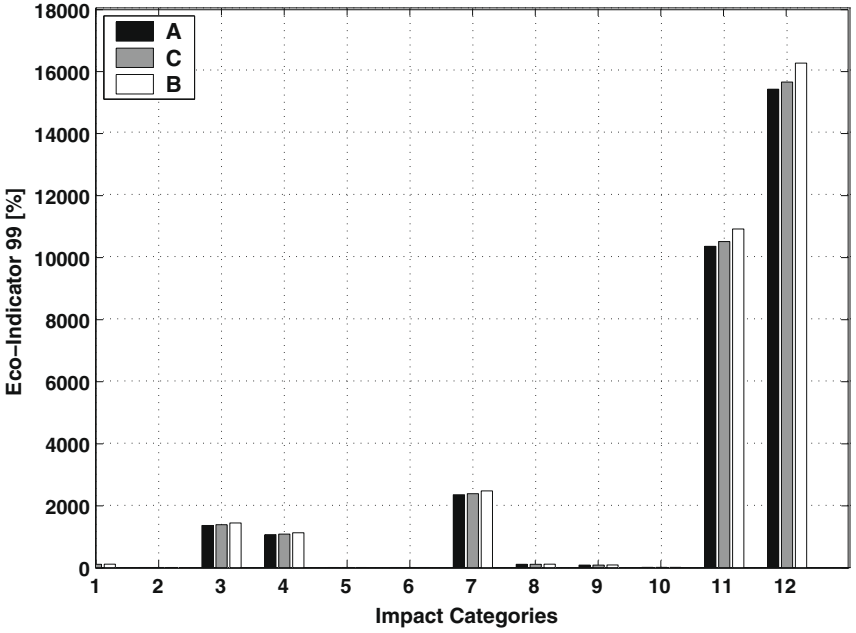

Fig. 7. Breakdown of Eco-indicator 99 for Pareto solutions A, B, and C.

data used in the analysis. We should also clarify at this point that the impact due to the equipment construction is usually very small compared to that caused by the energy generation. For this reason, it has been neglected in our work, although it could have been easily incorporated into the model.

Fig. 6 shows the direct relationship between the COP and the total Eco-indicator 99 value. Note that the COP is the ratio between the cooling load, which is constant, and the energy input to the system given in Eq. (9). As can be observed, when the energy input increases, both the COP and the Eco-indicator 99 value increase.

Tables 4–7 summarize the solutions A, B, and C. The information given includes the thermodynamic properties of each state point of the cycle, the mass flow rates, the design and operating variables of the heat exchangers, and the values of both objective functions. As can be seen, when the energy consumption increases, the solution temperature and the pressure level increase accordingly. As a result, the concentration gradient decreases, and the mass flow rate of the solution is increased in order to keep the cooling load constant.

Furthermore, in Table 7 one can see as the steam and electricity consumption increase, the total Eco-indicator 99 value increases accordingly, while the heat transfer area requirement decreases. For instance, the Eco-indicator 99 value of solution C is lower by 3.8% from solution B, and higher by 1.5% from A. On the other hand, its total annualized cost is 16.8% lower than solution A, and 4.8% higher than B. Therefore, taking B as reference, if we switch from B to C it leads to a 3.8% reduction in the total Eco-indicator 99 value at the expense of increasing the cost by 4.8%.

Table 8 shows the Eco-indicator 99 values and environmental impact of all 11 impact categories along with each contributors of Pareto solution C. As can be observed, the steam production is the main contributor to the total environmental impact in almost all damage categories, except for the damage to human health caused by ionization radiation, in which the electricity generation contributes more than 50% to the total impact.

Finally, Fig. 7 shows a breakdown of the Eco-indicator 99 value into its single impact categories for the Pareto solutions A, B, and C. As can be seen, the most significant environmental impact is the depletion of natural resources (impact 11) followed by the damage to the ecosystem quality caused by ecotoxic emissions (impact 7). The third and fourth damages are the respiratory effects on human health caused by inorganic substance (impact 3) and the damage to human health caused by climate change (impact 4), respectively.

Note that these specific results are very sensitive to the life cycle inventory data, which in our case were retrieved from the Ecoinvent databases. Hence, the conclusions and recommendations made may significantly change according to the specific features of the technologies employed for the generation of steam and electricity.

7. Conclusions

A systematic approach for the design of sustainable absorption cooling systems has been presented. The method introduced relies on formulating a bi-criteria nonlinear programming (NLP) problem that accounts for the minimization of the total annualized cost and the environmental impact of the cycle. The latter criterion has been measured according to the principles of life cycle assessment (LCA). The solution of such a problem, which is defined by a set of Pareto optimal design alternatives, can be obtained via standard techniques for multi-objective optimization.

The capabilities of the proposed approach have been illustrated through its application to the design of a typical absorption cooling system. It has been clearly shown that significant reductions in the environmental impact caused by the cycle can be attained if the decision-maker is willing to compromise the economic performance of the system. These reductions can be achieved by decreasing the energy consumption, which on the other hand leads to an increase in the total cost of the cycle. The methodology presented is intended to promote a more sustainable design of absorption cycles by guiding the decision-makers towards the adoption of alternatives that cause less environmental impact.

Acknowledgements

Berhane H. Gebreslassie expresses his gratitude for the financial support received from the University Rovira i Virgili. The authors also wish to acknowledge support of this research work from the Spanish Ministry of Education and Science (DPI2008-04099/DPI) and the Spanish Ministry of External Affairs (A/8502/07 and HS2007-0006).

References

[1] McMullan JT. Refrigeration and the environment – issues and strategies for the future. Int J Refrig 2002;25:89–99.
[2] Herold KE, Radermacher R, Klein SA. Absorption chillers and heat pumps. CRC Press; 1996.
[3] Florides GA, Kalogirou SA, Tassou SA, Wrobel LC. Modelling simulation and warming impact assessment of a domestic-size absorption solar cooling system. Appl Therm Eng 2002;22:1313–25.
[4] Palacios BR, Gonzales PR, Nebra SA. Thermoeconomic analysis of a single and double-effect LiBr/H_2O absorption refrigeration system. In: Andrzej Z, Zygmunt K, Wojciech S, editors. ECOS, 2008. p. 287–98.
[5] Misra PK, Sahoo RD, Gupta A. Thermoeconomic evaluation and optimization of an aqua-ammonia vapour-absorption refrigeration system. Int J Refrig 2006;29:47–59.
[6] Misra PK, Sahoo RD, Sahoo S, Gupta A. Thermoeconomic optimization of a single effect water/LiBr vapour absorption refrigeration system. Int J Refrig 2003;26:158–69.
[7] Kizllkan Ö, Sencan A, Kalogirou SA. Thermoeconomic optimization of a LiBr absorption refrigeration system. Chem Eng Process: Process Intens 2007;46:1376–84.
[8] Bejan A, Tsatsaronis G, Moran M. Thermal design & optimization. John Wiley & Sons; 1996.
[9] Guillén-Gosálbez G, Caballero JA, Jiménez L, Gadalla M. Application of life cycle assessment to the structural optimization of process flowsheets. Comput Aid Chem Eng 2007;24:1163–8.
[10] Stefanis SK, Livingston AG, Pistikopoulos EN. Minimizing the environmental impact of process plants: a process systems methodology. Comput Chem Eng 1995;19:39–44.
[11] Dantus MM, High KA. Evaluation of waste minimization alternatives under uncertainty: a multiobjective optimization approach. Comput Chem Eng 1999;23:1493–508.
[12] Azapagic A. Life cycle assessment and its application to process selection, design and optimisation. Chem Eng J 1999;73:1–21.
[13] Azapagic A, Clift R. The application of life cycle assessment to process optimisation. Comput Chem Eng 1999;10:1509–26.
[14] Azapagic A, Clift R. Life cycle assessment and multiobjective optimisation. J Clean Product 1999;7:135–43.
[15] Kotas TJ. The exergy method of thermal plant analysis. Krieger Publishing Company; 1995.
[16] Riva A, D'Angelosante S, Trebeschi C. Natural gas and the environmental results of life cycle assessment. Energy 2006;31:138–48.
[17] Prek M. Environmental impact and life cycle assessment of heating and air conditioning systems, a simplified case study. Energy Build 2004;36:1021–7.
[18] Masruroh NA, Li B, Klemes J. Life cycle analysis of a solar thermal system with thermochemical storage process. Appl Energy 2006;31:537–48.
[19] Góralczyk M. Life-cycle assessment in the renewable energy sector. Appl Energy 2003;75:205–11.
[20] Fu Y, Diwekar UM. Cost effective environmental control technology for utilities. Adv Environ Res 2004;8:173–96.
[21] Hugo A, Pistikopoulos EN. Environmentally conscious planning and design of supply chain networks. J Clean Product 2005;13:1471–91.
[22] PRé-Consultants. The Eco-indicator 99A damage oriented method for life cycle impact assessment. methodology report and manual for designers. Technical Report, PRé Consultants, Amersfoort, The Netherlands, 2000.
[23] Sencan A, Yakut KA, Kalogirou SA. Exergy analysis of lithium bromide/water absorption systems. Renew Energy 2005;30:645–57.
[24] Best R, Islas J, Martínez M. Exergy efficiency of an ammonia–water absorption system for ice production. Appl Energy 1993;45:241–56.
[25] Brooke A, Kendrik D, Meeraus A, Raman R, Rosenthal RE. GAMS – a user's guide. Washington: GAMS Development Corporation; 1998.

[26] Pátek J, Klomfar J. Simple functions for fast calculations of selected thermodynamic properties of the ammonia–water system. Int J Refrig 1995;18:228–34.
[27] Conde Engineering M. Thermophysical properties of $NH_3 + H_2O$ mixtures for the industrial design of absorption refrigeration equipment. Technical Report, 2006.
[28] Edgar TF, Himmelblau DM, Lasdon DS. Optimization of chemical processes. McGraw-Hill; 2001.
[29] Siddiqui MA. Economic analyses of absorption systems: part a – design and cost evaluation. Energy Convers Manage 1997;38:889–904.
[30] Wall G. Optimization of refrigeration machinery. Int J Refrig 1997;14:336–40.
[31] Al-Otaibi DA, Dincer I, Kalyon M. Thermoeconomic optimization of vapor-compression refrigeration systems. Int Commun Heat Mass Transfer 2004;31:95–107.
[32] IRAM-ISO 14040. Environmental management-Life cycle assessment-principles and frame work, 2006.
[33] Ecobalance-UK. TEAM and DEAM. Ecobalance UK, The Ecobilan Group, Arundel, UK, 1998. <http://www.ecobalance.com/uk_team.php>.
[34] PIRA-International. PEMS 4 Database. PIRA International, Leatherhead, UK, 1998. <http://www.pira.co.uk/pack/lca_software.htm>.
[35] PRé-Consultants. SimaPro 6 LCA software. The Netherlands, 1998. <http://www.pre.nl/simapro/default.htm>.
[36] Hugo A, Ciumei C, Buxton A, Pistikopoulos EN. Environmental impact minimization through material substitution: a multi-objective optimization approach. Green Chem 2004;6:407–17.
[37] Eliceche AM, Corvalán SM, Martínez P. Environmental life cycle impact as a tool for process optimisation of a utility plant. Comput Chem Eng 2007;31:648–56.
[38] Drud A. CONOPT solver manual. Bagsvaerd, Denmark: ARKI Consulting and Development; 1996.
[39] Drud A. BARON user manual. The Optimization Firm, LLC; 2004.

Applied Thermal Engineering 29 (2009) 3491–3500

Contents lists available at ScienceDirect

Applied Thermal Engineering

journal homepage: www.elsevier.com/locate/apthermeng

Economic performance optimization of an absorption cooling system under uncertainty

Berhane H. Gebreslassie [a], Gonzalo Guillén-Gosálbez [b], Laureano Jiménez [b], Dieter Boer [a,*]

[a] Department of Mechanical Engineering, University Rovira i Virgili, Av. Països Catalans, 26, 43007 Tarragona, Spain
[b] Department of Chemical Engineering, University Rovira i Virgili, Av. Països Catalans, 26, 43007 Tarragona, Spain

ARTICLE INFO

Article history:
Received 13 March 2009
Accepted 2 June 2009
Available online 6 June 2009

Keywords:
Absorption refrigeration
Stochastic programming
Multi-objective optimization
Uncertainty
Ammonia–water
Energy cost

ABSTRACT

Many of the strategies devised so far to address the optimization of energy systems are deterministic approaches that rely on estimated data. However, in real world applications there are many sources of uncertainty that introduce variability into the decision-making problem. Within this general context, we propose a novel approach to address the design of absorption cooling systems under uncertainty in the energy cost. As opposed to other approaches that optimize the expected performance of the system as a single objective, in our method the design task is formulated as a stochastic bi-criteria non-linear optimization problem that simultaneously accounts for the minimization of the expected total cost and the financial risk associated with the investment. The latter criterion is measured by the downside risk, which avoids the need to define binary variables thus improving the computational performance of the model. The capabilities of the proposed modeling framework and solution strategy are illustrated in a case study problem that addresses the design of a typical absorption cooling system. Numerical results demonstrate that the method presented allows to manage the risk level effectively by varying the area of the heat exchangers of the absorption cycle. Specifically, our strategy allows identifying the optimal values of the operating and design variables of the cycle that make it less sensitive to fluctuations in the energy price, thus improving its robustness in the face of uncertainty.

1. Introduction

Energy plays an important role in supporting our daily life, economic development and every human activity. Energy systems are complex as they involve various economic, technical, environmental, legal and political factors [1,2]. Due to the limitation of fossil energy resources, the impact on the environment, and the human health problems during the last decades, there has been a growing interest on developing modeling and optimization strategies for energy systems. In this challenging scenario, absorption cycles have emerged as a promising alternative in cooling and refrigeration applications, as they use refrigerant with zero global warming potential that do not contribute to the ozone layer depletion [3,4]. Moreover, another advantage of these systems is that they can use different forms of primary energy sources such as fossil fuels, renewable energy sources, and also waste heat recovered from other thermal systems.

Unfortunately, these systems require higher number of units than conventional vapor compression cycles, which leads to higher investment costs. Hence, there is a clear need to develop strategies able to optimize their design and operation from a thermodynamic and economic point of view so they can become a real alternative to the standard compression systems. Specifically, most of the methods proposed so far to accomplish this task rely on the concept of thermoeconomic analysis [5–7], an approach that combines in a single framework both, a thermodynamic model (usually based on exergy considerations) and an economic model (i.e., a cost model).

An alternative strategy that has been widely applied in the optimization of process industries is the simultaneous approach based on mathematical programming [8]. In this second method, the design task is posed as an optimization problem that is solved via standard techniques for linear, non-linear, mixed-integer linear and mixed-integer non-linear (LP, NLP, MILP, MINLP, respectively) programming. Although these strategies have been extensively used in the optimization of chemical processes (see [9]), their application to the design of absorption cooling systems has been rather limited, and only a few works can be found in the area [10,11] that deals with the optimization of an ammonia–water absorption cycle by application of MINLP following a deterministic approach.

Most of the strategies that address the optimization of thermal systems following either of the aforementioned approaches are deterministic. That is, they are typically based on nominal or estimated values for all the input data considered in the analysis

* Corresponding author. Tel.: +34 977559631; fax: +34 977559691.
E-mail address: Dieter.Boer@urv.cat (D. Boer).

1359-4311/$ - see front matter © 2009 Elsevier Ltd. All rights reserved.
doi:10.1016/j.applthermaleng.2009.06.002

Nomenclature

Abbreviations

A	absorber
C	condenser
D	desorber
E	evaporator
P	solution pump
RV	refrigerant expansion valve
SC	subcooler
SHX	solution heat exchanger
SV	solution expansion valve
yr	year

Indices

i	component of a stream
j	streams
k	unit

Sets

$IN(k)$	set of input streams to unit k
$OUT(k)$	set of output streams from unit k

Parameters

c_1	cost parameter $\left(\frac{€}{m^2}\right)$
c_2	cost parameter (€)
c_3	cost parameter $\left(\frac{€}{kW}\right)$
cq_s	unitary cost of steam in scenario s $\left(\frac{€}{MWh}\right)$
ce_s	unitary cost of electricity in scenario s $\left(\frac{€}{MWh}\right)$
cr	capital recovery factor (–)
$prob_s$	probability of total cost of scenario s
ir	interest rate (–)
t_{op}	operating hours $\left(\frac{h}{yr}\right)$
U_k	overall heat transfer coefficient of unit k $\left(\frac{kW}{m^2K}\right)$

Variables

A_k	area of heat exchanger k (m^2)
CC	total capital cost (€)
C_{exp}	cost of the expansion valves (€)
C_{hxs}	cost of the heat exchangers (€)
CO_s	total operating cost in scenario s (€)
C_p	cost of the pump (€)
COP	coefficient of performance (–)
$DRisk$	downside risk (€)
$E[TC]$	expected total cost (€)
ΔT_k^{lm}	logarithmic mean temperature difference in equipment k (°C or K)
ΔT_k^{h}	temperature difference in the hot end in equipment k (°C or K)
ΔT_k^{c}	temperature difference in the cold end in equipment k (°C or K)
ΔT	temperature difference of heat exchangers in equipment k (°C or K)
h_j	enthalpy of stream j $(\frac{kJ}{kg})$
m_j	mass flow rate of stream j $\left(\frac{kg}{s}\right)$
P_j	pressure of stream j (bar)
P	probability (–)
Q_k	heat transferred in unit k (kW)
TC	total cost (€)
TC_s	total cost in scenario s (€)
T_j	temperature of stream j (°C or K)
W_p	mechanical power of the pump (kW)
$x_{i,j}$	mass fraction of component i in stream j (–)
z_s	binary variable (1 if the cost in scenario s exceeds the target level, 0 otherwise)

Greek letters

Ω	target on the total cost (€)
δ	deviation of TC from Ω (€)
δ_s	deviation of TC_s from Ω (€)

[5,12–17]. This means that the key parameters that influence the optimization task are assumed to be perfectly known in advance, so the only situation assessed in the study is the most likely one. This type of strategies lead to decisions by far too optimistic, in which the variability of the parameters of the problem is disregarded. However, in real world applications there are many sources of uncertainty that introduce variability into the decision-making problem. This is especially true in the optimization of energy systems, in which the availability of energy sources, technology performance, energy cost and end user cooling and heating demand, among many others, are affected by a high degree of uncertainty [2,18–21].

In the process system engineering literature, the inclusion of uncertainty issues in the decision-making procedure has recently emerged as an active area of research. There are currently three main approaches that address optimization under uncertainty (for a detailed review see [19]): (1) stochastic programming [22–28], (2) fuzzy programming [1,2,20,29,30] and (3) stochastic dynamic programming [31]. The main applications of these tools have focused on process design [33–35], planning and scheduling of process plants [23,27,28,36–38] and also on the design and planning of entire chemical supply chains [22,26,39]. On the other hand, in the modeling and optimization of energy systems, uncertainty considerations have been usually neglected. Whereas there are few works that account for uncertainty issues in the planning of energy systems [1,2,20,29,30], to our knowledge the design under uncertainty of such systems has not yet been addressed.

Specifically, Cai et al. [2] studied the identification of optimal strategies for energy management planning where the total cost, energy demand, technology efficiency and energy import costs are considered as uncertain and represented by fuzzy sets. Lin et al. [1] have addressed the energy system planning by integration of interval-parameter and fuzzy programming into a two stage stochastic programming framework to handle energy demand uncertainty. Sadeghi et al. [20] studied the energy supply planning in Iran using fuzzy models to represent the investment cost uncertainty. Mavrotas et al. [29] used fuzzy linear programming to optimize energy planning in buildings by considering the fuel costs as uncertain or fuzzy parameters. Svensson et al. [32] developed a methodology for identifying robust process integration investments under uncertainty using a real options approach. Taylor et al. [40] performed an uncertainty analysis on the design of piping systems, piping networks, and cross-flow heat exchangers. The authors showed that uncertainty analysis is a viable paradigm for energy system analysis and design.

The objective of this work is to address the design of absorption cooling systems under uncertainty in the energy cost. The main novelties of this work are: (1) the explicit consideration of uncertainty issues at the design stage of absorption cooling cycles and (2) the development of a bi-criteria mathematical model that employs risk management techniques to deal with the associated decision-making problem under uncertainty. The approach presented relies on formulating the design task as a stochastic non-linear programming problem (NLP) that accounts

for the simultaneous minimization of the expected total cost and the financial risk of the investment. The capabilities of our modeling framework and solution strategy are illustrated through a case study problem, for which the set of Pareto solutions that represent the optimal compromise between cost and risk are obtained.

2. Problem statement

2.1. System description (absorption cycle)

Compared to a compression cooling cycle, the basic idea of an absorption system is to replace the electricity consumption associated with the vapor compression by a thermally driven absorption–desorption system [4]. This is accomplished by making use of absorption and desorption processes that employ a suitable working fluid pair. The working pair consists of a refrigerant and an absorbent. In this study, without loss of generality, an ammonia/water solution is used as working pair, with the ammonia being the refrigerant and water the absorbent.

Fig. 1 represents the considered absorption cycle in a pressure–temperature plot. The system provides chilled water for cooling applications and is steam driven. The basic components are the absorber (*A*), condenser (*C*), desorber (*D*) and evaporator (*E*). The cycle also includes the refrigerant subcooler (*SC*), refrigerant expansion valve (*RV*), solution heat exchanger (*SHX*), solution pump (*P*), and solution expansion valve (*SV*). The high pressure equipments are the solution heat exchanger, desorber, and condenser, whereas the low pressure ones are the evaporator and absorber.

The system operation is as follows: The refrigerant in vapor phase (stream 14) coming from the subcooler (*SC*) is absorbed in the absorber (*A*) by the diluted liquid solution (stream 6). The concentrated solution (stream 1) leaving the absorber is pumped by pump (*P*) to reach a higher pressure (stream 2) before being preheated in the solution heat exchanger (*SHX*). Then, the solution (stream 3) enters the desorber, in which the desorption of ammonia takes place. In this work, only the stripping section of the desorber is considered. Vapor refrigerant (stream 9) from the desorber condenses completely in the condenser (*C*). The liquid refrigerant (stream 10) from the condenser is then subcooled (stream 11) in the subcooler (*SC*) by the superheating stream (stream 13) that comes from the evaporator (*E*). The liquid refrigerant (stream 11) flows to the evaporator (*E*) through the refrigerant expansion valve (*RV*). The weak liquid solution (stream 4) from the desorber returns back to the absorber (*A*) through the solution heat exchanger (*SHX*), which preheats the concentrated solution (stream 2) before being introduced to the desorber. From the heat exchanger, the solution is finally sent to the expansion valve (*SV*), and then to the absorber (*A*).

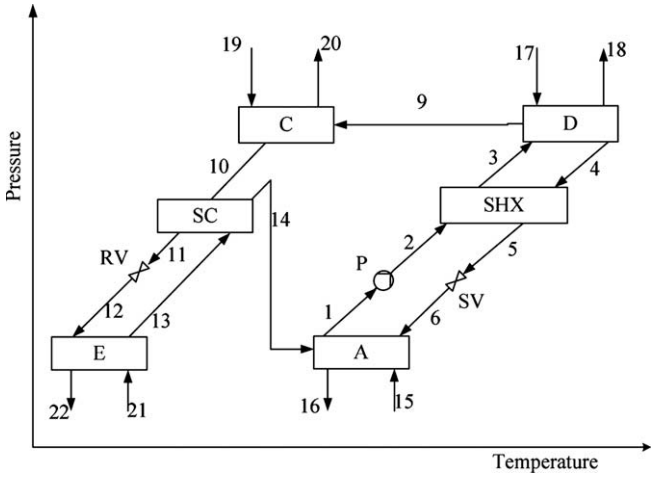

Fig. 1. Ammonia–water absorption cycle.

Note that streams 15–22 are external heat transfer fluids. In our case, water is used for energy supply and energy extracting. The useful output energy is the heat extracted in the evaporator (Q_E), whereas the input energy is supplied to the desorber (Q_D). The system includes a low pressure steam boiler where the primary energy resources are fossil fuels. For the sake of simplicity, the process of steam production has not been included in our model. However, the model could be easily modified in order to account for such a system.

Specifically, in this work we address the optimal design of an absorption cooling cycle like the one described before under uncertainty in the energy cost. Given are the cooling capacity of the system, the inlet and outlet temperatures of the external fluids and capital cost data. It is assumed that the energy cost cannot be perfectly forecasted, and that its variability can be represented by a set of scenarios with a given probability of occurrence. Hence, the goal of our study is to determine the optimal design and associated operating conditions that simultaneously minimize the total expected cost of the cycle and its risk level.

Note that, in general, the impact that the energy cost variability has in the overall economic performance of a process may vary from one type of industry to another, and will depend on the percentage of the total expenses that are due to the energy consumption. Furthermore, the energy consumption of a process industry and hence the energy cost, can be properly tuned by adjusting the associated design variables. Standard deterministic methods tend to optimize the economic performance of a process considering mean energy cost values. Stochastic methods can lead to more robust designs, in which the energy consumption is reduced in order to make the system less sensitive to fluctuations in the energy price. This allows to decrease the probability of unfavorable scenarios with large energy expenses.

3. Multi-objective stochastic model

This section introduces the mathematical model derived to address the problem described above. Specifically, in our work, the design task is posed as a multi-scenario bi-criteria NLP problem that simultaneously minimizes the expected total cost of the investment and its risk level. The solution of this problem is defined by a set of trade-off alternatives, each of which involves different structural and operating features. The choice of a scenario-based approach is motivated by the fact that it can deal with any type of probability distribution. This can be accomplished by using sampling techniques, such as a Monte Carlo sampling, that allow generating a set of representative scenarios from any type of probability function.

The mathematical model of the cycle is based on the one introduced by the authors in [41]. The major difference between the formulation presented in [41] and that described next is that in the latter one the model only considers the stripping section of the distillation, as proposed by Roriz et al. [42]. Note that since the evaporation temperature is above 0 °C, the enrichment process of ammonia in the rectification column does not bring significant performance improvement [43]. For the sake of completeness of this work, we next discuss the main features

of the formulation. The reader is referred to the original work for more technical details. Specifically, the model is based on the following assumptions:

- Steady state operation.
- Heat losses are not considered.
- Pressure losses are not considered.
- The refrigerant leaves the condenser as a saturated liquid.
- The solutions leave the absorber and desorber as saturated liquids.
- The solution and refrigerant valves are adiabatic.

The mathematical formulation includes two main parts: (1) general constraints (see Section 3.1) and (2) objective function related constraints (see Sections 3.2.1 and 3.2.2) that allow to assess the economic and risk performance of the cycle. Both parts are described in detail in the following sections.

3.1. General constraints

As mentioned before, these equations are added to enforce the mass and energy conservation. These principles are applied to all the units of the cycle, each of which is treated as a control volume with inlet and outlet streams, heat transfer and work interactions [4] (see Fig. 2). This is accomplished via the following equation:

$$\sum_{j\in IN(k)} m_j x_{i,j} - \sum_{j\in OUT(k)} m_j x_{i,j} = 0 \quad \forall\, k,i \tag{1}$$

Eq. (1) represents the mass balances, and states that the total amount of component i that enters unit k must equal the total amount of i that leaves k. In this equation, m_j denotes the mass flow of stream j, and $x_{i,j}$ is the mass fraction of component i in stream j. Note that j can be either an inlet or outlet stream. Hence, in this equation $IN(k)$ denotes the set of inlet streams of unit k, whereas $OUT(k)$ represents the set of outlet streams.

$$\sum_{j\in IN(k)} m_j h_j - \sum_{j\in OUT(k)} m_j h_j + Q_k^{IN} - Q_k^{OUT} - W_k = 0 \quad \forall\, k \tag{2}$$

Eq. (2) defines the energy balances in the system assuming no heat losses. The difference in energy content between the inlet and outlet streams, plus the heat supplied to the unit (Q_k^{IN}) must equal the heat removed (Q_k^{OUT}) plus the work done (W_k) by the unit. Note that the heat and work terms in Eq. (2) can take a zero value in some of the units, as shown in Eqs. (3)–(5):

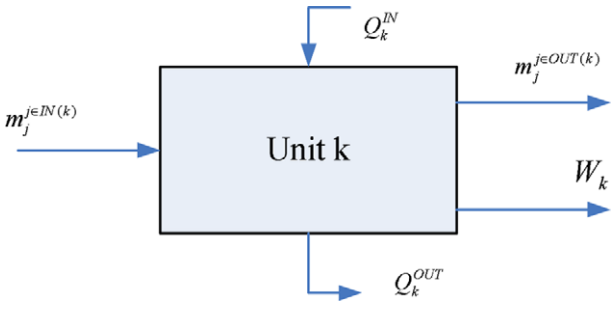

Fig. 2. A generic unit of the absorption cycle.

$$Q_k^{IN} = 0 \quad \text{if } k = \left\{ \begin{array}{l} \text{Absorber } (A) \\ \text{Condenser } (C) \\ \text{Subcooler } (SC) \\ \text{Solution heat exchanger } (SHX) \\ \text{Pump } (P) \\ \text{Expansion valves } (RV, SV) \end{array} \right\} \tag{3}$$

$$Q_k^{OUT} = 0 \quad \text{if } k = \left\{ \begin{array}{l} \text{Evaporator } (E) \\ \text{Desorber } (D) \\ \text{Subcooler } (SC) \\ \text{Solution heat exchanger } (SHX) \\ \text{Pump } (P) \\ \text{Expansion valves } (RV, SV) \end{array} \right\} \tag{4}$$

$$W_k = 0 \quad \forall\, k \neq \text{pump} \tag{5}$$

Furthermore, the enthalpy of a stream is determined from its temperature (T), pressure (P), and composition, as stated in Eq. (6)

$$h_j = f(T_j, P_j, x_{i,j}) \qquad \forall\, j \tag{6}$$

Specifically, the model makes use of the correlations proposed by Pátek and Klomfar [44] to estimate the thermodynamic properties of the ammonia–water mixture.

The heat exchangers are modeled using the logarithmic mean temperature difference (ΔT_k^{lm}), the heat transfer area (A_k) and the overall heat transfer coefficient (U_k), as shown in Eq. (7).

$$Q_k = U_k A_k \Delta T_k^{lm} \qquad \forall\, k \tag{7}$$

The logarithmic mean temperature difference, which is a function of the hot and cold end temperature differences (ΔT_k^h and ΔT_k^c, respectively), is calculated via the Chen's approximation. This avoids the discontinuity of the function at $\Delta T_k^h = \Delta T_k^c$, which in turn improves the robustness of the mathematical formulation and its numerical performance [41].

$$\Delta T_k^{lm} \cong \left[\Delta T_k^h \Delta T_k^c \frac{\Delta T_k^h + \Delta T_k^c}{2} \right]^{\frac{1}{3}} \quad \forall\, k \tag{8}$$

The coefficient of performance (COP) is determined via Eq. (9) as the ratio between the energy extracted from the chilled water and the total energy supplied to the system [4].

$$COP = \frac{Q_{k=E}}{Q_{k=D} + W_{k=P}} \tag{9}$$

3.2. Objective function

As mentioned before, the model considerers that the energy cost is uncertain and that its variability can be described through a set of scenarios with given probability of occurrence. As a result, the cost associated with the construction and operation of a cycle is not a single nominal value, instead it is a stochastic variable that follows a discrete probability function. In this context, the optimization method must identify the set of solutions (i.e., cycles) that simultaneously minimize the expected value of the cost distribution as well as its risk level.

The traditional approach to address optimization under uncertainty relies on formulating a single-objective optimization problem where the expected performance of the system is the objective to be optimized. This strategy does not allow controlling the variability of the objective function in the uncertain space. In

other words, optimizing the expected economic performance of a cycle does not imply that the process will yield better results at a certain level considering the whole cost distribution. The underlying idea in risk management is to incorporate the trade-off between financial risk and expected cost within the decision-making procedure. This gives rise to a multi-objective optimization problem in which the expected performance and a specific risk measure are the objectives considered. The solution of such a problem is given by a set of Pareto solutions that represent the optimal trade-off between expected performance and risk level. Specifically, in our work, the probability of meeting unfavorable scenarios is controlled by considering the downside risk as an additional objective to be minimized.

3.2.1. Expected cost performance

The expected total cost $E[TC]$, which is given by the mean value of the discrete distribution of the cost, can be calculated as follows:

$$E[TC] = \sum_s prob_s TC_s \tag{10}$$

where TC_s is the total cost corresponding to the realization of each scenario s, and $prob_s$ is the probability of occurrence of such scenario. Note that the set of scenarios considered in the analysis must be provided as input data by the decision-maker. In those cases where the uncertain parameters follow certain types of probability functions, they can be obtained, for instance, by performing a sampling on them.

The total annualized cost in each scenario s accounts for both, the capital and operating costs of the cycle (CC and CO_s, respectively):

$$TC_s = CC + CO_s \tag{11}$$

As can be observed, the uncertainty in the energy price only affects the operating cost. Hence, the capital cost is not scenario dependent, whereas the value of the operating cost depends on the specific scenario realization. The assumption of a deterministic capital investment is justified by the fact that this type of cost is usually agreed before the construction of the equipment, so it can be perfectly known in advance. On the other hand, the operating cost tends to fluctuate according to the market trends, so it cannot be predicted accurately at the design stage.

The annualized capital cost includes the cost of the heat exchangers (C_{hxs}), pumps (C_p) and expansion valves (C_{exp}) times the capital recovery factor (cr)

$$CC = (C_{hxs} + C_p + C_{exp})cr \tag{12}$$

The cost of the heat exchangers can be estimated using the linear correlation proposed by KizIlkan et al. [6].

$$C_{hxs} = \sum_{k=heat\ \ exchanger} (c_1 A_k + c_2) \tag{13}$$

In Eq. (13), c_1 and c_2 are the variable and fixed cost parameters, respectively, associated with the heat exchangers used in the system. These parameters relate the area of a heat exchanger with its cost. The cost of the pump can be calculated using the correlation introduced by Siddiqui [45]:

$$C_p = c_3 W_p^{0.4} \tag{14}$$

where W_p denotes the pump power and c_3 is a cost parameter. It should be noticed that in many applications the cost of the expansion valves can be neglected, since their contribution to the system cost is usually rather small. The capital recovery factor (cr) is a function of the interest rate (ir) and the life span (i.e., number of useful years, n) of the unit under consideration [7]:

$$cr = \frac{ir(ir+1)^n}{(ir+1)^n - 1} \tag{15}$$

Finally, the total annualized operating cost includes the cost of the steam used in the desorber, the electricity consumed by the pump and the cooling water. Usually, the latter term can be neglected compared to the remaining ones, so the operating cost can be finally calculated as follows:

$$CO_s = (cq_s Q_{k=D} + ce_s W_{k=P}) t_{op} \tag{16}$$

In this equation, cq_s and ce_s are the unitary costs of heat and electricity in scenario s, whereas t_{op} is the total annual operating time.

3.2.2. Financial risk

In mathematical terms, the financial risk associated with a design project can be defined as the probability of not meeting a certain target profit (maximization) or cost (minimization) level referred to as Ω [22,27]. Hence, the financial risk associated with a design x and a target Ω can be expressed as follows:

$$Risk(x, \Omega) = P[TC(x) \geqslant \Omega] \tag{17}$$

Here, $TC(x)$ is the actual total cost, that is, the cost resulting after the uncertainty has been unveiled and a scenario realized. The above probability can be expressed in terms of the probability of exceeding the target cost in each individual scenario realization:

$$Risk(x, \Omega) = \sum_s prob_s z_s(x, \Omega) \tag{18}$$

where z_s is a binary variable defined for each scenario, as follows:

$$z_s(x, \Omega) = \begin{cases} 1 & \text{if } TC_s \geqslant \Omega \\ 0 & \text{otherwise} \end{cases} \forall\ s$$

As can be observed, for a given design, the probability of exceeding the target cost in each particular scenario is either zero or one. A possible way of avoiding the use of binary variables when evaluating the financial risk is to utilize the definition of downside risk [46]. The financial risk associated with design x and target total cost (Ω) is given by the area under the probability curve from the target cost = Ω to $+\infty$ as shown in Fig. 3a. A more straight forward way of assessing the trade-off between risk and total cost is using the cumulative probability associated with a given design x and target level (see Fig. 3b). Here, the downside risk is the area enclosed above the cumulative probability curve between the target level and positive infinity. Mathematically, this metric can be determined as follows:

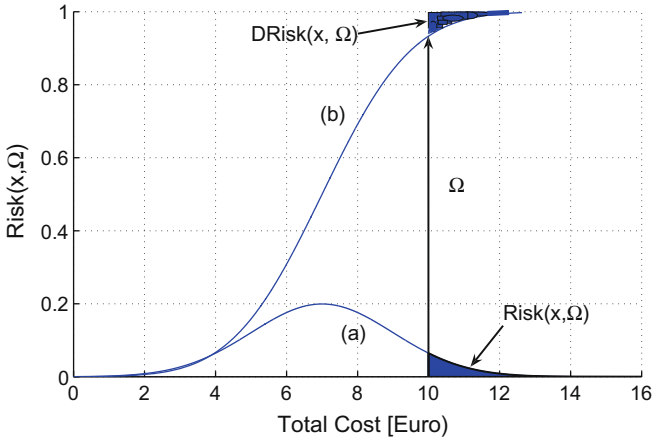

Fig. 3. Cumulative risk curve.

$$DRisk(x,\Omega) = \sum_s prob_s \delta_s(x,\Omega) \tag{19}$$

where $\delta(x,\Omega)$ is a positive variable that measures the deviation from a target Ω, that is:

$$\delta_s(x,\Omega) \geqslant TC_s - \Omega \quad \forall\, s \tag{20}$$

Notice that the downside risk is a continuous linear measure that does not require the definition of binary variables. This is a highly desirable property to potentially reduce the computational requirements of the models to manage risk.

3.3. Remarks

- The model presented accounts for the minimization of the expected total annualized cost of the cycle. To calculate the cost associated with a given time horizon, it suffices to multiply the annualized cost with the corresponding number of years. Note that the results of the optimization problem do not depend on the number of periods considered in the study, since the number of years is a constant value and hence can be removed from the objective function without affecting the calculations.
- By performing some algebraic transformations on the economic objective function of the model, it can be shown that minimizing the expected total cost is equivalent to minimizing the cost in the mean scenario, assuming that the same energy consumption is attained in all the scenarios:

$$\begin{aligned} E[TC] &= \sum_s prob_s TC_s \\ &= \sum_s prob_s [CC + (cq_s Q_{k=D} + ce_s W_{k=P}) t_{op}] \\ &= \sum_s prob_s CC + \sum_s prob_s cq_s Q_{k=D} t_{op} + \sum_s prob_s ce_s W_{k=P} t_{op} \\ &= CC \sum_s prob_s + Q_{k=D} t_{op} \sum_s prob_s cq_s + W_{k=P} t_{op} \sum_s prob_s ce_s \\ &= CC + Q_{k=D} t_{op} \overline{cq} + W_{k=P} t_{op} \overline{ce} \end{aligned} \tag{21}$$

  Here, $\overline{cq}$ and $\overline{ce}$ represent the expected values of the energy and electricity cost, respectively. In practice, it is convenient to replace constraint (10) by Eq. (21) in order to achieve a better numerical performance. Note that this simplification assumes that the operating conditions of the cycle are fixed once the design is decided on (i.e. Q_k is equal in all scenarios).
- As shown in [37], both the financial risk and downside risk can be effectively manipulated by minimizing the worst case (i.e., the total cost in the most unfavorable scenario). The worst case posses also the desired property of avoiding the definition of auxiliary binary variables.
- The model presented can handle uncertainties in any of the coefficients of the objective function, including the capital cost. This represents an important feature of the proposed approach.
- In those cases in which the uncertain coefficients follow specific types of probability functions (see [47]), it is possible to apply chance constrained programming techniques to perform an analytical integration of the probabilistic constraint defined by Eq. (17).

4. Solution method

The design task is finally posed as a bi-criteria non-linear programming (NLP) problem of the following form:

$$\begin{aligned} (\mathrm{M}) \quad & \min_x \quad U = \{E[TC], DRisk\} \\ & \text{s.t.} \quad \text{constraints } (1)-(16),\ (19) \text{ and } (20) \end{aligned} \tag{22}$$

The solution to this problem is given by a set of efficient or Pareto optimal points representing alternative process designs, each achieving a unique combination of economic performance and downside risk. For the calculation of the Pareto set of (M), two main methods exist in the literature. These are the weighted-sum method and the ϵ-constraint method [48]. The weighted-sum method is only rigorous for problems with convex Pareto sets, whereas the epsilon constraint (ϵ-constraint) method is rigorous for both, the convex and non-convex cases. In general, the thermodynamic correlations used to determine the enthalpies in model (M) will add non-convexities in the mathematical formulation. Thus, the ϵ-constraint method is better suited to our problem.

This method is based on formulating an auxiliary model (MA), which is obtained by transferring one of the objectives of the original problem (M) to an additional constraint. This constraint imposes an upper limit on the value of the secondary objective. Model (MA) is then solved for different values of the auxiliary parameter ϵ in order to generate the entire Pareto set of solutions:

$$\begin{aligned} (\mathrm{MA}) \quad & \min_x \quad E[TC] \\ & \text{s.t.} \quad DRisk(x,\Omega) \leqslant \epsilon \\ & \quad\quad \text{constraints } (1)-(16),\ (19) \text{ and } (20) \end{aligned} \tag{23}$$

The extreme points of the search interval of ϵ ($\epsilon \in [\underline{\epsilon}, \overline{\epsilon}]$), can be determined by optimizing each single objective separately.

5. Case study

The capabilities of our approach are illustrated through a case study that addresses the design of a typical absorption cooling system (see Fig. 1). The system is an absorption cooling cycle driven by low grade heat that utilizes ammonia–water as working pair. The input data of the problem, which includes the cooling capacity of the cycle and the external fluid (water) temperatures, are given in Table 1. A time horizon of 15 years was considered, so the annualized total cost was multiplied by 15 in the calculations. Note that, as commented before, the consideration of a specific time horizon does not affect the output of the optimization model.

The uncertain parameters (i.e., steam and electricity cost) were described through 100 equiprobable scenarios that were generated by performing a Monte Carlo sampling on a set of Gaussian probability functions. Specifically, we considered five distributions with mean values 1, 1.5, 2, 2.5 and 3 times larger than the nominal energy cost used in [41]. All these distributions assumed a standard deviation of 30 %. Figs. 4a and b show the histogram of frequencies associated with the resulting discrete probability distributions that characterize the heat and electricity cost.

6. Results and discussion

The problem was implemented in the modeling system GAMS [49] interfacing with CONOPT [50] as main optimization package. The resulting optimization problem features 713 continuous variables and 821 constraints. In general, the number of variables and constraints of the model is a function of the number of scenar-

Table 1
Process data of the absorption cooling cycle.

Heat transfer coefficients $U\left[\frac{kW}{m^2K}\right]$ and temperature data (°C)	Ref. [41]
Desorber heating steam temperature (°C)	110
Cost data	Ref. [41]
Operation time per year (h)	1000
Other data	Ref. [41]

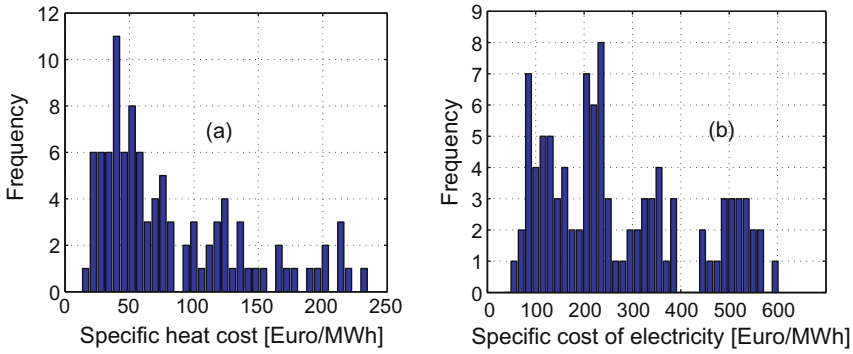

Fig. 4. Histograms of frequencies of the energy cost parameters.

ios considered, and the number of equipment units and streams. The number of scenarios is typically determined by applying a statistical analysis. On the other hand, the number of process units and streams is given by the topology of the absorption cycle.

Note that the global optimality of the solutions found cannot be guaranteed, since we are using a local optimizer. Thus, these solutions must be regarded as locally optimal unless a global optimization method is employed [51]. The application of this last type of techniques, which tend to be highly computationally intensive, is out of the scope of the current work. Hence, we consider that a local solution to the problem is sufficient for the purpose of the analysis performed.

6.1. Pareto optimal set of solutions

The model was first solved by optimizing each single objective separately. In the calculation of the downside risk, the target level Ω was set to 4.5×10^5 €. These single-objective optimizations provided the lower and upper limits of the search interval in which the downside risk must fall. This interval was next partitioned into 20 sub-intervals, and the model was then calculated for the limits of each of them. The total computation time was 2.91 s on a 1.81 GHz machine.

The Pareto points obtained by following this strategy are shown in Fig. 5. Note that each point of the Pareto set represents a different optimal design operating under a set of specific conditions. Furthermore, each trade-off solution involves a different compromise between expected total cost and risk. As can be observed in the figure, there is a clear trade-off between both objective functions, since a reduction in downside risk can only be achieved at the expense of an increase in the expected total cost.

The points A and B shown in Fig. 5 are the two extreme Pareto optimal designs. In design A, the expected total cost is 1.2% smaller than in B, whereas in B the downside risk is 6.1% smaller than in A. It is interesting to notice that in the upper part of the Pareto curve it is possible to achieve a substantial reduction of the downside risk at the expense of a marginal increase of the expected total cost. For example, in solution C, where $DRisk = 12,870$ € and

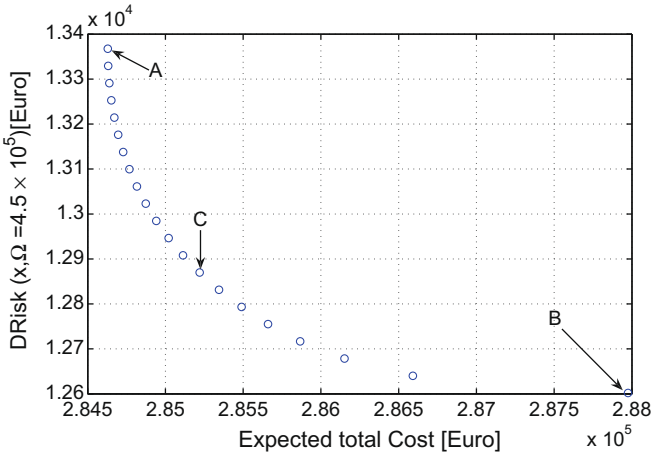

Fig. 5. Pareto optimal set.

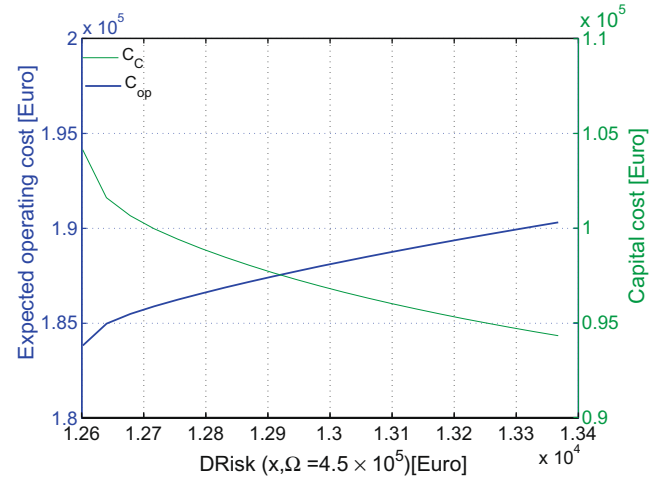

(a) Relationship between CC, CO and DRisk.

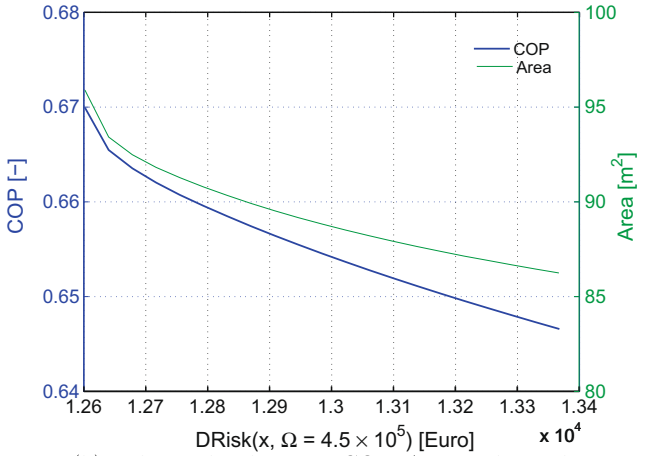

(b) Relationship between COP, Area and DRisk.

Fig. 6. Relationship between capital cost, expected operating cost, coefficient of performance, total area of the cycle and *DRisk*.

UNIVERSITAT ROVIRA I VIRGILI
OPTIMIZATION OF ENVIRONMENTALLY FRIENDLY SOLAR ASSISTED ABSORPTION COOLING SYSTEMS
Berhane Hagos Gebreslassie
ISBN: 978-84-693-7673-7/DL:T-1752-2010

$E[TC] = 285,220$ € it is possible to decrease the downside risk by 4% at the expense of increasing the total cost only by 0.21%. Hence, in view of these results, it seems convenient to select solutions close to cycle A, since they can reduce the risk level without compromising to a large extent the average economic performance of the system.

Furthermore, Fig. 6a depicts the capital cost and the expected operating cost of the cycles of the Pareto curve as a function of the downside risk. As can be observed, reducing the downside risk level leads to an increase in the capital cost, since this implies investing in heat exchangers with larger areas. In practice, the reduction of the expected operating cost that is attained by using bigger equipments does not compensate the extra capital investment required. Hence, the overall effect is that the expected total cost and downside risk tend to be conflictive criteria, as already discussed before. In Fig. 6b we show the relationship between the total area of the cycle, the coefficient of performance (COP) and the downside risk level. As can be seen, the minimization of the downside risk leads to cycles with better COPs and larger areas. Note that the reduction in the energy consumption makes the cycle less sensitive to the fluctuations in the price of steam, which is the main parameter affecting the operating cost. This leads to a more robust behavior of the system in the face of uncertainty.

6.2. Cumulative risk curves

Fig. 7 shows risk curves (cumulative probability vs total cost) associated with the extreme Pareto optimal designs. As can be observed, when the risk is reduced, the probability curve "rotates" in such a way that its lower part moves to the left whereas the upper one moves to the right. This is because the probability of highly undesirable scenarios (i.e., scenarios with high total cost) is reduced at the expense of lowering the probability of favorable situations (i.e., with a small total cost). For instance, in the minimum cost solution, the probability of exceeding a high cost level (like for instance 556,500 €), is 8%, whereas in the least risky one this probability drops to 5%. On the other hand, the probability of a total cost bellow 186,000 € is 26% in the minimum cost solution and 21% in the minimum downside risk one.

Finally, Fig. 8, depicts the total cost associated with each particular scenario realization. As shown in the figure, there are cases in which the minimum cost solution performs better than the minimum downside risk one, and others in which the opposite situation occurs. A more detailed analysis of these results reveals that, as expected, the minimum cost solution is superior when the energy price is low, whereas the other one yields better results when the energy cost increases.

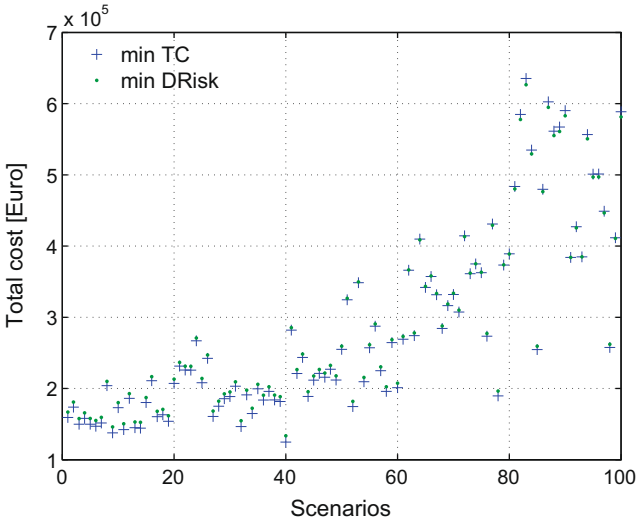

Fig. 8. Scenario realizations of the extreme solutions.

6.3. Sensitivity analysis

Note that the shape of the risk curves, and even the existence of a trade-off between expected cost and risk, will depend on the specific example being solved, and more precisely on the capital and operating cost data. In our example, it turns out that the difference between the curves is not very pronounced. In order to elucidate whether this was a particular feature of our example or not, we ran several case studies that differed in the values of the target level as well as the operating and capital cost parameters.

In first place, we solved the problem considering a risk-taker decision-maker with a preference for a small target level ($\Omega = 2 \times 10^5$ €). Fig. 9 shows the obtained results that illustrate how the risk curves of the extreme solutions of the problem tend to approximate when a small value of Ω is chosen. In other words, risk-takers will chose solutions close to the minimum expected cost one.

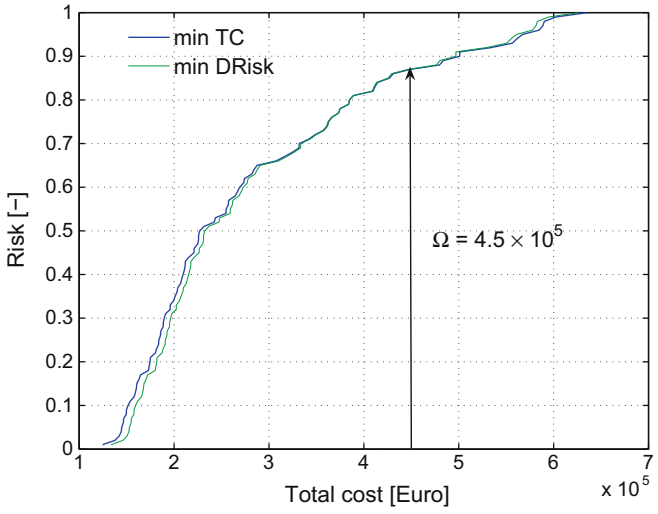

Fig. 7. Cumulative risk curves of the extreme solutions for $\Omega = 4.5 \times 10^5$ €.

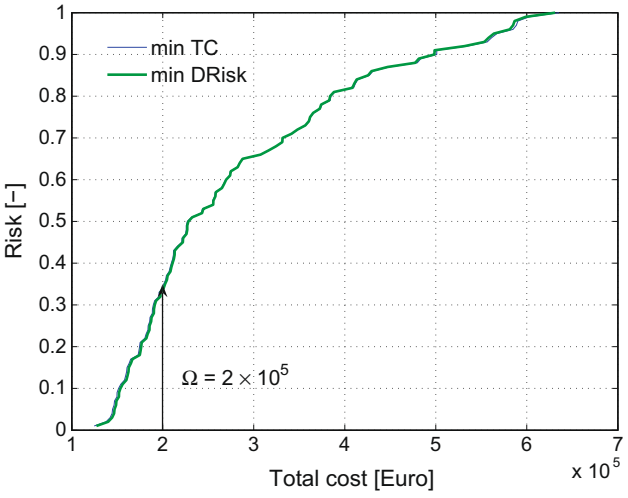

Fig. 9. Cumulative risk curves of the extreme solutions for $\Omega = 2 \times 10^5$ €.

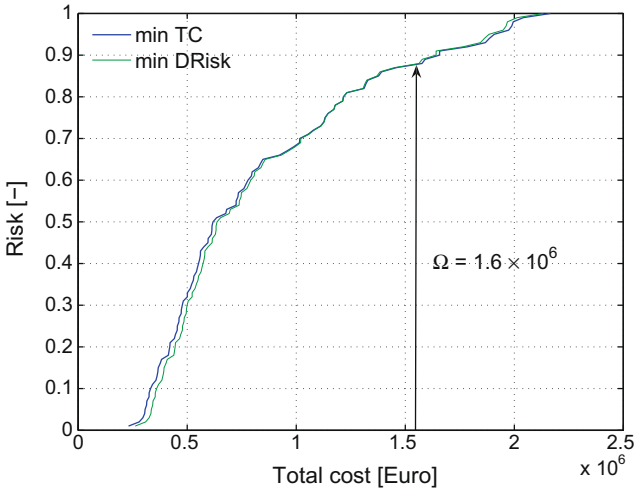

(a) Cumulative risk curves of the extreme solutions for t_{op}= 4,000 h

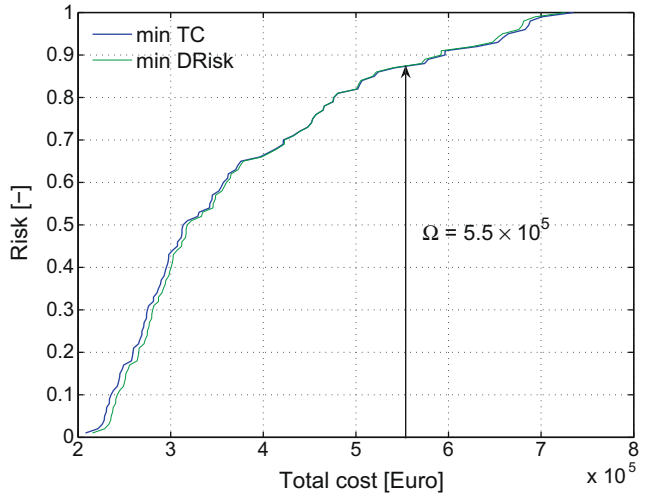

(b) Cumulative risk curves of the extreme solutions for doubled CC.

Fig. 10. Cumulative risk curves of the extreme solutions for $t_{op} = 4000$ h and doubled CC.

To study the impact that the operation and capital cost have in the risk curves, we next solved two examples which differed in the operating times and capital cost coefficients. In the first case, we considered an annual operating time of 4000 h per year in order to increase the weigh of the operating cost in the total cost of the system. The target level for this case was fixed to $\Omega = 1.6 \times 10^6$ €. Given this data, the model tries to minimize the operating cost by investing in equipments with larger areas. As a result, the trade-off between expected total cost and downside risk is small, since the areas of the heat exchangers are already large in order to minimize the energy consumption. Consequently, the cumulative risk curves of the extreme solutions are quite close, as depicted in Fig. 10a.

In the second example we doubled the coefficients of the capital costs and set $\Omega = 5.5 \times 10^5$ €. In this case, the optimization model minimizes the capital cost by investing in smaller heat exchangers, since they represent a large percentage of the total cost. As a result, the trade-off between expected cost and downside risk is more pronounced, and the risk curves move away, as shown in Fig. 10b.

As can be observed, in all the cases the probability curves of the extreme solutions are quite close. Hence, in view of these numerical results and in the absence of a more rigorous theoretical analysis, we conclude that the design problem is *per se* quite rigid (i.e., it is difficult to manipulate the risk associated with the investment). This might be attributed to the inherent trade-off that naturally exists between the capital and operating cost of an absorption cycle (i.e., to reduce the operating cost it is necessary to invest in larger equipments). In any case, as discussed and shown before, the risk level can still be manipulated to a certain extent by properly varying the areas of the equipments. This is an interesting insight that we get from the stochastic model, which shows how the optimal design of an absorption cycle is not very much affected by the uncertainty in the energy cost, since the potential savings that can be achieved by decreasing the energy consumption are compensated by the required increase in the capital investment. We should note, however, that such a conclusion strongly depends on the input data of the model.

7. Conclusions

This work has presented a systematic approach for the design of absorption cooling cycles under uncertainty in the energy cost. The design task has been formulated as a bi-criteria stochastic NLP model that seeks to minimize the expected total cost and the associated risk. The latter criterion has been measured by the downside risk, which avoids the definition of binary variables thus leading to better numerical performance. The solution to the problem is given by a set of Pareto optimal solutions that trade-off the objectives considered in the analysis. In this work, these solutions have been calculated via the epsilon constraint method.

The capabilities of the proposed modeling framework and solution strategy have been illustrated through the design of a typical absorption cooling system. It has been clearly shown that reductions in the downside risk can be attained by slightly increasing the expected cost of the cycle. This can be achieved by investing in heat exchangers with larger areas, which lowers energy consumption thus making the cycle less sensitive to fluctuations in the energy price.

Acknowledgements

Berhane H. Gebreslassie expresses his gratitude for the financial support received from the University Rovira i Virgili. The authors also wish to acknowledge support of this research work from the Spanish Ministry of Education and Science (Projects DPI2008-04099, PHB2008-0090-PC and BFU2008- 863 00196) and the Spanish Ministry of External Affairs (Projects A/8502/07, HS2007- 864 0006 and A/020104/08).

References

[1] Q.G. Lin, G.H. Huang, B. Bass, X.S. Qin, IFTEM: an interval-fuzzy two-stage stochastic optimization model for regional energy systems planning under uncertainty, Energy Policy 37 (3) (2009) 868–878.
[2] Y.P. Cai, G.H. Huang, Z.F. Yang, Q. Tan, Identification of optimal strategies for energy management systems planning under multiple uncertainties, Applied Energy 86 (4) (2009) 480–495.
[3] J.T. McMullan, Refrigeration and the environment – issues and strategies for the future, International Journal of Refrigeration 25 (2002) 89–99.
[4] K.E. Herold, R. Radermacher, S.A. Klein, Absorption Chillers and Heat Pumps, CRC Press, 1996.
[5] R.D. Misra, P.K. Sahoo, A. Gupta, Thermoeconomic evaluation and optimization of an aqua–ammonia vapour-absorption refrigeration system, International Journal of Refrigeration 29 (2006) 47–59.
[6] . Kizllkan, A. Sencan, S.A. Kalogirou, Thermoeconomic optimization of a LiBr absorption refrigeration system, Chemical Engineering and Processing: Process Intensification 46 (2007) 1376–1384.
[7] A. Bejan, G. Tsatsaronis, M. Moran, Thermal Design & Optimization, John Wiley & Sons Inc., 1996.
[8] I.E. Grossmann, J.A. Caballero, H. Yeomans, Mathematical programming approaches for the synthesis of chemical process systems, Korean Journal of Chemical Engineering 16 (1999) 407.

[9] L.T. Biegler, A.W. Westerberg, I.E. Grossmann, Systematic Methods of Chemical Process Design, Prentice-Hall, PTR, NJ, 1997.
[10] L.M. Chavez-Islas, C.L. Heard, I.E. Grossmann, Synthesis and optimization of an ammonia–water absorption refrigeration cycle considering different types of heat exchangers by application of mixed-integer nonlinear programming, Industrial & Engineering Chemistry Research 48 (6) (2009) 2972–2990.
[11] L.M. Chavez-Islas, C.L. Heard, Optimization of a simple ammonia–water absorption refrigeration cycle by application of mixed-integer nonlinear programming, Industrial & Engineering Chemistry Research 48 (4) (2009) 1957–1972.
[12] T. Savola, T-M. Tveit, C-J. Fogelholm, A MINLP model including the pressure levels and multiperiods for CHP process optimisation, Applied Thermal Engineering 27 (11–12) (2007) 1857–1867.
[13] T. Savola, C-J. Fogelholm, Minlp optimisation model for increased power production in small-scale CHP plants, Applied Thermal Engineering 27 (1) (2007) 89–99.
[14] J. Wang, Y. Dai, G. Lin, Parametric analysis and optimization for a combined power and refrigeration cycle, Applied Energy 85 (11) (2008) 1071–1085.
[15] G.Q. Zhang, L. Wang, L. Liu, Z. Wang, Thermoeconomic optimization of small size central air conditioner, Applied Thermal Engineering 24 (4) (2004) 471–485.
[16] Z. Yang, S.G. Zhang, H.B. Zhao, Optimization study of combined refrigeration cycles driven by an engine, Applied Energy 76 (4) (2003) 379–389.
[17] L. Ahlby, D. Hodgett, T. Berntsson, Optimization study of the compression absorption cycle, International Journal of Refrigeration-Revue Internationale Du Froid 14 (1) (1991) 16–23.
[18] S.W. Wallace, S-E. Fleten, A. Ruszczynski, A. Shapiro, Stochastic programming models in energy, Handbooks in Operations Research and Management Science, vol. 10, Elsevier, 2003, pp. 637–677.
[19] N.V. Sahinidis, Optimization under uncertainty: state-of-the-art and opportunities, Computers & Chemical Engineering 28 (6–7) (2004) 971–983.
[20] M. Sadeghi, H.M. Hosseini, Energy supply planning in iran by using fuzzy linear programming approach (regarding uncertainties of investment costs), Energy Policy 34 (9) (2006) 993–1003.
[21] E. Svensson, T. Berntsson. Economy and CO_2 emissions trade-off: a systematic approach for optimizing investments in process integration measures under uncertainty. Applied Thermal Engineering, in press, doi:10.1016/j.applthermaleng.2009.02.010 (Corrected Proof).
[22] G. Guillen, F.D. Mele, M.J. Bagajewicz, A. Espuña, L. Puigjaner, Multiobjective supply chain design under uncertainty, Chemical Engineering Science 60 (6) (2005) 1535–1553.
[23] S. Subrahmanyam, J.F. Pekny, G.V. Reklaitis, Design of batch chemical plants under market uncertainty, Industrial & Engineering Chemistry Research 33 (11) (1994) 2688–2701.
[24] R. Lahdelma, S. Makkonen, P. Salminen, Two ways to handle dependent uncertainties in multi-criteria decision problems, Omega 37 (1) (2009) 79–92.
[25] I.N. Durbach, T.J. Stewart, Using expected values to simplify decision making under uncertainty, Omega 37 (2) (2009) 312–330.
[26] A. Azaron, K.N. Brown, S.A. Tarim, M. Modarres, A multi-objective stochastic programming approach for supply chain design considering risk, International Journal of Production Economics 116 (1) (2008) 129–138.
[27] A. Barbaro, M.J. Bagajewicz, Managing financial risk in planning under uncertainty, AIChE Journal 50 (5) (2004) 963–989.
[28] A. Gupta, C.D. Maranas, Managing demand uncertainty in supply chain planning, Computers & Chemical Engineering 27 (8–9) (2003) 1219–1227.
[29] G. Mavrotas, H. Demertzis, A. Meintani, D. Diakoulaki, Energy planning in buildings under uncertainty in fuel costs: the case of a hotel unit in greece, Energy Conversion and Management 44 (8) (2003) 1303–1321.
[30] R. Yokoyama, K. Ito, Optimal design of energy supply systems based on relative robustness criterion, Energy Conversion and Management 43 (4) (2002) 499–514.
[31] S.B. Petkov, C.D. Maranas, Design of multiproduct batch plants under demand uncertainty with staged capacity expansions, Computers & Chemical Engineering 22 (Supp. 1) (1998) S789–S792.
[32] E. Svensson, T. Berntsson, A.B. Strömberg, M. Patriksson, An optimization methodology for identifying robust process integration investments under uncertainty, Energy Policy 37 (2) (2009) 680–685.
[33] H.S. Wellons, G.V. Reklaitis, The design of multiproduct batch plants under uncertainty with staged expansion, Computers & Chemical Engineering 13 (1989) 115–126.
[34] J. Acevedo, E.N. Pistikopoulos, Stochastic optimisation based algorithms for process synthesis under uncertainty, Computers & Chemical Engineering 22 (1998) 647–671.
[35] D.M. Cao, X.G. Yuan, Optimal design of batch plants with uncertain demands considering switch over of operating modes of parallel units, Industrial and Engineering Chemistry Research 41 (2002) 4616–4625.
[36] S.B. Petkov, C.D. Maranas, Multiperiod planning and scheduling of multipurpose batch plants under demand uncertainty, Industrial and Engineering Chemistry Research 36 (1997) 4864–4881.
[37] A. Bonfill, M. Bagajewicz, A. Espuña, L. Puigjaner, Risk management in scheduling of batch plants under uncertain market demand, Industrial and Engineering Chemistry Research 43 (2004) 741–750.
[38] J. Balasubramanian, I.E. Grossmann, Approximation to multistage stochastic optimization in multiperiod batch plant scheduling under demand uncertainty, Industrial and Engineering Chemistry Research 43 (2004) 3695–3713.
[39] F. You, I.E. Grossmann, in: L.G. Papageorgiou, M.C. Georgiadis (Eds.), Optimal Design and Operational Planning of Responsive Process Supply Chains, Supply Chain Optimization, vol. 3, Wiley-VCH, Weinheim, 2007 (Book chapter in Process System Engineering).
[40] R.P. Taylor, B.K. Hodge, C.A. James, Estimating uncertainty in thermal systems analysis and design, Applied Thermal Engineering 19 (1) (1999) 51–73.
[41] B.H. Gebreslassie, G. Guillen-Gosalbez, J. Laureano, D. Boer, Design of environmentally conscious absorption cooling systems via multi-objective optimization and life cycle assessment, Applied Energy 86 (9) (2009) 1712–1722.
[42] L. Roriz, A. Mortal, L.F. Mendes, Study of a plate heat exchanger desorber with a spray column for a small solar powered absorption machine, in: 3rd International Conference on Heat Powered Cycles, HPC, Cyprus, 2004.
[43] J. Fernández-Seara, J. Sieres, The importance of the ammonia purification process in ammonia–water absorption systems, Energy Conversion and Management 47 (13–14) (2006) 1975–1987.
[44] J. Pátek, J. Klomfar, Simple functions for fast calculations of selected thermodynamic properties of the ammonia–water system, International Journal of Refrigeration 18 (1995) 228–234.
[45] M.A. Siddiqui, Economic analyses of absorption systems: part A – design and cost evaluation, Energy Conversion and Management 38 (1997) 889–904.
[46] G.D. Eppen, R.K. Martin, L. Schrage, A scenario approach to capacity planning, Operations Research 37 (4) (1989) 517–527.
[47] S.L. Janak, X. Lin, C.A. Floudas, A new robust optimization approach for scheduling under uncertainty: II. uncertainty with known probability distribution, Computers & Chemical Engineering 31 (3) (2007) 171–195.
[48] M. Ehrgott, Multicriteria Optimization, Springer, 2000.
[49] A. Brooke, D. Kendrik, A. Meeraus, R. Raman, R.E. Rosenthal, GAMS-A User's Guide, GAMS Development Corporation, Washington, 1998.
[50] A. Drud, CONOPT Solver Manual, ARKI Consulting and Development, Bagsvaerd, Denmark, 1996.
[51] C.A. Floudas, Deterministic Global Optimization: Theory. In Methods and Applications, Kluwer, Academic Publishers, Dordrecht, The Netherlands, 2000.

Energy xxx (2010) 1–14

Contents lists available at ScienceDirect

Energy

journal homepage: www.elsevier.com/locate/energy

A systematic tool for the minimization of the life cycle impact of solar assisted absorption cooling systems

Berhane H. Gebreslassie [a], Gonzalo Guillén-Gosálbez [b], Laureano Jiménez [b], Dieter Boera [a,*]

[a] Departament d'Enginyeria Mecànica, Universitat Rovira i Virgili, Av. Països Catalans, 26 43007 Tarragona, Spain
[b] Departament d'Enginyeria Quimica, Universitat Rovira i Virgili, Av. Països Catalans, 26 43007 Tarragona, Spain

ARTICLE INFO

Article history:
Received 29 January 2010
Received in revised form
17 May 2010
Accepted 25 May 2010
Available online xxx

Keywords:
Absorption cooling
Solar assisted cooling
MINLP
Multi-objective optimization
Life cycle assessment (LCA)
Eco-indicator 99

ABSTRACT

In recent years, there has been a growing increase of the cooling demand in many parts of the world, which has led to major energy problems. In this context, solar assisted absorption cooling systems have emerged as a promising alternative to conventional vapor compression air conditioning systems, given the fact that in many cases the cooling demand coincide with the availability of solar radiation. In this work, we present a decision-support tool based on mathematical programming for the design of solar assisted absorption cooling systems. The design task is formulated as a bi-criteria mixed-integer nonlinear programming (MINLP) optimization problem that accounts for the minimization of the total cost of the cooling system and the associated environmental impact measured over its entire life cycle. The capabilities of the proposed method are illustrated in a case study that addresses the design of a solar assisted ammonia-water absorption cycle considering weather data of Barcelona (Spain).

1. Introduction

The cooling demand in many parts of the world has been increasing rapidly during the last decade, especially in moderate climates, such as in many European countries [1,2]. As a result, more air conditioning units have been installed, and the electricity demand has been rising, which has led to an increase in the use of fossil and nuclear energy. This trend threatens the stability of electricity grids, leading at the same time to major environmental problems. Particularly, during the last years there has been a fast proliferation of vapor compression air conditioning (*AC*) [1–3]. In Spain, the electricity consumption of these equipments is already affecting significantly the national energy system. For example, the summer peak electricity demand in the southern part of the country increased by 20% in 2003 and by another 20% in 2004, in which the summer peak consumption became even higher than the winter peak electricity demand [3].

Hence, it seems clear that a drastic change in the energy structure should be made in the developed countries in order to adopt more sustainable solutions for fulfilling the cooling demand. Particularly, environmentally friendly and energy efficient technologies have to be promoted so that the environmental impact of cooling applications is minimized without compromising the economic performance of the cooling system.

Solar cooling is one of the possible technological alternatives to vapor compression AC that has recently attracted an increasing interest. Solar cooling technology uses thermal energy provided by solar collectors to power an absorption cycle that produces cooling. The use of solar energy in cooling applications has a large potential to replace conventional cooling systems, given the fact that the cooling demand tends to coincide with the availability of solar radiation [2,4]. Although these technologies take advantage of a renewable source of energy, thus decreasing the associated environmental impact, they have the drawback that their cost is higher than that of conventional cooling systems (i.e., vapor compression cooling systems). Particularly, the required heat production subsystem, which includes the solar collectors as well as the auxiliary heating system, along with the absorption cooling cycle itself lead to higher capital costs than those of compression cycles.

In this context, it is necessary to develop tools for optimizing the performance of absorption cooling cycles, so they become a real alternative to compression cycles in the market place. In the literature, solar cooling systems have been typically optimized either component by component or variable by variable. Florides et al.

* Corresponding author. Tel.: +34 977559631; fax: +34 977559691.
E-mail address: Dieter.Boer@urv.cat (D. Boera).

0360-5442/$ – see front matter © 2010 Elsevier Ltd. All rights reserved.
doi:10.1016/j.energy.2010.05.039

Nomenclature

Abbreviations

AB	Absorber
ABS	Absorption cycle
Con	Condenser
Col	Solar collector
D	Desorber
E	Evaporator
ECO_{99}	Eco-indicator 99
GFH, *gfh*	Gas fired heater
LCA	Life cycle assessment
P	Solution pump
RV	Refrigerant expansion valve
SC	Subcooler
SHX	Solution heat exchanger
SV	Solution expansion valve
yr	Year

Indices

b	Chemical/feedstock
d	Damage category
c	Impact category
i	Collector model
j	Streams
k	Unit of the absorption cycle
n	Number of collectors
p	Component of a stream
t	Time period

Sets

$ID(d)$	Set of impact categories included in the damage category d
$IN(k)$	Set of input streams to unit k
$OUT(k)$	Set of output streams from unit k

Parameters

A_i^{col}	Absorber area of solar collector model i [m^2]
$cost_i^{col}$	Cost of solar collector model i per unit of capacity [€/m^2]
$cost_{elec}$	Unit cost of electricity [€/kWh^2]
$cost_{ng}$	Unit cost of heat from natural gas [€/kWh^2]
$c_{0,i}$	Optical efficiency of collector model i
$c_{1,i}$	Linear loss coefficient of collector model i
$c_{2,\ i}$	Quadratic loss coefficient of collector model i
Cp	Water heat capacity
df_{bc}	Damage factor associated with chemical/feedstock b and impact category c [impact/kg]
G_t	Global daily solar radiation for month t [W/m^2]
$IAM(\Theta)$	Incident angle modifier
ir	Interest rate [%]
$LCIE_b^{elec}$	Life cycle inventory entry associated with chemical/feedstock b per unit of electricity consumed [kg/MJ]
$LCIE_b^{heat(Col)}$	Life cycle inventory entry associated with chemical/feedstock b per unit of heat delivered by the solar collector [kg/kWh]
$LCIE_b^{heat(gfh)}$	Life cycle inventory entry associated with chemical b per unit of heat delivered by the heater [kg/MJ]
$LCIE_{bk}^{man}$	Life cycle inventory entry associated with chemical b per unit of capacity of equipment k constructed [$kg/unit$]
M and BM	Sufficiently large parameters
Q_t^E	Heat transferred in the evaporator in period t [kW]
T_t^{amb}	Ambient temperature in month t [$^\circ C$]
T_{op}	Operating hours per year [h/yr]
U_k	Overall heat transfer coefficient of unit k[$(kw)/(m^2K)$]
α_k	Purchase cost exponent
β_k	Purchase cost coefficient
δ_d	Normalization factor [points/impact]
η^{gfh}	Thermal efficiency of the gas fired heater
ψ	Capital cost coefficient
θ	Capital cost recovery factor
Θ	Incident angle
ϕ	Life span of the cooling system [*yrs*]
ξ_d	Weighting factor

Variables

A_k	Area of heat exchanger k
CAP_k	Capacity of equipment k
CC	Capital cost [€]
COP_t	Coefficient of performance of the absorption cycle in month t
$COP_{i,t}^S$	Solar cooling system efficiency using collector type i in month t
DAM_d	Damage in damage category d [*impact*]
EC_k	Capital cost of unit k [€]
ECO_{99}	Total Eco-indicator 99 [*points*]
f_t^{gross}	Gross solar fraction in month t
f_t^{net}	Net solar fraction in period t
$h_{j,\ t}$	Enthalpy of stream j in period t [kJ/kg]
IM_c	Damage in impact category c [*impact*]
LCI_b^{tot}	Life cycle inventory entry of chemical/feedstock b related to the construction and operation of the cycle [kg]
LCI_b^{man}	Life cycle inventory entry associated with chemical/feedstock b related to the manufacture of the system [kg]
LCI_b^{op}	Life cycle inventory entry associated with chemical/feedstock b related to the operation of the system [kg]
$m_{j,\ t}$	Mass flow rate of stream j in period t[kg/s]
OC	Operating cost [€]
$P_{j,\ t}$	Pressure of stream j in period t [bar]
PEC_k	Purchase equipment cost [€]
Q_t^{Col}	Solar heat collected in period t [kW]
Q_t^D	Heat demand of the absorption cycle generator in period t [kW]
Q_t^{gfh}	Heat provided by the gas fired heater in period t [kW]
$Q_{k,t}^{IN}$	Heat input to unit k in period t [kW]
$Q_{k,t}^{OUT}$	Heat output from unit k in period t [kW]
RC^{Col}	Running cost of the solar collectors [€]
RC^{cw}	Running cost of the cooling water [€]
RC^{gfh}	Running cost of the gas fired heater [€]
RC^P	Running cost of the pump [€]
$ry_{i,\ n}$	Relaxed binary variable
TC	Total cost [€]
T_t^{av}	Average temperature of the inlet and exit temperatures of the collector in period t [$^\circ C$]
$T_{j,\ t}$	Temperature of stream j in period t [$^\circ C$ *or* K]
$W_{k,\ t}$	Mechanical power of unit k in period t [kW]
$x_{p,\ j,\ t}$	Mass fraction of component p in stream j of period t
$y_{i,\ n}$	Binary variable (1 if n collectors of type i are selected, 0 otherwise)
$\Delta T_{k,t}^{lm}$	Logarithmic mean temperature difference of unit k in period t [$^\circ C$ *or* K]
$\Delta T_{k,t}^{h}$	Temperature difference in the hot end of unit k in period t [$^\circ C$ *or* K]
$\Delta T_{k,t}^{c}$	Temperature difference in the cold end of unit k in period t [$^\circ C$ *or* K]
ε	Auxiliary parameter
$\underline{\varepsilon}$	Lower bound on the auxiliary parameter
$\overline{\varepsilon}$	Upper bound on the auxiliary parameter
$\eta_{i,t}^{col}$	Efficiency of solar collector type i in period t

Please cite this article in press as: Gebreslassie BH, et al., A systematic tool for the minimization of the life cycle impact of solar assisted absorption cooling systems, Energy (2010), doi:10.1016/j.energy.2010.05.039

[5,6] addressed the optimization of a solar assisted air conditioning system installed in Nicosia. The optimization was aimed at selecting the appropriate solar collector type, slope, area, storage tank volume, and settings of the boiler thermostat so as to maximize the performance of the cooling system. Assilzadeh et al. [7] developed a model of a solar cooling system designed for the weather conditions of Malaysia that included evacuated tube solar collectors and a LiBr absorption chiller. These work used the dynamic simulation program *TRNSYS* in the modeling and analysis of the cooling system. The approach followed was a back and forth iterative one that consisted of running the model for a set of values that the variables of interest could take, and then identifying the best ones considering the performance of the solar system and the absorption cycle. The main drawback of this approach is that it is likely to fail in sub-optimal solutions, since the parameters search space is not explored in a systematic way.

Lecuona et al. [8] provided an explicit equation to optimize the hot water temperature of solar assisted absorption cooling systems. They used characteristic equation models that depended only on the external temperatures of the absorption refrigeration system. Their work assumed that as the hot water temperature increases, the coefficient of performance of the chiller increases, whereas the solar field efficiency decreases. In this context, there is a hot water temperature that leads to the best overall performance of the combined system [9,10].

Systematic methods based on mathematical programming techniques have also been applied to the optimization of absorption cycles. The use of these tools is rather convenient in this context, since they allow to explore in a systematic way a very large number of alternative solutions. This approach relies on posing the design task as an optimization problem, which is solved by standard techniques for linear, nonlinear, mixed-integer linear and mixed-integer nonlinear programming (LP, NLP, MILP, MINLP, respectively). These methods have been extensively used in many process systems engineering problems [11,12], including the optimization of energy systems [13,14] and more recently of ammonia-water absorption cycles [15–17].

Savola et al. [13] developed a MINLP model for the synthesis and operation of a combined heat and power (CHP) plant. Their objective was to maximize the power to heat production ratio. Tveit et al. [14] presented also a multi-period MINLP model to optimize a CHP plant by maximizing the benefits from the power generation and district heating.

The optimization of the operating conditions and the process scheme of an ammonia-water absorption refrigeration system was addressed in [15–17] using a MINLP model. In these works, various heat exchanger technologies were examined aiming at the minimization of the total capital cost of the absorption refrigeration system.

The aforementioned approaches focused on optimizing the economic performance of the absorption cycle. In contrast, other works in the literature have focused on evaluating the environmental performance of solar collectors following the Life Cycle Assessment (*LCA*) methodology [18–20]. The application of multi-objective optimization for integrating the environmental and economic performance of energy systems using evolutionary algorithm was also addressed in [21–24]. All the aforementioned contributions have concentrated on either the absorption cycle or the solar system. However, to our knowledge, the study of integrated solar assisted thermal systems has never been addressed in the literature.

In this paper, we fill in this research gap by proposing a novel MINLP model that optimizes the design and operating conditions of these systems considering economic and environmental concerns. Particularly, the two main goals of this work are: (i) to present a novel MINLP formulation that integrates a solar thermal system into a thermal energy driven absorption cooling model based on previous works by the authors [25,26], and (ii) to perform a LCA analysis of the integrated system in order to obtain a suitable environmental indicator to be optimized along with the standard economic criteria. The approach presented relies on a novel bi-criteria MINLP formulation in which the environmental impact is measured by an environmental metric based on LCA principles (i.e., Eco-indicator 99 [27]). To overcome the numerical difficulties associated with the model resolution, we propose an efficient solution strategy based on a customized branch and bound method that exploits the specific structure of the model.

The capabilities of the approach presented are illustrated through a case study that addresses the design of a solar assisted ammonia-water absorption cooling system that can operate with 7 different types of solar collectors: 3 evacuated tube collectors, 3 flat plate collectors and 1 compound parabolic collector, considering typical weather data of Barcelona (Spain).

The paper is organized as follows. The problem under study is formally stated in first place. The mathematical model is presented next along with the solution method devised to solve it. The case study is introduced in the next section, and the conclusions of the work are presented afterwards.

2. Problem statement

Compared to a compression cooling cycle, the basic idea of an absorption cooling cycle is to replace the electricity consumption associated with the vapor compression cycle by a thermally driven absorption–desorption system [28] that employs a suitable working fluid pair. The working pair consists of a refrigerant and an absorbent. In this study, without loss of generality, an ammonia-water solution is used as working pair, with the ammonia being the refrigerant and water the absorbent. We assume that the thermal energy that powers the absorption cooling cycle can be produced in different ways, including the use of gas fired heaters, steam boilers, waste heat and/or solar thermal panels.

Fig. 1 depicts the solar assisted absorption cooling system studied in this work. The hot water driven absorption cycle (Fig. 1 (*a*)) provides chilled water for cooling applications. The basic components of the absorption cycle are the absorber (AB), condenser (Con), desorber (D), evaporator (E), refrigerant subcooler (SC), refrigerant expansion valve (RV), solution heat exchanger (SHX), solution pump (P), and solution expansion valve (SV). The heat required by the desorber can be supplied by a fired water heater, by solar panels or by a combination of both. Therefore, the heat production subsystem includes two main components: a gas fired heater (GFH), and solar collectors (Col). The gas fired heater uses natural gas as primary energy resource. Different types of solar panels can be installed, including evacuated tube collectors (ETC), flat plate collectors (FPC) or compound parabolic collectors (CPC). Within each collector type, we consider different models. Details on the absorption cycle operation can be found in [25,26].

The hot water from the heat production subsystem is used in the generator of the absorption cycle, as shown in Fig. 1(b). If the temperature of the output stream from the solar collectors is high enough to power the absorption cycle, then the gas fired heater is by-passed. Otherwise, the water is further heated by passing through the gas fired heater in order to reach the appropriate operating temperature. If no solar collectors are chosen, then the cooled water directly enters the gas fired heater without any preheating.

The problem addressed in this paper can be formally stated as follows. Given are the cooling capacity of the system, the inlet and outlet temperatures of the external fluids (except the hot water

Please cite this article in press as: Gebreslassie BH, et al., A systematic tool for the minimization of the life cycle impact of solar assisted absorption cooling systems, Energy (2010), doi:10.1016/j.energy.2010.05.039

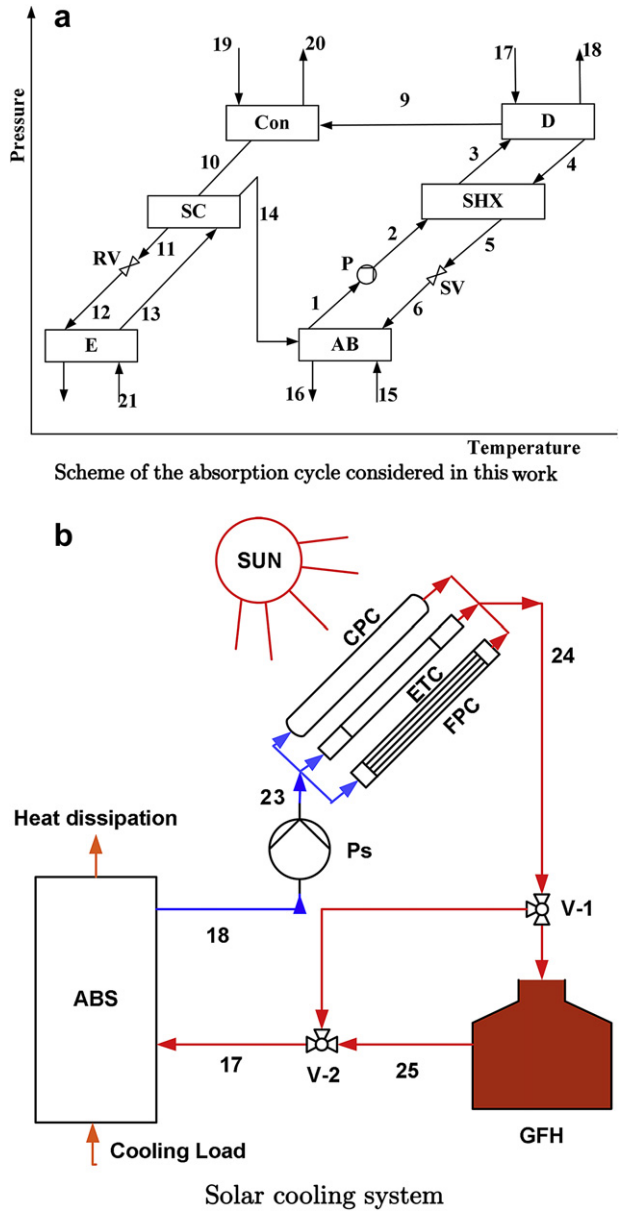

Fig. 1. Ammonia-water solar assisted absorption cooling system.

temperatures), the overall heat transfer coefficients of the heat exchangers, capital cost data, monthly weather data (ambient temperature and global daily solar radiation), performance equations of the solar collectors, and life cycle inventory of emissions

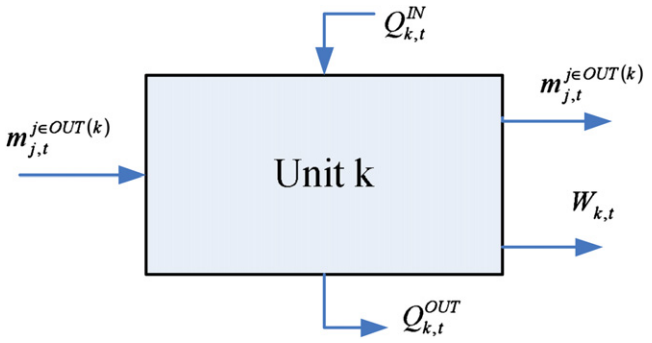

Fig. 2. A generic unit of the absorption cycle with its inlets and outlets.

and feedstock requirements associated with the construction and operation of the cooling system. The goal is to determine the optimal design and associated operating conditions that minimize simultaneously the total cost of the system and its environmental impact.

3. Mathematical formulation

In this work, the design task is posed as a bi-criteria MINLP that seeks to minimize the total cost and environmental impact of the cooling system. The solution to this bi-criteria problem is defined by a set of trade-off alternatives, each of which involves different structural and operating features. The mathematical model of the absorption cycle presented next is based on the formulation introduced by the authors in previous works [25,26]. Particularly, in this paper we have enlarged the scope of the aforementioned absorption cycle model in order to account for the performance equations of the heat production subsystem. The resulting formulation relies on the following assumptions:

- Weather conditions are expressed on a monthly basis without accounting for daily variations.
- Monthly steady state operation.
- Constant cooling demand, as is the case in many industrial applications.
- Other assumptions concerning the operation of the absorption cycle can be found in [25,26].

The mathematical formulation comprises two main parts: (i) general constraints that include mass and energy balance equations as well as equipment performance constraints; and (ii) objective function related constraints that allow to assess the economic and environmental performance of the solar assisted cooling system. Although some of these constraints have been already introduced in previous works by the authors [25,26], they are described in detail next for the sake of completeness of the overall mathematical formulation.

3.1. General constraints

The model considers that the total time horizon can be divided into t periods. The cycle can operate in a different manner in each of these periods in order to get adapted to the specific solar radiation of that time interval. We assume, without loss of generality, that each of these periods corresponds to one month, although in general we could specify any other length.

3.1.1. Mass balance constraints

The model is based on energy and materials balances that obey the laws of mass and energy conservation. These principles are applied to each unit of the system. Specifically, each process unit can be treated as a control volume with inlet and outlet streams, heat transfer and work interactions [28,29] (see Fig. 2). This is accomplished via the following equation:

$$\sum_{j\in IN(k)} m_{j,t}x_{p,j,t} - \sum_{j\in OUT(k)} m_{j,t}x_{p,j,t} = 0 \quad \forall k,p,t \tag{1}$$

Eqn. (1) represents the mass balances in period t, and ensures that the total amount of component p that enters unit k must equal the total amount of p that leaves k. In this equation, $m_{j,t}$ denotes the mass flow of stream j in period t, and $x_{p,j,t}$ is the mass fraction of component p in stream j and period t. Note that j can be either an inlet or outlet stream. Furthermore, $IN(k)$ denotes the set of inlet streams to unit k, whereas $OUT(k)$ includes the outlet streams.

3.1.2. Energy balance constraints

Eqn. (2) defines the energy balance for each equipment unit of the system, assuming no heat losses, in period t. The difference in energy content between the inlet and outlet streams, plus the heat supplied to the unit ($Q_{k,t}^{IN}$) must equal the heat removed ($Q_{k,t}^{OUT}$) plus the work done ($W_{k,t}$) by the unit. Note that the heat and work terms in eqn. (2) can take a zero value in some of the units, as shown in eqns. (3) to (5):

$$\sum_{j\in IN(k)} m_{j,t}h_{j,t} - \sum_{j\in OUT(k)} m_{j,t}h_{j,t} + Q_{k,t}^{IN} - Q_{k,t}^{OUT} - W_{k,t} = 0 \quad \forall k,t \tag{2}$$

$$Q_{k,t}^{IN} = 0 \text{ if } k = \left\{ \begin{array}{l} \text{Absorber}(AB) \\ \text{Condenser}(Con) \\ \text{Subcooler}(SC) \\ \text{Solution heat exchanger}(SHX) \\ \text{Pump}(P) \\ \text{Expansion valves}(RV, SV) \end{array} \right\} \tag{3}$$

$$Q_{k,t}^{OUT} = 0 \text{ if } k = \left\{ \begin{array}{l} \text{Evaporator}(E) \\ \text{Desorber}(D) \\ \text{Subcooler}(SC) \\ \text{Solution heat exchanger}(SHX) \\ \text{Pump}(P) \\ \text{Expansion valves}(RV, SV) \\ \textit{Sollar collectors}, (Col) \\ \text{Gas fired heater}, (GFH) \end{array} \right\} \tag{4}$$

$$W_{k,t} = 0 \quad \forall k \neq P \tag{5}$$

The thermodynamic properties of the ammonia-water mixture are determined with the correlations proposed by Patek and Klomfar [30]. The heat exchangers are modeled using the logarithmic mean temperature difference ($\Delta T_{k,t}^{lm}$), the heat transfer area (A_k) and the overall heat transfer coefficient (U_k), as shown in eqn. (6).

$$Q_{k,t} = U_k A_k \Delta T_{k,t}^{lm} \quad k = AB, Con, D, E, SC, SHX, \forall t \tag{6}$$

In order to improve the numerical performance of the model, the logarithmic mean temperature difference, which is a function of the hot and cold end temperature differences ($\Delta T_{k,t}^{h}$ and $\Delta T_{k,t}^{c}$, respectively), is calculated via the Chen's approximation [31].

$$\Delta T_{k,t}^{lm} \cong \left[\Delta T_{k,t}^{h} \Delta T_{k,t}^{c} \frac{\Delta T_{k,t}^{h} + \Delta T_{k,t}^{c}}{2} \right]^{\frac{1}{3}}$$
$$k = AB, Con, D, E, SC, SHX, \ \forall t$$

3.2. Heat production subsystem

As mentioned before, the model considers that the heat supplied to the absorption cycle is generated from the solar collectors and the fired heater. The equations associated with these systems are presented in the next sections.

3.2.1. Collector performance constraints

The model accounts for i different types of collectors. The selection of n number of solar collectors of type i is represented by the following disjunction [32,33]:

$$\bigvee_{i=1,\ldots I} \left[\begin{array}{c} Y_i \\ \bigvee_{n=1,\ldots N} \left[\begin{array}{c} Y_n \\ Q_t^{Col} = \eta_{i,t}^{Col} n A_i^{Col} G_t \end{array} \right] \\ \eta_{i,t}^{Col} = IAM(\Theta) c_{0,i} - c_{1,i} \frac{T_t^{av} - T_t^{amb}}{G_t} - c_{2,i} \frac{\left(T_t^{av} - T_t^{amb}\right)^2}{G_t} \end{array} \right]$$
$$Y_i, Y_n \in \{\text{True}, \text{False}\} \quad \forall i,n \tag{8}$$

where Y_i and Y_n are Boolean variables that decide whether the given disjunctive terms i and n in the disjunctions are true or false. They are true if n collectors of type i are selected, and false otherwise. If a given collector is chosen, then the associated equations inside the disjunction, which allow to determine the heat supplied by the solar system, are active. If the collector is not selected, the corresponding equations are all set to zero.

The useful heat collected from the solar system in each period t (Q_t^{Col}) is determined from the collector performance, which is given by the collector efficiency ($\eta_{i,t}^{Col}$), its area and the global solar incident radiation on the collector surface in t (G_t) [4]. The area of the collectors is obtained by multiplying the size of the collector model i (A_i^{Col}) with the corresponding number of collectors n installed in the system. The second equation inside the disjunction allows to determine the efficiency of a collector i in period t [4]. Here, $IAM(\Theta)$ is the incident angle modifier, which accounts for the effect of a non perpendicular incident radiation at incidence angle Θ, in relation to a normal incidence radiation (i.e., $\Theta = 0$). $T^{amb}{}_t$ is the monthly average ambient air temperature. $c_{0,\,i}$ denotes the optical efficiency of collector i, whereas $c_{1,\,i}$ and $c_{2,\,i}$ are the linear and quadratic loss coefficients, respectively, of collector i [4]. Finally, T_t^{av} is the monthly average fluid temperature in the collector, which can be determined from the monthly inlet ($T_{23,\,t}$) and exit ($T_{24,\,t}$) fluid temperatures as follows (see Fig. 1):

$$T_t^{av} = \frac{T_{23,t} + T_{24,t}}{2} \tag{9}$$

The above disjunction can be reformulated into standard algebraic equations by applying either the big-M or convex hull reformulations [33,34]. Particularly, in this work we use the big-M reformulation, which leads to the following equations:

$$Q_t^{Col} \leq \eta_{i,t}^{Col} n A_i^{Col} Gt + M\left(1 - y_{i,n}\right) \quad \forall i,n,t \tag{10}$$

$$Q_t^{Col} \geq \eta_{i,t}^{Col} n A_i^{Col} Gt - M\left(1 - y_{i,n}\right) \quad \forall i,n,t \tag{11}$$

$$\eta_{i,t}^{Col} \leq IAM(\Theta) c_{0,i} - c_{1,i} \frac{T_t^{av} - T_t^{amb}}{G_t} - c_{2,i} \frac{\left(T_t^{av} - T_t^{amb}\right)^2}{G_t} + BM\left(1 - \sum_n y_{i,n}\right) \quad \forall i,t \tag{12}$$

$$\eta_{i,t}^{Col} \geq IAM(\Theta) c_{0,i} - c_{1,i} \frac{T_t^{av} - T_t^{amb}}{G_t} - c_{2,i} \frac{\left(T_t^{av} - T_t^{amb}\right)^2}{G_t} - BM\left(1 - \sum_n y_{i,n}\right) \quad \forall i,t \tag{13}$$

where $y_{i,\,n}$ is an auxiliary binary variable that takes a value of 1 if n number of collectors of type i are selected and 0 otherwise, and M and BM are a sufficiently large parameters. Constraint (14) is added to ensure the selection of only one type of collector:

$$\sum_i \sum_n y_{i,n} = 1 \tag{14}$$

3.2.2. Linking constraints

Eqn. (15) links the heat provided by the collectors and the gas fired heater with that consumed by the cycle. Particularly, the heat consumed by the generator of the cycle in period t (Q_t^D) should be less than or equal to the summation of the heat supplied by the collector (Q_t^{Col}) and that provided by the gas fired heater (Q_t^{gfh}) in the same period:

Please cite this article in press as: Gebreslassie BH, et al., A systematic tool for the minimization of the life cycle impact of solar assisted absorption cooling systems, Energy (2010), doi:10.1016/j.energy.2010.05.039

$$Q_t^D \le Q_t^{Col} + Q_t^{gfh} \quad \forall t \tag{15}$$

The amount of heat provided by the heater in every time period must be less than or equal to its capacity, which is denoted by the continuous variable CAP_k.

$$Q_t^{gfh} \le CAP_k \quad k = gfh, \forall t \tag{16}$$

The heat provided by the collectors and the gas fired heater (Q_t^{Col} and Q_t^{gfh}, respectively) can be determined from the water flow rate $m_{j,t}$ and the inlet and exit temperatures of the heat production subsystem (see Fig. 1) as follows:

$$Q_t^{Col} = m_{23,t}Cp(T_{24,t} - T_{23,t}) \quad \forall t \tag{17}$$

$$Q_t^{gfh} = m_{24,t}Cp(T_{25,t} - T_{24,t}) \quad \forall t \tag{18}$$

3.2.3. Temperature constraints

The following equations enforce some conditions that the temperatures of the heat production subsystem must satisfy. The subscript numbers refer to the stream numbers in Fig. 1(b).

$$T_{17,t} \ge T_{18,t} \quad \forall t \tag{19}$$

$$T_{18,t} \le T_{23,t} \quad \forall t \tag{20}$$

$$T_{24,t} \ge T_{23,t} \quad \forall t \tag{21}$$

$$T_{25,t} \ge T_{24,t} \quad \forall t \tag{22}$$

$$T_{17,t} \le T_{25,t} \quad \forall t \tag{23}$$

3.2.4. Performance indicators

The equations given in this section are added to determine some indicators that provide information on the performance of the cooling system. In fact, these performance metrics can be easily determined once the model has been solved (i.e., in the post-optimal analysis of the solutions), since they do not affect the calculations. Nevertheless, they are described in detail next for completeness of the mathematical formulation.

The gross solar fraction f_t^{gross} is given by the ratio between the solar heat collected and the heat demand of the absorption cycle generator [4]:

$$f_t^{gross} = \frac{Q_t^{Col}}{Q_t^D} \quad \forall t \tag{24}$$

Furthermore, the net solar fraction f_t^{net} is defined as the ratio between the heat supplied by the solar collector and the heat demand of the generator [4].

$$f_t^{net} = \frac{Q_t^D - Q_t^{gfh}}{Q_t^D} \quad \forall t \tag{25}$$

Eqn. (26) defines the overall solar cooling system efficiency ($COP_{i,t}^S$) as the product of the collector efficiency $\eta_{i,t}^{Col}$ and the absorption cycle coefficient of performance COP_t [3].

$$COP_{i,t}^S = \eta_{i,t}^{Col} COP_t \quad \forall i,t \tag{26}$$

Where COP_t is given by eqn. (27).

$$COP_t = \frac{Q_t^E}{Q_t^D} \tag{27}$$

3.3. Objective functions

Our model includes two contradicting objective functions: minimum total cost and life cycle environmental impact.

3.3.1. Economic performance objective function

The total cost of the system (TC), which accounts for both, the capital and operating costs (CC and OC, respectively) during its entire life span, is given by eqn. (28).

$$TC = CC + OC \tag{28}$$

The capital cost includes the cost of the heat exchangers, solar collectors, gas fired heater, pumps and expansion valves, which are denoted by the continuous variable EC_k, as shown in eqn. (29).

$$CC = \varphi\theta\left(\sum_k EC_k\right) \tag{29}$$

Note that this equation makes use of the number of useful years (ϕ) and capital recovery factor (θ). The latter term, which is calculated via eqn. (30), is a function of the interest rate (ir) and the life span (ϕ) of the system [35].

$$\theta = \frac{ir(ir+1)^{\varphi}}{(ir+1)^{\varphi}-1} \tag{30}$$

Eqn. (31) is used to determine the capital cost associated with equipment k [35].

$$EC_k = \psi PEC_k \quad \forall k \neq Col \tag{31}$$

where ψ is a cost parameter that allows to determine the total capital cost of a given equipment (i.e., a heat exchanger, gas fired heater, pump or expansion valve) from the purchase equipment cost PEC_k [35]. The value of PEC_k is estimated using available correlations in the literature [36]. From these correlations, it is possible to derive the following exponential expression that is added to the model:

$$PEC_k = \beta_k (CAP_k)^{\alpha_k} \quad \forall k \neq Col \tag{32}$$

In this equation, CAP_k represents the capacity of unit k (i.e., a heat exchanger, gas fired heater or pump), whereas α_k and β_k are cost parameters. Typical values for the coefficient β_k, the exponent α_k and the range of capacities for the different equipments are shown in Table 1. The Chemical Engineering cost index [37] can be used for updating the equipment costs from the base year to the current one.

The capital cost associated with the solar collectors is determined from the specific collector cost and area ($cost_i^{Col}$ and A_i^{Col}, respectively) and number of collector units n purchased, as shown in eqn. (33).

$$EC_k = \sum_i \sum_n y_{i,n} n A_i^{Col} cost_i^{Col} \quad k = Col \tag{33}$$

The total operational cost accounts for the running cost associated with the gas fired heater (RC^{gfh}), pump (RC^P) and solar collectors (RC^{Col}), as well as the cooling water cost (RC^{cw}). It should be noted that the last two terms are typically neglected in the calculations.

$$OC = RC^{gfh} + RC^P + RC^{Col} + RC^{cw} \tag{34}$$

The running cost of the gas fired heater (RC^{gfh}) and the pump (RC^P) are given by eqns. (35) and (36), respectively.

$$RC^{gfh} = \frac{cost_{ng}\varphi T_{op}}{12\eta^{gfh}} \sum_t Q_t^{gfh} \tag{35}$$

$$RC^P = \frac{cost_{elec}\varphi T_{op}}{12} \sum_t W_t^P \tag{36}$$

Please cite this article in press as: Gebreslassie BH, et al., A systematic tool for the minimization of the life cycle impact of solar assisted absorption cooling systems, Energy (2010), doi:10.1016/j.energy.2010.05.039

Where ϕ and T_{op} represent the useful life of the system expressed in years and total number of operating hours per year, respectively. In this equation, Q_t^{gfh} and W_t^P are the monthly heat contribution of the gas fired heater and monthly electricity consumption of the pump, respectively, whereas η^{gfh} is the conversion efficiency of the gas fired heater. The parameters $cost_{ng}$ and $cost_{elec}$ are the unit costs of the heat from the gas fired heater and electricity, respectively.

3.3.2. Environmental performance objective function

To assess the environmental performance of the system, we follow a combined approach that integrates LCA principles with optimization theory [38,39]. In this framework, LCA is employed to assess the environmental performance of the process, whereas optimization techniques are used for generating in a systematic way different technological alternatives and identifying the best ones in terms of economic and environmental criteria. Examples on the application of this general framework to the development of sustainable processes can be found in [40–45].

In particular, the environmental performance of the system is measured by the Eco-indicator 99 metric. Note, however, that any other LCA indicator could be used. The Eco-indicator 99 accounts for 11 impact categories that are aggregated into three types of damages: human health, ecosystem quality and resource depletion. Details about the LCA methodology can be found elsewhere [46], whereas the Eco-indicator 99 is described in detail in [27].

The calculation of the Eco-indicator 99 follows the main LCA stages: (1) goal and scope definition, (2) inventory analysis, (3) damage assessment and (4) interpretation. We describe next these phases in the context of our study.

The goal of our LCA analysis, which is specified in phase 1, is to determine the life cycle impact of fulfilling a given cooling demand. The functional unit of the LCA analysis is therefore the amount of cooling demand satisfied. We perform a cradle to gate analysis that encompasses all the processes from the extraction of the raw materials required for the construction and operation of the cycle until the energy is delivered to the final customer.

The inventory analysis phase aims to determine the life cycle inventory of emissions and feedstock requirements associated with the cooling system. This inventory, which is represented by a continuous variable LCI_b^{tot}, accounts for the feedstock requirements and emissions of pollutant chemicals associated with the manufacture (LCI_b^{man}) and operation (LCI_b^{op}) of the cooling system, as shown in eqn. (37).

$$LCI_b^{tot} = LCI_b^{man} + LCI_b^{op} \tag{37}$$

The value of LCI_b^{man} can be determined from the sizes of the gas fired heater, solar collectors, heat exchangers and pumps of the cycle, as stated in eqn. (38).

$$LCI_b^{man} = \sum_k LCIE_{bk}^{man} CAP_k \tag{38}$$

Here, CAP_k represents, in each case, the area of the heat exchangers, capacity of heat delivered by the gas fired heater in kWh and solar collector absorber area in m^2. These variables are degrees of freedom in the optimization problem. On the other hand, $LCIE_{bk}^{man}$ denotes the life cycle inventory entries associated with each equipment unit k (i.e., the emissions/feedstock requirements of chemical b per unit of equipment capacity installed).

The values of $LCIE_{bk}^{man}$ should be obtained either from the literature or by performing an LCA analysis on the manufacture of each single equipment unit. At this point, it might be convenient to use rough estimates in the LCA calculations when there is little information available on the manufacture process. A possible way to do this consists of determining in first place the amount of metal contained in an equipment, and then translating this information into the corresponding life cycle inventory entries by using standard environmental databases that store emissions data associated with a wide range of processes [47–49]. Thus, in the absence of more accurate data, the life cycle inventory of emissions and feedstock requirements of any equipment unit will be approximated by the life cycle inventory of the material it is made of.

On the other hand, the value of $LCIE_b^{op}$ can be determined from the energy consumed by the gas fired heater, the energy consumed by the solar collectors, and the electricity consumed by the pump of the cycle, as shown in eqn. (39).

$$LCI_b^{op} = \varphi T_{op} \sum_t \left(\frac{Q_t^{gfh}}{\eta^{gfh}} LCIE_b^{heat(gfh)} + Q_t^{Col} LCIE_b^{heat(Col)} + W_t^P LCIE_b^{elec} \right) \tag{39}$$

Here, $LCIE_b^{heat(gfh)}$, $LCIE_b^{heat(Col)}$ and $LCIE_b^{elec}$ denote the life cycle inventory entries per unit of heat delivered by the heater and solar collectors, and unit of electricity consumed by the cycle, respectively. Note that these values, which can be retrieved from environmental databases [47–49], depend on the particular features of the cycle (i.e., type of primary energy sources used in the heater, type of solar collectors, electricity mix of the country in which the cycle operates, etc.).

The damage assessment phase aims at translating the life cycle inventory of emissions and feedstock requirements into the corresponding environmental impacts in each damage category. The Eco-indicator 99 framework accounts for 11 environmental impacts that are aggregated into three damage categories as follows:

- Human health, measured in Disability Adjusted Life Years (DALYs). This damage category includes the following impacts: carcinogenic effects on humans, respiratory effects on humans caused by organic substances, respiratory effects on humans caused by inorganic substances, damage to human health caused by climate change, human health effects caused by ionizing radiations and human health effects caused by ozone layer depletion.
- Ecosystem quality, measured in Potentially Disappear Fraction of Species per square meter and year (PDF·m^2·year), which includes the following impacts: damage to ecosystem quality caused by ecosystem toxic emissions, damage to ecosystem quality caused by the combined effect of acidification and eutrophication and damage to ecosystem quality caused by land occupation and land conversion.
- Depletion of resources, measured in MJ surplus energy, which accounts for the following impacts: damage to resources caused by extraction of minerals and damage to resources caused by extraction of fossil fuels.

The damage caused in each impact category c belonging to a specific damage category d (IM_c) is calculated from the life cycle inventory of emissions and feedstock requirements associated with the construction and operation of the cycle (i.e., LCI_b^{tot}) and the corresponding set of damage factors (df_{bc}), as stated in eqn. (40).

Table 1
Economic parameters.

Unit	β_k	α_k	Range
Heat exchanger	6880	0.430	5 m^2–1500 m^2
Gas fired heater	1633	0.584	100 kW–10000 kW
Pump	1942	1.110	1 kW–100 kW

Please cite this article in press as: Gebreslassie BH, et al., A systematic tool for the minimization of the life cycle impact of solar assisted absorption cooling systems, Energy (2010), doi:10.1016/j.energy.2010.05.039

$$IM_c = \sum_b df_{bc} LCI_b^{tot} \quad \forall c \tag{40}$$

As can be seen, the damage factors are used to translate the emissions and feedstock requirements into the associated impacts. The impact categories are next aggregated into the corresponding damage categories as follows:

$$DAM_d = \sum_{c \in ID(d)} IM_c \quad \forall d \tag{41}$$

where $ID(d)$ denotes the set of impact categories c that contribute to damage d. Finally, the Eco-indicator 99 is determined from the impact (DAM_d) in each damage category d (i.e., damage in human health, ecosystem quality and depletion of resources), by considering specific normalization (δ_d) and weighting (ξ_d) factors:

$$ECO_{99} = \sum_d \delta_d \xi_d \cdot DAM_d \tag{42}$$

With regard to the last stage of the LCA methodology (i.e., interpretation), let us note that in the context of our integrated framework, such phase corresponds to the post-optimal analysis of the Pareto solutions of the multi-objective problem.

4. Solution method

The design task is finally formulated as a bi-criteria mixed-integer nonlinear programming (MINLP) problem of the following form:

$$\begin{aligned} (\mathrm{M}) \quad \min_{x,y} \quad & U(x,y) = \{TC(x,y), ECO_{99}(x,y)\} \\ s.t. \quad & \text{constraints 1 } to \text{ 42} \\ & x \in \Re, y \in \{0,1\} \end{aligned} \tag{43}$$

In this formulation, x represents the state variables or design variables such as thermodynamic properties, mass flows, and sizes of equipments. The discrete variables are denoted by y, and are used in the selection of a specific number n of collectors of type i. On the other hand, $TC(x, y)$ and $ECO_{99}(x, y)$ denote the economic performance and environmental impact of the solar heat integrated absorption cooling system, respectively.

4.1. Epsilon constraint method

The solution to (M) is given by a set of Pareto optimal points that represent the trade-off between economic and environmental criteria.

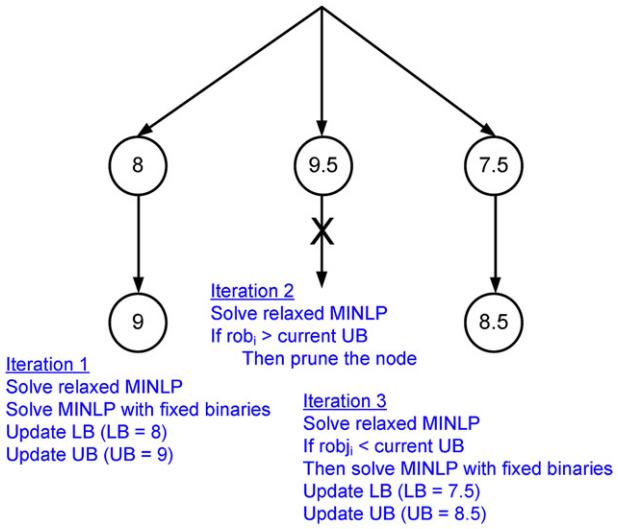

Fig. 3. Customized branch and bound example.

These points involve alternative process designs, each of which featuring a specific environmental and economic performance. These trade-off solutions are determined in this work by the ε-constraint method [50]. This technique is based on solving a set of single-objective problems in which one of the objectives is kept in the objective function and the others are transferred to auxiliary constraints as follows:

$$\begin{aligned} (\mathrm{MA}) \quad \min \quad & TC(x,y) \\ s.t. \ & \text{constraints 1 to 42} \\ & ECO_{99} \le \varepsilon \\ & \underline{\varepsilon} \le \varepsilon \le \overline{\varepsilon} \\ & x \in \Re, y \in \{0,1\} \end{aligned} \tag{44}$$

in which the lower and upper limits ($\underline{\varepsilon}$ and $\overline{\varepsilon}$, respectively) that define the interval within which the epsilon parameter must fall are obtained by optimizing each scalar objective separately.

A recent review on MINLP methods can be found in [51]. As pointed out in [51], one of the main difficulties that must be faced when solving MINLPs in synthesis problems, like the one addressed in this article, concerns the calculation of NLP subproblems with fixed values of the binary variables. In these subproblems, a significant number of equations and variables are often set to zero as they become redundant when units "disappear". This in turn often leads to singularities and poor numerical performance. In the context of our problem, this situation arises when a collector type is not selected, which forces the corresponding efficiency equations to take zero values.

To circumvent these difficulties, we propose in this paper a novel solution method that is based on the logic-based outer approximation for nonlinear Generalized Disjunctive Programming (GDP) problems [34,52], which has the important feature of generating subproblems where redundant equations and constraints of non-existing units are not included.

4.2. Customized branch and bound algorithm (CBB)

The proposed algorithm to solve (MA) is a customized branch and bound that exploits the model structure. The main idea consists of branching in first place on the type of collector and then solving a MINLP in which the only binary variables that are let free are those representing the number of collectors installed. The detailed steps of the algorithm are as follows.

- *Step 1: Initialization.* Set lower bound $LB = -\infty$, upper bound $UB = \infty$ and set of collector types $Col := \{1, \ldots, I\}$
- *Step 2: Branching.* Choose a collector type $i \in Col$.

Table 2
Different models of solar collectors considered.

Symbol	Name	Manufacturer	Type
ETC-1	Sydney SK-6	Microterm Energietechnik GmbH	Evacuated tube collector, cylindrical absorber, directly cooled, CPC Concentrator
ETC-2	Memotron TMO 600	Thermomax Ltd.	Evacuated tube collector, Flat absorber, heat pipe
ETC-3	VacuTube HP 65/30	Gasokol GmbH	Evacuated tube collector
FPC-1	SK 500	Sonnenkraft Vertriebs GmbH	Flat Plate collector, Selective coating
FPC-2	Euro C18	Wagner & Co Solartechnik GmbH	Flat Plate collector, Selective coating
CPC	CPC AO SOL 15	AO SOL Lda	Stationary CPC Collector (concentration 1.5) selective coating, teflon film
FPC-3	Sunbox HFK-S	Sun-Pro GmbH	Flat Plate collector, Selective coating, Roof integrated

Table 3
Characteristic values, module area and specific cost of different solar collector models.

	Unit	ETC-1	ETC-2	ETC-3	FPC-1	FPC-2	CPC	FPC-3
$c_{0,i}$	–	0.735	0.840	0.970	0.800	0.789	0.940	0.786
$c_{1,i}$	W/m^2	0.65	2.02	1.16	3.02	3.69	2.20	3.69
$c_{2,i}$	W/m^2	0.0021	0.0046	0.0060	0.0113	0.0070	0.0330	0.0070
A	m^2	0.984	1.975	2.973	2.215	2.305	1.590	2.305
$cost_i^{Col}$	€/m^2	771	777	783	271	265	377	196

- *Step 3: Lower bounding problem*. Solve a relaxed MINLP subproblem in which the binary variables associated to the collectors others than i are all set to zero ($y_{i'n}=0 \quad \forall i' \neq i$) and those denoting the number of collectors of type i are relaxed. Let $robj_i$ be the optimal objective function value. If $robj_i < LB$, then update the lower bound (i.e., $LB = robj_i$).
- *Step 4: Node fathoming*. If $robj_i > UB$, then prune the node.
- *Step 5: Upper bounding problem*. Solve a MINLP subproblem with fixed $y_{i'n}=0 \quad \forall i' \neq i$ in which the number of collectors are represented by integer variables (i.e., are not relaxed). Let obj_i be the optimal objective function value. If $obj_i < UB$, then update the upper bound (i.e., $UB = obj_i$).
- *Step 6: Termination criterion*. If all the collector types have been explored, then stop. Otherwise, exclude the current collector type i from the set of collectors (i.e., $Col = Col\backslash i$) and go to step 2.

An example of how the algorithm would proceed in a small problem with 3 collector types is given in Fig. 3. In this particular case, the method solves in first place node 1, which provides upper and lower bounds (9 and 8, respectively) on the optimal solution to the problem. Node 2 is then explored by solving the associated relaxed MINLP. Since this relaxed MINLP problem yields worst results than the current upper bound (i.e., 9.5 > 9), the method decides to prune it. In node 3, which is explored afterwards, the relaxed MINLP provides a lower bound that is below the current upper bound (i.e., 7.5 < 9). Thus, the method decides to further analyze the node by solving the MINLP associated with that collector type, in which the binaries denoting the number of collectors to be installed are not relaxed. This integer solution will be compared with the current upper bound in order to update it. This procedure is repeated until there are no more unexplored nodes in the tree.

4.2.1. Remarks

- The MINLP solved in step 3 is a reduced model in which all the equations included in the disjunctive terms associated with the collectors others than the one fixed in the node have been removed. This avoids singularities and poor numerical performance.
- The MINLP model solved in step 5 of the algorithm tends to show a very tight integer relaxation. Hence, a possible way to expedite the overall solution procedure consists of solving this problem by an heuristic based on rounding up the solution of the relaxed MINLP solved in step 3 of the method.
- The lower and upper bounds obtained by the algorithm are only rigorous if a global optimization package is used. In the context of our problem, these methods might lead to prohibitive CPU times. Hence, the solutions found when local optimizers are used must be regarded as locally optima.

Table 4
Barcelona and Tarragona monthly global solar radiation and ambient temperature for 45° inclination.

Period	Barcelona		Tarragona	
	G_t [W/m^2]	T_t^{amb} [°C]	G_t [W/m^2]	T_t^{amb} [°C]
January	297.0	8.2	323.6	10.0
February	350.7	9.4	380.8	11.3
March	415.3	11.1	447.0	13.1
April	460.4	13.1	491.0	15.3
May	478.5	17.0	503.5	18.4
June	482.4	20.9	503.5	22.2
July	483.8	23.5	502.8	25.3
August	477.5	24.1	495.4	25.3
September	445.8	21.6	460.6	22.7
October	385.0	17.3	395.1	18.4
November	320.6	12.1	330.3	13.5
December	282.2	9.9	297.0	10.7

5. Case study

The capabilities of the proposed approach are illustrated through a case study that addresses the design of a solar assisted absorption cooling system with 100 kW of cooling capacity.

We studied 7 types of non-tracking collectors. The associated data, which include the collector performance equations, the module area and the specific cost (Tables 2 and 3), were taken from [4] and [53]. For the calculations, we considered the global daily solar radiation of Barcelona (see Table 4) for an azimuth angle 0° and an inclination of 45° [54].

Regarding the calculation of the Eco-indicator 99, we followed the Hierarchist perspective combined with the default (average) weighting factors. The entries of the life cycle inventories of emissions were defined as follows.

- The values of $LCIE_{bk=gfh}^{man}$ and $LCIE_b^{heat(gfh)}$ were taken from the Ecoinvent database [55]. Specifically, the database provides the

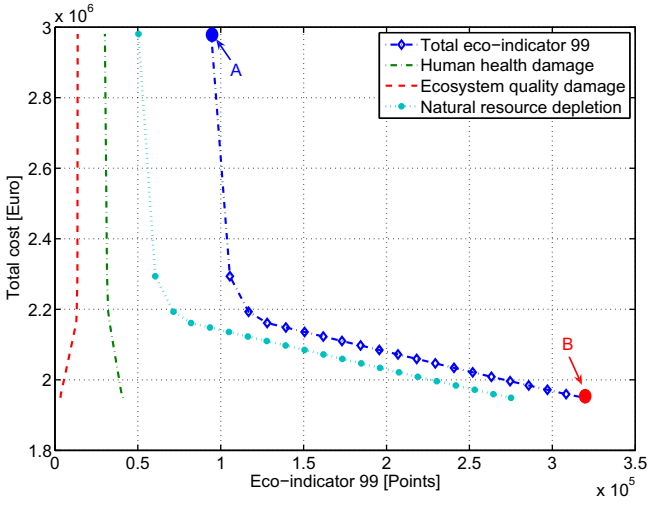

Fig. 4. Pareto set of the case study. For each Pareto solution, the total cost, Eco-indicator 99 and associated damage categories are depicted.

Please cite this article in press as: Gebreslassie BH, et al., A systematic tool for the minimization of the life cycle impact of solar assisted absorption cooling systems, Energy (2010), doi:10.1016/j.energy.2010.05.039

life cycle inventory associated with both, the manufacture and operation of the heater. This includes the infrastructure construction, as well as the electricity and natural gas consumed per *MJ* of heat delivered by the gas fired heater.

- The values of $LCIE^{man}_{bk=Col}$ and $LCIE^{heat(Col)}_{b}$ were determined as follows. For the life cycle inventory associated with the manufacture of the collectors, we first obtained the key construction elements per m^2 of absorber area of flat plate and evacuated tube collectors from the work by Jungbluth [56]. The life cycle inventory entries associated with the production of the mass of metal contained in these key elements were then retrieved from Ecoinvent. On the other hand, the life cycle inventory associated with the operation of the solar system, which includes the maintenance tasks and electricity consumed during their operation, were also retrieved from Ecoinvent.
- The values of $LCIE^{man}_{bk}$ for the heat exchangers (*AB*, *Con*, *D*, *E*, *SC*, *SHX*) and of $LCIE^{elec}_{b}$ were also taken from Ecoinvent. Particularly, the heat exchangers of the absorption cycles are assumed to be made of stainless steel. Hence, the mass of stainless steel contained in each heat exchanger was determined in first place from the heat exchanger area. The life cycle inventory associated with the production of this material was then retrieved from Ecoinvent. Finally, the life cycle inventory of the electricity consumed by the pump was also retrieved from Ecoinvent, considering the electricity mix of Spain. The aforementioned inventory accounts for the electricity production and also for its transportation through the transmission network.
- The impact associated with the construction of the pumps (i.e, $LCIE^{man}_{bk=P}$) was neglected in the analysis.

5.1. Validation

The model of the absorption cycle was validated by an error analysis that can be found in a recent work by the authors [57]. The efficiencies of the solar collectors are given in [4]. The optimization model was implemented in the Generic Algebraic Modeling System (GAMS). The process data considered in the model were taken from previous works by the authors [25,26].

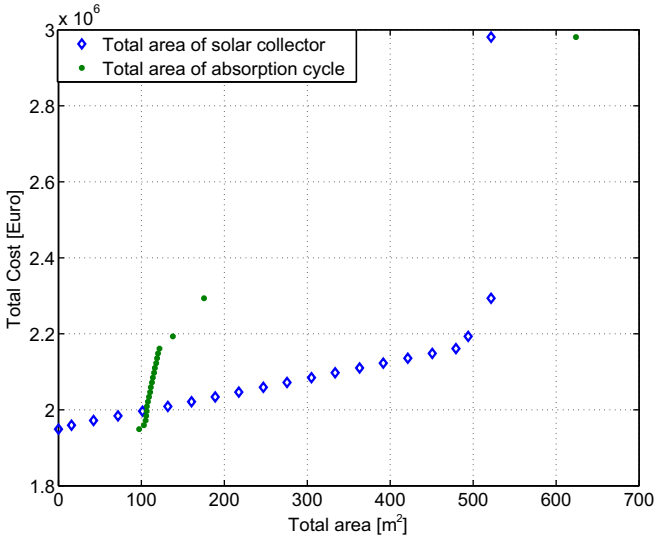

Fig. 5. Solar collectors and absorption cycle areas associated with each Pareto optimal solution.

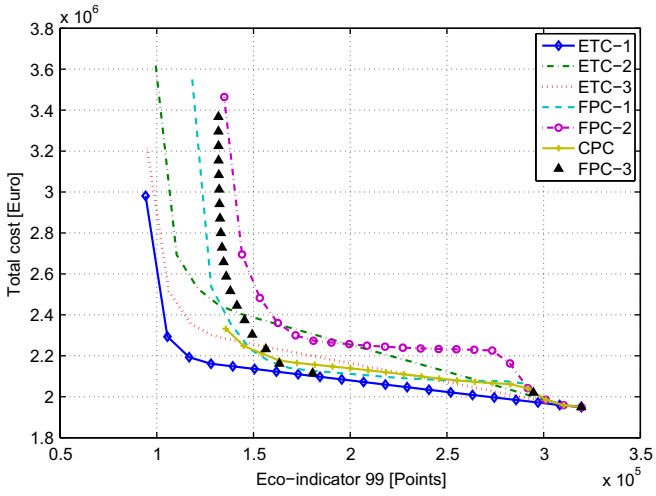

Fig. 6. Individual Pareto sets associated with each collector type.

5.2. Results and discussions

The model featured 11,869 constraints, 7004 continuous variables and 4557 binary variables. The solution procedure was implemented in GAMS [58] and solved with DICOPT, interfacing with SNOPT 6.2 and CPLEX 9.0. The upper bounding MINLP problems solved in each node of the tree were approximated by the rounding up heuristic discussed in section 4. The starting points used to initialize the NLPs were determined from a simulation model implemented in the Engineering Equation Solver [59] simulation environment, which was validated in [57]. Note that the model contains non-convex terms and for this reason the solutions found should be regarded as locally optimal unless a global optimization technique is employed.

5.2.1. Pareto optimal set of designs

The total computational time required to obtain 21 solutions of the Pareto set using the $\varepsilon-$ constraint method was *117.5* s in a *2.29* GHz machine. The Pareto points obtained by following the above strategy are shown in Fig. 4. Note that each point in the Pareto set represents a different optimal design operating under a set of specific conditions. Particularly, the figure shows the total cost

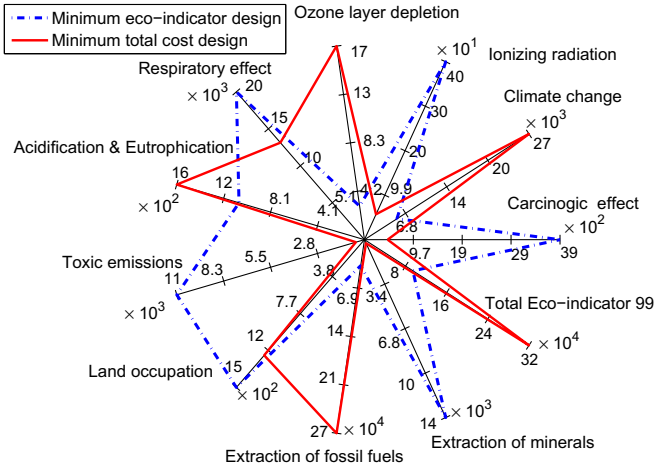

Fig. 7. Single impact categories and total Eco-indicator 99 associated with the extreme Pareto designs.

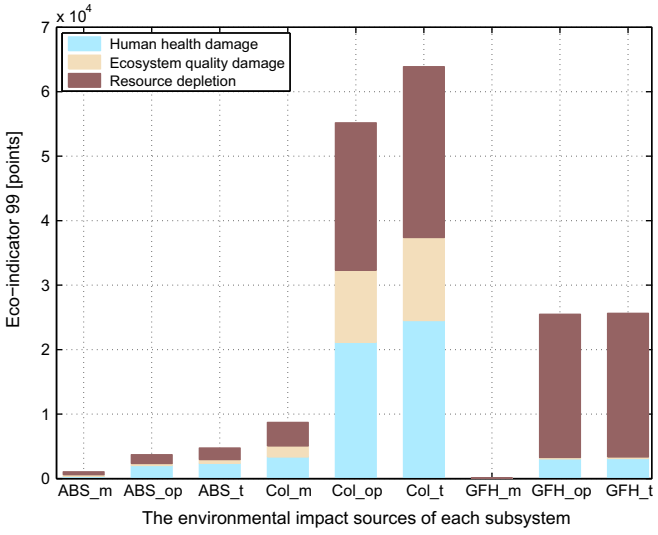

Fig. 8. Contribution of the manufacturing (m) and operation (op) stages associated with the absorption cycle (ABS), collectors (Col) and gas fired heater (GFH) in the total (t) environmental impact for the minimum environmental impact design (design A of Fig. 4).

associated with each Pareto design versus the Eco-indicator 99. For each Pareto point shown in the figure, we have also plotted the values of the single damage categories.

As observed in the figure, a conflict exists between the cost and environmental impact. Points A and B represent the minimum Eco-indicator and minimum total cost solutions, respectively. As can be seen, it is possible to reduce up to 70.5% the environmental impact of the most profitable design (point B), by increasing the cost in no more than 40%. As it will be discussed later on, this is achieved by increasing the amount of solar collectors installed, which reduces the fossil fuel needs. It is interesting to notice that the slope of the Pareto curve gradually decreases as we move from point A towards B. Hence, it is convenient to choose solutions close to point B, in which we can reduce to a large extent the environmental impact without having to compromise too much the economic performance.

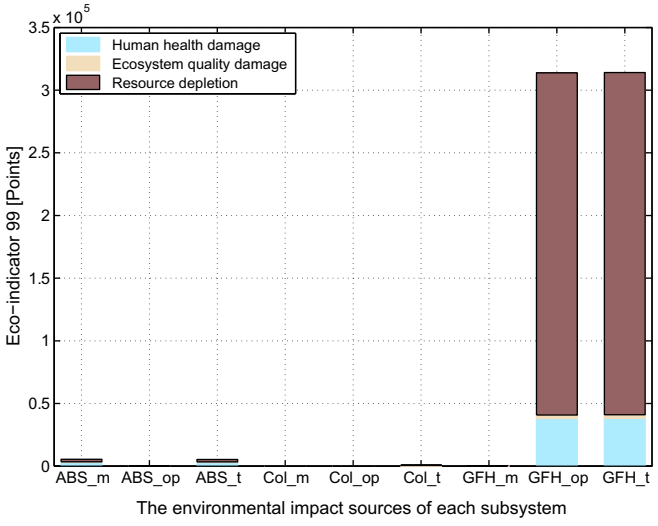

Fig. 9. Contribution of the manufacturing (m) and operation (op) stages associated with the absorption cycle (ABS), collectors (Col) and gas fired heater (GFH) in the total (t) environmental impact for the minimum total cost design (design B of Fig. 4).

Regarding the single damage categories included in the Eco-indicator 99, it is worthy to mention that the total impact is dominated by the depletion of natural resources followed by human health damage and finally by ecosystem quality. It is also interesting to notice that the first two damage categories behave in a similar way as the total Eco-indicator, whereas the ecosystem quality damage increases as the total impact is reduced. This is due to the increase in the emissions of heavy metals associated with the construction of the solar collectors. Particularly, the emissions of chromium steel and copper, both used in the production of the solar collectors, have a significant ecotoxic effect, which increases the damage in the ecosystem quality.

Fig. 5 shows for each point of the Pareto set depicted in Fig. 4, the total cost of the system and the areas of the solar collectors and absorption cycles. As can be seen, the environmental impact is lowered by increasing these areas. This reduces the contribution of the heat covered from the natural gas fired heater that is energy consumed by the cooling system, but on the other hand leads to an increase of the total cost.

Fig. 6 shows the individual Pareto sets associated with each collector type. These curves were obtained by solving for each collector type a reduced MINLP in which the binaries representing the associated collector model were fixed. Note that the Pareto set shown in Fig. 4 is nothing else but the envelope of the individual Pareto sets of each collector type. As observed, the Sydney SK-6 (ETC-1) collector model performs better than the remaining collectors, not only economically but also environmentally. As seen in the same figure, for small environmental impacts, Memotron TMO 600 (ETC-2) and VacuTube HP 65/30 (ETC-3) behave in a similar way as Sydney SK-6 (ETC-1). On the other hand, for low cost values, SK 500 (FPC-1), CPC AO SOL 15 (CPC) and ETC-1 perform all well.

These results are explained by the fact that the evacuated tube collectors show the highest efficiency in every month of the year. As a result, the total collector area required is considerably lower. This effect is more pronounced in the left region of the Pareto curve, in which the solar fraction increases. On the other hand, when the interest is shifted to the minimization of the total cost, the solar contribution decreases, since the cooling system tends to select the gas fired heater. In the latter region, the collectors operate at lower temperature, as most of the heat is supplied by the gas fired heater. Under these conditions (i.e., lower operating temperature) the efficiency of the flat plate collectors gets closer to that of the evacuated tube collectors. Therefore, because of their lower cost per

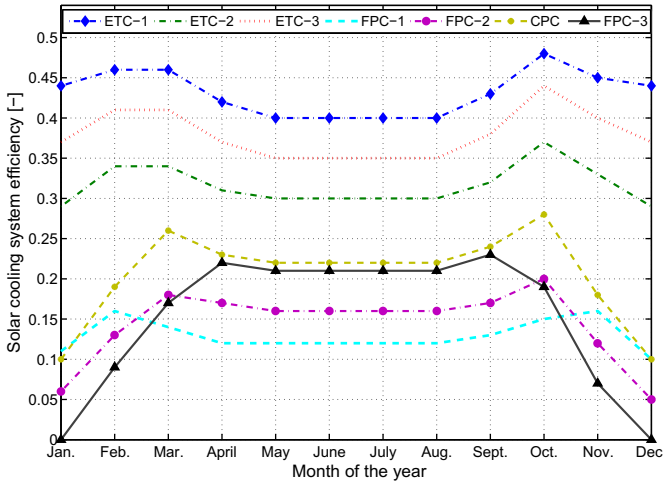

Fig. 10. Comparison of the solar cooling efficiency at each month of the year at minimum environmental impact for each collector type.

Please cite this article in press as: Gebreslassie BH, et al., A systematic tool for the minimization of the life cycle impact of solar assisted absorption cooling systems, Energy (2010), doi:10.1016/j.energy.2010.05.039

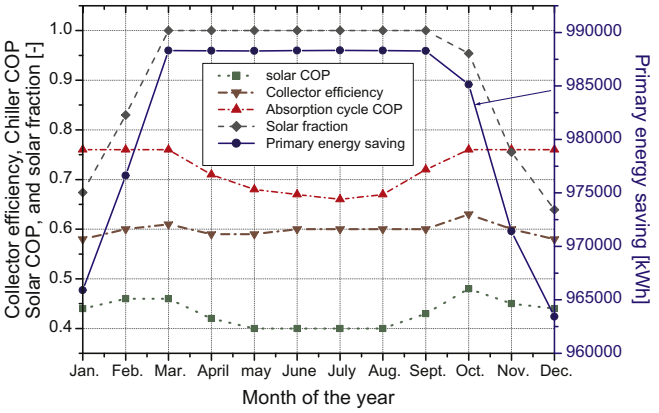

Fig. 11. Performance indicators associated with the minimum environmental impact design.

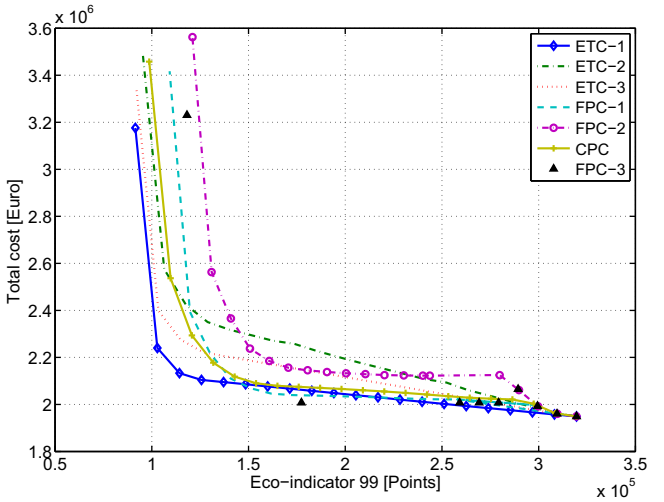

Fig. 13. Individual Pareto optimal sets associated with each collector type considering Tarragona weather data.

square meter, the flat plate collectors become more competitive, although they still cannot perform better than the ETC-1.

5.2.2. Extreme pareto optimal solutions

Fig. 7 depicts for the extreme Pareto optimal solutions, the environmental performance in each impact category expressed in normalized Eco-indicator 99 points. As observed, in some impact categories the minimum cost solution performs better than the minimum environmental impact one, whereas in some others the opposite situation occurs. In both designs, the main contribution to the overall impact is given by the extraction of fossil fuels followed by climate change, in the case of the minimum cost Pareto design, and by respiratory effects in the minimum environmental impact one. We can also observe in the same figure that the ozone layer depletion impact is rather low. This is because the cooling system uses natural working fluids.

Figs. 8 and 9 depict the contribution that the manufacturing and operation of the subsystems of the cooling system (i.e., absorption cycle itself, collectors and heater) have on the environmental performance of each extreme Pareto design. In general, the construction of the equipments have very little impact on the overall environmental damage. In fact, in the minimum total cost Pareto design, the main source of impact is the operation of the gas fired heater, whereas the contribution of the construction phase of the cooling system is negligible. In contrast, in the minimum environmental impact solution, the main contributor to the total impact is the operation of the solar collectors. These are operated using pumps that consume electricity. The electricity impact is determined assuming the Spanish electricity mix, which is mainly based on fuel oil and coal, and hence leads to large environmental impacts. In this latter case, the contribution of the manufacturing phase associated with the collectors is larger, mainly because of the emissions of heavy metals, as already mentioned. Hence, in view of these results, it seems convenient to account for this life cycle stage (i.e., construction of solar collectors) when performing the environmental analysis.

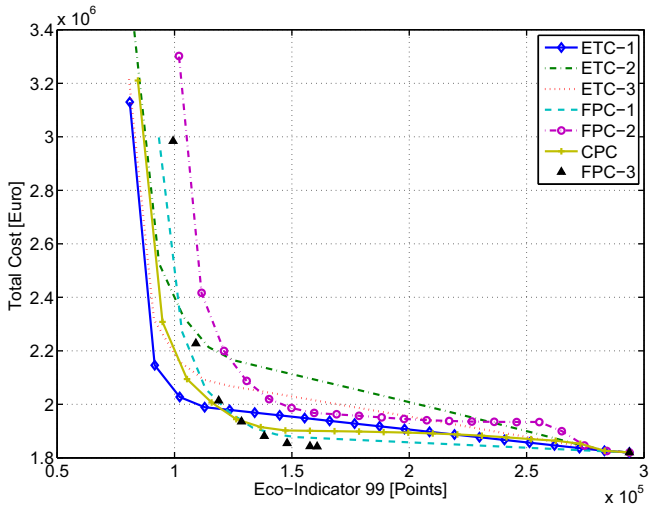

Fig. 12. Individual Pareto optimal sets associated with each collector type considering chilled and cooling water temperatures of 15/10 and 25/30 °C, respectively.

Fig. 10 shows the solar cooling system efficiency attained by each solar collector type in every month of the year when the Eco-indicator 99 value is minimized. As shown in the figure, the performance of the cooling system improves when the evacuated tube collector of type Sydney SK-6 (ETC-1) is used.

In Fig. 11 we show the performance indicators of the solar system, solar collector and the chiller in each month of the year for the minimum environmental impact design. The figure depicts also the total primary energy saved in each month relative to the consumption of primary energy at the minimum cost Pareto design. As observed, the savings in primary energy are larger from March to September, a period in which the solar radiation is higher.

5.2.3. Evaluation for different operation conditions

The outcome of the optimization depends on the specific case study under investigation. Among the key factors that affect the calculations, we find the operating conditions of the absorption cycle and the weather data of the location where the solar assisted system will be installed. In order to elaborate the dependency on the aforementioned variables, we conducted tests at different operating and weather conditions. The results of this analysis are presented in the next sections.

5.2.3.1. Operating conditions of the absorption cycle. The problem was solved for different values of the cooling and chilled water temperatures, which were varied from 27/35 °C to 25/30 °C, and from 10/5 °C to 15/10 °C, respectively.

The Pareto sets of alternatives associated with each solar collector type are presented in Fig. 12. As observed, the flat plate collectors (*FPC*)

Please cite this article in press as: Gebreslassie BH, et al., A systematic tool for the minimization of the life cycle impact of solar assisted absorption cooling systems, Energy (2010), doi:10.1016/j.energy.2010.05.039

are now selected in the lower region of the Pareto set (close to the minimum total cost design) and are used for preheating the water. The explanation for this is as follows. According to [60], the optimal generator temperature decreases when the cooling water temperature decreases and chilled water temperature increases. At lower generator temperature, and consequently lower solar collector temperatures, the flat plate collector performance improves, and because of their economic advantage, they are selected. On the other hand, in the left region of the Pareto curve, the contribution of the solar energy is more significant. Therefore, heating is carried out mainly by the solar collectors. In this case, those solar collectors that are more efficient at higher temperature perform better than the flat plate collectors and are therefore preferred.

5.2.3.2. Weather conditions. Taking as reference the base case, we next solved the problem considering weather data of Tarragona (Spain) (see Table 4) instead of Barcelona. This new location features higher solar radiations and ambient temperatures than Barcelona.

The Pareto set of the problem based on Tarragona weather data for each solar collector is presented in Fig. 13. Near the minimum total cost design, flat plate collectors are selected for preheating the water. This choice is explained by the following two observations: (i) the collector temperature is low because the solar collectors are used as preheater; (ii) as the ambient temperature and global daily solar radiation increases, the collector performance increases (see eqn. (8)). This improvement in the collector efficiency is more pronounced in the case of flat plate collectors. Hence, the flat plate collectors dominate in this region of the Pareto sets. On the other hand, close to the minimum environmental impact Pareto designs, evacuated tube collectors are selected. In this region, the heating is mainly covered by the solar collectors, so the collector temperature is higher. At higher temperatures, the performance of these collectors are by far better than that of the flat plate collectors and compound parabolic collectors and for this reason they become more competitive.

6. Conclusions

In this paper we have presented a systematic method for reducing the life cycle impact of cooling applications. The method introduced relies on formulating a bi-criteria MINLP problem that accounts for the minimization of the total cost and environmental impact of solar assisted absorption cooling cycles. The environmental performance has been measured according to the principles of LCA, which allows accounting for the damage caused in all the stages of the life cycle of the cooling system.

The capabilities of the proposed approach have been illustrated through its application to the design of a solar assisted ammonia-water absorption cooling system considering weather data of Barcelona and Tarragona. It has been clearly shown that significant reductions in the environmental impact can be achieved if the decision-maker is willing to invest on the solar collectors subsystem. These reductions can be attained by increasing the number of collectors installed, which increases the solar fraction of the cooling system. It has also been shown that the type of collector selected depends on the particular operating conditions and weather data considered in the analysis.

The systematic approach presented in this article has allowed to optimize integrated solar assisted absorption cycles in short CPU times under different conditions. The methodology presented in this work is intended to promote a more sustainable design of cooling applications by guiding the decision-makers towards the adoption of alternatives that cause less environmental impact and reduce the consumption of primary energy resources.

Acknowledgements

Berhane H. Gebreslassie expresses his gratitude for the financial support received from the University Rovira i Virgili. The authors also wish to acknowledge support of this research work from the Spanish Ministry of Education and Science (DPI2008-04099/DPI, CTQ2009-14420 and ENE2008-06687-C02-01) and the Spanish Ministry of External Affairs (A/8502/07, A/023551/09 and HS2007-0006).

References

[1] Balaras CA, Grossman G, Henning HM, Carlos A, Ferreira I, Podesser E, et al. Solar air conditioning in Europe—an overview. Renewable and Sustainable Energy Reviews 2007;2:299–314.
[2] Henning HM. Solar assisted air conditioning of buildings – an overview. Applied Thermal Engineering 2007;27:1734–49.
[3] Casals XG. Solar absorption cooling in spain: perspectives and outcomes from the simulation of recent instalations. Renewable Energy 2006;31:1371–89.
[4] Henning HM. Solar-assisted air-conditioning in buildings. Wien/New York: Springer, ISBN 3-211-00647-8; 2004.
[5] Florides GA, Kalogirou SA, Tassou SA, Wrobel LC. Modelling, simulation and warming impact assessment of a domestic-size absorption solar cooling system. Applied Thermal Engineering 2002;22:1313–25.
[6] Florides GA, Kalogirou SA, Tassou SA, Wrobel LC. Modelling and simulation of an absorption solar cooling system for cyprus. Solar Energy 2002;72:43–51.
[7] Assilzadeh F, Kalogirou SA, Ali Y, Sopian K. Simulation and optimization of a *LiBr* solar absorption cooling system with evacuated tube collectors. Renewable Energy 2005;30:1143–59.
[8] Lecuona A, Ventas R, Venegas M, Zacarías A, Salgado R. Optimum hot water temperature for absorption solar cooling. Solar Energy 2009;83:1806–14.
[9] Fathi R, Guemimi C, Ouaskit S. An irreversible thermodynamic model for solar absorption refrigerator. Renewable Energy 2004;29:1349–65.
[10] Wu C, Chen L, Sun F. Optimization of solar absorption refrigerator. Applied Thermal Engineering 1997;17:203–8.
[11] Biegler LT, Grossmann IE. Retrospective on optimization. Computers & Chemical Engineering 2004;28:1169–92.
[12] Grossmann IE, Biegler LT. Part ii. future perspective on optimization. Computers & Chemical Engineering 2004;28:1193–218.
[13] Savola T, Fogelholm CJ. *MINLP* optimisation model for increased power production in small-scale *CHP* plants. Applied Thermal Engineering 2007;27 (1):89–99.
[14] Tveit TM, Savola T, Gebremedhin A, Fogelholm CJ. Multi-period *MINLP* model for optimising operation and structural changes to *CHP* plants in district heating networks with long-term thermal storage. Energy Conversion and Management 2009;50:639–47.
[15] Chavez-Islas LM, Heard CL. Design and analysis of an ammonia-water absorption refrigeration cycle by means of an equation-oriented method. Industrial & Engineering Chemistry Research 2009;48(4):1944–56.
[16] Chavez-Islas LM, Heard CL. Optimization of a simple ammonia-water absorption refrigeration cycle by application of mixed-integer nonlinear programming. Industrial & Engineering Chemistry Research 2009;48(4):1957–72.
[17] Chavez-Islas LM, Heard CL, Grossmann IE. Synthesis and optimization of an ammonia-water absorption refrigeration cycle considering different types of heat exchangers by application of mixed-integer nonlinear programming. Industrial & Engineering Chemistry Research 2009;48(6):2972–90.
[18] Ardente F, Beccali G, Cellura M, Brano VL. Life cycle assessment of a solar thermal collector. Renewable Energy 2005;30(7):1031–54.
[19] Ardente F, Beccali G, Cellura M, Brano VL. Life cycle assessment of a solar thermal collector: sensitivity analysis, energy and environmental balances. Renewable Energy 2005;30(2):109–30.
[20] Battisti R, Corrado A. Environmental assessment of solar thermal collectors with integrated water storage. Journal of Cleaner Production 2005;13 (13–14):1295–300.
[21] Bernier E, Maréchal F, Samson R. Multi-objective design optimization of a natural gas-combined cycle with carbon dioxide capture in a life cycle perspective. Energy 2010;35(2):1121–8.
[22] Li H, Maréchal F, Burer M, Favrat D. Multi-objective optimization of an advanced combined cycle power plant including CO_2 separation options. Energy 2006;31:3117–34.
[23] Lazzaretto A, Toffolo A. Energy, economy and environment as objectives in multi-criterion optimization of thermal systems design. Energy 2004;29:1139–57.
[24] Burer M, Tanaka K, Favrat D, Yamada K. Multi-criteria optimization of a district cogeneration plant integrating a solid oxide fuel cell-gas turbine combined cycle, heat pumps and chillers. Energy 2003;28:497–518.
[25] Gebreslassie BH, Guillén-Gosálbez G, Jiménez L, Boer D. Design of environmentally conscious absorption cooling systems via multi-objective optimization and life cycle assesment. Applied Energy 2009;86:1712–22.
[26] Gebreslassie BH, Guillén-Gosálbez G, Jiménez L, Boer D. Economic performance optimization of an absorption cooling system under uncertainity. Applied Thermal Engineering 2009;29:3491–500.

Please cite this article in press as: Gebreslassie BH, et al., A systematic tool for the minimization of the life cycle impact of solar assisted absorption cooling systems, Energy (2010), doi:10.1016/j.energy.2010.05.039

[27] PRé-Consultants. The eco-indicator 99, a damage oriented method for life cycle impact assessment. methodology report and manual for designers. Amersfoort, The Netherlands: PRé Consultants; 2000. Technical report.
[28] Herold KE, Radermacher R, Klein SA. Absorption chillers and heat pumps. CRC Press; 1996.
[29] Kotas JT. The exergy method of thermal plant analysis. Krieger Publishing Company; 1995.
[30] Pátek J, Klomfar J. Simple functions for fast calculations of selected thermodynamic properties of the ammonia-water system. International Journal of Refrigeration 1995;18:228–34.
[31] Lasdon LS, Edgar TF, Himmelblau DM. Optimization of chemical processes. McGraw-Hill; 2001.
[32] Türkay M, Grossmann IE. Structural flowsheet optimization with complex investment cost functions. Computers & Chemical Engineering 1998;22:673–86.
[33] Vecchietti A, Lee S, Grossmann IE. Modeling of discrete/continuous optimization problems: characterization and formulation of disjunctions and their relaxations. Computers & Chemical Engineering 2003;27:433–48.
[34] Lee S, Grossmann IE. New algorithms for nonlinear generalized disjunctive programming. Computers & Chemical Engineering 2000;24:2125–41.
[35] Bejan A, Tsatsaronis G, Moran M. Thermal design & optimization. John Wiley & Sons Inc.; 1996.
[36] Turton R, Richard BC, Wallace WB, Joseph SA. Analysis, synthesis, and design of chemical processes. New Jersey: Prentice Hall PTR; 2003.
[37] Chemical Engineering. Chemical engineering plant cost index (CEPCI), Technical report; 2009.
[38] Azapagic A, Clift R. The application of life cycle assessment to process optimisation. Computers & Chemical Engineering 1999;10:1509–26.
[39] Puigjaner L, Guillén-Gosálbez G. Towards an integrated framework for supply chain management in the batch chemical process industry. Computers & Chemical Engineering 2008;32(4–5):650–70.
[40] Guillén-Gosálbez G, Caballero JA, Jiménez L. Application of life cycle assessment to the structural optimization of process flowsheets. Industrial & Engineering Chemical Research 2008;47:777–89.
[41] Hugo A, Ciumei C, Buxton A, Pistikopoulos EN. Environmental impact minimization through material substitution: a multi-objective optimization approach. Green Chemistry 2004;6:407–17.
[42] Bojarski AD, Guillén-Gosálbez G, Jiménez L, Espuña A, Puigjaner L. Life cycle assessment coupled with process simulation under uncertainty for reduced environmental impact: application to phosphoric acid production. Industrial & Engineering Chemical Research 2008;47(21):8286–300.
[43] Guillén-Gosálbez G, Grossmann IE. Optimal design and planning of sustainable chemical supply chains under uncertainty. AIChE Journal 2009;55 (1):99–121.
[44] Guillén-Gosálbez G, Mele F, Grossmann IE. A bi-criterion optimization approach for the design and planning of hydrogen supply chains for vehicle use. AIChE Journal 2010;56(3):650–67.
[45] Guillén-Gosálbez G, Grossmann IE. A global optimization strategy for the environmentally conscious design of chemical supply chains under uncertainty in the damage assessment model. Computers & Chemical Engineering 2010;34(1):42–58.
[46] Environmental management-life cycle assesment-principles and framework. IRAM-ISO 14040; 2006.
[47] Ecobalance-UK. TEAM and DEAM. Ecobalance UK. Arundel, UK: The Ecobilan Group, www.ecobalance.com/uk_team.php; 1998.
[48] SimaPro 6 LCA software. The Netherlands: PRé-Consultants, www.pre.nl/simapro/default.htm; 1998.
[49] PIRA-International. PEMS 4 database. Leatherhead, UK: PIRA International, www.pira.co.uk/pack/lca_software.htm; 1998.
[50] Ehrgott M. Multicriteria optimization. Springer; 2000.
[51] Grossmann IE. Review of nonlinear mixed-integer and disjunctive programming techniques. Optimization and Engineering 2002;3:227–52.
[52] Türkay M, Grossmann IE. Logic-based *MINLP* algorithms for the optimal synthesis of process networks. Computers & Chemical Engineering 1996;20:959–78.
[53] SPF Solartechnik Prüfung Forschung, *www.solarenergy.ch*.
[54] Comerç i Turisme Generalitat de Catalunya. ATLAS DE RADIACIÓ SOLAR A CATALUNYA. Departament d'Indústria, www.icaen.net; 2000.
[55] The ecoinvent Center. A competence centre of ETH, PSI, EMPA& ART, www.ecoinvent.ch/. ecoinvent data v2.1.
[56] Jungbluth N. Sonnenkollektor-anlagen. Dübendorf, CH: Swiss Centre for Life Cycle Inventories; 2007. ecoinvent report No. 6-XI.
[57] Gebreslassie BH, Medrano M, Mendes F, Boer D. Optimum heat exchanger area estimation using coefficients of structural bonds: application to an absorption chiller. International Journal of Refrigeration 2010;3(3):529–37.
[58] Brooke A, Kendrik D, Meeraus A, Raman R, Rosenthal RE. GAMS – a user's guide. Washington: GAMS Development Corporation; 1998.
[59] F-Chart Software. Engineering equation solver, (EES), *www.fchart.com*.
[60] Fernández-Seara J, Vázquez M. Study and control of the optimal generation temperature in NH_3–H_2O absorption refrigeration systems. Applied Thermal Engineering 2001;21:343–57.

Please cite this article in press as: Gebreslassie BH, et al., A systematic tool for the minimization of the life cycle impact of solar assisted absorption cooling systems, Energy (2010), doi:10.1016/j.energy.2010.05.039

UNIVERSITAT ROVIRA I VIRGILI
OPTIMIZATION OF ENVIRONMENTALLY FRIENDLY SOLAR ASSISTED ABSORPTION COOLING SYSTEMS
Berhane Hagos Gebreslassie
ISBN: 978-84-693-7673-7/DL:T-1752-2010

Solar assisted absorption cooling cycles for reduction of global warming: a multi-objective optimization approach

Berhane H. Gebreslassie[a], Gonzalo Guillén-Gosálbez[b], Laureano Jiménez[b], Dieter Boer[a,*]

[a] *Departament d'Enginyeria Mecânica, Universitat Rovira i Virgili*
Av. Països Catalans, 26, 43007, Tarragona, Spain
[b] *Departament d'Enginyeria Quimica, Universitat Rovira i Virgili*
Av. Països Catalans, 26, 43007, Tarragona, Spain

Abstract

This work studies the use of absorption cycles combined with solar energy for reducing the green house gas emissions in the energy sector. The problem of satisfying a given cooling demand at minimum cost and environmental impact is formulated as a bi-criterion nonlinear optimization problem that seeks to minimize the total cost of the cooling application and its contribution to global warming. The latter metric, which is assessed following the principles of life cycle assessment, accounts for the impact caused during the construction and operation of the system. The concept of Pareto optimality is employed to discuss different alternatives for reducing the contribution to global warming that differ in their economic and environmental performance. We show that reducing the contribution to global warming considering the current energy prices and taxes on carbon dioxide emissions is technically viable but economically not appealing. We also discuss the conditions under which reducing the CO_2 emissions could become economically attractive.

Keywords: Solar assisted cooling, NLP, Multi-objective optimization, Life

*Corresponding author
Email address: Dieter.Boer@urv.cat (Dieter Boer)

UNIVERSITAT ROVIRA I VIRGILI
OPTIMIZATION OF ENVIRONMENTALLY FRIENDLY SOLAR ASSISTED ABSORPTION COOLING SYSTEMS
Berhane Hagos Gebreslassie
ISBN: 978-84-693-7673-7/DL:T-1752-2010

cycle assessment (LCA), Global warming potential

1. Introduction

The human pattern of development has led to a significant increase in greenhouse gas (GHG) emissions and consequently in global warming [1]. Based on the Intergovernmental Panel on Climate Change ($IPCC$) [2] global GHG emissions increased by 70% between 1970 and 2004, growing from 28.7 to 49 Gigatonnes of carbon dioxide equivalents ($GtCO_{2\,eq}$). CO_2 emissions grew by 80% in the same period representing 77% of the GHG emissions in 2004.

Nowadays, 94% of the CO_2 emissions in Europe are attributed to the energy sector as a whole, and particularly to the combustion of fossil fuels. Oil consumption accounts for 50% of the CO_2 emissions in the European Union, natural gas for 22% and coal for 28% [1]. Particularly, the building sector represents 40% of the total primary energy demand in European Union countries and it is responsible for one third of the GHG emissions [3].

A large percentage of the emissions attributed to the building sector are due to air conditioning (AC) systems, most of which are based on electricity driven compression cycles. These systems show the best economic performance and for this reason they have dominated the market in the last years. Unfortunately, they consume non-renewable primary energy resources and contribute to major environmental problems such as the Ozone layer depletion (due to the refrigerants) and global warming (because of their electricity consumption [4]). With the recent trend of developing more sustainable processes, there has been a growing interest on thermal energy activated cooling machines. These systems represent an environmentally friendly alternative to standard compression chillers, as they can be driven by waste heat, natural gas, solar energy or biomass. This can lead to significant reductions in GHG emissions [5–7].

Among all the alternatives to standard AC systems, solar assisted cooling cycles are seen by many as a promising option. By using solar energy

ISBN: 978-84-693-7673-7/DL:T-1752-2010

autonomous cooling systems, it is possible to achieve virtually zero CO_2 emissions. Unfortunately, the current electricity cost and fuel prices make it difficult to compete with conventional cooling systems [8]. Hence, the adoption of alternative AC systems raises the question of to which extent decision-makers are willing to compromise the economic performance in order to obtain environmental benefits.

Mathematical programming methods, and in particular, multi-objective optimization, offer a suitable framework for addressing this type of problems. These techniques allow for the inclusion of environmental concerns in the decision-making process by generating a set of trade-off solutions that balance economic and environmental criteria called the Pareto set. From these points, decision-makers can identify the best ones according to their strategic guidelines and applicable legislation.

Several optimization studies have been carried out on cooling systems [13–16]. Most of them addressed the optimization of the economic performance of the cooling application and neglected the associated environmental impact. A reduced number of approaches have applied multi-objective optimization to the design of energy systems [17–19]. However, to our knowledge, none of them focused on integrated solar absorption systems.

One of the key issues in multi-objective optimization as applied to environmentally conscious process design is the definition of a suitable environmental metric. Works incorporating environmental concerns through multi-objective optimization have typically focused on minimizing the impact at the plant level [19, 20], thus neglecting the damage caused in other stages of the life cycle. This approach can lead to solutions that transfer the environmental problem to other echelons of the energy supply chain, thereby failing in reducing the environmental damage globally [21]. A proper evaluation of the environmental performance of a system requires the application of life cycle assessment (LCA) principles [11, 12, 22, 23] for quantifying the impact from the extraction of raw materials to the delivery of energy to the final customer. Despite recent advances in LCA methodology, the current

UNIVERSITAT ROVIRA I VIRGILI
OPTIMIZATION OF ENVIRONMENTALLY FRIENDLY SOLAR ASSISTED ABSORPTION COOLING SYSTEMS
Berhane Hagos Gebreslassie
ISBN: 978-84-693-7673-7/DL:T-1752-2010

situation is that the literature on the application of LCA to energy systems is limited.

With the aforementioned observations in mind, the goals of this work are: (i) to perform an LCA analysis on solar assisted absorption cooling systems; and (ii) to explore their environmental benefits in terms of reducing the GHG emissions by employing a multi-objective optimization framework. Specifically, in this work we will elaborate, among others, the following points.

i. Under which circumstances the use of solar energy in cooling applications is economically competitive with fossil fuels? (*i.e.*, which are the values of the fuel cost and CO_2 taxes that make the use of solar energy in absorption cooling systems profitable?)

ii. How much can be saved in terms of GHG emissions by integrating solar collectors with absorption cooling systems?

This work is structured in seven sections. The section that follows presents a motivating example that illustrates the environmental benefits of the solar assisted absorption chiller over the counter part vapor compression cycle. The next section discuses the mathematical formulation of the multi-objective optimization problem. Special emphasis is given to the solar system performance constraints and the equations added to quantify the environmental impact (*i.e.*, contribution to global warming). The fourth and fifth sections concentrate on the solution method of the problem and the case study used to test its capabilities. A detailed discussion of the results is presented in section six. The conclusions of the work are finally drawn in the last section of the paper.

2. Motivating example

We present first a straightforward example that helps to briefly illustrate the environmental advantages of integrating solar collectors with absorption cycles for reducing the GHG emissions in cooling applications. Three chillers,

ISBN: 978-84-693-7673-7/DL:T-1752-2010

the conventional electricity driven one and two thermal energy driven chillers, are considered at this point. Particularly, we will study single effect absorption and vapour compression cycles with coefficients of performance of 0.7 and 3, respectively. The vapour compression cycle motor efficiency (η^{mot}) is 95%. The solar fraction (SF) of the absorption chillers are 0% (100% natural gas) and 70%. A life span of 20 years and 2000 working hours per year are assumed.

These systems are compared in terms of their global warming potential (GWP) expressed in equivalent tons of CO_2 per unit of cooling capacity generated. In the case of the electricity driven chiller, the calculation of the GWP accounts only for the electricity generation. For the thermal energy driven chillers, the environmental analysis considers the extraction and combustion of natural gas as well as operation of the solar collectors. It should be noted that, for the sake of simplicity, in both cases the impact associated with the construction of the cycle has been neglected. The electricity consumed by the pump of the absorption cycle has also been neglected, since it represents a very low percentage of the total energy consumption. With regard to the GWP associated with the electricity generation, we consider different electricity generation mixes (*i.e.*, Spain, USA and China). The associated GWP values per unit of energy generated have been retrieved from the environmental database Ecoinvent [24]. For the countries considered in this example, these are 0.6035, 0.751 and 1.148 $[kg\,CO_{2\,eq}/kWh]$, respectively. On the other hand, the GWP due to the combustion of natural gas in the gas fired heater, which has also been retrieved from Ecoinvent, is 0.256 $[kg\,CO_{2\,eq}/kWh]$. The latter value includes also the impact associated with the construction of the boiler.

[***Figure 1 Could be placed here***]

The results of the analysis are shown in Fig. 1. Particularly, Fig. 1(a) represents 100 kW cooling capacity powered by natural gas. The total GWP

ISBN: 978-84-693-7673-7/DL:T-1752-2010

is 1463 $ton\,CO_{2\,eq}$ with a natural gas consumption of 142.8 kW. Fig. 1(b) represents the same cycle but this time powered by combination of natural gas and solar energy. With this integration, the natural gas consumption drops to 42.9 kW, with a total GWP of 438.8 ton $CO_{2\,eq}$. Fig. 1(c) represents a 100 kW cooling capacity vapour compression cycle powered by electricity. The GWP of this chiller is 847, 1054 and 1612 $ton\,CO_{2\,eq}$ in Spain, USA and China, respectively.

Comparing chillers (a) and (b), it can be seen that it is possible to reduce up to 70% the primary energy demand of the cycle by integrating it with solar energy. This reduces the GWP from 1463 to 438.8 $ton\,CO_{2\,eq}$.

The comparison between chillers (a) and (c) depends on the electricity production mix. The use of absorption chillers in China reduces the GWP by 9%. On the other hand, in Spain and USA, vapour compression chillers are environmentally more attractive than the considered absorption chillers. It should be noted that absorption chillers become competitive from an environmental perspective if they had higher COPs. This could be accomplished by using double or triple effect configurations. Besides, their impact could also be reduced by using less contaminant heat sources or free driving energy as waste heat.

The comparison between chillers (b) and (c) reveals that solar assisted absorption chillers are environmentally more attractive than electric chillers. The magnitude of the GWP reduction depends again on the electricity production mix of the country. We can see from the results that reductions in GWP of 48%, 52% and 73% can be achieved in Spain, USA and China, respectively. In these cases, the advantages are twofold: (i) the mitigation of global warming; and (ii) the reduction in the consumption of those non-renewable primary energy resources consumed for generating the electricity required by the compression chillers.

UNIVERSITAT ROVIRA I VIRGILI
OPTIMIZATION OF ENVIRONMENTALLY FRIENDLY SOLAR ASSISTED ABSORPTION COOLING SYSTEMS
Berhane Hagos Gebreslassie
ISBN: 978-84-693-7673-7/DL:T-1752-2010

3. Mathematical formulation: a multi-objective optimization approach

After proving the environmental advantages of integrating solar collectors with absorption cycles, we next derive a multi-objective mathematical formulation for analyzing systematically these systems considering environmental and economic criteria simultaneously.

3.1. System description

In order to derive our formulation, we consider a typical ammonia/water mixture supported solar assisted absorption chiller (see Fig. 2). The detail description of the absorption cycle could be found [14]. It is assumed that the heat demand required to activate the chiller can be supplied either by the gas fired heater using natural gas as primary energy resource or by solar energy captured by solar collectors. Evacuated tube collectors are used to convert the solar energy into usable forms of thermal energy. It is also possible to cover the heat demand of the absorption chiller by a combination of the aforementioned heat sources.

[***Figure 2 could be placed here***]

The problem addressed in this paper can be formally stated as follows. Given are the cooling capacity of the cooling system, the inlet and outlet temperatures of the external fluids (except the generator temperatures), capital cost data, monthly weather data (ambient temperature and global daily solar radiation), performance equations of the solar collector, and GHG emissions associated with the construction and operation of the cooling system. The goal is to minimize simultaneously the contribution to global warming and the total cost of the cooling system.

3.2. Mathematical formulation

We present next a multi-objective optimization model that provides as output a set of technical alternatives for satisfying the cooling demand, each

ISBN: 978-84-693-7673-7/DL:T-1752-2010

featured by a different economic and environmental performance. The mathematical model of the absorption cycle is based on the formulation presented in detail in previous works [14, 25]. The model described here extends the original formulation by integrating the absorption cycle with solar collectors. For completeness of the work, we present the main equations of the absorption cycle already described elsewhere [14, 25] in the Appendix. On the other hand, the solar collector performance constraints and the equations associated with the calculation of the GHG emissions are given next.

The mathematical formulation is a multi-period one that allows to follow a given cooling demand pattern while accounting for varying meteorological conditions over time. It is assumed that the cycle can operate in a different manner in each time period t in order to get adapted to the specific solar radiation available. The model is based on mass and energy balances (see Appendix) and objective function constraints that allow to assess the economic and environmental performance of the cooling system.

3.2.1. Heat production subsystem

The model considers that the heat supplied to the absorption cycle is provided from the solar collectors and the gas fired heater. The associated solar collector constraints are presented in the following sections.

3.2.2. Collector performance constraints

Solar collectors absorb solar radiation and convert it into useful heat. The useful heat collected is transported by working fluids flowing through the solar collectors [26]. The collector performance is denoted by a continuous variable η_t^{col} whose value is determined via eqn. (1). On the other hand, the heat collected from the solar collector in period t ($Q_{k=col,t}$) is given by eqn. (2).

$$\eta_t^{col} = IAM(\Theta)c_0 - c_1\frac{T_t^{av} - T_t^{amb}}{G_t} - c_2\frac{(T_t^{av} - T_t^{amb})^2}{G_t} \qquad \forall t \tag{1}$$

$$Q_{k,t} = \eta_t^{col} A_{col} G_t \qquad k = Col, \forall t \tag{2}$$

UNIVERSITAT ROVIRA I VIRGILI
OPTIMIZATION OF ENVIRONMENTALLY FRIENDLY SOLAR ASSISTED ABSORPTION COOLING SYSTEMS
Berhane Hagos Gebreslassie
ISBN: 978-84-693-7673-7/DL:T-1752-2010

In eqn. (1), $IAM(\Theta)$ is the incident angle modifier, which accounts for the effect of a non perpendicular incident radiation at incidence angle Θ in relation to a normal incidence radiation ($i.e., \Theta = 0$); T_t^{av} is the monthly average inlet and exit fluid temperature in the collector; and T_t^{amb} is the monthly average ambient air temperature. The daily global solar radiation is represented by G_t. Finally, c_0 denotes the optical efficiency of the collector, whereas c_1 and c_2 are the linear and quadratic loss coefficients, respectively [8]. On the other hand, in eqn. (2), n represents the number of collectors and A_{col} is the absorber area of a single collector. For the sake of simplicity, in this work we treat the integer variable n as a continuous one. It should be noted that from numerical examples we have observed that this can be done without compromising the quality of the final solution. This simplification greatly helps the computations.

3.2.3. Linking constraints

Eqn. (3) relates the heat consumed by the absorption cycle with that produced by the solar collector and the gas fired heater. More precisely, the sum of the heat produced by the solar collector ($Q_{k=Col,t}$) and gas fired heater ($Q_{k=GFH,t}$) should cover at least the heat demand ($Q_{h=D,t}$) of the absorption cycle in period t.

$$Q_{k,t} \leq Q_{k',t} + Q_{k'',t} \qquad k = D, k' = Col, k'' = GFH, \forall t \tag{3}$$

Furthermore, the heat produced by the heater in every time period must be less than or equal to its capacity ($CAP_{k=GFH}$) as given by eqn. (4).

$$Q_{k,t} \leq CAP_k \qquad k = GFH, \forall t \tag{4}$$

3.3. Objective functions

The model seeks to minimize two contradicting objective functions simultaneously: total cost and contribution to global warming. Details on the calculations of both performance metrics are given in the next subsections.

UNIVERSITAT ROVIRA I VIRGILI
OPTIMIZATION OF ENVIRONMENTALLY FRIENDLY SOLAR ASSISTED ABSORPTION COOLING SYSTEMS
Berhane Hagos Gebreslassie
ISBN: 978-84-693-7673-7/DL:T-1752-2010

3.3.1. Economic performance

The economic assessment of the absorption cycle is discussed in detail in [14, 25]. Specifically, the total cost (TC) accounts for the capital and operating cost of the integrated system (TCC and TOC, respectively) as shown in eqn. (5).

$$TC = TCC + TOC \tag{5}$$

In this equation, TCC accounts for the cost of the heat exchangers of the cycle, solar collectors, gas fired heater, pump and expansion valves. On the other hand, the operating cost (TOC) includes the running cost of the gas fired heater, pump and solar collectors, as well as the cooling water cost. The capital and operation cost constraints are included in the Appendix.

3.3.2. Environmental impact

The environmental impact is quantified according to LCA principles. The combined use of LCA and multi-objective optimization has been shown to be a suitable framework for identifying, in a systematic way, opportunities for environmental improvements in different applications [9–12]. In this approach, LCA is employed to assess the environmental performance of a system, whereas optimization techniques enable us to generate feasible process alternatives and identify the best ones in terms of economic and environmental criteria. General details on the LCA methodology can be found elsewhere [21].

The calculation of the life cycle impact of the cooling application follows the four LCA steps: (1) goal and scope definition; (2) inventory analysis; (3) damage assessment; and (4) interpretation. We describe next these phases in the context of our study.

Goal and scope definition: In this step, the system boundaries, the functional unit and the environmental damages are defined. We perform a cradle-to-gate analysis that accounts for the generation of the utilities consumed by the cooling system as well as the impact during the construction phase. The functional unit is the amount of cooling demand satisfied during the time

ISBN: 978-84-693-7673-7/DL:T-1752-2010

horizon. The environmental damage is quantified through the global warming potential (GWP). This is a measure of how much a given mass of a GHG emission contribute to global warming. It is a relative scale which compares the impact of a given chemical with that of the same mass of carbon dioxide (whose GWP by convention equals 1). The GWP is calculated over a specific time interval that must be stated beforehand [2, 27]. Particularly, we follow the Intergovernmental Panel on Climate Change IPCC 2007 framework considering a time horizon of 100 years, which is the time frame used in the Kyoto Protocol [27].

Inventory analysis: This step aims at quantifying the total GHG emissions associated with the absorption cooling. These emissions are represented by a continuous variable (LCI_b^{tot}), that is determined from the emissions during the manufacturing (LCI_b^{man}) and operation (LCI_b^{op}) of the cooling system, as shown in eqn. (6).

$$LCI_b^{tot} = LCI_b^{man} + LCI_b^{op} \qquad \forall b \tag{6}$$

The life cycle GHG emissions during the construction phase, which are denoted by the continuous variable LCI_b^{man}, can be determined from the sizes of the gas fired heater, solar collectors, heat exchangers and pumps of the cycle, as stated in eqn. (7).

$$LCI_b^{man} = \sum_k LCIE_{b,k} CAP_k \tag{7}$$

Here, the continuous variable CAP_k represents, in each case, the mass of the heat exchangers and expansion valve in kg, heat capacity of the gas fired heater and pump capacity expressed in kW, power of and solar collector absorber area in m^2. The parameter $LCIE_{b,k}$ denotes the life cycle inventory of emissions of chemical b released during the construction phase per unit of capacity of equipment k. The values of $LCIE_{b,k}$ should be obtained either from the literature or by performing an *ad hoc* LCA analysis on the construction of each single equipment.

The second term in eqn. (6) (LCI_b^{op}) accounts for the emissions due to the extraction and combustion of natural gas, operation of the solar collectors

UNIVERSITAT ROVIRA I VIRGILI
OPTIMIZATION OF ENVIRONMENTALLY FRIENDLY SOLAR ASSISTED ABSORPTION COOLING SYSTEMS
Berhane Hagos Gebreslassie
ISBN: 978-84-693-7673-7/DL:T-1752-2010

and generation of the cooling water and electricity consumed by the heat exchangers and pumps of the cycle, respectively:

$$\begin{aligned} LCI_b^{op} = \sum_t \varphi T_{op} \Big(& Q_{k,t} LCIE_b^{heat(gfh)} + Q_{k',t} LCIE_b^{heat(col)} \\ & + m_{j,t} LCIE_b^{cw} + W_{k'',t} LCIE_b^{elec} \Big) \\ & \forall b, j = cooling\, water, k = GFH, k' = Col, k'' = Pump \end{aligned} \tag{8}$$

In this equation, T_{op} and φ are the annual operation hours of the cooling system and life span in years. $LCIE_b^{heat(gfh)}$, $LCIE_b^{heat(col)}$, $LCIE_b^{cw}$ and $LCIE_b^{elec}$ appearing in the same equation denote the life cycle inventory of emissions of chemical b contributing to global warming per unit of reference flow (*i.e.*, heat, amount of cooling water and electricity, respectively). These values, which can be retrieved from environmental databases [28, 29], depend on the particular features of the absorption cycle (*i.e.*, type of primary energy sources used in the heater, type of solar collectors, electricity mix of the country in which the cycle operates, etc.). Finally, the continuous variables $m_{j=cooling\, water,t}$ and $W_{k=Pump,t}$ denote the cooling water and electricity consumption, respectively, in period t. Note that the consumption of cooling water is obtained from the energy balance applied to the heat exchangers.

Impact assessment: In this step, the life cycle inventory of emissions is translated into the corresponding contribution to global warming.

$$GWP = \sum_b LCI_b^{tot} df_b \tag{9}$$

Here, the parameter df_b is a damage factor that accounts for the global warming potential of chemical b compared to that of CO_2. These values are available in the $IPCC$ report [30]. It should be noted that environmental databases such as Ecoinvent provide both the life cycle inventory of emissions as well as the associated environmental impacts per unit of reference flow. Hence, it might be possible to omit eqn.(9) in those cases in which the GWP values are directly available in the database.

Interpretation: In the context of the approach presented, the interpretation phase entails analyzing the Pareto solutions of the following multi-objective

ISBN: 978-84-693-7673-7/DL:T-1752-2010

environmental problem:

$$\begin{array}{lll} \text{(M)} & \min\limits_{x} & U\left(x\right)=\left\{TC\left(x\right),GWP\left(x\right)\right\} \\ & \text{s.t.} & h(x)=0 \\ & & g(x)\leq 0 \\ & & x\in\Re \end{array} \tag{10}$$

In this formulation, x denotes state or design variables (*i.e.*, thermodynamic properties, flows, operating conditions, and sizes of equipment units). The equality constraints $h(x) = 0$ represent thermodynamic property relations, mass and energy balances, cost, and LCA calculations. On the other hand, the inequality constraints $g(x) \leq 0$ are added to model design specifications (*i.e.*, capacity limits, bounds on process variables, etc.). The objective function includes two terms: *TC(x)* is the total cost of the cooling system, and *GWP(x)* represents its environmental impact (*i.e.*, contribution to global warming). The solution to this problem is given by a set of efficient or Pareto optimal points representing trade-off designs [12].

4. Solution method

To obtain the Pareto solutions of model (M), we apply the ϵ-constraint method, which is based on solving a set of instances of an auxiliary model (MA) for different target values on the environmental performance (*i.e.*, *GWP(x)*) as follows:

$$\begin{array}{lll} \text{(MA)} & \min\limits_{x} & U(x)=TC\left(x\right) \\ & \text{s.t.} & GWP\left(x\right)\leq\epsilon \\ & & \underline{\epsilon}\leq\epsilon\leq\overline{\epsilon} \\ & & h(x)=0 \\ & & g(x)\leq 0 \\ & & x\in\Re \end{array} \tag{11}$$

Note that the lower and upper limits imposed on epsilon can be obtained by minimizing each scalar objective separately.

UNIVERSITAT ROVIRA I VIRGILI
OPTIMIZATION OF ENVIRONMENTALLY FRIENDLY SOLAR ASSISTED ABSORPTION COOLING SYSTEMS
Berhane Hagos Gebreslassie
ISBN: 978-84-693-7673-7/DL:T-1752-2010

5. Case study

The capabilities of the proposed approach were illustrated through a case study that addresses the design of a solar assisted absorption cooling system with 100 kW cooling capacity. The process data for the absorption cycle are given in [14, 25]. We considered a water cooled ammonia/water absorption chiller with a generator temperature in the range of 95 to 120^{o}C. Note that this temperature range cannot be reached by flat plate collectors with acceptable efficiencies [26]with acceptable efficiencies. For this reason in this work assumed to operate with evacuated tube collectors. More precisely, the cycle operates with a Sydney SK-6 from Microterm Energietechnik GmbH, which is a directly cooled evacuated tube collector with a cylindrical absorber and a CPC concentrator collector [8]. Global daily solar radiation of Barcelona (see Table 1) for an azimuth angle 0^{o} and an inclination of 45^{o} was considered [31].

[***Table 1 could be placed here***]

The entries of the life cycle inventory of GHG emissions associated with the construction and operation of the cooling system were defined as follows:

- *Heat exchangers:* The life cycle inventory of GHG emissions released during the construction of the heat exchangers was approximated by that associated with production of the equivalent mass of stainless steel. This amount of mass can be easily determined from the exchange area. The associated environmental information was taken from Ecoinvent [24].

- *Solar collectors:* The emissions due to the construction and operation of the evacuated tube collector were retrieved from Ecoinvent [24]. The operation emissions account for the maintenance of the solar collector and the generation of the electricity consumed by its pump.

- *Gas fired heater:* The emissions associated with the generation and combustion of natural gas in the fired heater were retrieved from Ecoin-

UNIVERSITAT ROVIRA I VIRGILI
OPTIMIZATION OF ENVIRONMENTALLY FRIENDLY SOLAR ASSISTED ABSORPTION COOLING SYSTEMS
Berhane Hagos Gebreslassie
ISBN: 978-84-693-7673-7/DL:T-1752-2010

vent. This term accounts for the emissions given by the fuel generation, construction of the boiler, direct emissions, and electricity consumed during the boiler operation. For the calculations, we assumed an average net efficiency of 0.95 based on the lower heating value.

- *Pump:* The life cycle inventory of GHG emissions associated with the electricity consumed by the pump consdering the electricity mix of Spain, was also retrieved from Ecoinvent [24]. The emissions during the construction of the pump and expansion valve were neglected.

6. Results and Discussions

6.1. Pareto set for the base case

The NLP model of the solar assisted cooling system was implemented in GAMS 23.0 [28] and solved with the NLP solver CONOPT [29] in a 2.29 GHz machine. The Pareto solutions were calculated following the method described before. The model contained 2634 constraints and 2116 variables. It took 22 seconds of CPU time to generate 21 Pareto solutions.

Fig. 3 depicts the Pareto set of alternatives, each of which represents a different integrated absorption cycle with a specific solar fraction. The y axis on the right hand side of the figure shows the solar fraction associated with each Pareto design (*i.e.*, amount of energy covered by solar energy divided by the total energy consumed by the cycle), whereas that on the left axis provides the total cost.

[***Figure 3 could be placed here***]

As can be seen, there is a clear trade off between the economic (total cost) and environmental (GWP) indicators. Particularly, one can reduce up to 82.3% the GWP potential at the expense of increasing the total cost by 115%. Further inspection of the Pareto points reveals that reductions in GWP with respect to the minimum cost design are achieved by reducing the primary

UNIVERSITAT ROVIRA I VIRGILI
OPTIMIZATION OF ENVIRONMENTALLY FRIENDLY SOLAR ASSISTED ABSORPTION COOLING SYSTEMS
Berhane Hagos Gebreslassie
ISBN: 978-84-693-7673-7/DL:T-1752-2010

energy consumption rate of the cycle. This is accomplished by increasing the area of the heat exchangers of the cycle and also by replacing the primary energy source (natural gas) by solar energy. Note that reducing the natural gas consumption decreases the operating cost of the cooling system, but also increases the capital cost due to the installation of solar collectors. In practice, the latter effect dominates the former one, so an increase in the total cost is observed when the GWP is minimized.

As observed in the figure, the slope of the Pareto curve is smooth in the region close to the minimum cost design (point D), but becomes steeper as we move towards the minimum GWP solution (point A). This is because in order to fulfill more stringent environmental limitations (near to Pareto design A), the model is forced to increase the area of the solar collectors drastically in order to cover the energy requirements in months with low radiations. This causes a large increase in the slope of the curve, as observed in the figure.

In Fig. 3 we have also depicted the economic and environmental performance of a standard vapour compression chiller, considering only the impact during the operation phase. This chiller has a cooling capacity of 100 kW and a COP of 3. Data for the Spanish electricity grid retrieved from Ecoinvent [24] was considered in its environmental assessment. A simulation model of the chiller was implemented in EES [32] in order to perform the calculations. As observed, this system dominates part of the Pareto designs, as it shows better environmental and economic performance for a GWP above 2100 $ton\,CO_{2\,eq}$. However, the vapour compression chiller have the limitation that it cannot reduce the GWP below that point. Hence, it can be concluded from these results that depending on the part of the Pareto frontier in which decision-makers are interested, it might be convenient to select a traditional vapour compression cycle instead of a solar assisted cooling system.

[***Figure 4 could be placed here***]

UNIVERSITAT ROVIRA I VIRGILI
OPTIMIZATION OF ENVIRONMENTALLY FRIENDLY SOLAR ASSISTED ABSORPTION COOLING SYSTEMS
Berhane Hagos Gebreslassie
ISBN: 978-84-693-7673-7/DL:T-1752-2010

Fig. 4 depicts for some of the Pareto designs shown in Fig. 3, the solar fraction attained in each month of the year. Note that the model assumes that the cycle operates in the same way during all the years of the time horizon. As seen, in the minimum environmental impact design (design A), 98% of the heat demanded by the absorption chiller is covered by solar energy. On the other hand, in the Pareto designs B, C, and D the contribution of the solar energy decreases depending on the environmental limit imposed by the epsilon constraint method. Pareto design D is not visible in the figure because at the minimum total cost design the cooling system does not have any contribution of solar energy.

[***Figure 5 could be placed here***]

Fig. 5 shows the life cycle GWP associated with the operation of the cycle for some Pareto alternatives (*i.e.*, points A, B, C and D in Fig. 3) in each month of the year. As we can see in Fig. 5, the GWP is lower in May, June, July and August, due to the high global daily solar radiation (see Table 1). In these months, the natural gas consumption is reduced and the GHG emissions are decreased.

6.2. Taxes on GHG emissions

Ideally, decision-makers should analyze the Pareto set of alternatives given in Fig. 3, and finally choose the best one according to their preferences. Unfortunately, this is not done in practice. Instead, the total cost is usually minimized as single-objective and the unique solution obtained by doing so is implemented as far as it fulfills the environmental legislation. Hence, by setting taxes on GHG emissions, policy makers can guide decision-makers towards the adoption of more sustainable alternatives.

With this observation in mind, we conducted an analysis whose goal was to assess the impact of a given tax on CO_2 emissions on the optimal absorption cycle configuration considering only its economic performance. More precisely, we aimed at determining how the areas of the heat exchangers of

UNIVERSITAT ROVIRA I VIRGILI
OPTIMIZATION OF ENVIRONMENTALLY FRIENDLY SOLAR ASSISTED ABSORPTION COOLING SYSTEMS
Berhane Hagos Gebreslassie
ISBN: 978-84-693-7673-7/DL:T-1752-2010

the cycle and number of solar collectors changed as a function of the charges tax_{CO_2} on the CO_2 emissions. This study was performed by solving the following single-objective optimization model that minimizes the total cost for different possible values of tax_{CO_2}:

$$\begin{array}{lll} \text{(MT)} & \min\limits_{x} & U(x) = TC(x) + GWP(x)tax_{CO_2} \\ & \text{s.t.} & h(x) = 0 \\ & & g(x) \leq 0 \\ & & x \in \Re \end{array} \tag{12}$$

Note that this is indeed equivalent to applying the weighted sum method (REF) to the multi-objective problem (M). In fact, each single run of model (MT) for a given tax value on the GHG emissions provides a different Pareto solution. Conversely, each point of the Pareto set "total cost" vs "GWP" has an associated tax rate, that is to say, a value of the tax rate that would make that Pareto point optimal if the total cost was minimized as a single objective without any restriction on the GHG emissions. It should be noted that since the problem is nonconvex, the weighted sum method is not guaranteed to provide all the solutions of the Pareto set. In fact, it can only provide the points that lie in the convex envelope of the Pareto set [33]. This implies that there might be points of the Pareto set that cannot be obtained by solving (MT) (*i.e.*, there is not any tax rate for which the Pareto point is the maximum of MT).

[***Table 2 could be placed here***]

The results obtained by applying the above commented procedure are given in Table 2. The table shows for each tax rate value, the total cost, GWP and solar fraction of the cycle that minimizes the cost as unique criterion. As observed, increasing the tax rate has the effect of leading to optimal designs with larger solar fractions and consequently less GHG emissions. This is an interesting result that shows how policy makers can influence on the GHG emissions in the energy sector by properly adjusting the tax rates. It

ISBN: 978-84-693-7673-7/DL:T-1752-2010

is worthwhile to mention that in the last Pareto optimal high jump in the total cost is observed. This could be explained that once the solar energy contribution reaches certain percentage further increase in the solar fraction alone does not lead to a reduction in environmental load but also it has to be accompanied by significant increase in the area of the absorption cycle. The increase in the area of the absorption cycle allows decreasing the higher temperature energy demand thus reducing the primary energy needs. However, it leads to a large increase of the total cost.

6.3. Influence of fuel cost

We recalculated next the Pareto set shown in Fig. 3 for different fuel prices in order to assess the impact of this parameter on the performance of the integrated system. Fig. 6 shows the new Pareto sets obtained for different fuel prices.

[***Figure 6 could be placed here***]

As expected, the Pareto set moves upwards and to the left when the fuel cost is increased. Particularly, the minimum total cost design shows a solar fraction of 8% for a fuel price of 0.0635 €/kWh, and of 77% when the fuel price is 0.0700 €/kWh. This is due to the fact that the increase in the fuel cost makes the integration of the cycle with solar collectors more profitable.

[***Table 3 could be placed here***]

Table 3 shows for each Pareto point in Fig. 6, the carbon dioxide tax rate (tax_{CO_2}), the solar fraction (SF) and the associated GWP for fuel prices of 0.0474 €/kWh, 0.0635 €/kWh and 0.07 €/kWh. Note that the tax rate given in the table is that for which the Pareto point would become optimal considering only the total cost as single objective.

As observed, by increasing the fuel cost, we get larger solar fractions and lower tax rates. This is an interesting observation that suggests that the tax

UNIVERSITAT ROVIRA I VIRGILI
OPTIMIZATION OF ENVIRONMENTALLY FRIENDLY SOLAR ASSISTED ABSORPTION COOLING SYSTEMS
Berhane Hagos Gebreslassie
ISBN: 978-84-693-7673-7/DL:T-1752-2010

rate should be adapted to the cost data in order to achieve always a given reduction in GHG emissions rather than being fixed independently of the market trends.

Results in Table 3 indicate also that at a given fuel cost, it is possible to obtain Pareto designs with significant reductions in GWP by slightly increasing the tax rate on CO_2 emissions. For instance, for a fuel cost of 0.0474 €/kWh and a tax rate of 77.8 €/$ton\,CO_2$, the optimal solar fraction is 0.06. However, by slightly increasing the value of tax_{CO_2} up to 4.4%, we obtain a solar fraction of 0.75 and a reduction of GWP of 62.8%. Moreover, Table 3 shows that when the fuel cost is increased to 0.07 €/kWh, the first four Pareto designs show a negative value of the charges on CO_2 emissions. This is because in these cases the use of solar energy becomes profitable not only economically but also environmentally.

[***Figure 7 could be placed here***]

Fig. 7 depicts (1) the total life cycle GWP, the life cycle GWP associated with the manufacturing (2) and operation (3) of the cooling system, and (4) the CO_2 emissions released during the cycle operation for the minimum total cost solution under different fuel prices. The emissions values were determined as follows: (4) includes the CO_2 released in the combustion of natural gas in the fired heater; (3) accounts for the same emissions as in (4) plus those associated with the generation of the electricity and natural gas consumed by the cycle; (2) includes the life cycle GHG emissions associated with the construction of the cycle; and (1) is the summation of (2) and (3).

As observed, for high fuel cost values, the model tends to select the solar energy over the natural gas. Consequently, the GWP is reduced because the GHG emissions released during the operation of the cycle are decreased. This reduction in GWP is not significant for fuel cost values lower than 0.065 €/kWh. This is because below this point the economic savings in fuel expenditures are not compensated by the increase in capital cost due to

UNIVERSITAT ROVIRA I VIRGILI
OPTIMIZATION OF ENVIRONMENTALLY FRIENDLY SOLAR ASSISTED ABSORPTION COOLING SYSTEMS
Berhane Hagos Gebreslassie
ISBN: 978-84-693-7673-7/DL:T-1752-2010

the purchase of solar collectors. Fig. 7 also shows how the GHG emissions released during the manufacturing phase can be neglected, since their contribution to the total GWP of the cycle is rather small. Furthermore, it can be observed how the GHG emissions released in the combustion of natural gas represent a large percentage of the total life cycle GHG emissions of the process.

It should be noted that the results obtained in the environmental analysis depend largely on the data used to calculate the life cycle inventory, which in our case were retrieved from the Ecoinvent database.

7. Conclusions

This paper has addressed the use of solar collectors coupled with absorption cooling cycles as a manner to reduce the GHG emissions in the cooling sector. The design of these systems has been formulated in mathematical terms as a multi-objective nonlinear programming (NLP) problem that seeks to minimize simultaneously the economic and environmental performance of the cooling application.

This work has extended our previously developed methodology [25] in the following ways: (i) it focuses on a different environmental performance measure (*i.e.*, global warming potential, GWP); (ii) it includes the option of using solar energy as a heat source to activate the cooling system; (iii) it assesses the impact that taxes on GHG emissions have on the optimal absorption cycle configuration considering only the economic performance; and (iv) it evaluates the impact of the fuel cost on the performance of the integrated system.

The results obtained show that with the current energy price and without considering governmental subsides on solar technologies, the use of solar energy in cooling applications is not profitable.

The method presented in this paper is aimed at facilitating the task of policy makers when deciding on the tax rates to be fixed in order to promote more sustainable technological alternatives in the energy sector.

ISBN: 978-84-693-7673-7/DL:T-1752-2010

8. Nomenclature

Abbreviations

AB	Absorber
ABS	Absorption cycle
AC	Air conditioning
Col	Solar collector
Con	Condenser
D	Desorber
E	Evaporator
ETC	Evacuated tube collector
Exp	Solution and subcooler expansion valve
GFH	Gas fired heater
GHG	Greenhouse gas emissions
$IPCC$	Intergovernmental Panel on Climate Change
LCA	Life cycle assessment
NLP	Nonlinear programming
$Pump$	Solution pump
SC	Subcooler
SHX	Solution heat exchanger

Indices

b	Chemical emission
i	Component of a stream
j	Streams
k	Equipment unit of the absorption cycle
t	Time period

Sets

$IN(k)$	Set of input streams to unit k
$OUT(k)$	Set of out put streams from unit k

ISBN: 978-84-693-7673-7/DL:T-1752-2010

Parameters

A_{col}	Absorber area of solar collector model i $[m^2]$
$cost_{col}$	Specific cost of solar collector model i $[\frac{€}{m^2}]$
$cost_{elec}$	Specific cost of electricity $[\frac{€}{kWh}]$
$cost_{ng}$	Specific cost of heat from natural gas $[\frac{€}{kWh}]$
c_0	Optical efficiency value of solar collector model
c_1	Linear loss coefficient of solar collector model
c_2	Quadratic loss coefficient of solar collector model
$CEPCI_{1996}$	Chemical engineering cost index in year 1996
$CEPCI_{2008}$	Chemical engineering cost index in year 2008
FC	Fuel cost $[€/kWh]$
G_t	Global daily solar radiation in period t $[\frac{W}{m^2}]$
$IAM(\Theta)$	Incident angle modifier $[-]$
ir	Interest rate $[-]$
$LCIE_b^{cw}$	Life cycle inventory entry associated with chemical b per kg of cooling water used $[\frac{kg}{unit}]$
$LCIE_b^{elec}$	Life cycle inventory entry associated with chemical b per reference flow of electricity consumed $\frac{kg}{MJ}$
$LCIE_b^{heat(col)}$	Life cycle inventory entry associated with chemical b per kWh of heat delivered by the solar collector $[\frac{kg}{kWh}]$
$LCIE_b^{heat(gfh)}$	Life cycle inventory entry associated with chemical b per MJ of heat delivered by the heater $[\frac{kg}{MJ}]$
$LCIE_{b,k}$	Life cycle inventory entry associated with chemical b per unit of capacity of equipment k constructed $[\frac{kg}{unit}]$
T_t^{amb}	Ambient temperature in period t $[^oC]$
T_{op}	Operational hours per year $[\frac{h}{yr}]$
U_k	Overall heat transfer coefficient of unit k $\left[\frac{kW}{m^2K}\right]$
α_k	Purchase cost exponent of unit k $[-]$
β_k	Purchase cost coefficient $[-]$
ϵ	Auxiliary parameter
$\underline{\epsilon}$	Lower bound on the auxiliary parameter ϵ
$\overline{\epsilon}$	Upper bound on the auxiliary parameter ϵ

UNIVERSITAT ROVIRA I VIRGILI
OPTIMIZATION OF ENVIRONMENTALLY FRIENDLY SOLAR ASSISTED ABSORPTION COOLING SYSTEMS
Berhane Hagos Gebreslassie
ISBN: 978-84-693-7673-7/DL:T-1752-2010

η^{gfh}	Thermal efficiency of the gas fired heater $[-]$
η^{mot}	Compressor motor efficiency $[-]$
ψ	Capital cost coefficient $[-]$
θ	Capital cost recovery factor $[-]$
Θ	Incident angle
φ	Life span of the cooling system $[years]$
df_b	Global warming potential of chemical b with respect to CO_2 $[kg\,CO_{2\,eq}]$

Variables

A_k	Area of heat exchanger k $[m^2]$
CAP_k	Capacity of equipment k
CC_k	Capital cost of equipment k [€]
COP	Coefficient of performance of the absorption cycle $[-]$
GWP	Global warming potential $[kg\,CO_{2\,eq}]$
LCI_b^{man}	Life cycle inventory of chemical b associated with the manufacture of the cooling system $[kg]$
LCI_b^{op}	Life cycle inventory entry of chemical b associated with the operation of the cooling system $[kg]$
LCI_b^{tot}	Total life cycle inventory entry of chemical b $[kg]$
$h_{j,t}$	Enthalpy of stream j in period t $\left[\frac{kJ}{kg}\right]$
$m_{j,t}$	Mass flow rate of stream j in period t $\left[\frac{kg}{s}\right]$
n	Number of collectors (relaxed integer variable)
PEC_k	Purchase cost of unit k [€]
$P_{j,t}$	Pressure of stream j in period t $[bar]$
$Q_{k,t}^{IN}$	Heat input to unit k in period t $[kW]$
$Q_{k,t}^{OUT}$	Heat output from unit k in period t $[kW]$
RC_{cw}	Running cost associated with cooling water consumption [€]
RC_{gfh}	Running cost of the gas fired heater [€]
RC_{pump}	Running cost of the pump [€]
SF_t	Solar fraction in period t [-]
tax_{CO_2}	Tax on carbon dioxide emissions $[€/ton\,CO_2]$

ISBN: 978-84-693-7673-7/DL:T-1752-2010

TC	Total cost [€]
TCC	Total capital cost [€]
TOC	Total operating cost [€]
T_t^{av}	Average temperature of collector inlet and exit temperatures in period t $[^oC]$
$T_{j,t}$	Temperature of stream j in period t $[^oC \, or \, K]$
$W_{k,t}$	Mechanical power of unit k in period t $[kW]$
$x_{i,j,t}$	Mass fraction of component i in stream j in period t $[-]$
$\Delta T_{k,t}^c$	Temperature difference in the cold end of unit k in period t $[^oC \, or \, K]$
$\Delta T_{k,t}^h$	Temperature difference in the hot end of unit k in period t $[^oC \, or \, K]$
$\Delta T_{k,t}^{lm}$	Logarithmic mean temperature difference of unit k in period t $[^oC \, or \, K]$
η_t^{col}	Solar collector efficiency in period t

UNIVERSITAT ROVIRA I VIRGILI
OPTIMIZATION OF ENVIRONMENTALLY FRIENDLY SOLAR ASSISTED ABSORPTION COOLING SYSTEMS
Berhane Hagos Gebreslassie
ISBN: 978-84-693-7673-7/DL:T-1752-2010

Acknowledgements

Berhane H. Gebreslassie would like to acknowledge his gratitude for the financial support received from the University Rovira i Virgili, the Spanish Ministry of Education and Science (DPI2008-04099 and CTQ2009-14420-C02) and the Spanish Ministry of External Affairs (A/016473/08, HS2007-0006 and A/023551/09). We would also like to thank the MSc. student Melanie Jiménez for helping to produce the numerical result for the case studies.

ISBN: 978-84-693-7673-7/DL:T-1752-2010

References

[1] Commission of the European Communities . Towards a european strategy for the security of energy supply. Tech. Rep.; 2001.

[2] PRé-Consultants. SimaPro 7 LCA software. The Netherlands (www.pre.nl/simapro/default.htm); 2008.

[3] Casals XG. Solar absorption cooling in spain: Perspectives and outcomes from the simulation of recent instalations. Renewable Energy 2006;31:1371–89.

[4] McMullan JT. Refrigeration and the environment – issues and strategies for the future. International Journal of Refrigeration 2002;25:89–99.

[5] Jaruwongwittaya T, Chen G. A review: Renewable energy with absorption chillers in thailand. Renewable and Sustainable Energy Reviews 2010;14(5):1437 –44.

[6] Rosiek S, Batlles F. Integration of the solar thermal energy in the construction: Analysis of the solar-assisted air-conditioning system installed in $CIESOL$ building. Renewable Energy 2009;34(6):1423 –31.

[7] Doukas H, Patlitzianas KD, Kagiannas AG, Psarras J. Renewable energy sources and rationale use of energy development in the countries of gcc: Myth or reality? Renewable Energy 2006;31(6):755 –70.

[8] Henning HM. Solar-Assisted Air-Conditioning in Buildings. Springer Wien/New York; ISBN: 3-211 - 00647-8; 2004.

[9] Azapagic A, Clift R. The application of life cycle assessment to process optimisation. Computers and Chemical Engineering 1999;10:1509–26.

[10] Azapagic A, Clift R. Life cycle assessment and multiobjective optimisation. Journal of Cleaner Production 1999;7:135–43.

ISBN: 978-84-693-7673-7/DL:T-1752-2010

[11] Guillén-Gosálbez G, Caballero JA, Esteller LJ. Application of life cycle assessment to the structural optimization of process flowsheets. Industrial & Engineering Chemistry Research 2008;47:777–89.

[12] Hugo A, Ciumei C, Buxton A, Pistikopoulos EN. Environmental impact minimization through material substitution: a multi-objective optimization approach. Green Chemistry 2004;6:407–17.

[13] Chavez-Islas LM, Heard CL. Design and analysis of an ammonia-water absorption refrigeration cycle by means of an equation-oriented method. Industrial & Engineering Chemistry Research 2009;48(4):1944–56.

[14] Gebreslassie BH, Guillén-Gosálbez G, Jiménez L, Boer D. Economic performance optimization of an absorption cooling system under uncertainity. Applied Thermal Engineering 2009;29:3491–500.

[15] Misra RD, Sahoo PK, Gupta A. Thermoeconomic evaluation and optimization of an aqua-ammonia vapour-absorption refrigeration system. International Journal of Refrigeration 2006;29:47–59.

[16] Gebreslassie BH, Medrano M, Mendes F, Boer D. Optimum heat exchanger area estimation using coefficients of structural bonds: Application to an absorption chiller. International Journal of Refrigeration 2010;33:529–37.

[17] Bernier E, Maréchal F, Samson R. Multi-objective design optimization of a natural gas-combined cycle with carbon dioxide capture in a life cycle perspective. Energy 2010;35:1121–8.

[18] Molyneaux A, Leyland G, Favrat D. Environomic multi-objective optimisation of a district heating network considering centralized and decentralized heat pumps. Energy 2010;35:751 –8.

[19] Li H, Maréchal F, Burer M, Favrat D. Multi-objective optimization of an advanced combined cycle power plant including co_2 separation options. Energy 2006;31:3117 –34.

ISBN: 978-84-693-7673-7/DL:T-1752-2010

[20] Svensson E, Berntsson T. Economy and co_2 emissions trade-off: A systematic approach for optimizing investments in process integration measures under uncertainty. Applied Thermal Engineering 2010;30(1):23–9.

[21] IRAM-ISO 14040. Environmental management-Life cycle assesment-Principles and frame work. 2006.

[22] Azapagic A. Life cycle assessment and its application to process selection, design and optimisation. Chemical Engineering Journal 1999;73:1–21.

[23] Guillén-Gosálbez G, Grossmann IE. A global optimization strategy for the environmentally conscious design of chemical supply chains under uncertainty in the damage assessment model. Computers & Chemical Engineering 2010;34(1):42–58.

[24] The ecoinvent Center. A competence centre of $ETH, PSI, EMA\&ART$, http://www.ecoinvent.ch/. ecoinvent data v21.

[25] Gebreslassie BH, Guillén-Gosálbez G, Jiménez L, Boer D. Design of environmentally conscious absorption cooling systems via multi-objective optimization and life cycle assesment. Applied Energy 2009;86:1712–22.

[26] Kalogirou SA. Solar thermal collectors and applications. Progress in Energy and Combustion Science 2004;30(3):231 –95.

[27] Gian-Kasper P, Stocker T, Midgley P, Tignor M. $IPCC$ Expert Meeting on the Science of Alternative Metrics. 2009.

[28] Brooke A, Kendrik D, Meeraus A, Raman R, Rosenthal RE. GAMS - A User's Guide. GAMS Development Corporation, Washington; 1998.

[29] Drud A. $CONOPT$ Solver Manual. ARKI Consulting and Development, Bagsvaerd, Denmark; 1996.

ISBN: 978-84-693-7673-7/DL:T-1752-2010

[30] Solomon S, Qin D, Manning M, Chen Z, Marquis M, Averyt K, Tignor M, Miller HL. Contribution of working group I to the fourth assessment report of the intergovernmental panel on climate change. Tech. Rep.Cambridge University Press, Cambridge, United Kingdom and New York, NY, USA; 2007.

[31] Generalitat de Catalunya, Departament d'Indústria, Comerç i Turisme. ATLAS DE RADIACIÓ SOLAR A CATALUNYA. *http* : *//www*20.*gencat.cat/docs/icaen*; 2000.

[32] F-Chart Software. Engineering equation solver, (EES). www.fchart.com.

[33] Bérubé JF, Gendreau M, Potvin JY. An exact ϵ-constraint method for bi-objective combinatorial optimization problems: Application to the traveling salesman problem with profits. European Journal of Operational Research 2009;194(1):39 – 50.

[34] Pátek J, Klomfar J. Simple functions for fast calculations of selected thermodynamic properties of the ammonia-water system. International Journal of Refrigeration 1995;18:228–34.

[35] Edgar TF, Himmelblau DM, Lasdon LS. Optimization of chemical processes. McGraw-Hill; 2001.

[36] Bejan A, Tsatsaronis G, Moran M. Thermal Design & Optimization. John Wiley & Sons Inc.; 1996.

[37] Turton R, Bailie RC, Whiting WB, Shaeiwitz JA. Analysis, Synthesis, and Design of Chemical Processes. Prentice Hall PTR, New Jersey; 2003.

[38] Chemical Engineering. Chemical engineering plant cost index $(CEPCI)$. Tech. Rep., Chemical engineering. www.CHE.com; 2009.

UNIVERSITAT ROVIRA I VIRGILI
OPTIMIZATION OF ENVIRONMENTALLY FRIENDLY SOLAR ASSISTED ABSORPTION COOLING SYSTEMS
Berhane Hagos Gebreslassie
ISBN: 978-84-693-7673-7/DL:T-1752-2010

List of Figures

UNIVERSITAT ROVIRA I VIRGILI
OPTIMIZATION OF ENVIRONMENTALLY FRIENDLY SOLAR ASSISTED ABSORPTION COOLING SYSTEMS
Berhane Hagos Gebreslassie
ISBN: 978-84-693-7673-7/DL:T-1752-2010

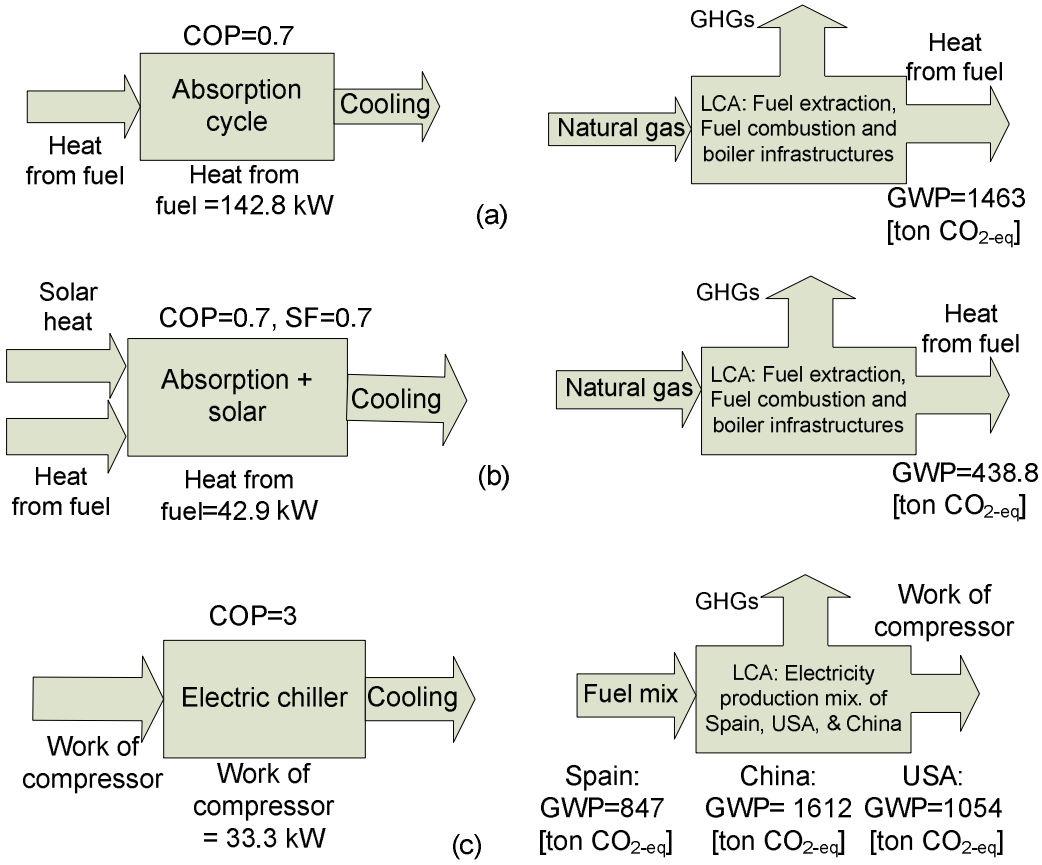

Figure 1: Environmental analysis of the electricity and thermal energy driven chillers.

UNIVERSITAT ROVIRA I VIRGILI
OPTIMIZATION OF ENVIRONMENTALLY FRIENDLY SOLAR ASSISTED ABSORPTION COOLING SYSTEMS
Berhane Hagos Gebreslassie
ISBN: 978-84-693-7673-7/DL:T-1752-2010

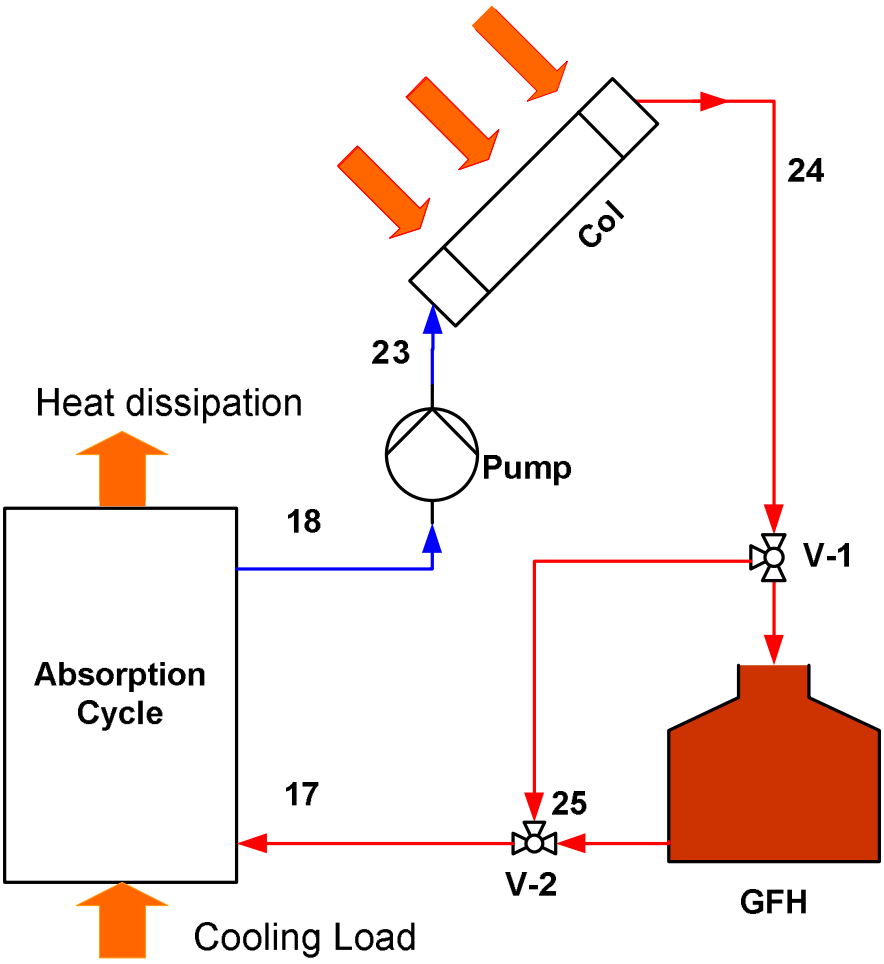

Figure 2: Solar assisted absorption chiller.

UNIVERSITAT ROVIRA I VIRGILI
OPTIMIZATION OF ENVIRONMENTALLY FRIENDLY SOLAR ASSISTED ABSORPTION COOLING SYSTEMS
Berhane Hagos Gebreslassie
ISBN: 978-84-693-7673-7/DL:T-1752-2010

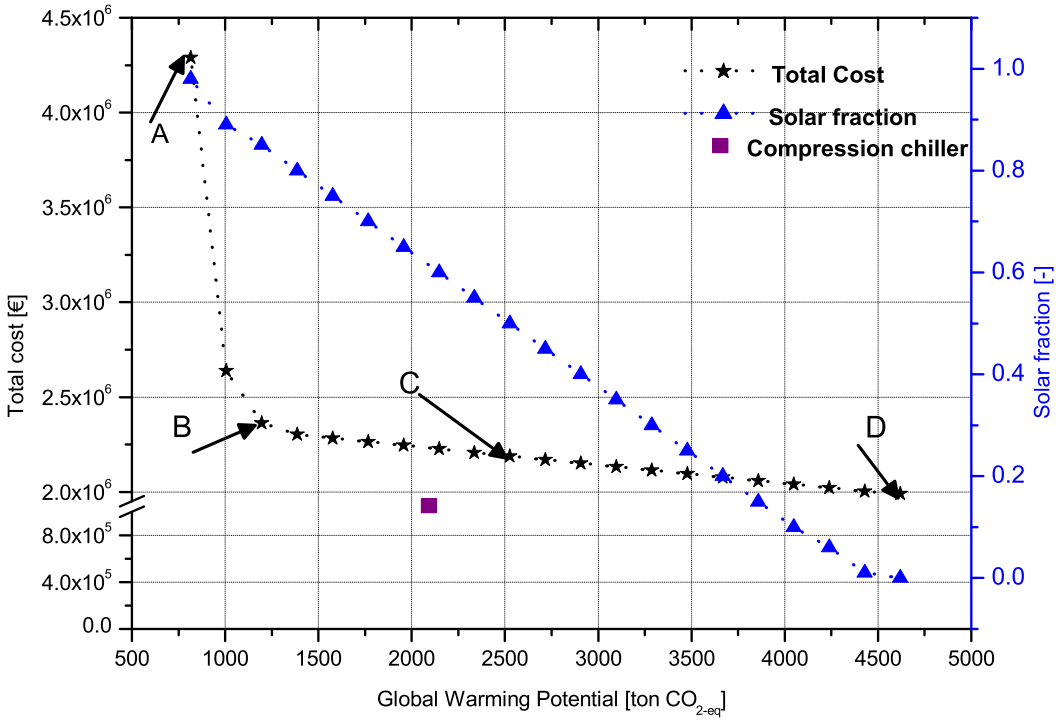

Figure 3: Pareto optimal designs of the base case.

UNIVERSITAT ROVIRA I VIRGILI
OPTIMIZATION OF ENVIRONMENTALLY FRIENDLY SOLAR ASSISTED ABSORPTION COOLING SYSTEMS
Berhane Hagos Gebreslassie
ISBN: 978-84-693-7673-7/DL:T-1752-2010

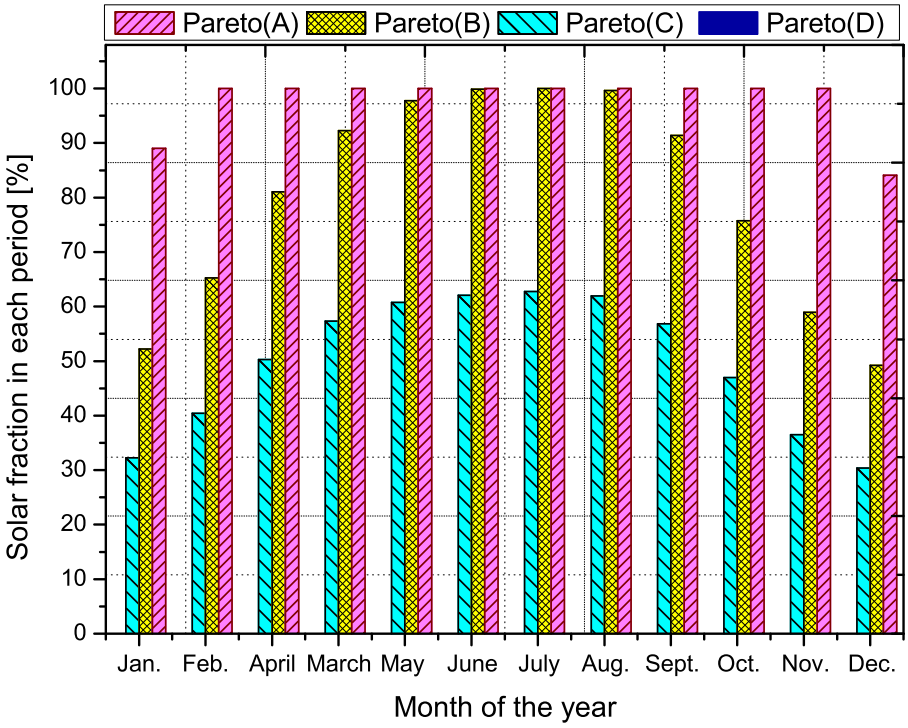

Figure 4: Solar fraction in each month for the selected Pareto optimal designs.

UNIVERSITAT ROVIRA I VIRGILI
OPTIMIZATION OF ENVIRONMENTALLY FRIENDLY SOLAR ASSISTED ABSORPTION COOLING SYSTEMS
Berhane Hagos Gebreslassie
ISBN: 978-84-693-7673-7/DL:T-1752-2010

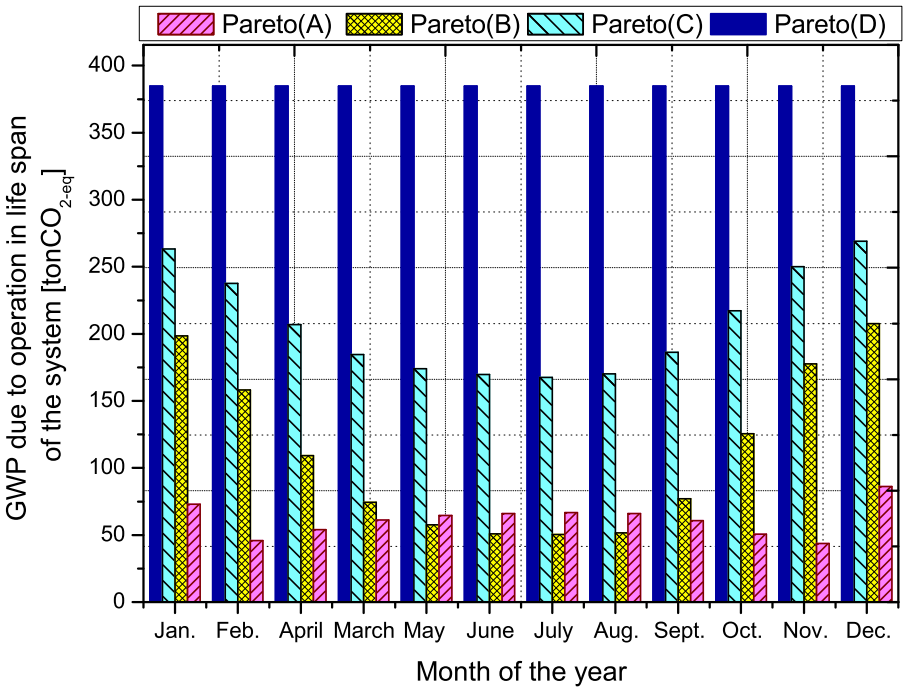

Figure 5: GWP during the operation of the cooling system for the selected Pareto optimal designs.

UNIVERSITAT ROVIRA I VIRGILI
OPTIMIZATION OF ENVIRONMENTALLY FRIENDLY SOLAR ASSISTED ABSORPTION COOLING SYSTEMS
Berhane Hagos Gebreslassie
ISBN: 978-84-693-7673-7/DL:T-1752-2010

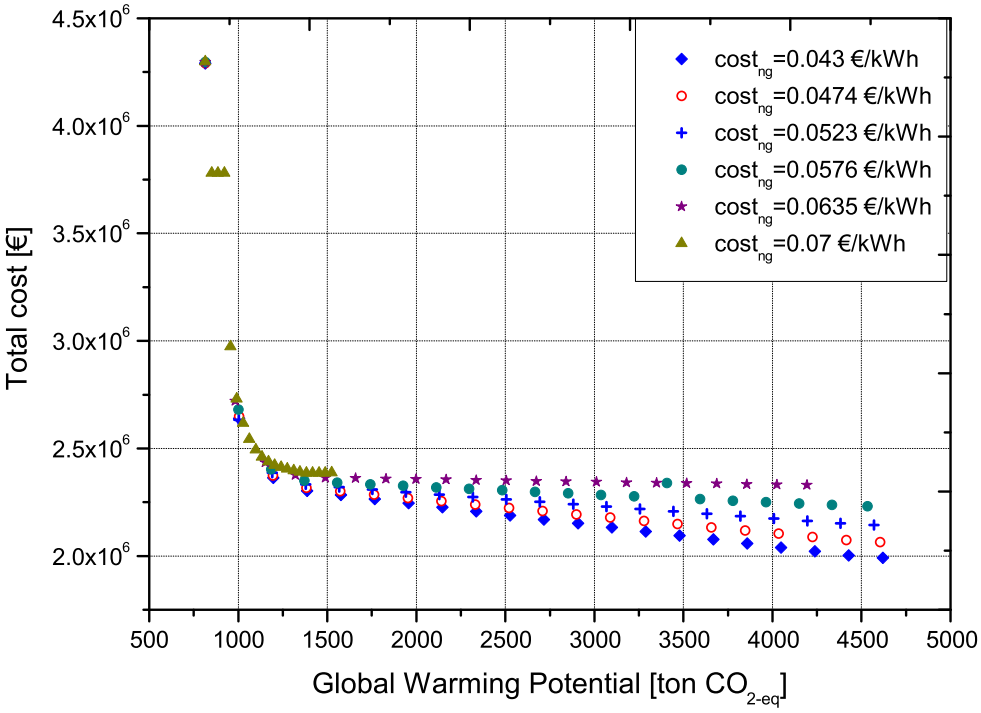

Figure 6: Pareto optimal designs for different fuel prices.

UNIVERSITAT ROVIRA I VIRGILI
OPTIMIZATION OF ENVIRONMENTALLY FRIENDLY SOLAR ASSISTED ABSORPTION COOLING SYSTEMS
Berhane Hagos Gebreslassie
ISBN: 978-84-693-7673-7/DL:T-1752-2010

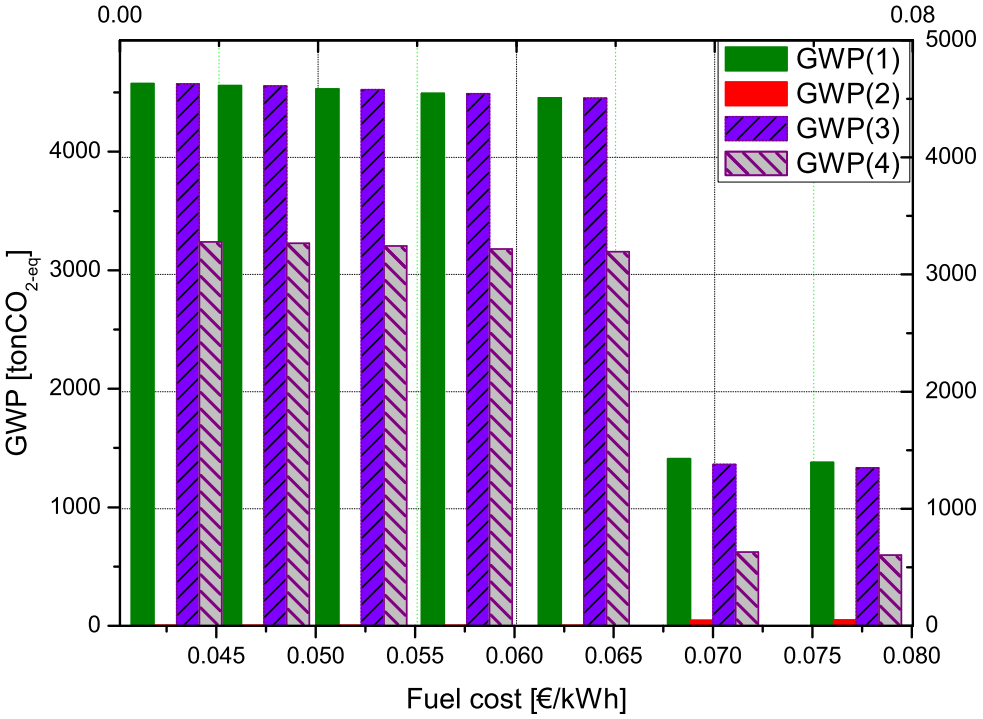

Figure 7: The minimum cost solutions GWP at different fuel costs of the Pareto sets given in Fig. 6. In the figure, (1) refers to the total life cycle GWP; (2) to the life cycle GWP associated with the manufacturing of the cycle; (3) to the life cycle emissions during the operation of the cooling system; and (4) to the CO_2 emissions in the gas fired heater.

.

UNIVERSITAT ROVIRA I VIRGILI
OPTIMIZATION OF ENVIRONMENTALLY FRIENDLY SOLAR ASSISTED ABSORPTION COOLING SYSTEMS
Berhane Hagos Gebreslassie
ISBN: 978-84-693-7673-7/DL:T-1752-2010

List of Tables

UNIVERSITAT ROVIRA I VIRGILI
OPTIMIZATION OF ENVIRONMENTALLY FRIENDLY SOLAR ASSISTED ABSORPTION COOLING SYSTEMS
Berhane Hagos Gebreslassie
ISBN: 978-84-693-7673-7/DL:T-1752-2010

Table 1: Barcelona daily global solar radiation and ambient temperature for 45^0 inclination.

Period	G_t $[W/m^2]$	T_t^{amb} $[^oC]$
January	297.0	8.2
February	350.7	9.4
March	415.3	11.1
April	460.4	13.1
May	478.5	17.0
June	482.4	20.9
July	483.8	23.5
August	477.5	24.1
September	445.8	21.6
October	385.0	17.3
November	320.6	12.1
December	282.2	9.9

UNIVERSITAT ROVIRA I VIRGILI
OPTIMIZATION OF ENVIRONMENTALLY FRIENDLY SOLAR ASSISTED ABSORPTION COOLING SYSTEMS
Berhane Hagos Gebreslassie
ISBN: 978-84-693-7673-7/DL:T-1752-2010

Table 2: The Pareto optimal design tax_{CO_2} and solar fraction of Fig. 3.

TC [€]	GWP $[ton\,CO_{2-eq}]$	tax_{CO_2} $[\frac{€}{ton\,CO_2}]$	SF [-]
1992007	4620	0.00	0.00
2260393	4429	58.10	0.01
2429149	4239	96.20	0.06
2430839	4049	96.60	0.10
2432453	3859	97.00	0.15
2434353	3669	97.50	0.20
2435437	3478	97.80	0.25
2436125	3288	98.00	0.30
2437741	3098	98.50	0.35
2438631	2908	98.80	0.40
2439192	2717	99.00	0.45
2439714	2527	99.20	0.50
2440204	2337	99.40	0.55
2440423	2147	99.50	0.60
2440626	1957	99.60	0.65
2435402	1766	96.64	0.70
2440797	1576	99.70	0.75
2448339	1386	104.50	0.80
2742809	1196	317.00	0.85
4098633	1005	1451.00	0.89
11365723	815	8679.00	0.98

Table 3: GWP, Solar fraction and tax_{CO_2} for some of the fuel costs of the Pareto optimal designs shown in Fig. 6.

fuel cost= 0.0474 $\frac{€}{kWh}$			fuel cost= 0.0635 $\frac{€}{kWh}$			fuel cost= 0.07 $\frac{€}{kWh}$		
GWP $[ton\,CO_{2-eq}]$	tax_{CO_2} $\frac{€}{ton\,CO_2}]$	SF $[-]$	GWP $[ton\,CO_{2-eq}]$	tax_{CO_2} $\frac{€}{ton\,CO_2}]$	SF $[-]$	GWP $[ton\,CO_{2-eq}]$	tax_{CO_2} $\frac{€}{ton\,CO_2}]$	SF $[-]$
4604	0.0	0.00	4194	0.0	0.08	1524	-18.4	0.77
4414	48.7	0.01	4025	10.2	0.11	1489	-18.3	0.78
4225	77.8	0.06	3856	11.0	0.16	1453	-14.1	0.79
4035	78.5	0.11	3687	11.3	0.20	1418	-11.2	0.80
3846	78.8	0.16	3518	11.6	0.24	1382	20.9	0.80
3657	79.0	0.21	3349	11.9	0.29	1347	109.0	0.81
3467	79.5	0.25	3180	12.2	0.33	1311	175.5	0.82
3278	79.8	0.30	3011	12.4	0.37	1276	221.8	0.83
3088	80.0	0.35	2842	12.6	0.42	1241	225.0	0.84
2899	80.3	0.40	2674	12.8	0.46	1205	271.5	0.85
2709	80.6	0.45	2505	13.0	0.51	1170	477.0	0.86
2520	80.7	0.50	2336	13.1	0.55	1134	636.0	0.86
2331	80.8	0.55	2167	13.2	0.60	1099	935.0	0.87
2141	81.0	0.60	1998	13.2	0.64	1063	1398.0	0.88
1952	81.0	0.65	1829	13.3	0.69	1028	2082.5	0.89
1762	81.1	0.70	1660	13.3	0.73	992	3180.0	0.89
1573	81.2	0.75	1491	13.3	0.78	957	6861.0	0.90
1383	86.5	0.80	1322	69.5	0.82	922	7597.1	0.91
1194	304.0	0.85	1153	356.5	0.86	886	7597.1	0.91
1005	1460.0	0.89	984	1694.0	0.90	851	7597.1	0.91
815	8671.0	0.98	815	9325.0	0.98	815	14608.0	0.98

UNIVERSITAT ROVIRA I VIRGILI
OPTIMIZATION OF ENVIRONMENTALLY FRIENDLY SOLAR ASSISTED ABSORPTION COOLING SYSTEMS
Berhane Hagos Gebreslassie
ISBN: 978-84-693-7673-7/DL:T-1752-2010

UNIVERSITAT ROVIRA I VIRGILI
OPTIMIZATION OF ENVIRONMENTALLY FRIENDLY SOLAR ASSISTED ABSORPTION COOLING SYSTEMS
Berhane Hagos Gebreslassie
ISBN: 978-84-693-7673-7/DL:T-1752-2010

Appendices

Appendix A. Energy and material balance applied to each unit of the cooling system

The model of the integrated absorption cycle is based on mass and energy conservation laws. It includes also equations for assessing the economic and environmental performance of the cooling system. We provide next the main constraints of the model. Further details can be found in [14, 25].

- Mass balance: The total mass of component i that enters unit k in period t is equal to the total mass of the same component i that leaves the unit.

$$\sum_{j \in IN(k)} m_{j,t} x_{i,j,t} - \sum_{j \in OUT(k)} m_{j,t} x_{i,j,t} = 0 \qquad \forall k, i, t \tag{A.1}$$

  In this equation, $m_{j,t}$ is the mass flow rate of stream j in time period t, $x_{i,j,t}$ is the composition of component i in stream j and period t, and $IN(k)$ and $OUT(k)$ are the set of input and output streams associated with unit k.

- Energy balance: The difference in heat content between the inlet and outlet streams of a unit k plus the difference in heat supplied ($Q^{IN}_{k,t}$) and removed ($Q^{OUT}_{k,t}$) minus the work done ($W_{k,t}$) must equal zero in each period t. Furthermore, the input and output heat terms are zero in some units of the cycle.

$$\sum_{j \in IN(k)} m_{j,t} h_{j,t} - \sum_{j \in OUT(k)} m_{j,t} h_{j,t} + Q^{IN}_{k,t} - Q^{OUT}_{k,t} - W_{k,t} = 0 \qquad \forall k, t \tag{A.2}$$

$$Q^{IN}_{k,t} = 0 \quad if \quad k = \left\{ \begin{array}{l} Absorber\,(AB) \\ Condenser\,(Con) \\ Subcooler\,(SC) \\ Solution\ heat\ exchanger\,(SHX) \\ Pump\,(Pump) \\ Expansion\ valves\,(Exp) \end{array} \right\} \tag{A.3}$$

UNIVERSITAT ROVIRA I VIRGILI
OPTIMIZATION OF ENVIRONMENTALLY FRIENDLY SOLAR ASSISTED ABSORPTION COOLING SYSTEMS
Berhane Hagos Gebreslassie
ISBN: 978-84-693-7673-7/DL:T-1752-2010

$$Q_{k,t}^{OUT} = 0 \quad if \quad k = \left\{ \begin{array}{l} Evaporator\,(E) \\ Desorber\,(D) \\ Subcooler\,(SC) \\ Solution\ heat\ exchanger\,(SHX) \\ Pump\,(Pump) \\ Expansion\ valves\ (Exp) \\ Solar\ collectors(Col) \\ Gas\ fired\ heater,(GFH) \end{array} \right\} \tag{A.4}$$

$$W_{k,t} = 0 \qquad \forall k \neq Pump \tag{A.5}$$

In eqn. (A.2), $h_{j,t}$ denotes the specific enthalpy of stream j in period t.

- The thermodynamic properties of the ammonia-water working pair are determined with the correlations of Patek and Klomfa [34]

$$h_{j,t} = f(T_{j,t}, P_{j,t}, x_{i,j,t}) \quad \forall t \tag{A.6}$$

where, $T_{j,t}$ and $P_{j,t}$ are the temperature and pressure of stream j in period t, and $x_{i,j,t}$ is the mass fraction of component i in stream j in period t

- The heat exchangers are modeled based on the logarithmic mean temperature difference, as shown in eqn. (A.7).

$$Q_{k,t} = U_k A_k \Delta T_{k,t}^{lm} \qquad k = AB, Con, D, E, SC, SHX, \ \forall t \tag{A.7}$$

Here, $Q_{k,t}$ is the heat transfer in heat exchanger k in period t; U_k is the overall heat transfer co-efficient; A_k is the heat transfer area of the heat exchanger k; and $\Delta T_{k,t}^{lm}$ is the logarithmic mean temperature difference.

- In order to improve the numerical performance of the model, the logarithmic mean temperature difference, which is a function of the hot

UNIVERSITAT ROVIRA I VIRGILI
OPTIMIZATION OF ENVIRONMENTALLY FRIENDLY SOLAR ASSISTED ABSORPTION COOLING SYSTEMS
Berhane Hagos Gebreslassie
ISBN: 978-84-693-7673-7/DL:T-1752-2010

and cold end temperature differences ($\Delta T^h_{k,t}$ and $\Delta T^c_{k,t}$, respectively), is calculated via the Chen's approximation [35], as shown in eqn. (A.8).

$$\Delta T^{lm}_{k,t} \cong \left[\Delta T^h_{k,t}\Delta T^c_{k,t}\frac{\Delta T^h_{k,t}+\Delta T^c_{k,t}}{2}\right]^{\frac{1}{3}} \qquad k = AB, Con, D, E, SC, SHX, \ \forall t \tag{A.8}$$

- The total useful heat absorbed by the collector ($Q_{k=Col,t}$) and the heat generated by the gas fired heater ($Q_{k=GFH,t}$) in period t are determined using the following equations:

$$Q_{k,t} = m_{23,t}C_p(T_{24,t} - T_{23,t}) \qquad k = Col, \forall t \tag{A.9}$$

$$Q_{k,t} = m_{24,t}C_p(T_{25,t} - T_{24,t}) \qquad k = GFH, \forall t \tag{A.10}$$

in which the numbers refer to those in Fig. 2.

Appendix B. Equations for calculating the capital and operation costs of the cooling system

- The capital cost of the cooling system includes the cost of the heat exchangers, solar collectors, gas fired heater, pump, and expansions valves, which are denoted by the continuous variable CC_k.

$$TCC = \varphi\theta\left(\sum_k CC_k\right) \tag{B.1}$$

Here, φ is the life span of the cooling system and θ is the capital recovery factor, which is determined from eqn. (B.2),

$$\theta = \frac{ir\,(ir+1)^{\varphi}}{(ir+1)^{\varphi}-1} \tag{B.2}$$

where ir is the annual interest rate. On the other hand, The capital cost of unit k is estimated from the purchase cost of the unit (PEC_k)

UNIVERSITAT ROVIRA I VIRGILI
OPTIMIZATION OF ENVIRONMENTALLY FRIENDLY SOLAR ASSISTED ABSORPTION COOLING SYSTEMS
Berhane Hagos Gebreslassie
ISBN: 978-84-693-7673-7/DL:T-1752-2010

given by eqn. (B.5) and the cost parameter ψ, which has been taken from Bejan et al. [36].

$$CC_k = \psi PEC_k \quad \forall k \neq Col, \forall t \tag{B.3}$$

The purchase cost of unit k in year 1996 (PEC_k^{1996}) is estimated following Turton et al. [37].

$$PEC_k^{1996} = \beta_k \left(CAP_k\right)^{\alpha_k} \qquad \forall k \neq Col \tag{B.4}$$

Where CAP_k is the capacity measure of unit k. α_k and β_k are the cost parameters, which are given in Table B.4, that have been obtained from Turton et al. [37]. The purchase equipment cost is updated from year 1996 to year 2008 using the Chemical Engineering plant cost index [38] as follows:

$$PEC_k = PEC_k^{1996} \frac{CEPCI_{1996}}{CEPCI_{2008}} \qquad \forall k \tag{B.5}$$

Here, the parameters $CEPCI_{1996}$ and $CEPCI_{2008}$ refer to the Chemical Engineering plant cost index in years 1996 and 2008, respectively.

The capital cost of the solar collector, which is given by eqn. (B.6), is a function of the number of collectors (n), absorber area (A_{col}) and collector cost per m^2 of absorber area [8].

$$CC_k = nA_{col}cost_{col} \qquad k = Col \tag{B.6}$$

- The operating cost (TOC) of the cooling system accounts for the running cost of the gas fired heater (RC_{gfh}), the running cost of the pump (RC_{pump}), and the cooling water cost (RC_{cw}):

$$TOC = RC_{gfh} + RC_{pump} + RC_{cw} \tag{B.7}$$

$$RC_{gfh} = \frac{cost_{ng}\varphi T_{op}}{12\eta^{gfh}} \left(\sum_t Q_{k,t}\right) \qquad k = GFH \tag{B.8}$$

UNIVERSITAT ROVIRA I VIRGILI
OPTIMIZATION OF ENVIRONMENTALLY FRIENDLY SOLAR ASSISTED ABSORPTION COOLING SYSTEMS
Berhane Hagos Gebreslassie
ISBN: 978-84-693-7673-7/DL:T-1752-2010

$$RC_{pump} = \frac{cost_{elec}\varphi T_{op}}{12}\left(\sum_{t} W_{k,t}\right) \qquad k = Pump \tag{B.9}$$

$$RC_{cw} = cost_{cw}\varphi T_{op}\left(\sum_{t} m_{j,t}\right) \qquad j = cooling\,water \tag{B.10}$$

Where $cost_{ng}$, $cost_{elec}$ and $cost_{cw}$ are the prices of the natural gas, electricity and cooling water, respectively. T_{op} and η^{gfh} denote the annual operating hours, and gas fired heater efficiency, respectively.

Table B.4: Economic Parameters

Unit	β_k	α_k	Range
Heat exchanger	6880	0.430	$5 - 1500m^2$
Gas fired heater	1633	0.584	$100 - 10000kW$
Pump	1942	1.110	$1 - 100kW$